# AN *IN VITRO* INVESTIGATION OF *MYCOBACTERIUM TUBERCULOSIS* BIOFILM FORMATION AND ITS EFFECT ON THE HOST INNATE IMMUNE RESPONSE

by

THOMAS OLIVER KEATING

A thesis submitted to the University of Birmingham for the degree of DOCTOR OF PHILOSOPHY

The Institute of Microbiology and Infection
School of Biosciences
College of Life and Environmental Sciences
University of Birmingham
August 2017

UNIVERSITY OF
BIRMINGHAM

## University of Birmingham Research Archive

### e-theses repository

This unpublished thesis/dissertation is copyright of the author and/or third parties. The intellectual property rights of the author or third parties in respect of this work are as defined by The Copyright Designs and Patents Act 1988 or as modified by any successor legislation.

Any use made of information contained in this thesis/dissertation must be in accordance with that legislation and must be properly acknowledged. Further distribution or reproduction in any format is prohibited without the permission of the copyright holder.

# ABSTRACT

*Mycobacterium tuberculosis* is ostensibly an intracellular pathogen, which may form pellicle-like biofilms in the peripheries of tuberculosis cavities. Environment-induced cell wall modifications and extracellular polymeric substance production may alter host-pathogen interactions. Specifically, expectorated mycobacteria from cavities, which establish infection in new hosts, may have distinct phenotypic adaptations to impair early clearance by the innate immune system. *M. tuberculosis* H37Rv biofilm extracellular polymeric substance was identified using scanning electron microscopy. Biofilm phenotype non-covalently-bound extracts of cell wall lipids and carbohydrates were compared to planktonic phenotype and a relative reduction in the proportion of constituent glucose in biofilm carbohydrate extracts was discovered, indicative of a reduction in α-glucan prevalence. Comparison of carbohydrate extracts' potency in stimulating cytokine and chemokine secretion in whole blood and complement activation elucidated reduced C3b/iC3b deposition onto biofilm carbohydrate extracts. Labelling live dispersed *M. tuberculosis* planktonic and biofilm samples with fluorescent antibodies showed C3b/iC3b, C5b-9, MBL and C1q deposition was reduced on biofilm phenotype cells, using flow cytometry. The relative contribution of each major pathway of complement activation was investigated and greater dependence on classical pathway activation by *M. tuberculosis* biofilm cells compared to planktonic cells was observed. Implications of these findings in *M. tuberculosis* pathogenesis are discussed.

*Dedicated to my parents*

# ACKNOWLEDGEMENTS

First and foremost I would like to thank my supervisors, Joanna Bacon, Stephen Taylor (Public Health England (PHE)) and Luke Alderwick (University of Birmingham) for all their support, training, encouragement and feedback.

I would like to thank the PHE TB group and Pathogen Immunology group for all their training and support. Especially Samuel Lethbridge, Charlotte Hendon-Dunn, Rose Jeeves, Jon Allnut, Steve Thomas and Holly Humphries.

Thank you to all those in the IMI lab at the University of Birmingham who helped me and always made me feel welcome and the Chemistry department for performing gas chromatography on my samples.

Thanks to Howard Tolley at the PHE EM department for imaging my samples.

Thank you Nicole N van der Wel and Zehui Zhang for immuno gold labelling my samples at the University of Amsterdam.

Finally I want to thank Public Health England for providing funding for the PhD studentship.

I hope this thesis is above the threshold of acceptability to all those who dedicated time and effort to help with my research.

# TABLE OF CONTENTS

# LIST OF ILLUSTRATIONS

# LIST OF TABLES

# 1 INTRODUCTION

## 1.1 Overview

Biofilms are environment-adapted single or multi-species aggregates of microorganisms embedded in a self-secreted matrix of extracellular polymeric substance (EPS), which attaches the organisms to each other and/or to a surface (Vert et al., 2012). EPS is the amalgamation of extracellular hydrated biopolymers such as polysaccharides, proteins nucleic acids and lipids (Flemming and Wingender, 2010). This thesis investigates the importance of *M. tuberculosis* biofilm formation in the modulation of the innate human immune response, using *in vitro* techniques to characterise *M. tuberculosis* biofilms and measure their effect on human cytokine/chemokine production and complement activation. Before these findings are presented it is pertinent to review tuberculosis pathogenesis, drawing particular attention to the role of the innate immune response in host-pathogen interaction and incorporating advances in research into *M. tuberculosis* biofilms and the *M. tuberculosis* cell wall.

## 1.2 What is Tuberculosis?

Tuberculosis (TB) is an airborne disease that infected an estimated 10.4 million people in 2015 including 1 million children. In that same year 1.4 million people died as a result of TB (Anderson et al., 2016). The causative agent of TB is *Mycobacterium tuberculosis*, a rod shaped bacteria first discovered by Robert Koch in 1882 (Koch, 1882). TB is treatable with a multidrug regimen including isoniazid, rifampicin, pyrazinamide and ethambutol over 6 months (Pai et al., 2016). However, the length of treatment increases the risk of patient non-compliance. More concerning are incidences of rifampicin and multidrug resistant tuberculosis, which together accounted for almost 600 000 cases in 2015 (Anderson et al.,

2016). Tuberculosis causes a significant disease burden in developing countries with India, Indonesia, China, Nigeria, Pakistan and South Africa accounting for 60% of all new infections. It also remains a problem in many developed countries for example in the United Kingdom, reducing tuberculosis incidence was named as one of the top 7 priorities for Public Health England (PHE, 2014). TB cases in London are reported at 26 per 100 000 of the population (PHE, 2016), which is greater than the average of the 30 highest-burden TB countries in the world at 25 per 100 000 of the population (Anderson et al., 2016).

Bacillus Calmette-Guérin (BCG) vaccine is currently the only licenced vaccine against tuberculosis and it is approaching 100 years since the first human 'trial' (Luca and Mihaescu, 2013). The vaccine is effective against extrapulmonary TB in infants (Trunz et al., 2006) but shows wildly variable efficacy against pulmonary TB in adults ranging from 0 to 80% (Andersen and Doherty, 2005). This is particularly problematic since 80% of clinical cases and nearly 100% of *M. tuberculosis* transmission is due to pulmonary TB, triggered after a period of non-symptomatic latent infection (Hunter, 2011).

### 1.3 Part I Transmission

*M. tuberculosis* bacteria are expectorated in aerosolised droplets from the lungs of infected individual with active tuberculosis. Aerosols have been shown to harbour viable bacteria predominantly when particle size ranges from 0.65 – 4.7 μm in aerodynamic diameter (Fennelly et al., 2004; Fennelly and Jones-López, 2015). *M. tuberculosis* bacterium are rod-shaped, on average 2 - 4 μm in length (Eum et al., 2010) and around 0.44 μm in diameter (Takade et al., 2003) suggesting single or small aggregates of mycobacteria are primarily responsible for transmission. Sputum samples from tuberculosis patients are predominately composed of viable but non-culturable *M. tuberculosis* bacteria, which are undetected by conventional culture but may still be transmissible (Mukamolova et al., 2010).

## 1.4 Part II Air to Alveolus

*M. tuberculosis* bacteria are inhaled deep into the respiratory tract but are unable to cross the respiratory epithelium which poses a physical barrier between host and pathogen (Stevenson et al., 2006). Furthermore, an *M. tuberculosis* bacterium must contend with its first adversary in the war of attrition between host and pathogen, the airway surface liquid (ASL). ASL consists of two layers: The aqueous layer immerses cilia in the airway epithelium and enables them to beat efficiently, resulting in the gradual upward movement of the ASL to the throat. Floating on top of this is a viscous mucus layer, which can trap inhaled bacteria. This process of capture and gradual removal is known as mucocilliary clearance (Stevenson et al., 2006). Antimicrobial proteins and peptides that are also present in the ASL include lysozyme (Fleming, 1922), beta-defensin-1 (hBD-1) (Singh et al., 1998) and LL-37 (Bals et al., 1998). Lysozyme is only weakly active against *M. tuberculosis* (Kanetsuna, 1980) and the concentration of hBD-1 required to kill virulent *M. tuberculosis* is higher than the concentration found in the lung (Fattorini et al., 2004). While two studies have shown bactericidal activity of of LL-37 against *M. tuberculosis* (Rivas-Santiago et al., 2013; Sonawane et al., 2011) another research group found minimal inhibitory activity of LL-37 against *M. tuberculosis* (Jiang et al., 2011).

*M. tuberculosis* bacteria that avoid the ASL travel deep into the lung through bronchioles to the alveoli. Each alveolus is a spherical construct of type I epithelial cells. The importance of type I epithelial cells in *M. tuberculosis* infection has not yet been determined however type II epithelial cells, present at cell junctions as well as resident alveolar macrophages, dendritic cells can be infected with *M. tuberculosis* as illustrated in **Figure 1.4.1**(Lerner et al., 2015). Before phagocytosis of *M. tuberculosis* is described, it is necessary to review the intricate structure of the *M. tuberculosis* cell wall.

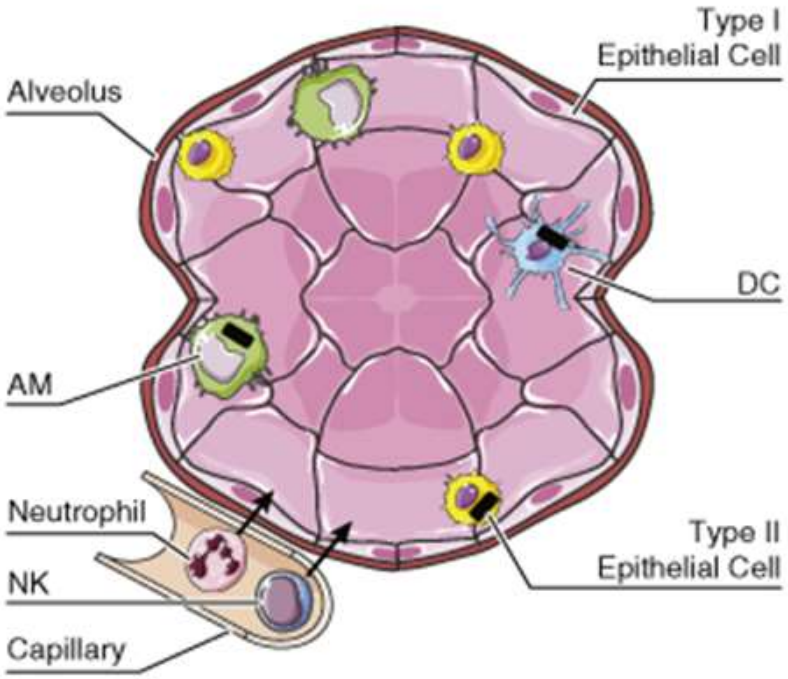


**Figure 1.4.1:** Alveolus structure. Adapted from Lerner et al., 2015, (permission to reuse via Creative Commons Attribution License) each alveolus is structured from Type I epithelial cells with type II epithelial cells at cell junctions. *M. tuberculosis* (black rods) is able to infect type II epithelial cells, alveolar macrophages (AMs), dendritic cells (DCs) as well as recruited neutrophils while recruited natural killer (NK) cells are able to lyse infected cells.

## 1.5 The *M. tuberculosis* cell wall

In the absence of biofilm formation, the *M. tuberculosis* cell wall is the host-pathogen interface and contains a variety of immunomodulatory molecules. The thick envelope surrounding the bacterium has low permeability and is also thought to be responsible for *M. tuberculosis'* antibiotic tolerance (Brennan and Nikaido, 1995; Lopez-Marin, 2012). *M. tuberculosis* is classed in the order *Actinomycetales* and the sub-order *Corynebacterineae* which specifically produce mycolic acids (Verschoor et al., 2012).

Mycobacteria produce mycolic acyl acid chains ranging from 60 to 90 carbons in length, the longest fatty acids known in nature (Lopez-Marin, 2012; Portevin et al., 2004; Verschoor et al., 2012; Vilcheze et al., 2000). There are three classes, α-mycolates, methoxy-mycolates and keto-mycolates, all of which contain cyclopropane rings in their carbon chains. α-mycolates tend to only form an extended 'U' shape, keto mycolates tend to form a 'W' shape and methoxy-mycolates are found in 'W' shape and intermediate semi-folded 'sZ' shape forms (**Figure 1.5.1**) (Minnikin et al., 2015). The majority of mycolic acids are covalently attached via ester linkages to the arabinogalactan, which is in turn covalently attached to peptidoglycan forming the mycolyl-arabinogalactan-peptidoglycan (mAGP) complex (McNeil et al., 1991, 1990). This structure forms the core of the mycobacterial cell wall (Brennan, 2003). Importantly these mycolic acids form the inner leaflet of an outer membrane (OM).

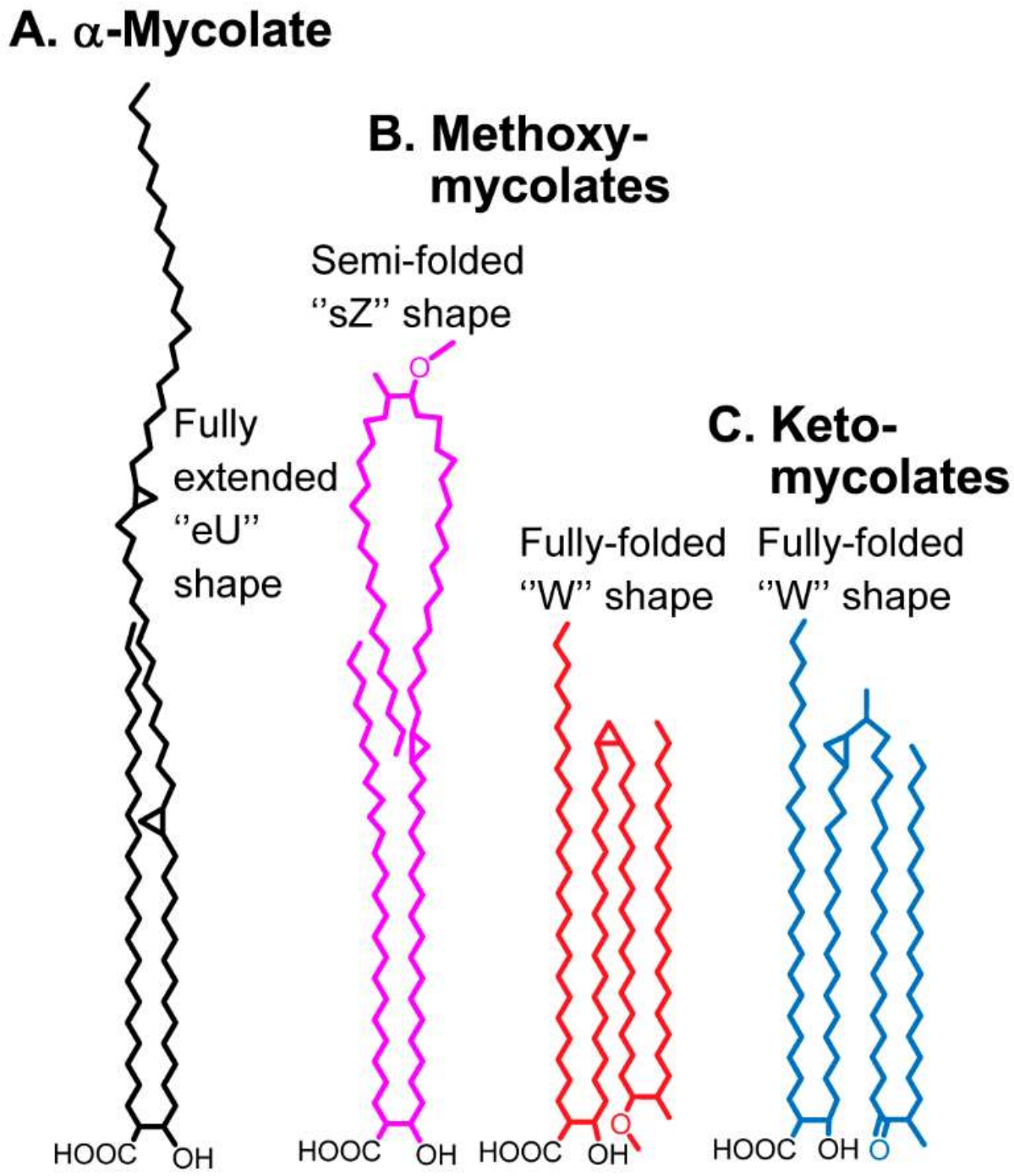


**Figure 1.5.1:** *M. tuberculosis* mycolic acids. Adapted from (Minnikin et al., 2015) (permission to reuse via Creative Commons Attribution License) A. α-mycolate. B. methoxy-mycolate in two alternative conformations. C. keto-mycolate

Between the mycobacterial inner membrane (IM) and the mAGP complex are phosphatidylinositol-anchored lipoglycans lipoarabinomannan (LAM) and lipomannan (LM) (**Figure 1.5.2**). LAM and LM are extensions of phosphatidyl-*myo*-inositol mannosides (PIMS). PIMs are glycolipids with fatty acids attached to glycerol, linked by a phosphodiester moiety to *myo*-inositol. *Mycobacterium* species can have mono or diacyl PIMs ($AC_1$ and $AC_2$ respectively) (Minnikin et al., 2015). Furthermore PIMs can be dimannoside or hexamannoside (Minnikin et al., 2015; Mishra et al., 2011; Vilkas and Lederer, 1956). 21-34 α-D-mannopyranosyl residues form the backbone of LM. With LAM, this is further extended by an additional highly branched arabinan domain and this is capped with around seven residues of mannose per molecule of LAM (Mishra et al., 2011).

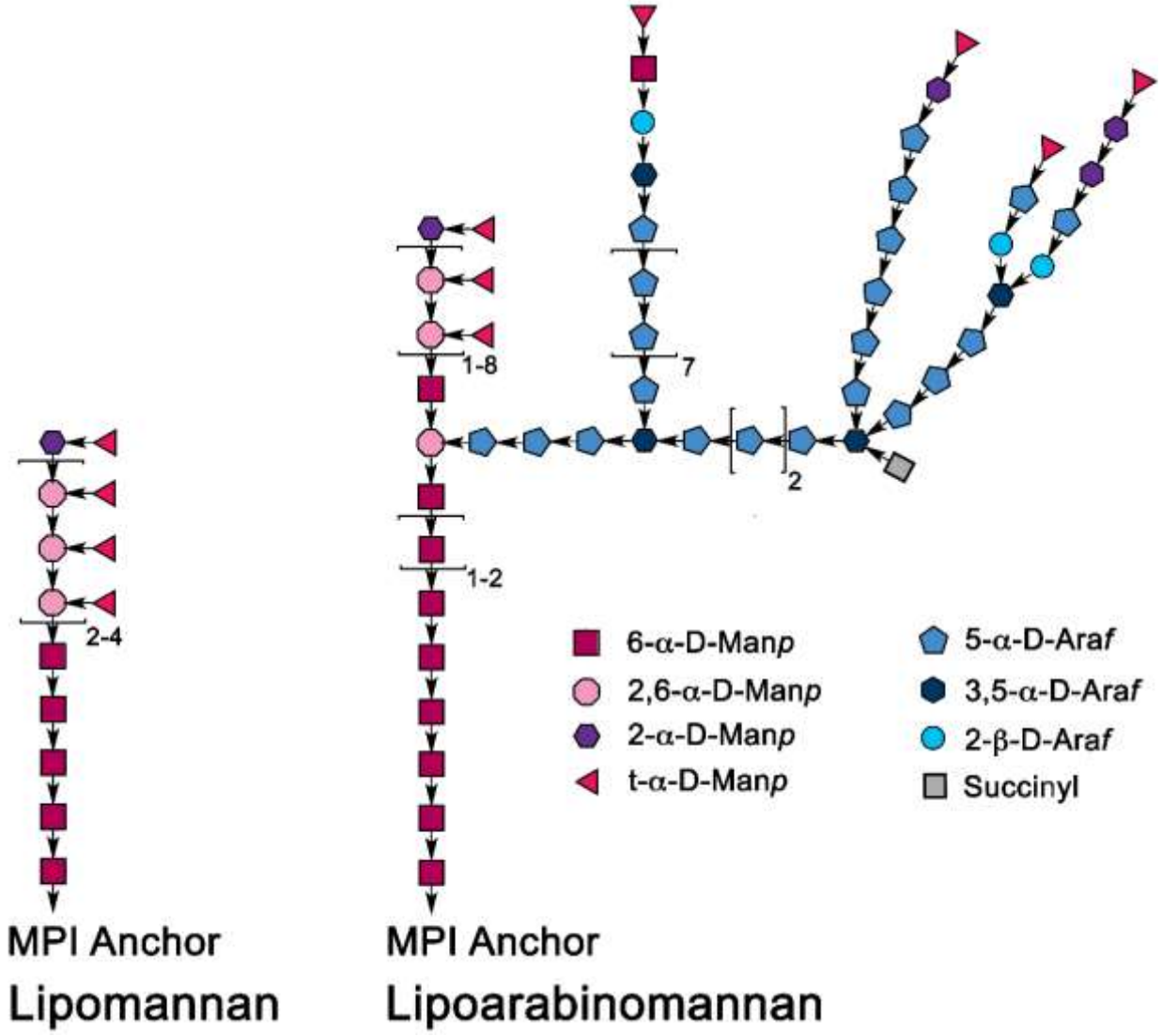


**Figure 1.5.2:** Structural topography of *M. tuberculosis* lipomannan and lipoarabinomannan. Adapted from (Minnikin et al., 2015) (permission to reuse via Creative Commons Attribution License) MPI is manno-phosphatidylinositol.

The mycolic acids terminus of the mAGP complex has been shown to form the inner leaflet of a second bilayer surrounding the bacilli, an outer membrane analogous to that of Gram negative bacteria but more complex. The 3D ultrastructure of the outer membrane has yet to be fully established. The outer leaflet of the outer membrane is composed of non-covalently attached free lipids (Bansal-Mutalik and Nikaido, 2014; Hoffmann et al., 2008; Zuber et al., 2008).

Recently cell wall lipids have been quantified in *M. smegmatis* using a method known as reverse micellar solution (RMS) extraction. This method completely and selectively removes non-covalently bound outer membrane (OM) lipids in the *Corynebacteria–Mycobacteria–Nocardia* group (Bansal-Mutalik and Nikaido, 2014, 2011). The OM inner leaflet was found to contain covalently bound mycolic acids (4.6% dcm). The OM outer leaflet comprised of mostly glycopeptidolipids (GPLs) 5.56% dcm, triacylglycerols (TAG) 2.54%, free mycolic acids and fatty acids (MA and FA) 2.06% dcm, diacyl glycerols 0.45% dcm, unidentified apolar lipids 0.28% dcm, trehalose dimycolate (TDM) 0.23% dcm and trace amounts of sulpholipid (SL). These lipids were found to be more than sufficient to form a complete bilayer. Notably the authors reason that a surplus of free mycolic acid required to form the outer-membrane is probably due to contamination of the RMS extract with extracellular material (Bansal-Mutalik and Nikaido, 2014). This contamination is due to mycobacterial biofilm formation, which will be discussed later in section 1.11. It would be interesting to see the same method applied to *M. tuberculosis* to identify the lipid constituents of the outer membrane and to identify which outer leaflet lipids form the complete bilayer. A recent model of the cell envelope as proposed by Minnikin et al., (2015) is shown in **Figure 1.5.3**.

Surrounding the OM is a capsule layer rich in the polysaccharides α-glucan, arabino-D-mannan, and D-mannan (Lemassu and Daffé, 1994; Ortalo-Magne et al., 1996; Ortalo-Magné

et al., 1995). This fragile layer can be stripped by culturing with detergents such as Tween-80, agitation alone and agitation with glass beads (Ortalo-Magné et al., 1995; Sani et al., 2010). Notably the discovery of the *M. tuberculosis* capsule was dependent on the culture of *M. tuberculosis* biofilms (surface pellicles). It is therefore possible that the mycobacterial extracellular polymeric substance (EPS) also contains the polysaccharides of the *M. tuberculosis* capsule in addition to the presence of free mycolic acids (Ojha et al., 2008) see section 1.11 for a review of *M. tuberculosis* biofilms.

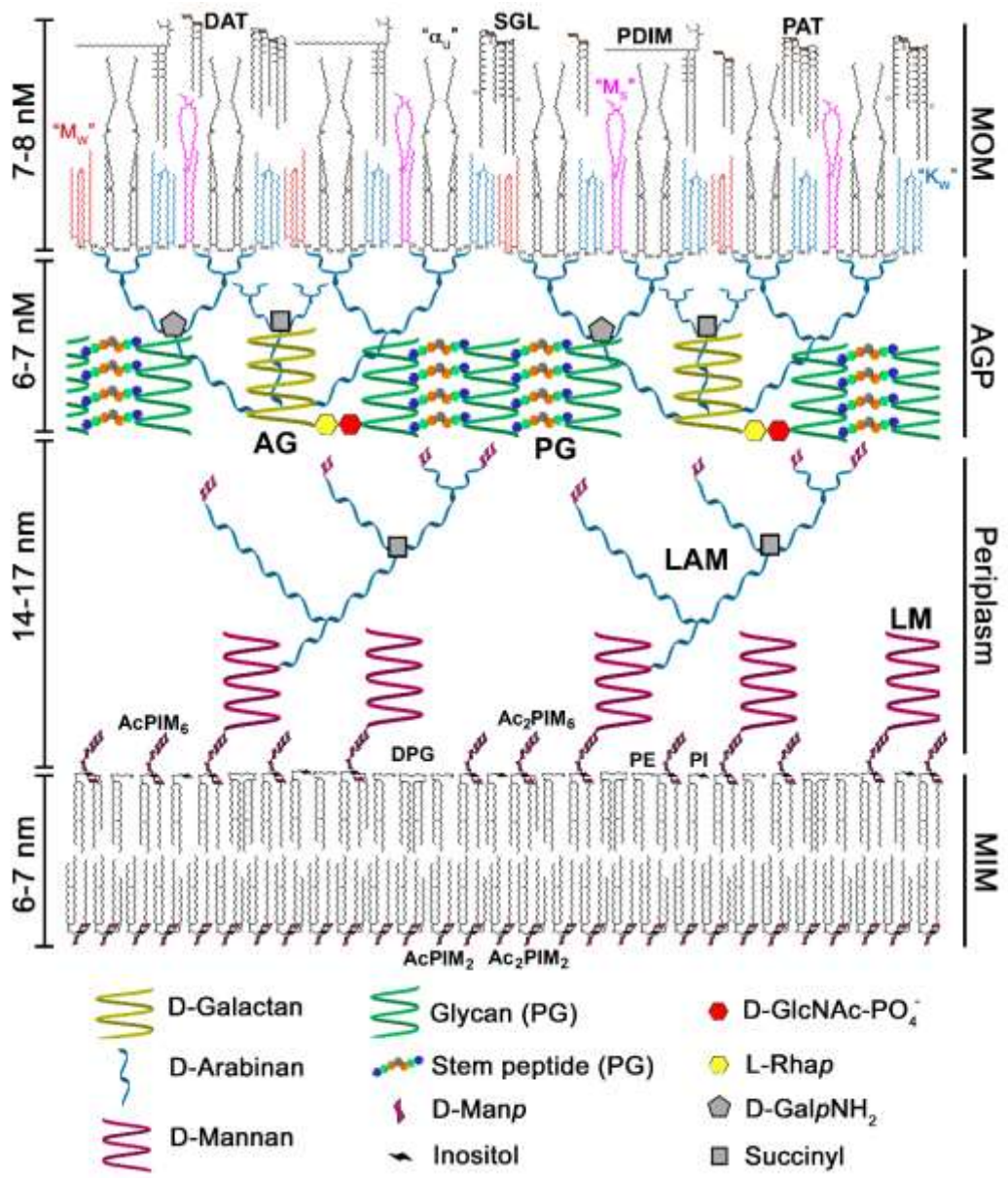


**Figure 1.5.3:** The cell envelope of *M. tuberculosis*. Schematic of the *M. tuberculosis* cell wall adapted from (Minnikin et al., 2015) (Permission to reuse via Creative Commons Attribution License). Dimensions correlate to cryo-electron microscopy and cell wall proteins are not shown. Depicts the mycobacterial inner membrane (MIM), arabinogalactan peptidoglycan (AGP), the mycobacterial outer membrane (MOM). The capsule is not shown. DAT, diacyltrehaloses; SGL, Sulfoglycolipid; PDIM, phthiocerol dimycocerosates; PAT, Pentaacyl trehalose; αu, fully extended α-mycolate; Kw and Mw, folded keto and methoxy-mycolate respectively; Ms, semi-folded methoxymycolate; AG, arabinogalactan; PG, peptidoglycan; LAM, lipoarabinomannan; LM, lipomannan; $Ac_1/Ac_2PIM_6$, acyl/diacyl phosphatidylinositol hexamannosides respectively; DPG, diphosphatidylglycerol; PE, phatidylethanolamine; PI, phosphatidylinositol; $Ac_1/Ac_2PIM_2$ acyl/diacyl phosphatidylinositol dimannosides respectively.

## 1.6 Part III Pathogen recognition proteins in the alveolus

Residing in the alveolus are soluble pattern recognition receptors (PRRs) such as complement protein C1q (Watford et al., 2000), Ficolin-1 (Liu et al., 2005) Ficolin-3 (Plovsing et al., 2016) and surfactant proteins A and D (Ferguson et al., 1999; Watford et al., 2001). These soluble PRRs interact with pathogen associated molecular patterns (PAMPs) on the surface of *M. tuberculosis* bacteria and opsonise the bacteria. However, uptake of *M. tuberculosis* can occur in the presence or absence of opsonins via PRRs present on host immune cells.

Soluble PRRs present in the alveolus recognise PAMPs on the *M. tuberculosis* cell wall such as capsular polysaccharides: mannans, α-glucans and arabinomannans as well as OM lipids and extracellular proteins. Surfactant proteins SP-A and SP-D are members of the collectin family (calcium dependent lectins) unlike SP-B and SP-C which are the other main mammalian surfactant proteins (Bernhard, 2016). Surfactant proteins SP-A and SP-D show saccharide selectivity, SP-A preferentially binds to mannose over glucose (Jakel et al., 2013). This suggests it would preferentially bind to *M. tuberculosis* capsular mannans and Man-AMs over capsular α-glucans. Whereas SP-D preferentially binds to maltose but shows an equal but less potent binding preference to glucose and mannose (Jakel et al., 2013) suggesting it interacts with all *M. tuberculosis* capsular polysaccharide components, mannans, α-glucans and Man-AMs, with similar affinity. Surprisingly, ficolin-3 does not bind to Man-LAM but instead to the secreted mycobacterial protein antigen 85 complex (Świerzko et al., 2016). Uptake of SP-A opsonised *M. tuberculosis* shows a decrease in the expression of reactive nitrogen intermediates (RNIs) (Pasula et al., 1997) whereas SP-D opsonisation of *M. tuberculosis* inhibits uptake by macrophages and independently causes agglutination (Ferguson et al., 2002). Incubation of *M. tuberculosis* with sub-agglutinating concentrations of SP-D reduces the adherence of bacteria to macrophages by 62.7% (Ferguson et al., 2002, 1999). Trying to piece together the role of alveolus resident soluble PRRs interacting *M.*

*tuberculosis* is further complicated by observation that SP-A binds to complement protein C1q and prevents the formation of active C1 complexes (Watford et al., 2001). Ferguson *et al.* speculate that exclusion of *M. tuberculosis* from their intracellular niche by SP-D may be a protective response. Notably, SP-A levels are increased in HIV-infected patients: Bronchoalveolar lavages of HIV-infected individuals with corresponding raised SP-A levels led to a 3-fold increase in *M. tuberculosis* attachment to alveolar macrophages compared control non-HIV infected individuals (Downing et al., 1995). Tsolaki suggests the relative levels of SP-A and SP-D may correlate with risk of infection (Tsolaki, 2009). The effect of bacterial agglutination on *M. tuberculosis* pathogenesis is unknown but is thought to aid mucociliary clearance (Ferguson et al., 2002). Notably SP-A and SP-D were both found to be dispensable in the immune control of tuberculosis in mice (Lemos et al., 2011). This may be because there is redundancy in the mechanisms *M. tuberculosis* utilises to enter cells as it can gain access to phagocytes via PRRs expressed on their cell surface regardless of prior opsonisation (Hossain and Norazmi, 2013).

Many sPRRs such as C1q and MBL are initiators of the complement cascade, which is a major mechanism *M. tuberculosis* utilises to gain access to its intracellular niche. The complement system also regulates inflammation and can directly kill some Gram negative bacteria through the deposition of the C5b-9 membrane attack complex which forms pores on the bacterial membrane. The cascade is triggered by multiple pathways and converges on deposition of C3b, which is quickly degraded to iC3b (**Figure 1.6.1**) (Murphy, 2012). Complement deposition onto *M. tuberculosis* complex can be initiated through opsonisation via antibodies or direct binding of C1q, (the classical pathway) (Carroll et al., 2009), via the lectin pathway activators, MBL and ficolins (Bartlomiejczyk et al., 2014; Hoppe et al., 1997; Luo et al., 2013) or the positive feedback loop of C3b deposition by the alternative pathway

(Schlesinger et al., 1990). Furthermore, *M. tuberculosis* forms a C3 convertase by recruiting C2a providing another mechanism of opsonisation (Schorey et al., 1997).

During the establishment of infection, before the recruitment of systemic lectins such as MBL (Fidler et al., 2009), opsonisation via resident lectins such as C1q (in the absence of SP-A interactions) and ficolin-3 may trigger the complement cascade. Although complement activation has not been shown to lead to direct killing of mycobacteria, it has been implicated in bacterial control through the release of C5a anaphylatoxin in mice (Actor et al., 2001). Additionally, complement activation has been shown to be increased in tuberculosis patients (Senbagavalli et al., 2009).

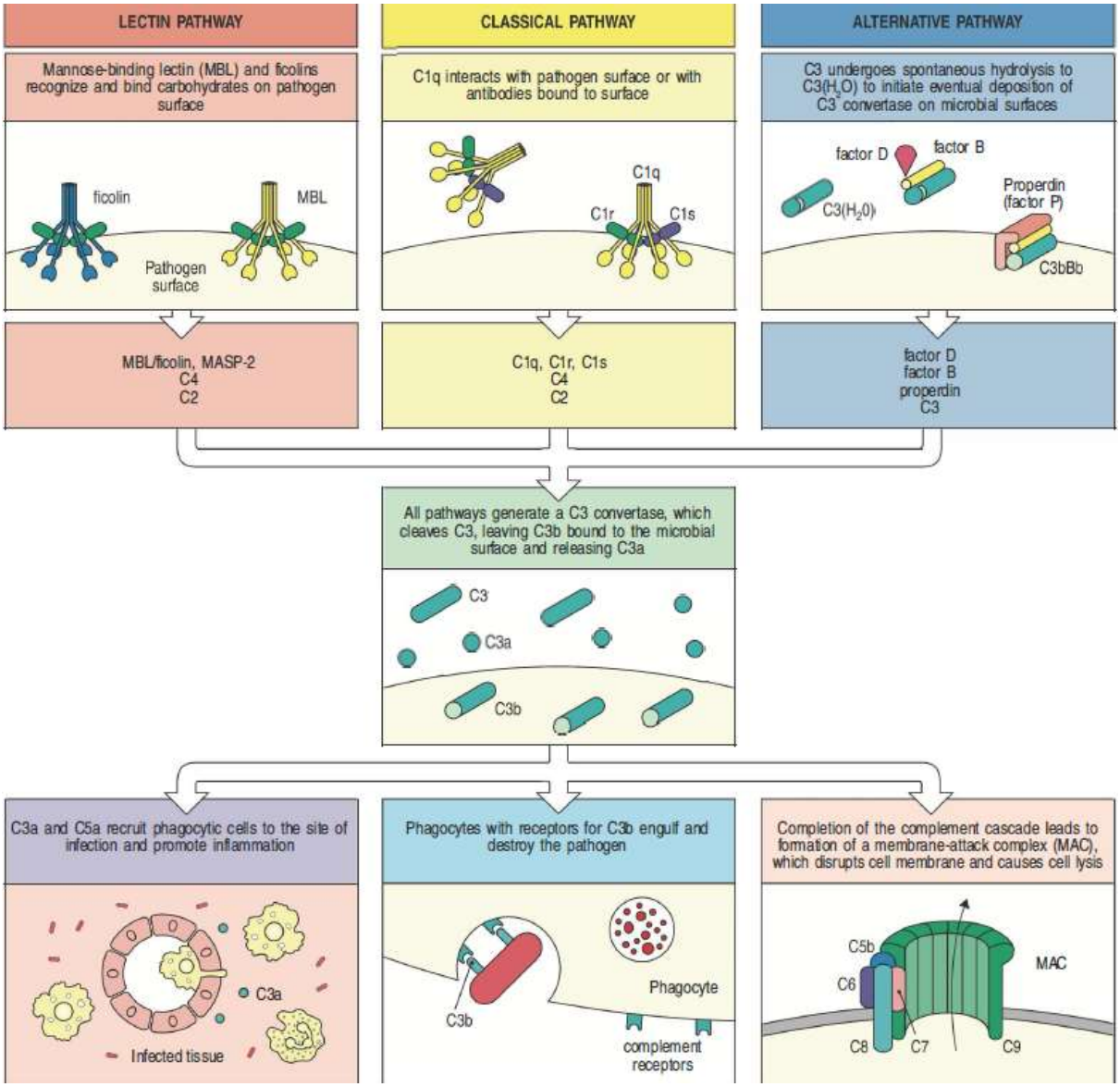


**Figure 1.6.1:** The complement system. Adapted from Murphy, (2012), Copyright © 2012 by Garland Science, Taylor & Francis Group, LLC. Used by permission of W. W. Norton & Company, Inc. All pathways converge on the generation of a C3 convertase and the deposition of C3b on the surface of a pathogen. This can be triggered by lectin pathway activators (complement activating collectins and ficolins), classical pathway activation through antibodies or the direct binding of C1q, or the spontaneous hydrolysis of C3 and generation of a fluid phase C3 convertase through the alternative pathway. The alternative pathway also amplifies C3b deposition by all pathways. Pathogenic mycobacteria also recruit C2a to their surface to form a C3 convertase and trigger C3b deposition (not shown) (Schorey et al., 1997). The effector functions of the complement pathway include the production of inflammatory modulators C3a and C5a, opsonisation and uptake of pathogens by phagocytes, and the formation of a membrane attack complex (a pore on the pathogen surface) which has been shown to be ineffective at killing Gram positive bacteria but may have other roles specific to certain pathogens still to be elucidated (Berends et al., 2013).

## 1.7 Part IV Phagocytosis

PRRs expressed on the cell surface of phagocytes include complement receptors (CR), toll-like receptors (TLRs), C-type lectin receptors such as dendritic cell-specific intercellular adhesion molecule-3-grabbing non-integrin (DC-SIGN), mannose receptors (MR) and Mincle (Kleinnijenhuis et al., 2011; Lang, 2013). PRR-PAMP binding between pathogens and immune cells usually triggers cytokine/chemokine production and/or phagocytosis followed by phagosome-lysosome fusion and bacterial killing. This process is subverted by *M. tuberculosis* bacteria, which are able to exploit uptake mechanisms and inhibit phagosome maturation to turn immune cells into a benign replicative niche.

It is thought the complement receptor CR3 can bind *M. tuberculosis* directly via its β-glucan lectin site interacting with *M. tuberculosis* capsular polysaccharides (Cywes et al., 1997). Or after deposition of complement proteins, which covalently bind to the surface of *M. tuberculosis* (Schlesinger et al., 1990). Complement receptor 3 (CR3), CR4 and to a lesser extent CR1 are capable of inducing complement-opsonised *M. tuberculosis* phagocytosis. It was shown using CR-specific antibodies and acid-fast staining that CR3 and CR1 are the primary CRs for *M. tuberculosis* uptake by monocyte-derived macrophages (Schlesinger et al., 1990) whereas CR4 was the primary CR in alveolar macrophages (Hirsch et al., 1994). Schlesinger *et al.* also used monoclonal antibodies (mAbs) against monocyte receptor antigens and showed that mAb against CR1 inhibited bacterial adherence by 40%. A combination of two mAbs against CR3, which targeted distinct epitopes, inhibited adherence by 81%. When these antibodies were used in combination with anti-CR1 it resulted in no greater inhibition. Schlesinger *et al.* used EDTA, which inhibits the classical and alternative complement pathways, and EGTA and $MgCl_2$, which inhibits only the classical pathway, to show that C3b can be fixed to *M. tuberculosis* by the alternative pathway (Schlesinger et al., 1990). Complement-opsonised uptake via CR3 prevents $Ca^{2+}$ increase and inhibits

phagosome lysosome fusion (Malik et al., 2000). Notably C3 deficient mice have been shown to have comparable bacterial burdens, granuloma formation and survival patterns to wild type mice suggesting *M. tuberculosis* is able to enter host cells via other receptors to establish infection (Hu et al., 2000).

TLR2 recognises mycobacterial components including Man-LAM, PIMs, LM and TDM (Bowdish et al., 2009; Pitarque et al., 2008) TLR4 recognises mycobacterial proteins such as heat shock protein 65 (Bulut et al., 2005). They form as heterodimers TLR2/TLR1, TLR2/6 and homodimers TLR2/2 and TLR4/4 on the plasma membrane of phagocytes (Saraav et al., 2014). While TLRs do not directly induce phagocytosis they are associated with the release of proinflammatory cytokines and chemokines as well as increased membrane ruffling and adhesion which can result in nonspecific phagocytosis (Underhill and Goodridge, 2012)

Mannose receptors (MRs) play a role in phagocytosis of only virulent strains of *M.* tuberculosis and directly recognises mannose residues such as those present in Man-LAM (Schlesinger, 1993). MRs are highly expressed in mouse alveolar macrophages (Hussell and Bell, 2014). Uptake via MR due to direct binding to Man-LAM directs *M. tuberculosis* to a phagosomal compartment with limited fusion to lysosomes (Kang et al., 2005). Hence, the intracellular niche provided through uptake via both CRs and MRs provides a safe haven for *M. tuberculosis* to replicate and persist.

Mincle and DC-SIGN have been shown to bind to mycobacterial TDM and Man-LAM. respectively (Geijtenbeek et al., 2002; Lang, 2013). DC-SIGN is expressed on both macrophages and dendritic cells (Tailleux et al., 2005). Uptake of *M. tuberculosis* via DC-SIGN induces IL-10 expression and prevents dendritic cell maturation (Geijtenbeek et al., 2002). Mincle deficient macrophages show impaired production of proinflammatory

cytokines after stimulation with *M. bovis* BCG and TDM (Behler et al., 2012; Schoenen et al., 2010).

Once inside macrophages, *M. tuberculosis* prevents phagosome-lysosome fusion through the action of immunomodulatory lipids and lipoglycans (Mishra et al., 2011). PIMs interfere with phagosome maturation arrest by stimulating Rab5 GTPase to enhance fusion between phagosomes and early endosomes, and involves inducing the acquisition of endosomal SNARE protein syntaxin-4 and the transferrin receptor (Fratti et al., 2003; Vergne et al., 2004a, 2004b). Through this process *M. tuberculosis* gains access to nutrients necessary for mycobacteria residing in phagosomal compartments (Kelley and Schorey, 2003; Vergne et al., 2004b). LM is recognised by TLR2 leading to the induction IL-12 and apoptosis, Man-LAM does not induce this response (Dao et al., 2004). Man-LAM inhibits cytosolic $Ca^{2+}$ increase during phagocytosis by excluding EEA1 from the early endosome, as shown in experiment using Man-LAM-coated beads, although the exact mechanism is not known (Fratti et al., 2001; Mishra et al., 2011). LAM is known to accumulate in lipid rafts in human macrophages via its glycosylphosphatidylinositol anchor and this coincides with reduced phagosome maturation (Welin et al., 2008).

A recent paper used mCherry labelled *M. tuberculosis* bacteria and time-lapse confocal microscopy to investigate the importance of mycobacterial aggregation on the cellular fate of the bacteria after phagocytosis. They found internalisation of large aggregates caused macrophage necrosis and *M. tuberculosis* replication, leading to a positive feedback loop of increasing macrophage cell death and increasing aggregate size (Mahamed et al., 2017). Aggregates, clumps or flocs in microbiology are interchangeable descriptions of a mass of bacteria that are often stuck together via a self-secreted matrix i.e. biofilms. Hence, if a single *M. tuberculosis* bacterium enters an alveolar macrophage, it prevents phagosome-lysosome fusion and is able to replicate and produce EPS. As the intracellular biofilm grows and

effectors of disease are secreted, a threshold is reached at which point the infected macrophage undergoes necrosis. The biofilm can then continue to grow extracellularly even more rapidly in the nutrient rich cellular debris until another phagocytosis event.

The mechanism by which *M. tuberculosis* aggregates triggers necrosis of infected macrophages is an area currently being studied but is likely to involve active secretion of mycobacterial effectors via the ESX-1 secretion system. For example, ESAT-6 mediates escape from the phagosome into the cytosol (Houben et al., 2012) and can trigger necrosis (Welin et al., 2011).

## 1.8 Part IV Granuloma formation

Either via taxis of infected macrophages across the lung epithelium or direct infection of lung epithelial cells, *M. tuberculosis* enters the parenchyma where additional macrophages aggregate (Pai et al., 2016). Some macrophages gradually transform into lipid saturated foam cells, epithelioid cells or fuse into multinucleated giant cells. The concurrent release of cytokines and chemokines draws neutrophils, dendritic cells, natural killer (NK) cells as well as activated T and B cells after the onset of adaptive immunity (Ramakrishnan, 2012). These events culminate in the formation of a tuberculosis granuloma, a distinctive feature in tuberculosis disease (**Figure 1.8.1**). Tuberculosis granulomas are heterogeneous in nature and are not all associated with disease progression. Early granuloams are non-necrotizing and can heal through calcification or progress into necrotic granulomas associated with high bacilliary load in their central caseous necrosis. The immune cell granuloma becomes surrounded by a fibrotic rim of fibroblasts, collagen and interspersed immune cells (Lenaerts et al., 2015).

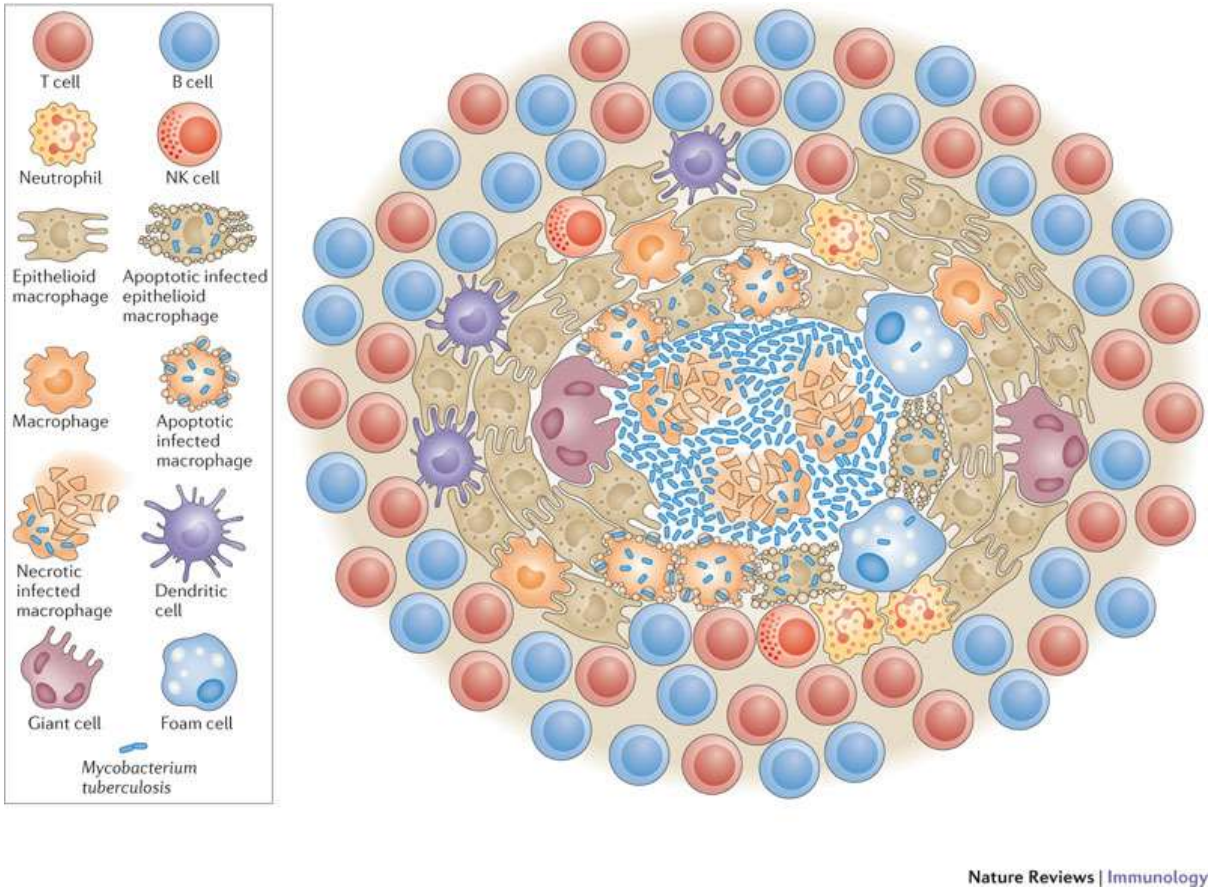


**Figure 1.8.1**: The tuberculosis caseating granuloma. Adapted from Ramakrishnan, 2012 (permission to reuse via Springer Nature Licence number 4274221181184). From the outside inwards; activated T and B cells accumulate around the peripheries of the granuloma after the onset on adaptive immunity 14 – 17 day after exposure (O'Garra et al., 2013). The bulk of the granuloma is comprised of epithelioid macrophages with interspersed NK cells, dendritic cells and neutrophils. Towards the inner-rim of the granuloma, some macrophages have transformed into multinucleated giant cells and foam cells. *M. tuberculosis* is prevalent in the central area of caseous necrosis and its periphery, where aggregates infect host cells (Irwin et al., 2015).

## 1.9 Part V Adaptive immunity and latency

In order to initiate adaptive immunity to tuberculosis, *M. tuberculosis* infected dendritic cells and monocytes migrate from early forming granulomas to the pulmonary lymph nodes for T cell priming (Pai et al., 2016). *M. tuberculosis* protein and lipid antigens are loaded onto the surface of antigen presenting cells via MHC and CD1 expression respectively (Lopez-Marin, 2012). Subsequently activated $CD4^+$ T cells travel back to the site of infection and secrete cytokine IFN-γ to mediate mycobacterial killing mechanisms in phagocytes such as the production of reactive oxygen and nitrogen species to control and contain the infection (O'Garra et al., 2013).

However, the induction of a strong $CD4^+$ T cell response that controls the infection (often indefinitely) yet fails to eradicate all the bacteria may be central to the pathogen's success. A landmark study has shown *M. tuberculosis* T cell epitopes are hyperconserved (Comas et al., 2010). T cells are mainly primed to epitopes on secreted proteins such as the immunodominant antigens CFP10 and Ag85B and hence T-cell responses to these antigens are dependent on their secretion (Woodworth et al., 2008). This enables *M. tuberculosis* to exert some control over $CD4^+$ T cell responses through the controlled expression and secretion of these 'immunological decoys' (Baena and Porcelli, 2009; Rogerson et al., 2006). There is not an evolutionary pressure for *M. tuberculosis* to evade the activation of a T-cell response because secreted antigens induce T-cell responses that are incapable of completely eradicating *M. tuberculosis* (Baena and Porcelli, 2009). Potent T-cell activation may also benefit *M. tuberculosis* by contributing to the pathology required for *M. tuberculosis* transmission; via a chronic proinflammatory response which leads to tissue damage, possibly driven by the upregulation of matrix metalloproteinases, leading to cavity formation (Behr, 2013; Comas et al., 2010; Elkington et al., 2011).

However in the vast majority of cases, the onset of adaptive immunity triggers a prolonged and often permanent period of latent disease where the infected individual is no longer infectious. 80-95% of latently infected individuals will never progress to post-primary tuberculosis and the remaining 5-20% of the infected population will develop active TB, most likely around 2 to 5 years after the initial infection (Baddeley et al., 2013). Despite the low likelihood of an individual progressing to the contagious phase of TB, the reservoir of latently infected individuals worldwide is colossal with an estimated third of the world's population estimated to be latently infected with TB (Russell et al., 2010). Latent TB is defined by the immune response directed against *M. tuberculosis* rather than directly observing the presence of the bacteria. Therefore the latently infected population may include exposed individuals who have cleared the infection through an effective innate and/or adaptive immune response but remain tuberculin skin test positive ($TST^+$) and IFN-γ release assay positive ($IGRA^+$), because their adaptive immune response remains detectable (O'Garra et al., 2013). Further confounding the identification of latent TB is the fact that a false positive TST can sometimes occur in BCG vaccinated individuals, of which there are 3 billion (Andersen and Doherty, 2005) and through exposure to environmental non-tuberculosis mycobacteria (Horsburgh, 2004; Van Rhijn et al., 2009). Nevertheless, failed immune facilitated suppression of true latent *M. tuberculosis* infection leads to the reactivation of tuberculosis, also known as post-primary tuberculosis (Hunter, 2011).

### 1.10 Part VI Cavitation

In immunocompetent individuals, the most prominent signature of post-primary tuberculosis is the development of a pulmonary cavities and this is seen in 40 – 87% of pulmonary TB cases (Saeed, 2012). There are two competing theories of how *M. tuberculosis* cavities arise, one is based on animal models and argues that cavities arise from the liquefaction of a

caseating granuloma (Dannenberg, 1994) and the other, based on human pathology states that cavities arise independent of granulomas due to a tuberculosis pneumonia (Hunter, 2016). Cavities form when necrotic lung fragments are coughed out. As cavities mature they are characterised by a layer of caseous necrotic material over a fibrotic layer. The surface of the cavities provide the perfect growth conditions for the extensive extracellular *M. tuberculosis* biofilm formation over there surface of the cavity (**Figure 1.10.1**) (Hunter, 2011). *M. tuberculosis* cavity biofilms produce more TDM compared to extrapulmonary sites and resemble *in vitro* pellicle cultures (Arora et al., 2016; Hunter, 2016; Robert L. Hunter et al., 2006). Early studies from the 1940s to 1960 often described the extensive bacterial growth in open cavities, where '*the soft necrotic layer and abundant oxygen supply provide an excellent culture medium for tubercle bacilli*' (Canetti, 1965). One historical report, prior even to the discovery of the bacillus itself, describe the lumen of tuberculosis cavities as coated in an expansive soft semi-transparent greyish-white '*membrane*' which can detach into sputum (Laennec and Forbes, 1821). Robert Hunter and colleagues have repeatedly published evidence that *M. tuberculosis* residing in cavities resemble *in vitro* pellicle biofims (Arora et al., 2016; Hunter, 2016, 2011; Hunter et al., 2014; Robert L. Hunter et al., 2006).

Despite catastrophic lung damage during cavity formation, infected immunocompetent individuals with mature cavities can show remarkable constitution, able to remain mobile, relatively active with a persistent cough and thereby capable of spreading the disease for decades unless treated (Hunter, 2016). Since the majority of tuberculosis transmission occurs via infected individuals with cavities, and these cavities are likely to be associated with pellicle biofilm formation, it is plausible that the majority of expectorated *M. tuberculosis* bacteria are shed from biofilms. Hence biofilm phenotype *M. tuberculosis* bacteria may directly compete with the innate immune system of a newly infected host to establish

infection. This theory is the cornerstone of this thesis. Prior to presenting an outline of the primary aims of this thesis, it is appropriate to review the current literature regarding *M. tuberculosis* biofilm formation.

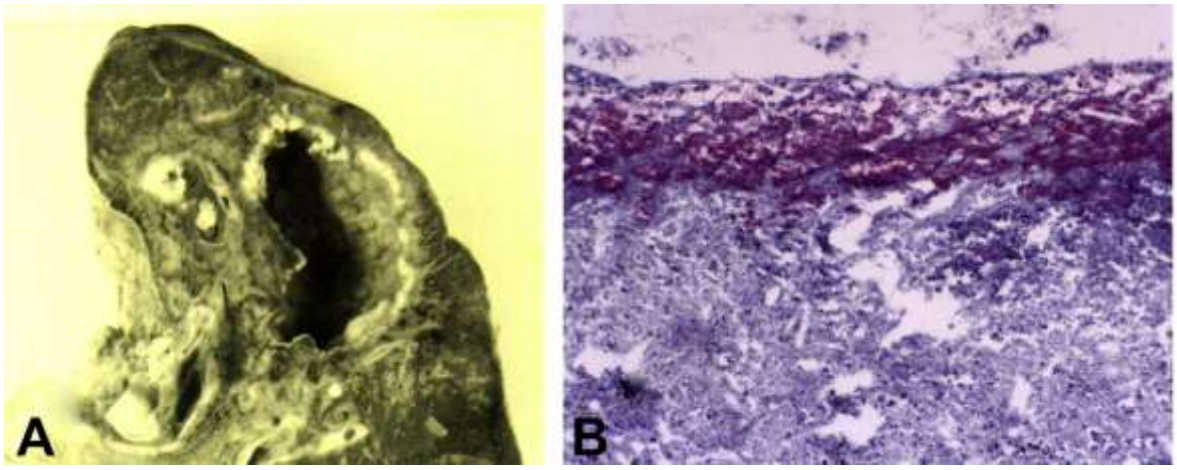


**Figure 1.10.1:** The tuberculosis cavity. Adapted from (Hunter, 2011) (Permission to reuse via Elsevier licence number 4274730590976). (A) A cavity from a largely asymptomatic tuberculosis patient who died of an unrelated illness. (B) 200x acid-fast stain with enormous numbers of *M. tuberculosis* bacteria at the cavity surface.

## 1.11 *M. tuberculosis* biofilm formation

Biofilms are surface-associated microbial communities surrounded by an extracellular polymeric substance (EPS) matrix (Hall-Stoodley and Stoodley, 2009). The exact composition of EPS varies between bacterial species but is thought to be primarily polysaccharides (Donlan, 2002). The extracellular polymeric substance (EPS) secreted by mycobacteria to form the biofilm matrix has yet to be fully characterised. In other bacteria that form single-species biofilm, the principle substance in EPS is composed of exopolysaccharides; alginate in *Pseudomaonas aeruginosa* biofilms and colanic acid in *Escherichia coli* biofilms (Watnick and Kolter, 2000). Scrutiny of mycobacterial genomes suggest that mycobacteria lack the capability for exopolysaccharide production, but instead may be held together by free mycolic acids (Ojha et al., 2005; Sochorová et al., 2014; Zambrano and Kolter, 2005). On the contrary, exocellular polysaccharides glucan and arabinomanannan and mannan are present in crude exocellular extracts of *M. tuberculosis* pellicles (biofilms) which have only traces of lipids (Lemassu and Daffé, 1994; Ortalo-Magné et al., 1995). Therefore, it is feasible that these polysaccharides also contribute to the mycobacterial EPS in addition to free mycolic acids (Ojha et al., 2008), and TDM (Robert Lee Hunter et al., 2006), secreted proteins and other lipids.

The classical definition of biofilms, whether mono or multispecies, includes surface attachment and a typical model of biofilm formation is shown in **Figure 1.11.1**, taken from Zoubos et al., (2012). Notably, while surface-attachment is often a key defining characteristic of microbial biofilms (Watnick and Kolter, 2000), host-pathogen *in vivo* studies show bacterial aggregates that appear to have grown uncoupled from attachment; such as mucoid-phenotype *Pseudomonas aeriginosa* clusters in sputum (a mixture of airway mucus, immune system factors , bacteria and bacterial products) in the cystic fibrosis lung (Yang et al., 2008).

This raises the notion that aggregation may not always require surface attachment. Indeed, *Staphylococcus aureus* clusters in joint-fluid aspirates may have derived from surface-attached biofilm shedding or grown as clusters in the fluid (Hall-Stoodley and Stoodley, 2009; Stoodley et al., 2008). Recently in comprehensive reviews of the role of biofilms in chronic infections, biofilms are defined as '*a coherent cluster of bacterial cells embedded in a matrix, which is more tolerant of most antimicrobials and host defences compared with planktonic bacterial cells*'(Bjarnsholt, 2013; Burmølle et al., 2010).

In addition to pellicle-type biofilm formation, aggregates of *M. tuberculosis* in animal model infections have been visualised. Both the guinea pig and C3HeB/FeJ mouse models of tuberculosis show human-like pathology. Aggregates of extracellular *M. tuberculosis* have been observed using acid fast staining of guinea pig model (Hoff et al., 2011; Lenaerts et al., 2007; Ryan et al., 2010). Also a more sensitive acid fast method using SYBR Gold nucleic acid stain has shown the existence of aggregates within foamy macrophages in the rim of caseous granulomas and in extracellular necrosis in the C3HeB/FeJ mouse infection model (Driver, 2014; Irwin et al., 2015). An *in vitro* macrophage infection model has suggested aggregates are more cytotoxic than multiple phagocytosis events of the same number of bacteria (Mahamed et al., 2017), suggesting aggregates are more than simply multiple bacteria in close proximity and are held together by an immunomodulatory EPS matrix.

There remains reluctance in the field to define any *M. tuberculosis* aggregates as biofilms. This may be due a tendency to regard *in vitro* clumps that occur in detergent-free shaken cultures as disorganised masses of cells, whereas biofilms must be surface associated and highly organised. Recently *M. tuberculosis* has been shown to gradually accumulate distinctive extracellular material during progression from exponential growth phase to a non-replicating persistent growth phase (NRP) with concurrent gradual depletion of Tween 80.

This material was visible by scanning electron microscopy (Bacon et al., 2014). It is argued in this thesis that all self-formed *M. tuberculosis* aggregates are biofilms. In defence of this assumption, here are two important points: Firstly, *in vitro* mycobacterial clumps grown in shaken cultures are not a mass of cells that can be dispersed by simple methods such as vortexing or pipetting. They require harsher methods to disperse such as the introduction of detergents into the medium (Ojha and Hatfull, 2012). This is due to the EPS that glues the bacteria together in the turbulent conditions of shaken cultures and is presumably a phenotypic adaptation to protect the mycobacterial cell wall from the shearing forces inside the flask. Secondly, in shaken cultures *M. tuberculosis* clumps are biofilms formed around the surface of pre-existing mycobacteria rather than the walls of the flask. There is no reason why a surface for biofilm establishment could not be other mycobacteria. After all, that is in essence how all biofilms continue to grow following establishment on any surface, building upon an existing framework of bacteria and EPS. The turbulent conditions inside a shaken flask are very different to the conditions present in static cultures during pellicle formation probably resulting in considerable differences in the amount of EPS secreted and its composition. Although the latter resembles *in vivo* cavity biofilms the former environment bears little relation to *in vivo* necrosis associated biofilms (Basaraba and Ojha, 2017), where EPS constituents may differ again. A biofilm is a biofilm regardless of whether it is intracellular e.g. an aggregate within a foamy macrophage (Irwin et al., 2015), or extracellular e.g. an aggregate in caseous necrosis (Lenaerts et al., 2007).

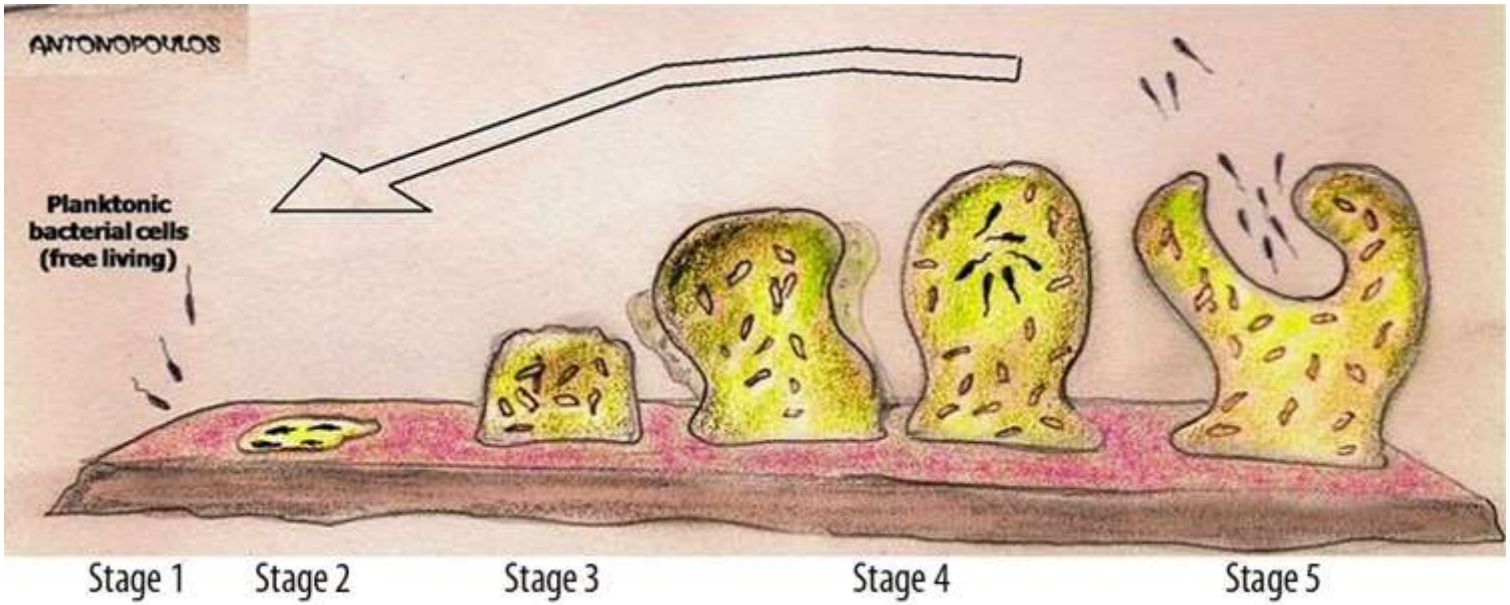


**Figure 1.11.1:** Biofilm formation. Adapted from (Zoubos et al., 2012) (Permission to reuse via Creative Commons Attribution License). Cartoon of the classic model of biofilm development. Stage 1: Planktonic bacteria attach to a surface. Stage 2: EPS production begins. Stage 3: The bacterial population becomes established and biofilm structure begins to develop. Stage 4: Growth continues until maturation of biofilm as a highly organised structure with oxygen/nutrient gradients and physical features such as air channels. Stage 5: Planktonic bacteria are released from the mature biofilm when environmental conditions become unfavourable. Note *M. tuberculosis* biofilms in cavities do not release flagellated bacteria. The biofilm can spread across the cavity surface via sliding motility and bacteria may be shed by the mechanical forces of human aspiration and expiration into the respiratory tract to transport the bacteria to a new host. In the case of *in-vitro* pellicle biofilms on the air-liquid interface, surface-association with settled liquid rather than solid-surface attachment allows for biofilm formation.

*In vitro M. tuberculosis* pellicle biofilms are surface associated, forming a confluent membrane across the air-liquid interface of the culture vessel with some growth up the sides and can easily be scraped off their associated surfaces. Pellicle biofilms grow in limited $O_2$, high $CO_2$ conditions and show retarded growth in low iron or low zinc medium (Ojha et al., 2008). In the same paper Ojha et al., show pellicle formation is genetically distinct from planktonic growth, as it requires gene Rv1013 (polyketide synthase pks16). In addition, the genes Rv2454c and Rv2455c, which encode 2-oxoglutarate dehydrogenase enzymes, are required for mature biofilm formation. Triacylglycerides in the cell wall are reduced in *M. tuberculosis* pellicle biofilms, possibly being used as an intracellular carbon source. Pellicles have increased free mycolic acids compared to planktonic cultures. Synthesis of free mycolic acids has been shown to be due to cleavage of TDM in *M. smegmatis* by a specific serine esterase also present in *M. tuberculosis* (Ojha et al., 2010, 2008).

A genetic screen revealed 12 genes that result in biofilm formation deficiency after transposon insertion including, *pks1,* a component of the *pks15/1* gene required for the production of phenolic glycolipid in some strains (not H37Rv) (Pang et al., 2012). Pellicle formation (in the conditions tested) was shown to not be a universal trait among clinical isolates. From a sample of 15 clinical isolates, 3 strains formed mature pellicles, 9 strains partially formed pellicles and 3 strains failed to produce any pellicle. The pellicles were grown in Sauton's medium-filled wells of microplates wrapped in parafilm and incubated at 37$^{o}$C for 5 weeks without shaking. Laboratory strain H37Rv formed the thickest pellicle, and importantly pellicle formation was seen in all four clades suggesting pellicle biofilm formation is not specific to any particular lineage (Pang et al., 2012).

Pellicle formation can occur without cording, a specific form of organised growth in mycobacteria where the mycobacteria are aligned pole-to-pole in linear strands, as a cording mutant has been shown to still produce a pellicle with a similar morphology to wildtype *M.*

*tuberculosis* H37Rv (Sambandan et al., 2013). Through the production of mutants deficient in the production of either α, methoxy and keto or keto only mycolic acids, keto mycolic acids have been shown to be required for pellicle formation despite the greater accumulation of free α and methoxy mycolic acids present in pellicles compared to free keto mycolic acids (Sambandan et al., 2013). *M. tuberculosis* produces highly aggregative curli pili that are antigenic and bind to extracellular matrix protein laminin *in vitro* (Alteri, 2005; Alteri et al., 2007). The *mtp* curli pili gene is not upregulated during biofilm formation, although *mtp* mutants show a 68.43% reduction in biofilm biomass suggesting curli pili contribute to cell-cell contact and surface association during biofilm formation (Ramsugit et al., 2013). Furthermore putative MtrAB two component system accessory lipoprotein LpqB, which has a homologue in *M. tuberculosis*, has been shown to be required for mature biofilm formation in *M. smegmatis,* a non-pathogenic species (Nguyen et al., 2010).

A recent study of pellicle formation in *M. smegmatis* used scanning electron microscopy and proteomics to investigate mycobacterial changes between the early and late stages of pellicle development. The authors found that the cell size of *M. smegmatis* significantly decreased (2 fold in length and 25% in width) over time. Proteins expressed highly during pellicle formation include several proteins involved in cell-wall biosynthesis and modifications (Sochorová et al., 2014). GroEL1 showed highest expression during the transition from floating flocks to a compact pellicle (Sochorová et al., 2014). GroEL1, a chaperone protein thought to be involved in the early stages of TMM transport prior to free mycolate production via synthesis and cleavage of TDM (Ojha et al., 2010) has been shown to be required for mycobacterial biofilm formation and is involved in the regulation of the synthesis of mycolic acids (Ojha et al., 2005). Other proteins upregulated during pellicle formation include antigen 85A a secreted mycolyl transferase involved in the addition of mycolic acids to arabinogalactan and TDM (Huygen, 2014) and two proteins involved in the synthesis of

inositol; inositol-3-phosphate synthase and methylmalonate-semialdehyde dehydrogenase (Sochorová et al., 2014). Inositol is a monosaccharide incorporated into lipoglycans, PIMs, LM and LAM (Mishra et al., 2011).

Kerns et al., (2014 ) used proteomics and western blots to identify 9 *M. tuberculosis* H37Ra antigenic and pellicle-specific proteins. These proteins were consistently expressed since they were isolated from 3 week, 5 week and 7 week old pellicle cultures but not from control shaken cultures in the same medium. The western blots were incubated with 60-day old low-dose *M. tuberculosis* H37Rv-infected guinea pig serum and probed with horseradish peroxidase-labelled anti-Guinea Pig IgG to identify antigenic proteins. Proteins were identified by matrix-assisted laser desorption ionization time-of-flight/time-of-flight (MALDI-TOF/TOF) mass spectrometry (Kerns et al., 2014). Some interesting pellicle specific proteins were identified in this study. The signal transducer FhaA is believed to repress peptidoglycan synthesis following activation by a peptidoglycan sensor (Gee et al., 2012). This could be a response to nutrient starvation (Kerns et al., 2014). CeoB is involved in potassium uptake (Cholo et al., 2006) and has been shown to restore isoniazid resistance when complementing an *E. coli oxyR* mutant (Chen and Bishai, 1998). This may therefore help explain the phenotypic isoniazid resistance by *M. tuberculosis* biofilms, although overexpression of *ceoBC* gene pair in *M. bovis* BCG had no effect on isoniazid susceptibility (Chen and Bishai, 1998). Rv3519 has been suggested as a putative acetoacetate decarboxylase which could be used by *M. tuberculosis* to obtain acetone from acetoacetate (Kerns et al., 2014; May et al., 2013). *M. tuberculosis* could utilise acetone as a carbon source as seen in *M. smegmatis* (Lukins and Foster, 1963) and more intriguingly has been speculated to perhaps be a diffusible signalling model (Kerns et al., 2014). The case for a mycobacterial acetone-quorum sensing mechanism is made stronger by the discovery that MimR is an

acetone responsive transcriptional regulator in *M. smegmatis* (Furuya et al., 2011; Kotani et al., 2007).

Bacon et al., (2014) has shown infection of guinea pigs with NRP phase *M. tuberculosis* H37Rv, which forms aggregate biofilms with distinct EPS, results in reduced pathology and delayed onset of disease. Two studies have linked mycobacterial biofilm formation with *in vivo* persistence using *M. bovis* (Chandra et al., 2010; Flores-Valdez et al., 2015). In the first study, a mutant for the cell wall and culture medium associated glutamate synthetase, encoded by the gene *glnA-1* had reduced levels of intracellular glutamate and abolished extracellular levels. The mutant had a 50% reduction in biofilm formation and did not persist as long as the wild type in BALB/c mice (Chandra et al., 2010). Flores-Valdez and colleagues showed the importance of bis-(3′-5′)-cyclic-dimeric guanosine monophosphate (c-di-GMP) in regulating biofilm formation in mycobacteria for the first time. c-di-GMP has been shown to regulate between planktonic and biofilm phenotypes in many bacteria (Hengge, 2009). *M. tuberculosis* has two genes involved in the synthesis and regulation of c-di-GMP. *Rv1354c* encodes a protein with diguanylate cyclase and phosphodiesterase domains while *Rv1357c* encodes a protein with a phosphodiesterase domain only (Gupta et al., 2010) Flores-Valdez et al., deleted the phosphodiesterase gene *Rv1357c* from *M. bovis* BCG, required for the degradation of c-di-GMP. This enhanced pellicle biofilm formation, as did supplementation of growth medium with c-di-GMP. Notably the authors were unable to detect c-di-GMP levels in *M. bovis* BCG directly. The mutant also displayed resistance to *in vitro* nitrosative stress and persisted in infected BALB/c mice for longer compared to the wild type, measured by viable counts. Interestingly a different study where deletion of the same gene in *M. tuberculosis* H37Rv was performed showed that the mutant was less able to persist in C57BL/6 mice after 10 weeks (Hong et al., 2013). Notably no assessment of biofilm formation was performed and the mutant was not complemented in the mouse infection

experiment. It would be interesting to see what effect on biofilm formation deletion of *Rv1357c* has in H37Rv and whether the reduced pathogenicity is consistent with other animal models with more human-like pathology. Flores-Valdez and colleagues have suggested since *M. tuberculosis* actively replicates and increases its burden in the host unlike *M. bovis* BCG, c-di-GMP may have different roles in two strains. *M. bovis* BCGΔ*Rv1357c* is no more virulent than parental *M. bovis* BCG in nude mice and has been tested in BALB/c mice as a vaccine (Pedroza-Roldán et al., 2016). It was found to perform better than BCG after *M. tuberculosis* H37Rv challenge, with increased local IFNγ producing T cells, reduced tissue damage, and lower bacterial burden and even increased the threshold of corticosterone dependent immunosuppression required for disease progression of chronically infected mice.

This study highlights how improved understanding of *M. tuberculosis* biofilm formation and its effect on host immune responses can be utilised to develop vaccines with greater efficacy than BCG (Pedroza-Roldán et al., 2016). Future studies could also identify novel pathogen or host targets for adjuvant therapies, which inhibit biofilm formation/EPS production with the aim of enhanced cell-mediated clearance and antibiotic activity. Such an approach could reduce the lengthy current treatment regimen for tuberculosis.

## 1.12 Thesis aims

*M. tuberculosis* biofilm formation has only recently been acknowledged as a fundamental aspect of its growth and its importance in pathogenesis is still being researched. In this thesis *in vitro* pellicle *M. tuberculosis* biofilms are used due to their resemblance of *in vivo M. tuberculosis* biofilms in cavities (Arora et al., 2016; Hunter, 2016). Comparisons are made between these biofilms and planktonic cultures. Planktonic *M. tuberculosis* cultures refer to exponential phase shaken cultures, grown using the same medium as used for biofilm culture. Despite not being single-cell dispersed, these cultures are still referred to as planktonic similarly to another study (Kerns et al., 2014).

Primary aims for this thesis are as follows:

- Measure growth and viability of *M. tuberculosis* biofilms over time (2.3).
- Define exponential phase planktonic *M. tuberculosis* (2.3).
- Find evidence for *M. tuberculosis* pellicle biofilm EPS from growth data and microscopy (2.3 and 2.4).
- Identify changes to cell wall and EPS carbohydrates/lipoglycans and lipids specific to *M. tuberculosis* pellicle biofilms (3.3 and 3.4).
- Assess whether changes in carbohydrates/lipoglycans extracts and capsule extracts specific to *M. tuberculosis* pellicle biofilms alter innate human cytokine and chemokine responses in a whole blood stimulation assay and multiplex analysis (4.3 and 4.6)
- Optimise the dispersion of planktonic and biofilm phenotype *M. tuberculosis* cultures for flow cytometry analysis (5.3).
- Compare live biofilm and planktonic cells induction of complement activation (5.4, 5.5 and 5.6).

- Investigate if carbohydrate changes specific for *M. tuberculosis* pellicle biofilms affect human complement activation using ELISAs (5.7).

The discussion sections of each chapter will be limited to technical evaluations of the methods applied with further discussion on key aspects of the results in the context of published literature on tuberculosis pathogenesis and the innate immune response presented in chapter 6.

# 2 OPTIMISATION OF BIOFILM AND PLANKTONIC *M. TUBERCULOSIS* CULTURE

## 2.1 Introduction

The classical definition of 'planktonic' phenotype is a transient, motile life stage to transport the bacterium to a favourable environment on which to attach and form a biofilm (Watnick and Kolter, 2000). There are multiple mechanisms of bacterial motility including swimming by use of flagellum, twitching and gliding (Madigan et al., 2010). Mycobacteria are nonflagellated and were thought to be nonmotile, although fast growing *M. smegmatis* and slow growing *M. avium* have been shown to exhibit sliding motility on solid surfaces (Martínez et al., 1999) and it is likely that *M. tuberculosis* shares this characteristic. Sliding motility is defined as surface translocation of cells over a substrate, often assisted by EPS to reduce friction, and caused by the outward force of a growing culture (Henrichsen, 1972). Since mycobacterial sliding is a passive process, moving a population of bacteria as a single unit, the planktonic classical definition is not appropriate. Rather, due to the bacteria's reliance on growth, sliding motility could be regarded a mechanism for directional growth during biofilm expansion.

Mycobacterial cell division is different to many bacteria as the division is asymmetrical (Kieser and Rubin, 2014). The suggested advantage of this form of growth is that the host environment is heterogeneous and can also be in a state of flux meaning differentially sized cells may have specific survival advantages dependent on their environment (Kieser and Rubin, 2014). Asymmetrical cell division is due to faster growth at the old pole relative to the new pole after cytokinesis (Santi et al., 2013). Furthermore, asymmetrical cell division coupled with sliding motility may provide a simple mechanism of directional growth towards

a favourable environment. Mycobacterial cording could be a manifestation of this process (Julián et al., 2010).

The term planktonic *M. tuberculosis* has previously been used to describe *in vitro* cultures grown in shaking flasks with or without Tween-80 detergent (Kerns et al., 2014; Ojha et al., 2008). Likewise, in this project the term 'planktonic' is defined as *M. tuberculosis* grown in shaking, vented flasks without Tween-80 and using the same medium as used for pellicle growth. Under these conditions, *M. tuberculosis* forms macroscopic clumps, which are harvested during exponential growth. In the presence of Tween-80 the bacteria are single-cell dispersed but the native capsule layer of each bacterium is shed into the medium. In the absence of Tween-80, the bacteria clump together and capsule shedding is less pronounced (Sani et al., 2010). The mycobacteria within clumps may have oxygen/nutrient gradients (Islam et al., 2012) and therefore a proportion of the population within the clump may not be exponentially growing. Effectively, mycobacterial clumps in shaking cultures are a type of biofilm in their own right. The use of the term planktonic bacteria is therefore a little misleading. For clarity, the terms planktonic and biofilm in this thesis are used to differentiate between younger exponentially growing shaking cultures and older mature pellicles respectively. This has been adopted by Kerns et al., (2014) in their study of *M. tuberculosis* biofilms.

## 2.2 Chapter 2 hypothesis

*M. tuberculosis* pellicle biofilms produce EPS and show organised morphology, which is distinct from exponential phase shaken planktonic cultures grown in the same detergent-free medium.

## 2.3 *M. tuberculosis* planktonic and biofilm culture

*M. tuberculosis* biofilms were cultured as described in methods section 7.1. Briefly, *M. tuberculosis* H37Rv was cultured in modified Sauton's medium, grown on 24-well plates (which for containment reasons were placed in an airtight container) and incubated for 5 weeks at 37$^{o}$C. In each of the wells, a thick hydrated yellowish pellicle biofilm formed. A photograph of a typical *M. tuberculosis* biofilms in a 24-well plate and a close-up of one of the wells is shown in **Figure 2.3.1**. Notably this biofilm culture was incubated for 6 weeks before harvesting instead of the typical 5 week incubation period. The pellicles did not dry out during incubation since humidity was maintained in a sealed box.

To assess the growth of *M. tuberculosis* biofilms, two independent cultures were used to inoculate a series 24-well plates individually sealed in boxes. Therefore, any one plate per time point contained two biological replicate *M. tuberculosis* cultures in x12 technical replicate wells each. This allowed sacrificial sampling without altering the aeration of other plates. To quantify the number of viable bacteria in a biofilm, the number of colony forming units (CFU) per gram of wet-weight biofilm was calculated at weekly intervals between the third and seventh week of culture (method 7.2). On day 0 the inoculum was calibrated to 0.05 $OD_{540\ nm}$ in PBS pH 7.4. Viable counts were performed following serial dilution in detergent-containing PBS to remove clumps to ensure accuracy. A viable count of $1.94 \times 10^{6} \pm 2.23 \times 10^{5}$ CFU mL$^{-1}$ was calculated. Prior to re-suspension in modified Sauton's medium, the inoculum was pelleted and the wet-weight pellet was weighed to determine the number of viable bacteria per gram (CFU g$^{-1}$). This was determined to be $4.92 \times 10^{8} \pm 2.83 \times 10^{8}$ CFU g$^{-1}$. On day 21 and subsequent sampling days, one plastic container was opened and the liquid medium in each well of the 24-well plate was removed from underneath the biofilm. x6 technical replicate wells of each independent culture were sampled and weighed before being dispersed using 1% Tween-80 to determine CFU g$^{-1}$ (**Figure 2.3.1c**) and the 12 remaining

wells were used for a crystal violet assay in the same fashion (**Figure 2.3.1d**) to quantify biomass (method 7.3). Regression analysis between weeks 3 and 5 showed a statistically significant downward trend in CFU $g^{-1}$ $R^2 = 0.9968$ P= 0.0358. Since CFU $g^{-1}$ essentially measures the density of bacteria within the biofilm, this result suggests that either there were an increasing proportion of dead or dormant bacteria between weeks 3 and 5 or an increasing proportion of biomass was attributable to EPS between weeks 3 and 5. The CFU $g^{-1}$ between weeks 5 and 7 appeared to plateau, which would not be expected if cell death was occurring as a death phase would result in a continuing drop in CFU $g^{-1}$. Likewise a plateau would not be expected if an ever increasing proportion of the population was entering a dormant and non-culturable phase due to exhaustion of one or more of the environmental factors required for growth. Therefore, the downward trend in CFU $g^{-1}$ between weeks 3 and 5 is indicative of an increasing proportion of EPS. This is supported by the time-series crystal violet assay which showed statistically significant positive trend towards increasing biomass between weeks 3 and 6, $R^2 = 0.9634$ P = 0.0185. Therefore, while the density viable bacteria decreases between weeks 3 and 5 and plateaus between weeks 5 - 7, the biomass of the biofilm increases between weeks 3 to 6. Together these data suggest that *M. tuberculosis* biofilms cultured by the method described above produce sufficient EPS between weeks 3 and 5 to lower the density of the bacterial population.

The inoculum was derived from Tween-80 containing chemostat culture (Bacon and Hatch, 2009), which harbours dispersed planktonic bacteria. This means most EPS is shed into the culture liquid. Prior to inoculation the culture was washed in PBS and pelleted. Therefore the viable count (CFU $g^{-1}$) of the inoculum represents a crude estimation of the density of *M. tuberculosis* bacteria in the absence of EPS. It is then possible to estimate the percentage of the biofilm that is EPS at each time-point by dividing the viable counts of the biofilm (at T3 – 7) by the viable count of planktonic bacteria (T0) (**Figure 2.3.1e**).

$$\% \text{ EPS} = \frac{\text{Viable count of biofilm (CFU g}^{-1}\text{)}}{\text{Viable count of planktonic inoculum (CFU g}^{-1}\text{)}} = \frac{\text{(Cells + EPS) g}^{-1}}{\text{Cells g}^{-1}}$$

These results suggest that during biofilm culture, significant pellicular EPS production does not occur until week 4 where it represents around 11% of the biofilm biomass. Between weeks 5 and 7 EPS represents consistently around 50% of the biofilm biomass.

Planktonic control culture medium was identical to the biofilm medium. In the absence of detergents, shaken cultures are clumpy. In addition, rather than use a control the same age as mature 5-week pellicle biofilms, it was decided that comparing biofilm phenotype bacteria to exponential phase shaking cultures would provide a more useful control to determine the specific immunological effects of pellicle biofilms. This is because a comparison of biofilms to healthy, exponential phase shaken cultures in the same medium is more typical of *M. tuberculosis* cultures routinely used in biochemical and immunological studies.

To identify the exponential phase of planktonic growth, viable counts of three biological replicate cultures were taken on day 0, 4, 10 and 14 (**Figure 2.3.1f**) (method 7.4). Each culture was inoculated at 0.05 $OD_{540\ nm}$, which equated to $1.69x10^6 \pm 5.52 \times 10^5$ CFU $mL^{-1}$. By day 4 this had risen slightly to $4.06x10^6 \pm 1.2x10^6$ CFU $mL^{-1}$ indicating a lag phase. After 10 days there was an increase in the number of viable bacteria consistent with exponential growth. The viable count reached $1.34x10^8 \pm 8.43x10^7$ CFU $mL^{-1}$. The final viable count taken on day 14 was $9.53x10^7 \pm 5.69x10^7$ CFU $mL^{-1}$. This was lower than expected but still may be consistent with stationary phase. For consistent reproducible planktonic controls, mid-exponential phase bacilli were used for comparison with mature 5 week *M. tuberculosis* pellicle biofilms. Therefore, it was decided that planktonic cultures would be harvested on day 7. The generation time of *M. tuberculosis* in modified Sauton's medium during exponential phase was calculated to be approximately 28.7 hours.

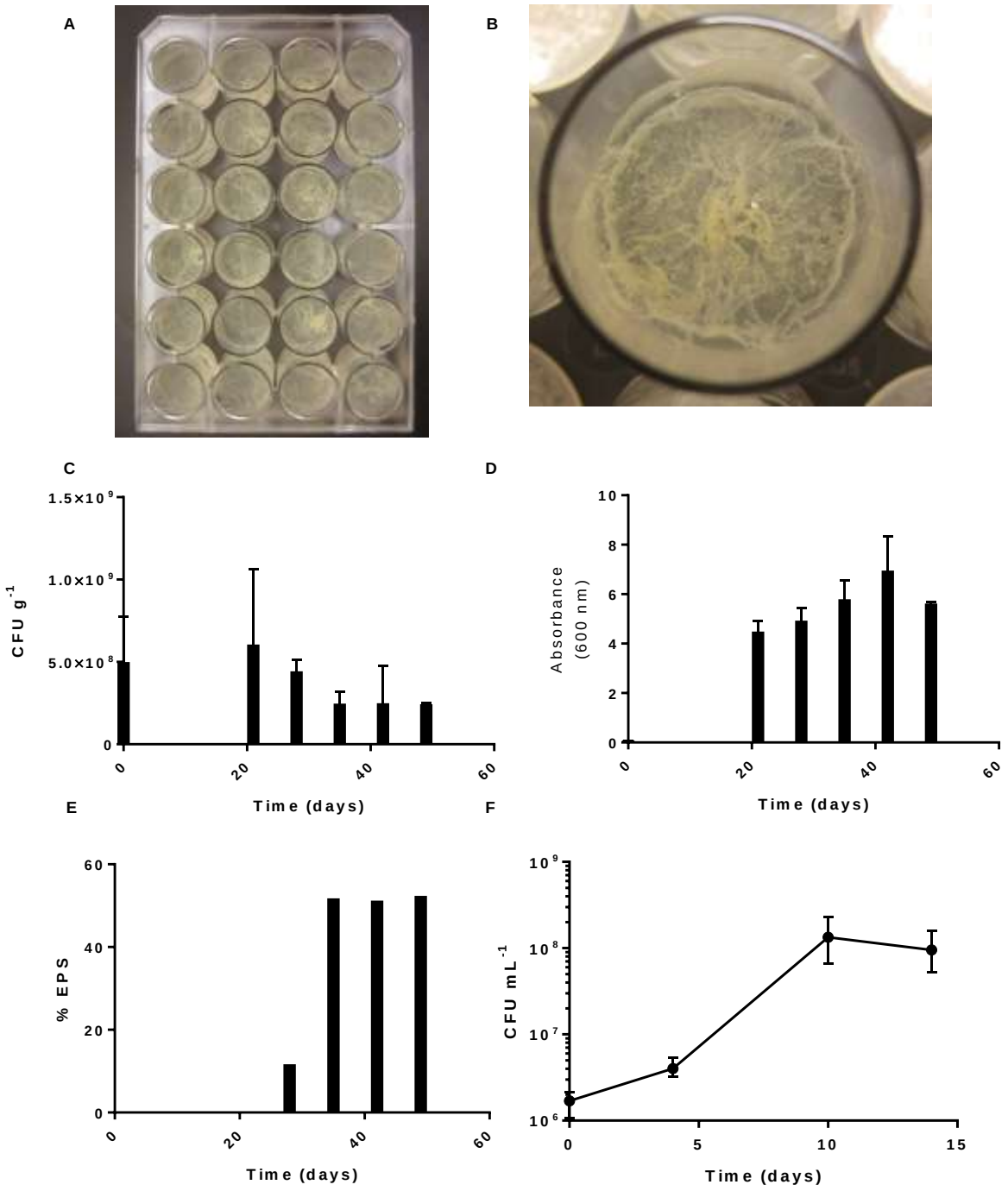


**Figure 2.3.1:** Culture of biofilm and planktonic phenotype *M. tuberculosis*. (A) Photograph of *M. tuberculosis* biofilms cultured using a 24-well plate and modified Sauton's medium over 6 weeks. (B) Close-up photograph of an *M. tuberculosis* pellicle biofilm. (C) Viable counts of wet-weighed pellet inocula (T0) and biofilms to determine the density of viable *M. tuberculosis* (CFU $g^{-1}$) harvested at 0, 3, 4, 5, 6 and 7 weeks (x2 biological replicates, error bars = standard deviation). (D) Crystal violet assay of pelleted innocula (T0) and biofilms to quantify biomass of *M. tuberculosis* harvested at 0, 3, 4, 5, 6 and 7 weeks (x2 biological replicates, error bars = standard deviation). (E) Percentage of extracellular polymeric

substance (EPS) present in *M. tuberculosis* biofilms, calculated after dividing the mean density of biofilm biomass at weeks 3, 4, 5, 6 and 7 by the mean density of planktonic biomass (T0), to determine the proportion of biomass attributable to the bacteria only. (F) Planktonic growth curve showing mean total viable count over two weeks, sampled on days 0, 4, 10 and 14 (x3 biological replicates, error bars = standard deviation)

## 2.4 Microscopy of *M. tuberculosis* biofilms

To image the native state of *M. tuberculosis* pellicle biofilms (method 7.5), biofilms were cultured for 5 weeks with a sterilised plastic coverslip placed on the bottom of each well prior to the addition of the inoculum. At the point of harvest, the pellicles were gently separated from the edges of the wells using a sterile spatula and the medium was removed so that the intact pellicle rested on the plastic coverslip. These could then be removed using tweezers and fixed using formaldehyde for scanning electron microscopy (SEM). SEM was performed by Howard Tolley, PHE.

SEM analysis showed *M. tuberculosis* pellicle biofilms contained areas of cording, where the majority of bacteria within the cord were oriented pole-to-pole and these cords showed variable thickness (**Figure 2.4.1a**, **b** and **Figure 2.4.2**) Sheets of confluent growth were also observed (**Figure 2.4.3**). Air-dried samples better preserved the EPS of the biofilm (**Figure 2.4.1a**, **Figure 2.4.2a**, **c**, **e**, **Figure 2.4.3a**, **c**) while processing the samples through graduated solvents stripped away the EPS and revealed the bacteria within the biofilm in greater detail (**Figure 2.4.2b**, **d**, **f**, **Figure 2.4.3b**, **d**). **Figure 2.4.2a** and **Figure 2.4.3b** appear to show mycobacterial cords growing on top of a layer of confluent growth. **Figure 2.4.3b**, a sample stripped of EPS, showed a complex network of serpentine cords on top of the layer. It is possible that the confluent growth on the right of the image reveals an area where during sample preparation the pellicle had been folded over itself, revealing the confluent bacteria on the liquid interface. **Figure 2.4.2a** has the EPS preserved and shows an area where cording has formed a pile or stack. Surrounding this area, cords are completely shrouded by EPS. The crevices visible in the EPS may represent air channels or be artefacts of the dehydration process of fixation and air-drying.

To investigate the vagaries surrounding the distinction between capsule and EPS, fixed planktonic and biofilm samples were sent to Dr. Nicole N van der Wel, University of Amsterdam for capsule immuno gold EM labelling of the capsule using anti-PIM/LAM antibody. This antibody binds to α(1-2) mannosyl residues, present on the mannose caps of PIM, LM and LAM and their non-lipdated counterparts. SEM analysis performed by Zehui Zhang, a researcher at the University of Amsterdam revealed both planktonic clumps and biofilm clumps labelled with α(1-2) mannosyl residues (**Figure 2.4.4**). The clumps often contained few distinguishable individual bacteria and large areas of heavily labelled EPS. Interestingly biofilm phenotype showed what appeared to be two types of EPS which were both labelled (**Figure 2.4.4**b). This suggests that similar to the capsule, *M. tuberculosis* EPS also contains α(1-2) mannosyl residues.

To investigate whether there was a difference in the extent of α(1-2) mannosyl residues present on planktonic and biofilm phenotypes, individual bacterium from fixed samples of both cultures were identified and the number of gold labels present on each bacterium was calculated and the measurements were normalised to the length of each bacterium (method 7.6). Both planktonic and biofilm bacterium showed an electron transparent zone which was heavily labelled suggesting this was the mycobacterial capsule (**Figure 2.4.1c**, **d**). Interestingly, bacterium from biofilm cultures were on average significantly longer than bacterium from planktonic cultures (**Figure 2.4.1e**) ($P<0.0001$ Welch's t-test $n\geq38$). Bacterium from planktonic cultures measured 2.803 ± 0.720 μm (mean ± standard deviation) while bacterium from biofilm cultures measured 3.842 ± 0.874 μm. This could be because the mature biofilm bacteria have ceased dividing after elongation in response to nutrient and/or oxygen depletion, whereas the planktonic bacteria divide rapidly following elongation, during their exponential growth phase. There was no significant difference in the extent of α(1-2) mannosyl labelling between bacterium from planktonic and biofilm cultures.

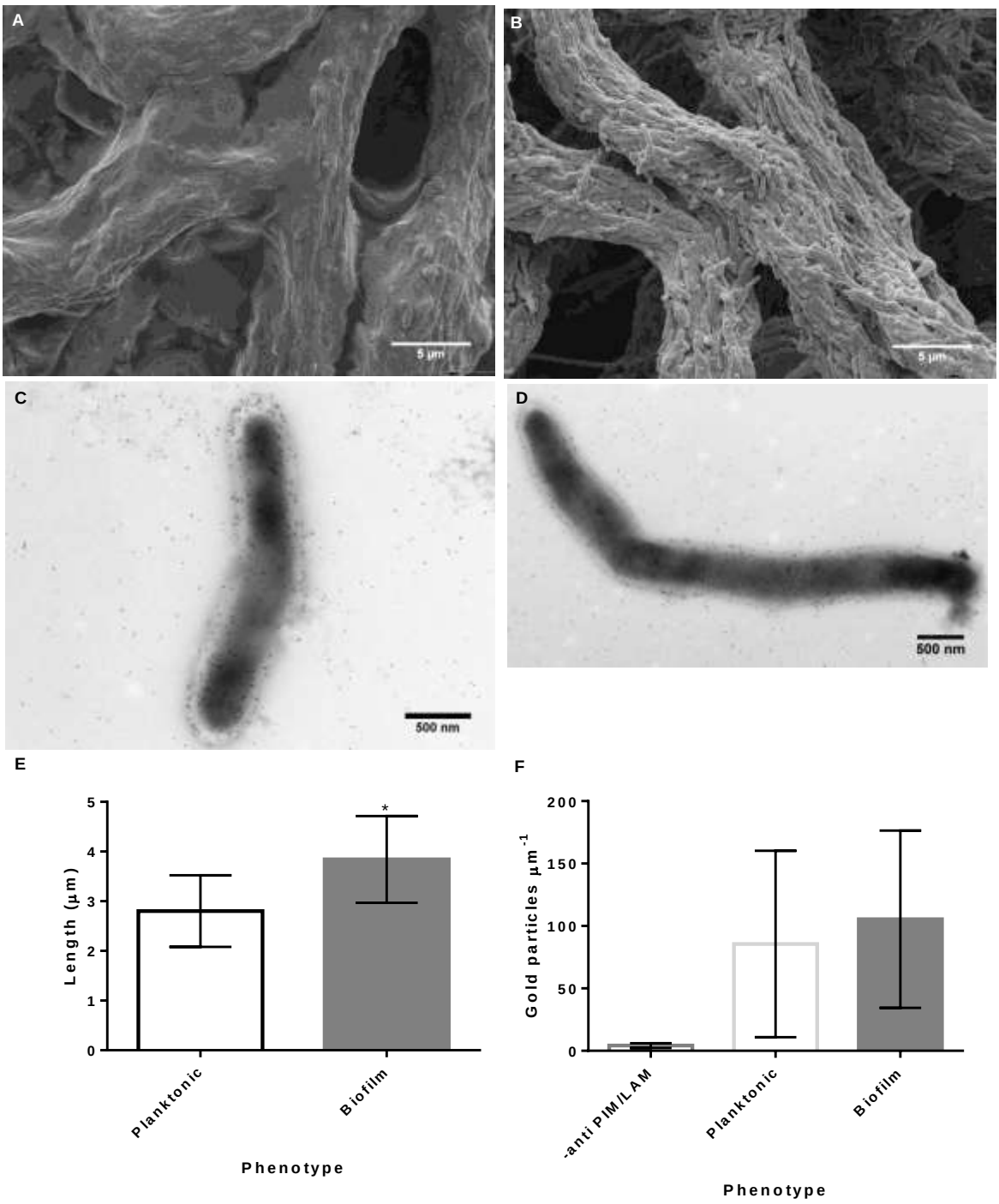


**Figure 2.4.1:** Scanning electron microscopy and immuno gold labelling of *M. tuberculosis* biofilms. (A) Scanning electron micrograph (SEM) of formaldehyde-fixed and air-dried *M. tuberculosis* biofilm. (B) SEM of formaldehyde fixed and graduated solvent treated *M. tuberculosis* biofilm. Immuno gold anti-PIM/LAM labelled planktonic (C) and biofilm (D) *M. tuberculosis*. (E) Mean length of *M. tuberculosis* cells. (F) Quantification of immuno gold anti-PIM/LAM dots visible on each micrograph associated with a bacterium/length of bacterium. n of planktonic and biofilm samples ≥38. * $P<0.05$ Welch's t-test. Error bars = standard deviation.

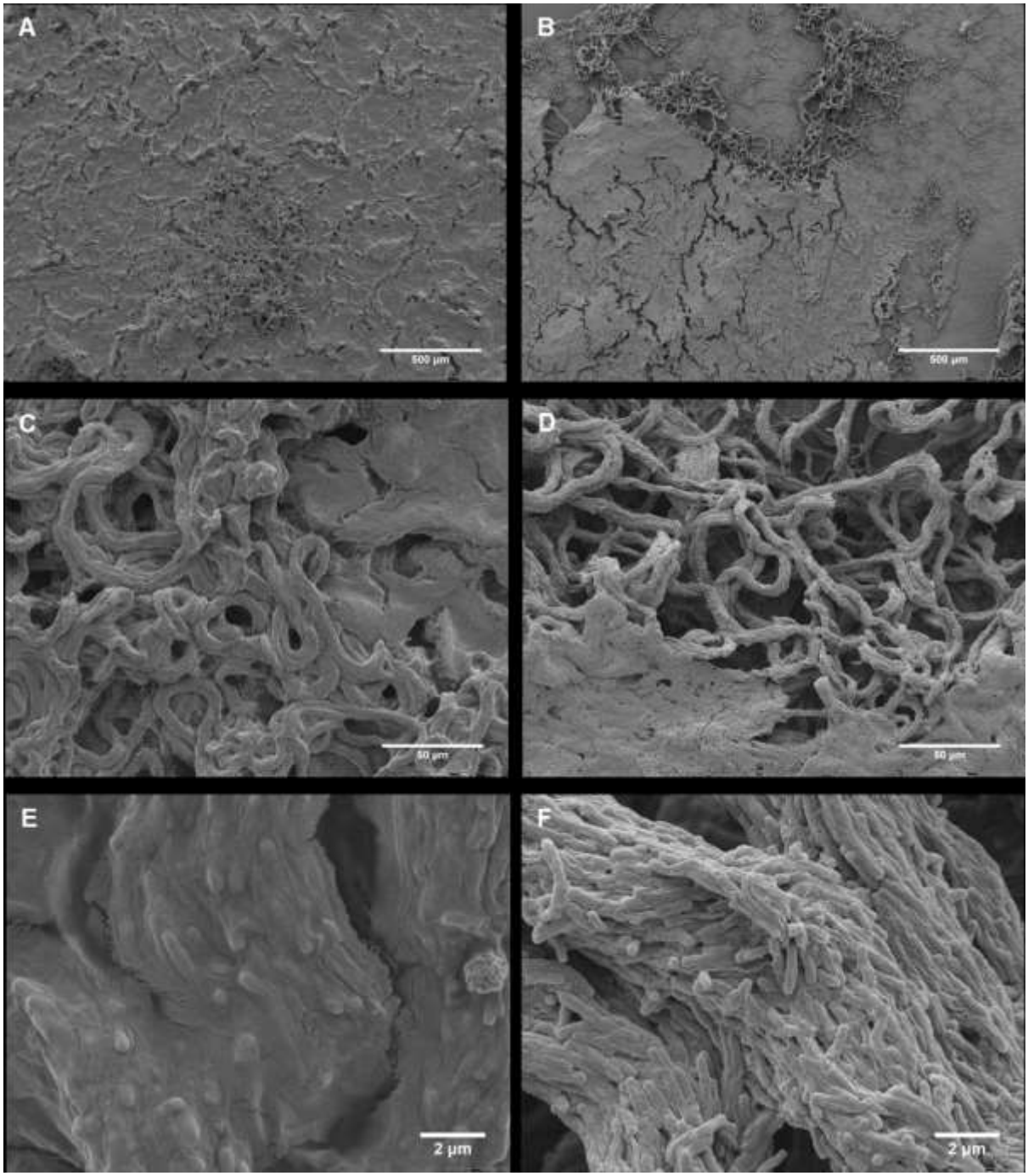


**Figure 2.4.2:** Scanning electron micrographs of cording bacteria within *M. tuberculosis* biofilms. Samples prepared by air drying (left column) and graduated solvent dehydration (right column). (A) and (B) 50x magnification, (C) and (D) 500x magnification, (E) and (F) 8000x magnification.

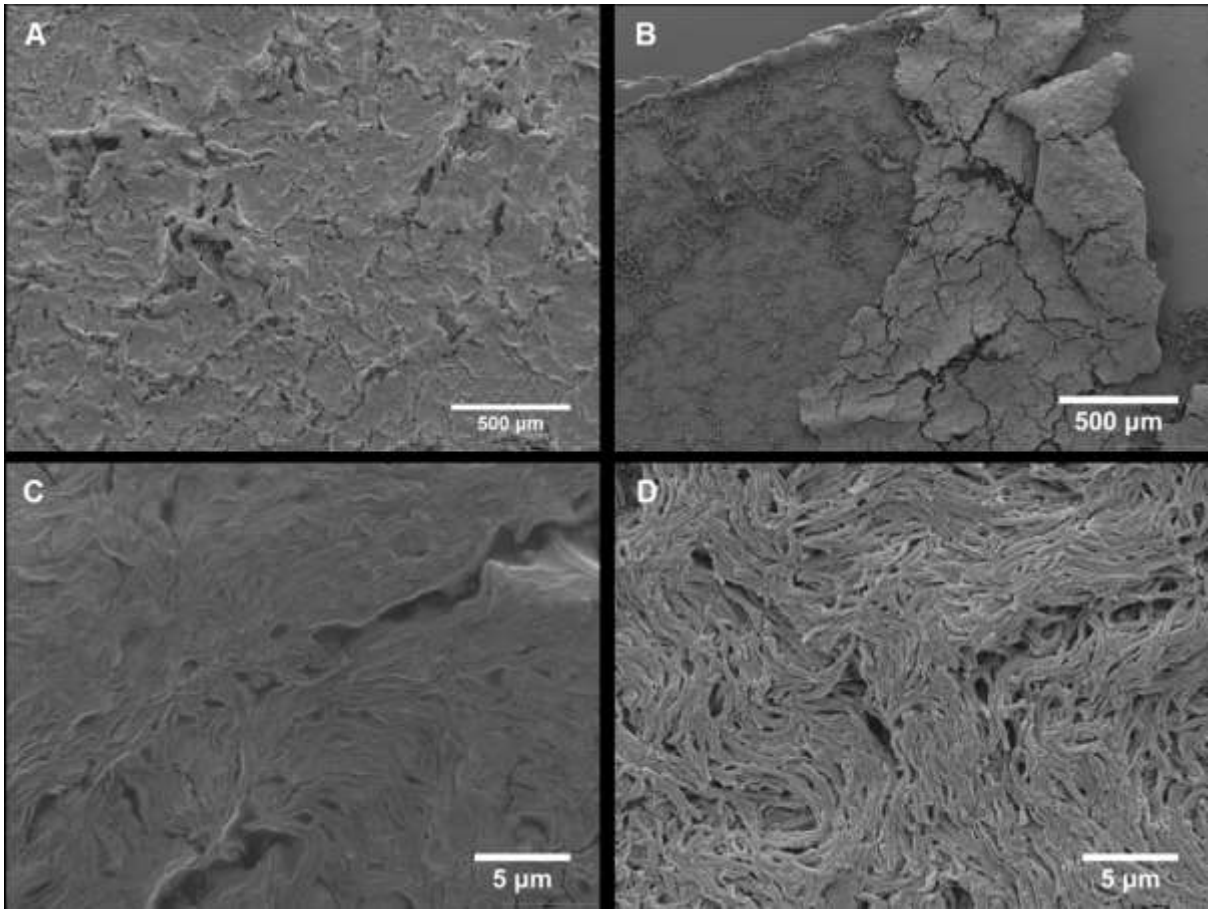


**Figure 2.4.3:** Scanning electron micrographs of surface spreading bacteria within *M. tuberculosis* biofilms. Samples prepared by air drying (left column) and graduated solvent dehydration (right column). (A) and (B) 50x magnification, (C) and (D) 4000x magnification

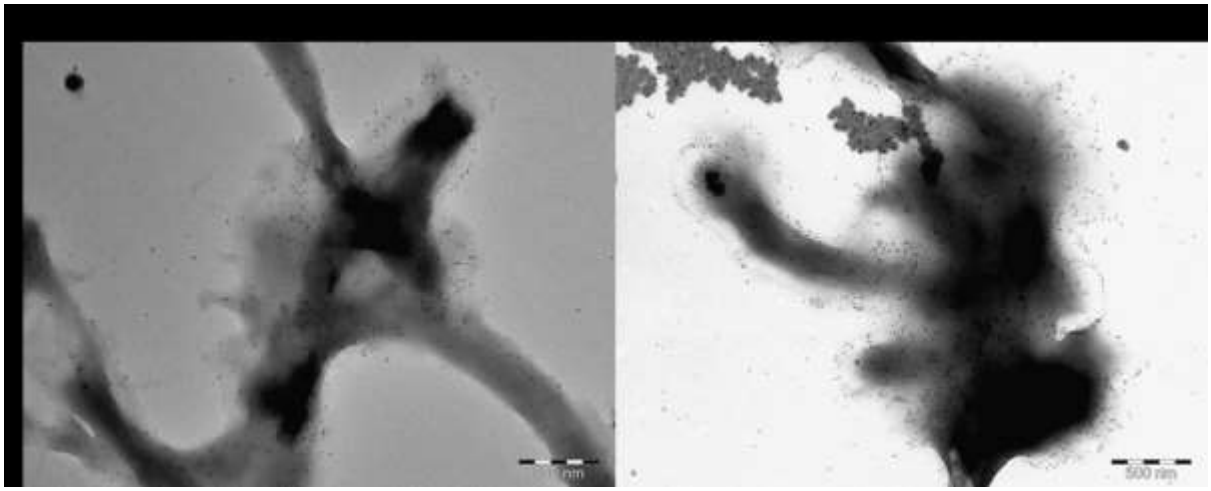

**Figure 2.4.4**: SEM image of immuno gold anti-PIM/LAM labelled *M. tuberculosis* aggregates. Representative images of fixed *M. tuberculosis* samples from planktonic (shaken flask) (A) and biofilm (pellicle) (B) cultures. Anti-PIM/LAM antibody binds to α(1-2) mannosyl residues.

## 2.5 Technical discussion

To summarise the results presented in this chapter, *M. tuberculosis* pellicle biofilms produce EPS. Pellicular EPS, as distinct from EPS present in aggregates of shaken cultures, does not appear as a major constituent of microbial biomass in cultures until between weeks 3 and 4 of biofilm culture and EPS production does not increase indefinitely but plateaus around 50% from week 5 of culture. *M. tuberculosis* planktonic cultures (in identical detergent-free medium) also grow as aggregates and reach exponential phase growth between days 4 and 10 of culture. Planktonic and biofilm *M. tuberculosis* aggregates label with α(1-2) mannosyl residues which appears to be present both in the capsule layer of each bacterium at similar levels and in EPS. Bacteria from *M. tuberculosis* biofilms appear to be on average longer than bacteria from exponentially growing cultures in shaken flasks. SEM analysis of native state *M. tuberculosis* pellicle biofilms show copious EPS, which can be removed by immersing samples in graduated solvents. *M. tuberculosis* pellicles show networks of intertwined cords as well as areas of confluent growth.

*M. tuberculosis* strain H37Rv was used for all *M. tuberculosis* experiments described in this thesis. It has been shown to produce thicker biofilms than most clinical isolates (Pang et al., 2012), which may be a phenotypic adaptation to laboratory culture methods. However, H37Rv is virulent and as previously mentioned, *M. tuberculosis* pellicle biofilm formation is not particular to any specific lineage (Pang et al., 2012) suggesting it is an ideal strain to investigate biofilm formation and innate immune responses. Sauton's medium was modified with a 10-fold reduction in monopotassium phosphate, which has previously been shown to lead to faster pellicle formation (Lethbridge, 2012 pers. comm.). Therefore this culture medium was used to follow on from this previous work. The biofilm culture method also differed from a published protocol (Kulka et al., 2012) because there was limited gas exchange. The published protocol used microplates wrapped in parafilm to maintain humidity

and incubated at 37°C in 5% $CO_2$ (Kulka et al., 2012). The biofilm cultures described in this thesis were in x12 plate batches, sealed within a 5.5L box for the generation of cell wall material and frozen biofilm bacteria stocks. In addition, individual biofilm culture plates in a 550 mL sealed box were used to analyse *M. tuberculosis* biofilm growth over time.

Biofilm culture in a sealed box abided the safety considerations for manipulating containment level 3 organisms, which require double containment at all times. Humidity was maintained since water could not escape the closed system. However, gas composition and pH may have changed over the course of culture. Consistent air composition could be provided in future experiments by using specially designed chambers fitted with double 0.2 μm filters, end-capped with parafilm in a 5% $CO_2$ incubator. This would prevent the release of aerosolised bacteria and water vapour, while also ventilating the cultures with a maintained supply of 5% $CO_2$ supplemented atmospheric air, similar to the method used by Kulka but with double containment. The $CO_2$ concentration of the human lung fluctuates between atmospheric levels during inhalation and around 5% during expiration (Krogh and Lindhard, 1914) and hence neither a closed system or consistent 5% $CO_2$ supply are likely to replicate *in vivo* fluctuations in air composition within tuberculosis cavities. The effect of a limited oxygen supply on the biofilm cultures was not assessed and one can only infer that over the 5 week period the surrounding atmosphere of the biofilm cultures gradually altered as *M. tuberculosis* bacteria respired. There would be a gradual increase in $CO_2$ and waste metabolised products and a decrease in $O_2$. An increase in $CO_2$ concentration may also lower the pH of the medium over time as it dissolves. Such changes may be detected by two component systems expressed by *M. tuberculosis* such as the DosRST system which responds to hypoxia and leads to downregulation of protein synthesis and upregulation of the Dos regulon to assist in redox homestasis to maintain energy levels through catabolism of nutrients and anabolism of cellular components in a low oxygen environment (Poole et al.,

2012). Notably previous studies have shown pellicles with unlimited gas exchange mature after 5 weeks of culture (Kulka et al., 2012) and the cultures described in this thesis similarly mature after 5 weeks incubation, suggesting oxygen may not be fully depleted and the pH remains high enough for maximal biofilm growth within the well (**Figure 2.3.1**). The rate of oxygen depletion, $CO_2$ increase and pH could be measured by including sensors in the closed system or for example with oxygen concentration; methylene blue could be used in one of the wells as a simple indicator of depletion. Additionally comparative crystal violet assays to measure growth of ventilated and sealed biofilm cultures would highlight the cumulative effects of any air composition and pH changes on *M. tuberculosis* biofilm formation.

The spread plate method was used to quantify viable counts of planktonic and biofilm phenotype *M. tuberculosis*. Future work could include improvements in the approach to quantify bacterial numbers in the cultures studied since the cultures did not contain the commonly used detergent Tween-80 for mycobacterial dispersal, which allowed clumping to occur. The approach of sampling instantly after using a vortex on the vessel was used in an attempt to minimise sedimentation and randomly distribute the clumps throughout the medium. Serial dilutions in PBS-Tween-80 were also performed to disperse visible clumps for viable counts.

Quantification of the number of viable bacteria in *M. tuberculosis* pellicle biofilms was performed by calculating the number of colony forming units per gram of wet-weight biofilm. Six technical replicates for each biological replicate were included to reduce the effect of weight variation between cell pastes. However, an improvement to the method would have been to measure dry weights of the biomass with the caveat that the sample dried and weighed would not be the same sample spread onto plates.

To quantify pellicle-specific EPS (**Figure 2.3.1e**), viable counts (CFU $g^{-1}$) of biofilm samples were divided by the viable count (CFU $g^{-1}$) of the planktonic inoculum. Estimates of the percentage of biomass that is EPS are commonly used in biofilm EPS extraction as they allow the estimation of EPS extraction efficiency (Nielsen and Jahn, 1999).

The planktonic cultures used in this thesis comprised of aggregates and therefore did not harbour truly planktonic dispersed bacteria. Yet clumps are even seen in Tween-80 containing chemostat cultures (James et al., 2000). This has implications for the comparisons made between planktonic and biofilm cultures. Firstly since the clumps contain oxygen/nutrient gradients it suggests there may be additional heterogeneity in the population with bacteria at the peripheries of the clump replicating more rapidly than those in the centre (Islam et al., 2012). Therefore it is possible not all the bacteria harvested on day 7 of culture were in an exponential phase growth state (**Figure 2.3.1f**) with structurally similar cell envelopes. Importantly, *M. tuberculosis* replication generates heterogeneity in part controlled through expression of the gene *LamA* during replication to produce daughter cells of different sizes and growth rates (Hesper Rego et al., 2017). This variation would be present regardless of aggregation. However, the additional heterogeneity due to aggregation may further increase variability when measuring innate immune responses.

The incorporation of a detergent such as tyloxapol into the planktonic cultures, which cannot be hydrolysed by the bacteria, unlike Tween-80 (de Carvalho et al., 2010) may have provided some advantages since it would have dispersed the bacteria effectively. This would have allowed more accurate quantitation for growth curves and (as to be discussed in chapter 3) would likely enhance the low yield of planktonic cells for biomass because each bacterium would have optimal surface area for gas exchange and nutrient uptake. However, this approach was not taken because the defining of detergent-free shaken cultures as planktonic has been used previously (Kerns et al., 2014). Secondly, the addition of detergents induces a

shedding effect on the capsules of the bacteria, which is reduced in detergent-free shaken cultures (Sani et al., 2010). Therefore the use of detergents would likely exaggerate any disparate innate immune responses between planktonic and biofilm *M. tuberculosis* due to the shedding cell wall components of planktonic cells and these changes could not be attributed to pellicle biofilm formation but to the presence/absence of detergent. Notably, α(1-2) mannosyl immuno-gold EM capsule labelling of detergent free aggregates showed the capsule layer of *M. tuberculosis* to be barely distinguishable from biofilm EPS in aggregates from both planktonic and biofilm cultures (**Figure 2.4.4**). Therefore, it may be difficult to retain capsule but remove EPS and a planktonic state using detergents.

Another possible approach to determining the effect of biofilm formation on innate immune responses to *M. tuberculosis* that future researchers could pursue, which would complement the approach taken here, would be to utilise biofilm-deficient mutants. A mutant *M. tuberculosis* strain in which biofilm formation was inhibited and dispersed planktonic growth was observed, compared to wild type (WT) and a complemented mutant strain, cultured in exactly the same conditions as WT *M. tuberculosis* biofilms, would provide an elegant study of biofilm formation. One possibility would be to modulate cyclic dimeric guanosine monophosphate (c-di-GMP) production, which in turn regulates biofilm formation. Modulation of this pathway has been shown to affect *M. tuberculosis* biofilm formation (Flores-Valdez et al., 2015). Deletion of the only known GGDEF domain (with diguanylate cyclase activity) in *M. tuberculosis* H37Rv gene *Rv1354c* does not affect aerobic planktonic growth in Middlebrook 7H9 medium (Hong et al., 2013) but may severely inhibit pellicle biofilm growth since it would cease c-di-GMP production (Hengge, 2009). Therefore, these mutants and complemented strains could be ideal for further study of biofilm formation.

The SEM investigations performed here (2.4) using *M. tuberculosis* and other mycobacteria have utilised the contrast between air-drying fixed samples, which preserves EPS, and

dehydrates samples using a graded series of ethanol washes, which removes the EPS (Julián et al., 2010; Sambandan et al., 2013). The use of plastic coverslips in the bottom of *M. tuberculosis* biofilm cultures allowed removal of the fragile pellicles into formaldehyde for SEM with large section still intact. The use of formaldehyde to fix the samples was sufficient to preserve biofilms and was the only validated fixative for killing *M. tuberculosis* biofilms. The contrast between air drying samples and gradual dehydration using ethanol in preserving EPS of mycobacteria or removing it respectively has previously been shown in *M. tuberculosis* (Sambandan et al., 2013) and non-tuberculosis bacteria (Julián et al., 2010). Although their methods used secondary fixation with osmium vapour, this appeared to be unnecessary since SEM of formaldehyde only fixed biofilms still preserved *M. tuberculosis* EPS (**Figure 2.4.1**, **Figure 2.4.2**, **Figure 2.4.3**).

Treatment of fixed biofilms through graded alcohols effectively removed EPS from the bacteria (**Figure 2.4.1**, **Figure 2.4.2**, **Figure 2.4.3**). Unfortunately the use of ethanol to extract EPS, leaving behind intact cells would be hampered due to the leakage of intracellular components as ethanol penetrates the cell membrane (Ingram, 1990). It would be interesting to use the air drying EPS preserving technique and EPS removal through graded alcohols on planktonic cultures to compare the morphology to pellicle biofilms.

The biofilm samples sent for α(1,2) mannosyl immuno gold EM labelling were not preserved on coverslips but were instead broken-up into clumps use of a vortex and fixed. This released enough individual bacteria from both biofilm and planktonic cultures for visualising the capsule. However, it would be useful to use this technique on intact biofilms to identify the EPS constituents with more specific antibodies in addition to α(1,2) mannose caps. Targets could include other capsular components e.g. α-glucan (Sani et al., 2010), known biofilm EPS components such as free mycolate and TDM (Robert Lee Hunter et al., 2006) and identify whether virulence associated secreted proteins such as CFP10, ESAT-6 and PE/PPE

are associated with biofilm EPS. The quantification of gold labelling has been used before to discriminate between labelled and unlabelled bacteria (Sani et al., 2010). Since biofilm cells were on average longer than planktonic cells (**Figure 2.4.1e**), and *M. tuberculosis* width is uniform (Kieser and Rubin, 2014), it was possible to quantify the extent of labelling on both planktonic and biofilm cells. The accuracy of the quantification may be effected by dark regions on the micrographs and large labelled aggregates where counting could have been underestimated. The large sample size of individual bacterium (≥38) should cumulatively reduce the overall effect of errors in quantitation on each bacterium.

# 3 ANALYSIS OF THE OUTERMOST LIPIDS AND CARBOHYDRATES OF PLANKTONIC AND BIOFILM PHENOTYPE *M. TUBERCULOSIS*

## 3.1 Introduction

In chapter 2, it was shown that pellicle biofilms are distinct from planktonic bacteria in shaken flasks. Therefore, to determine the biochemical changes that occur, *M. tuberculosis* biomass from planktonic and biofilm cultures was heat-inactivated, evaporated to dryness and taken to the University of Birmingham where lipid and carbohydrate analyses was performed.

*M. tuberculosis* biofilm lipids have been characterised previously (Ojha et al., 2008). Ojha compared $mc^2$7000 strain planktonic cultures in Middlebrook 7H9 with 0.05% Tween 80 to $mc^2$7000 strain cultured as pellicle biofilms in Sauton's medium. They observed a reduction in triacylglycerol in biofilm *M. tuberculosis* lipid extracts and an increase in free mycolic acids, predominantly α and methoxy mycolates, with 10% keto-mycolates. The planktonic and biofilm models described in chapter 2, which use the same detergent-free medium, were used to try to replicate and expand on the findings of Ojha et al., (2008). *M. tuberculosis* lipid profiles have been annotated in detail (Besra, 1998; Dobson et al., 1985; Wheeler, 2009). Although the growth medium used in the more recent protocols is not stated, Dobson *et al.*, used Sauton's medium, but as to whether the biomass was derived from shaken or pellicle cultures is not specified.

An established method for non-covalently attached cell wall carbohydrate/lipoglycan extraction was followed (Besra, 1998). This method removes lipid-anchored lipoarabinomannan (LAM), lipomannan (LM), phosphtidylinsitol mannans (PIMs), capsular α-glucan, arabinomannan (AM) and mannan (M) from the mAGP cell wall core. It also

removes any carbohydrates associated with secreted EPS. Comparison of planktonic and biofilm phenotype *M. tuberculosis* carbohydrates/lipoglycans has not been performed previously. Once differences in lipid and carbohydrate extracts have been identified, their ability to modulate innate immune responses can be assessed through multiplex and ELISA based techniques.

## 3.2 Chapter 3 hypothesis

1) Pellicle biofilm phenotype *M. tuberculosis* has a lipid profile distinct from exponential phase planktonic *M. tuberculosis*, cultured in shaken flasks with identical medium.
2) Pellicle biofilm phenotype *M. tuberculosis* has a carbohydrate profile distinct from exponential phase planktonic *M. tuberculosis*, cultured in shaken flasks with identical medium.

### 3.3 Analysis of polar and apolar lipids

To determine whether there was differential expression of lipids in planktonic and biofilm cultures grown using identical medium, three independent biological replicates of both *M. tuberculosis* planktonic and biofilm phenotypes were cultured according to methods section 7.1 and were harvested according to methods section 7.7. Polar and apolar lipids were extracted by the method described in section 7.8 and analysed by two direction thin layer chromatography (2D-TLC) described in section 7.9 using the solvent systems shown in **Table 3.3-1**.

| Solvent system | Direction 1 solvent | Direction 2 solvent |
|---|---|---|
| A (apolar) | Petroleum ether/ethyl acetate 98:2 x3 times | Petroleum ether/acetone 98:2 x1 time |
| B (apolar) | Petroleum ether/acetone 92:8 x3 times | Toluene/acetone 95:5 x1 time |
| C (apolar and polar) | Chloroform/methanol 96:4 x1 time | Toluene/acetone 80:20 x1 time |
| D (apolar and polar) | Chloroform/methanol/water 250:75:4 x1 time | Chloroform/acetone/methanol/water 100:120:5:6 x1 time |
| E (polar) | Chloroform/methanol/water 60:30:6 x1 time | Chloroform/acetic acid/methanol/water 40:25:3:6 |

**Table 3.3-1**: The solvent systems used for analysis of polar and apolar lipids of *M. tuberculosis* by 2D-TLC.

Densitometry analysis of the scanned raw images of TLC plates was performed as described in section 7.10 to quantify changes in lipids between planktonic and biofilm phenotype *M. tuberculosis*.

Inspection of equally loaded triplicate biological replicate planktonic and biofilm apolar 2D TLCs, developed using system A (**Figure 3.3.1**) revealed a lipid smear in each biofilm replicate, which is likely to be triacylglycerols (TAG). This smear was not present in each planktonic replicate but a faint spot could be seen in the vicinity. Since TAG did not appear as a uniform spot it was not possible to perform densitometry. Phthiocerol dimycocerosates

(PDIMs) and menaquinone (MK) were also identifiable. Densitometry analysis (**Figure 3.3.8**) showed the biofilm PDIMs spots had a relative density of 63% ± 11% (mean ± standard deviation) compared to planktonic spots 36% ± 11%. Densitometry analysis also showed the biofilm MK spots had a relative density of 81% ± 6% compared to planktonic spots 19% ± 6%. An unidentifiable spot was also present in both planktonic and biofilm lipid extracts. This spot labelled $?_1$ was prominent enough for densitometry analysis and the biofilm replicates had a relative density of 71% ± 9% compared to planktonic replicates 29% ± 9%. T-tests corrected for multiple comparisons by false discovery rate (Q=5%) showed a significant difference in MK and $?_1$ lipid spot density but not PDIM spot density between planktonic and biofilm lipid extracts ($P<0.05$).

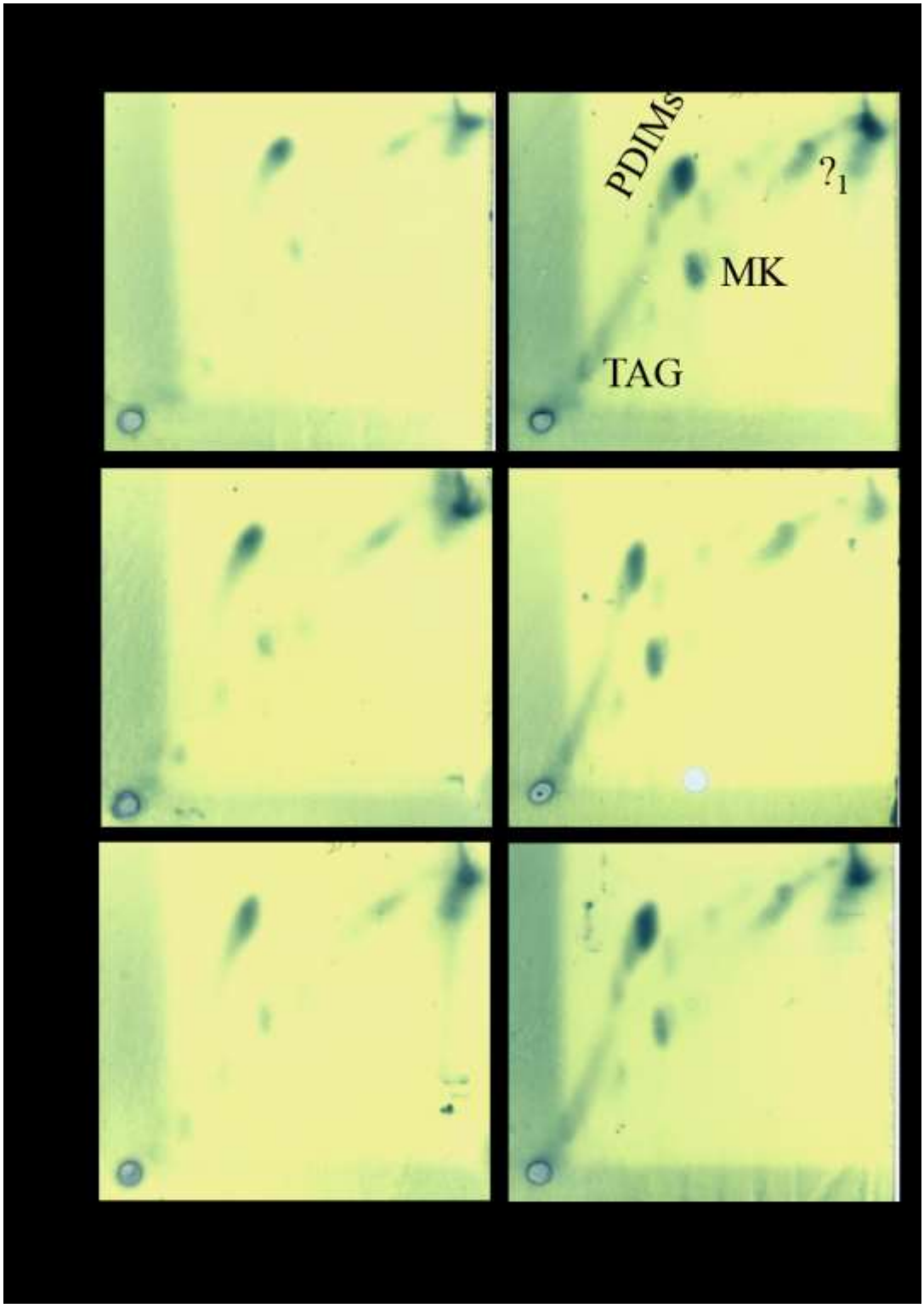


**Figure 3.3.1:** Apolar lipid analysis of planktonic and biofilm phenotype *M. tuberculosis* (Solvent system A ). 2D-TLC plates of apolar fractions from three replicate (independently inoculated cultures) of planktonic (left column) and biofilm (right column) phenotype *M. tuberculosis* stained with molybdophosphoric acid (MPA). Phthiocerol dimycocerosates PDIMs, Menaquinone (MK), Triacylglycerol (TAG), Unidentified lipid ($?_1$).

System B identified trehalose mycolipenates (TMPs) and free fatty acids (FFA). Densitometry analysis (**Figure 3.3.8**) showed biofilm FFA spots had a relative density of 58% ± 5% compared to planktonic replicates 42% ± 5%. The relative density of biofilm phenotype TMPs was 45% ± 8% compared to planktonic spots 55% ± 8%. 2/3 biofilm replicates showed an unidentified spot in the top left corner of the TLC, which was not present on the planktonic TLCs and the remaining biofilm replicate TLC ($?_2$) (**Figure 3.3.2**). Also adjacent to the free fatty acid spot, present in both planktonic and biofilm apolar lipid extracts, is another unidentified spot ($?_3$). The biofilm $?_3$ spots had a relative density of 48% ± 19% compared to the planktonic spots 52% ± 19%. T-tests corrected for multiple comparisons by false discovery rate (Q=5%) showed a significant difference in FFA lipid spot density but not TMPs and $?_3$ spot density between planktonic and biofilm lipid extracts ($P<0.05$).

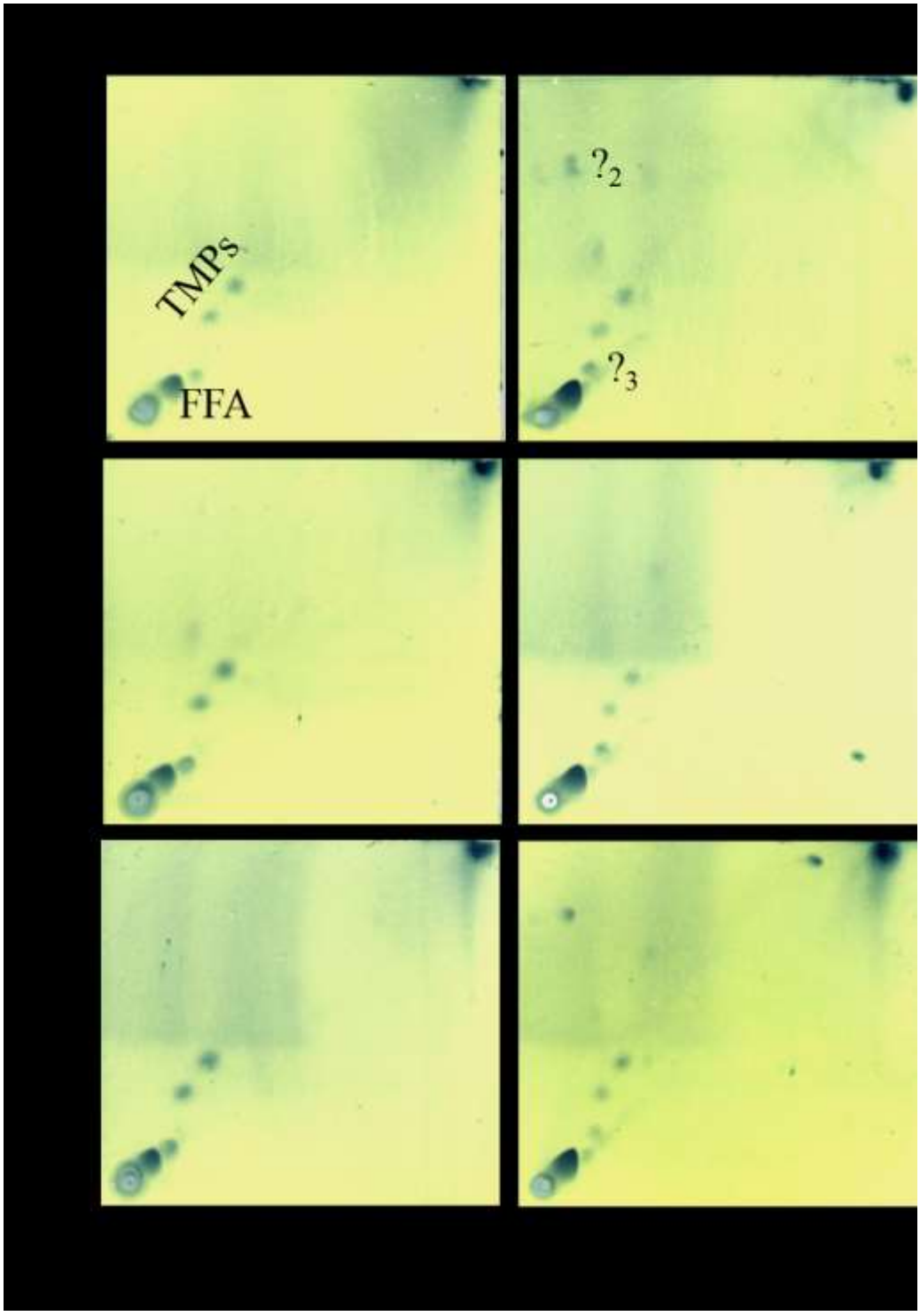


**Figure 3.3.2:** Lipid analysis of planktonic and biofilm phenotype *M. tuberculosis* (Solvent System B). 2D-TLC plates of apolar fractions from three replicate (independently inoculated cultures) of planktonic (left column) and biofilm (right column) phenotype *M. tuberculosis* stained with molybdophosphoric acid (MPA). Free fatty acid (FFA), Trehalose mycolipenates (TMPs), Unidentified lipid ($?_2$), Unidentified lipid ($?_3$).

System C identified an increase in free mycolic acids (FMA) in the biofilm non-polar lipid extract replicates relative to the planktonic replicates (**Figure 3.3.3**). Densitometry analysis (**Figure 3.3.8**) showed the relative density of biofilm FMA to be 61% ± 4% compared to planktonic spots 39% ± 4%. The FMA spot may in fact be two overlapping spots in the *M. tuberculosis* replicates. Additionally two unidentified lipid spots $?_4$ and $?_5$ were present in the top right corner of most replicates. Another unidentified lipid spot $?_6$ was present on 2/3 biofilm replicates. These spots were too faint for accurate densitometry analysis. T-tests corrected for multiple comparisons by false discovery rate (Q=5%) showed a significant difference in FMA lipid spot density between planktonic and biofilm lipid extracts ($P<0.05$).

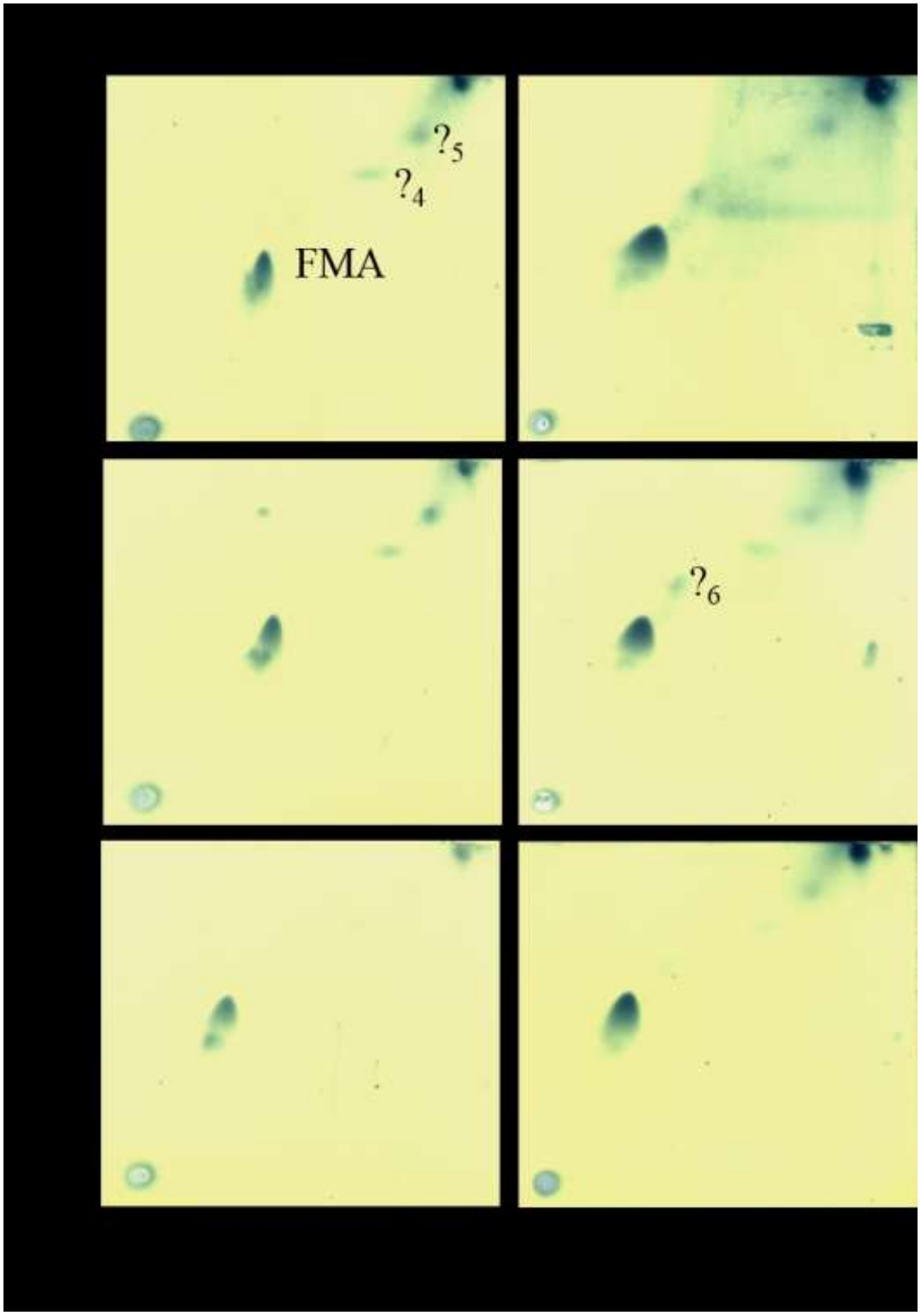


**Figure 3.3.3:** Lipid analysis of planktonic and biofilm phenotype *M. tuberculosis* (Solvent system C). 2D-TLC plates of apolar fractions from three replicate (independently inoculated cultures) of planktonic (left column) and biofilm (right column) phenotype *M. tuberculosis* stained with molybdophosphoric acid (MPA). Free mycolic acid (FMA), Unidentified lipid ($?_4$), Unidentified lipid ($?_5$), Unidentified lipid ($?_6$).

Inspection of apolar 2D TLCs developed using system D did not show prominent lipid spots in some of the replicates (**Figure 3.3.4**). Sulfolipid-1 (SL-I) and trehalose dimycolate (TDM) appeared consistently in the biofilm replicates and in 2/3 planktonic replicates. Trehalose monomycolate (TMM) did not consistently show up in either planktonic or biofilm replicates. All spots from the non-polar extracts were too faint for densitometry analysis.

The separation of polar lipids into an aqueous phase and apolar lipids into an organic phase using a separatory funnel does not result in complete separation of both apolar and polar lipids but rather an equilibrium, meaning apolar lipids may be detectable in the polar fraction. TDM and TMM and SL-I were also present in the polar fraction of the *M. tuberculosis* lipid extracts and were present in both planktonic and biofilm phenotypes (**Figure 3.3.5**). Unfortunately, one planktonic and biofilm replicate polar lipid extract was contaminated due to a technical error and could not be used. Only the SL-I spot was prominent enough in the polar lipid fractions for densitometry analysis. The biofilm SL-I spots had a relative density of 67% ± 3% compared to the planktonic replicates 33% ± 3%. T-tests corrected for multiple comparisons by false discovery rate (Q=5%) showed a significant difference in SL-I lipid spot density between planktonic and biofilm lipid extracts ($P<0.05$).

To confirm that these spots were glycolipids, TLC plates were stained with α-napthol (**Figure 3.3.6**). Inspection of polar lipid TLCs developed using system D and stained with α-napthol showed TMM, TDM and SL-I spots, confirming them to be glycolipids. TDM and SL-I were too faint to visualise on one of the planktonic replicates.

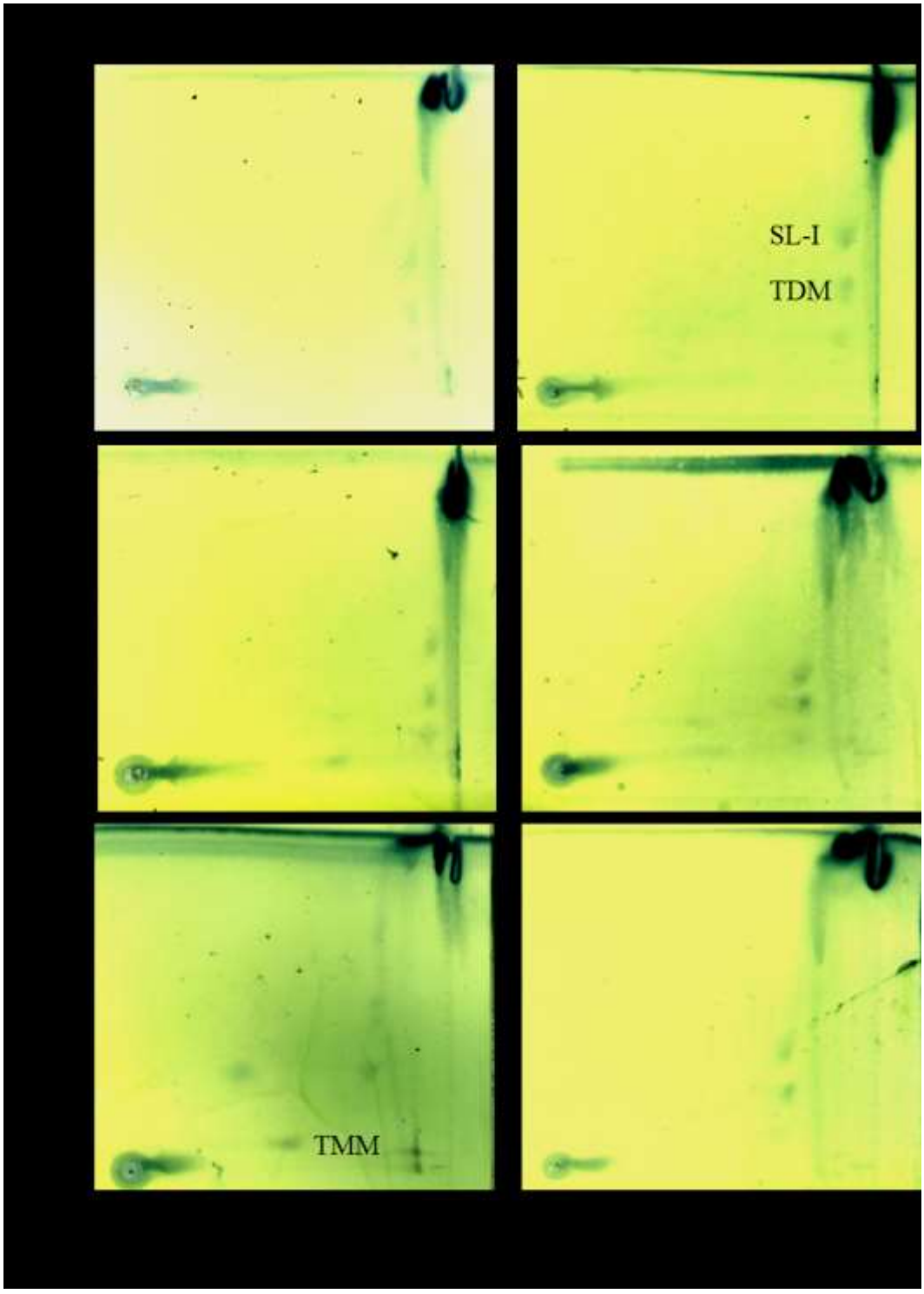


**Figure 3.3.4:** Apolar lipid analysis of planktonic and biofilm phenotype *M. tuberculosis* (Solvent System D). 2D-TLC plates of apolar fractions from three replicate (independently inoculated cultures) of planktonic (left column) and biofilm (right column) phenotype *M. tuberculosis* stained with molybdophosphoric acid (MPA). Trehalose monomycolate (TMM), Trehalose dimicolate (TDM), Sulfolipid I (SL-I).

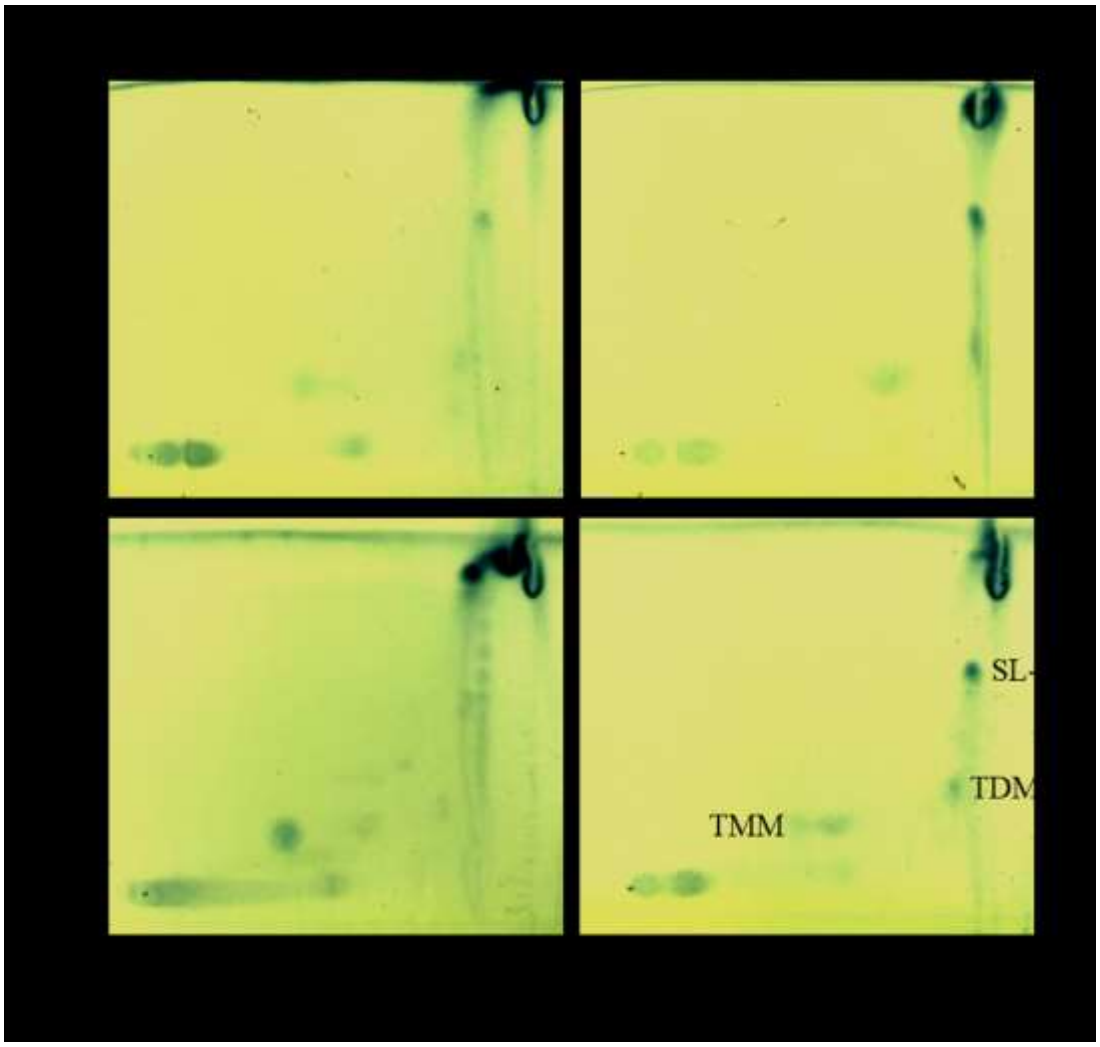


**Figure 3.3.5:** Polar lipid analysis of planktonic and biofilm phenotype *M. tuberculosis* (Solvent System D). 2D-TLC plates of polar fractions from two replicate (independently inoculated cultures) of planktonic (left column) and biofilm (right column) phenotype *M. tuberculosis* stained with molybdophosphoric acid (MPA). Sulfolipid-I (SL-I), Trehalose monomycolate (TMM), Trehalose dimicolate (TDM).

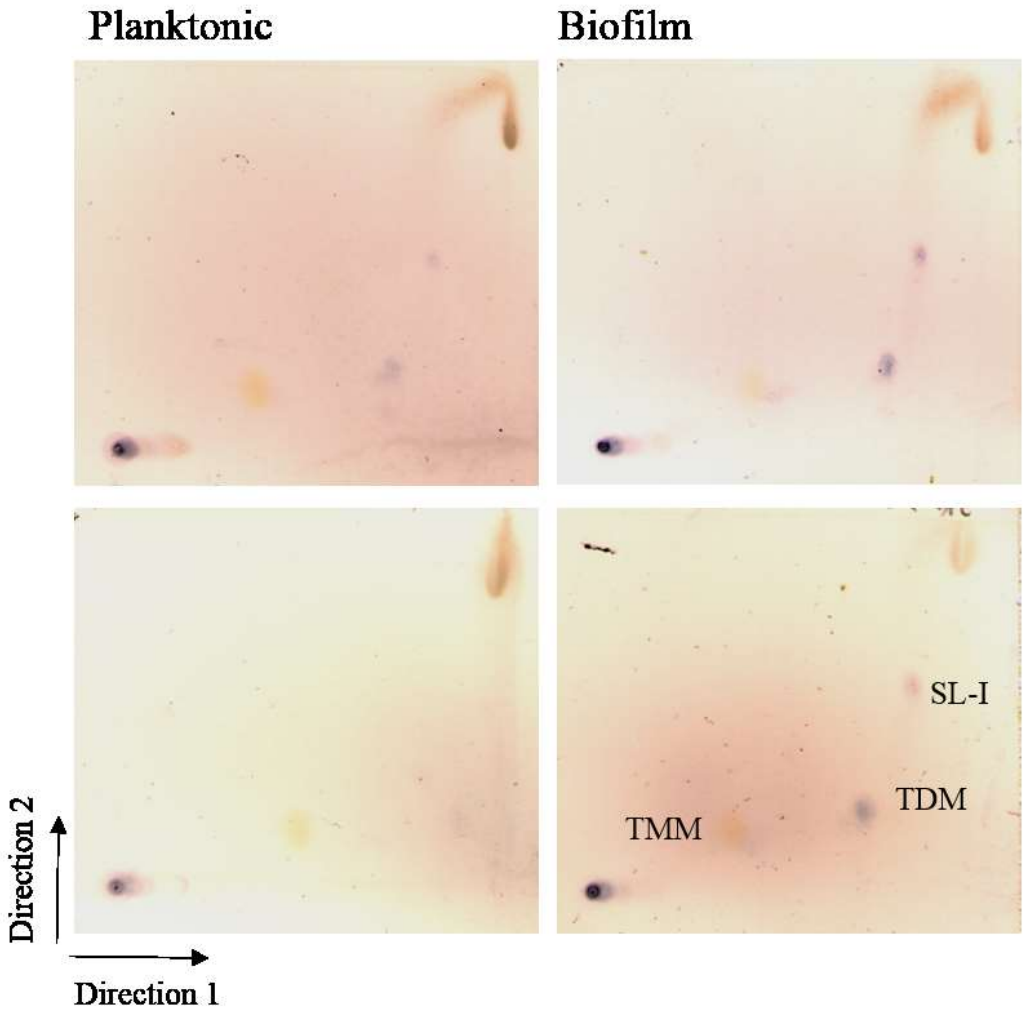


**Figure 3.3.6:** Polar glycolipid analysis of planktonic and biofilm phenotype *M. tuberculosis* (Solvent system D). 2D-TLC plates of polar fractions from two replicate (independently inoculated cultures) of planktonic (left column) and biofilm (right column) phenotype *M. tuberculosis* stained with α-napthol. Sulfolipid-I (SL-I), Trehalose monomycolate (TMM), Trehalose dimicolate (TDM).

System E was developed after spraying with α-napthol to stain mycobacterial glycolipids and identified phosphatidylinositol mannosides (PIMs) with no major changes between planktonic and biofilm phenotype *M. tuberculosis* (**Figure 3.3.7**). Only the Monoacyl phospho-*myo*-inositol-dimannoside ($Ac_1PIM_2$) spot was prominent enough for densitometry analysis. The analysis (**Figure 3.3.8**) revealed biofilm $Ac_1PIM_2$ spots had a relative density of 45% ± 11% compared to the planktonic replicates 55% ± 11%. **Figure 3.3.7** also shows additional spots ($?_7$) and ($?_8$) present in the top right corner of both planktonic and biofilm polar lipid extract TLCs which are an unidentified glycolipids. T-tests corrected for multiple comparisons by false discovery rate (Q=5%) showed no significant difference in $Ac_1PIM_2$ lipid spot density between planktonic and biofilm lipid extracts ($P<0.05$).

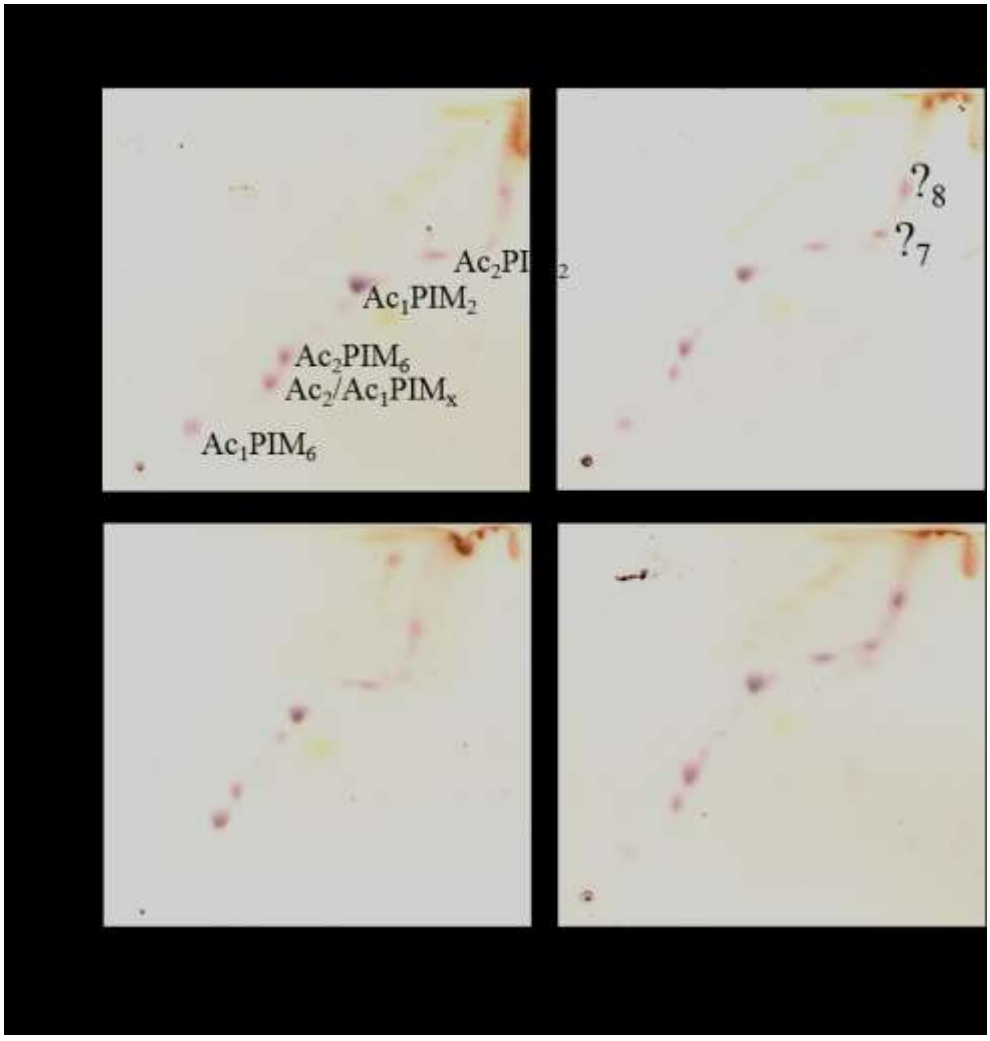


**Figure 3.3.7:** Polar glycolipid analysis of planktonic and biofilm phenotype *M. tuberculosis* (Solvent system E). 2D-TLC plates of polar fractions from two replicate (independently inoculated cultures) of planktonic (left column) and biofilm (right column) phenotype *M. tuberculosis* stained with α-napthol. Monoacyl phospho-*myo*-inositol- hexamannoside ($Ac_1PIM_6$), Diacyl phospho-*myo*-inositol- hexamannoside ($Ac_2PIM_6$), intermediate PIMs ($Ac_1PIM_x$), Monoacyl phospho-*myo*-inositol- dimannoside ($Ac_1PIM_2$), Diacyl phospho-*myo*-inositol- dimannoside ($Ac_2PIM_2$), Unidentified glycolipid ($?_7$), Unidentified glycolipid ($?_8$)

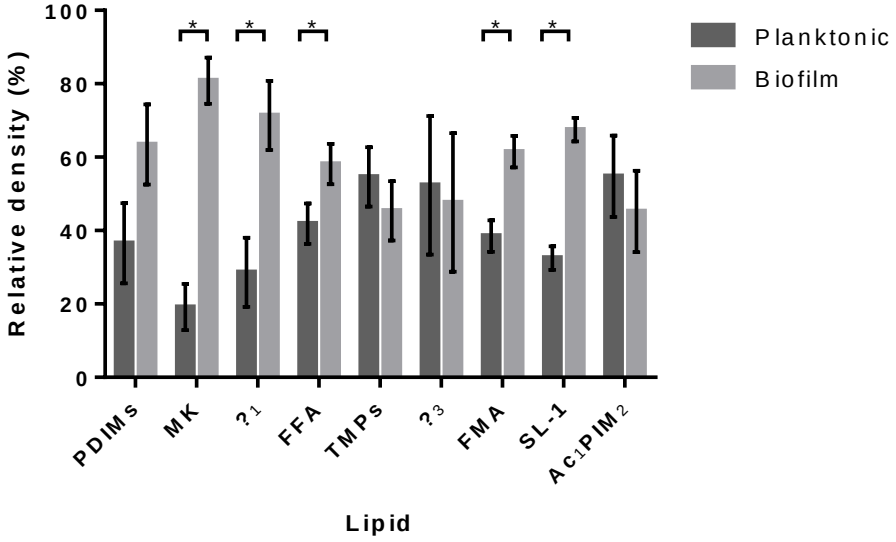


**Figure 3.3.8:** Densitometry of lipid spots. Relative density (%) of planktonic and biofilm *M. tuberculosis* lipid spot size from equally loaded TLC plates. Relative percentage was calculated from integrated density measurements on scanned raw data images, processed using ImageJ software (Schindelin et al., 2012), method 7.10. Phthiocerol dimycocerosates (PDIMs), Menaquinone (MK), Unidentified lipid from solvent system A ($?_1$), Free fatty acid (FFA), Trehalose mycolipenates (TMPs), Free mycolic acid (FMA), Sulfolipid-I (SL-I), Monoacyl phospho-*myo*-inositol-hexamannoside ($Ac_1PIM_2$). Graph shows mean of x3 biological replicates. SL-1 and $Ac_1PIM_2$ data is mean of x2 biological replicates. Error bars show standard deviation. Significant differences calculated by t-tests corrected for multiple comparisons by false discovery rate (Q= 5%).

To determine if biofilm formation alters the inner leaflet outer membrane mycolic acid profiles of *M. tuberculosis*, MAMES and FAMES analysis was performed. Mycolyl-arabinogalactan-peptidoglycan (mAGP) extracts from planktonic and biofilm samples were purified and processed as described in methods sections 7.11 and 7.12 to create methyl ester derivatives. The samples were spotted on a single direction TLC plate and the TLC plate was developed and sprayed with MPA. α-mycolates, methoxy-mycolates and keto-mycolates were present in both biofilm and planktonic samples (**Figure 3.3.9**). Fatty acids were also present in the samples. There appeared to be an additional fatty acid spot in the biofilm sample which was not seen in the planktonic sample. A biological replicate of the MAMES analysis using independently grown planktonic and biofilm cultures is also shown (**Figure 3.3.10**). Analysis of the replicate samples showed a similar profile of mycolic acids. However, fatty acids were not seen in the planktonic sample. In addition, the three fatty acid spots in the biofilm sample appeared to show that the relative proportions of each fatty acid were altered compared to the MAMES and FAMES analysis shown in **Figure 3.3.9**.

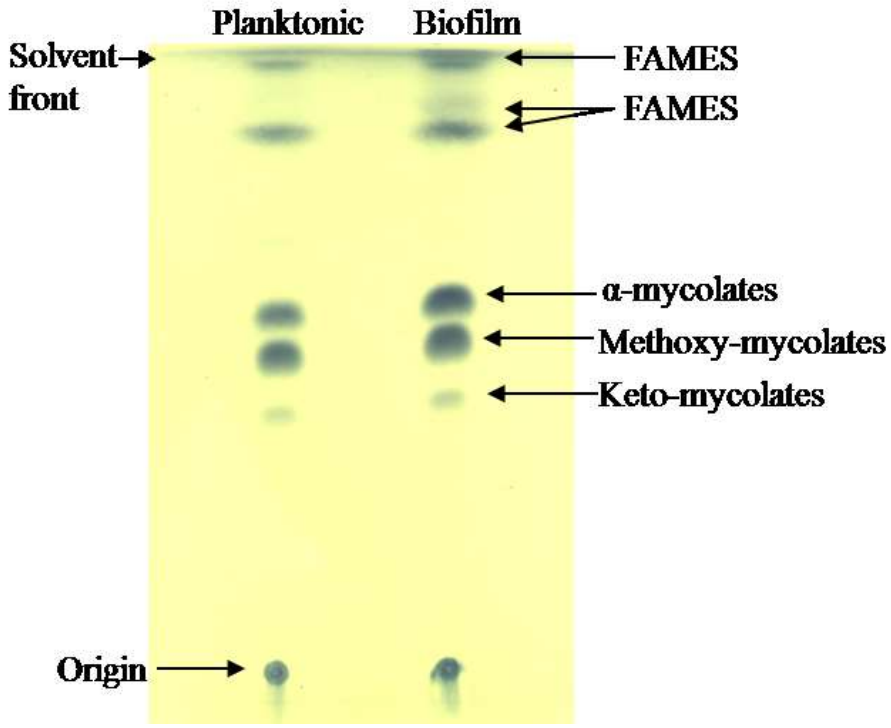


**Figure 3.3.9:** Analysis of mycolic acid methyl esters (MAMES) and fattty acid methyl esters (FAMES). Derived *M. tuberculosis* mycolyl-arabinogalactan-peptidoglycan extracts planktonic (left lane) and biofilm (right lane). MAMES: α-mycolates, Methoxy-mycolates and keto-mycolates

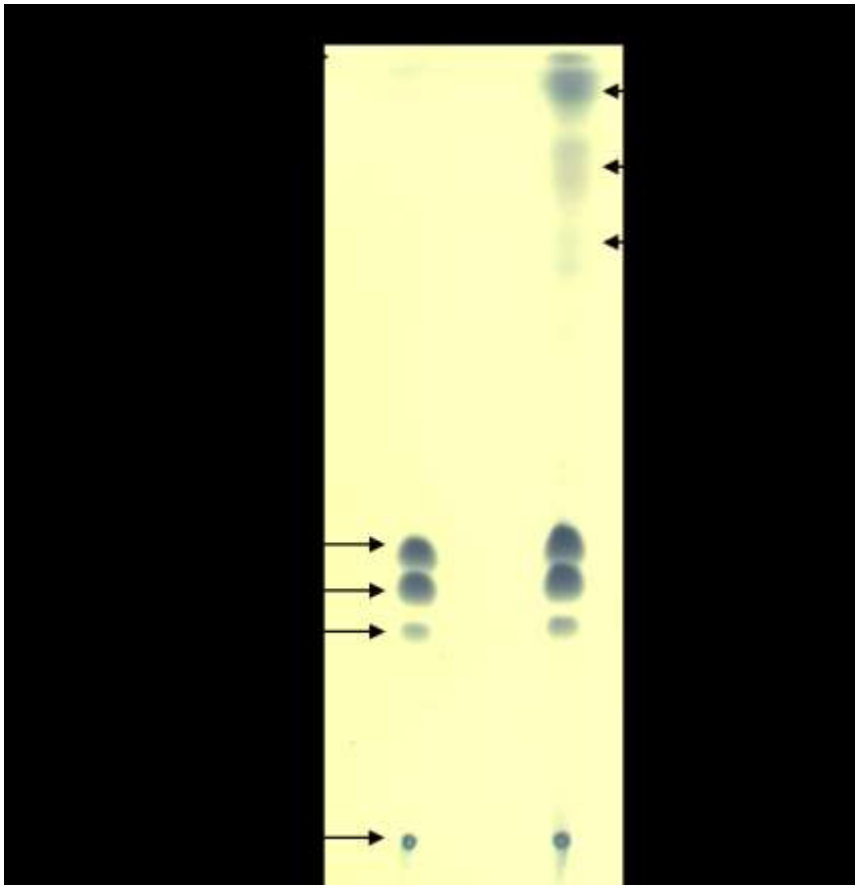

**Figure 3.3.10**: Analysis of replicate mycolic acid methyl esters (MAMES) and fatty acid methyl esters (FAMES). Derived *M. tuberculosis* mycolyl-arabinogalactan-peptidoglycan extracts planktonic (left lane) and biofilm (right lane). MAMES: α-mycolates, Methoxy-mycolates and keto-mycolates. Biological replicate repeat of analysis shown in **Figure 3.3.9**.

### 3.4 Analysis of outermost carbohydrates of the *M. tuberculosis* cell wall

To identify whether any changes to the outermost lipoglycans and carbohydrates occur when *M. tuberculosis* adopts a biofilm phenotype, non-covalently bound cell wall components from the cell wall core were extracted. Three separate extractions were performed using independently grown planktonic and biofilm *M. tuberculosis* cultures. The samples were heat inactivated and dried as described in methods section 7.7. Heat-inactivated planktonic and biofilm dried biomass samples were heated under ethanol reflux and phenol-treated to remove contaminating proteins and obtain the outermost non-covalently bound cell wall carbohydrate/lipoglycan fraction (method 7.13). Non-covalently bound lipoglycans and carbohydrates were visualised using ProQ Emerald 300 carbohydrate (and glycoprotein) stain according to the method described in section 7.14. **Figure 3.4.1** shows the results of the third extraction where 150 µg of pooled-planktonic and three independent biofilm phenotype *M. tuberculosis* carbohydrate samples along with *M. smegmatis* LAM standard was loaded onto a gel and visualised greyscale as a coloured spectrum, which approximates the quantity of carbohydrate in each band. Planktonic biomass was pooled due to low a yield of dried biomass. The ≈120 kDa α-glucan band was not clearly detected in any sample run on the gel. There may be a faint band in the planktonic sample but this bleeds into the background so could be an artefact. LAM and LM were detected in both planktonic and biofilm samples at similar quantities.

**Figure 3.4.2** shows the results from carbohydrate extractions 1 and 2. Extraction 1 revealed the presence of α-glucan (visible in the biofilm sample) and PIMs in addition to LAM and LM. Extraction 2 did not reveal α-glucan and PIMs. Furthermore, the LAM to LM ratio in extraction 1 showed that the biofilm extract had a greater proportion of LAM to LM. Contrary to this, extraction 2 showed the reverse; with a greater proportion of LM to LAM. In

extraction 3 (**Figure 3.4.1**) the ratio of LM to LAM was roughly equal between planktonic and biofilm phenotype.

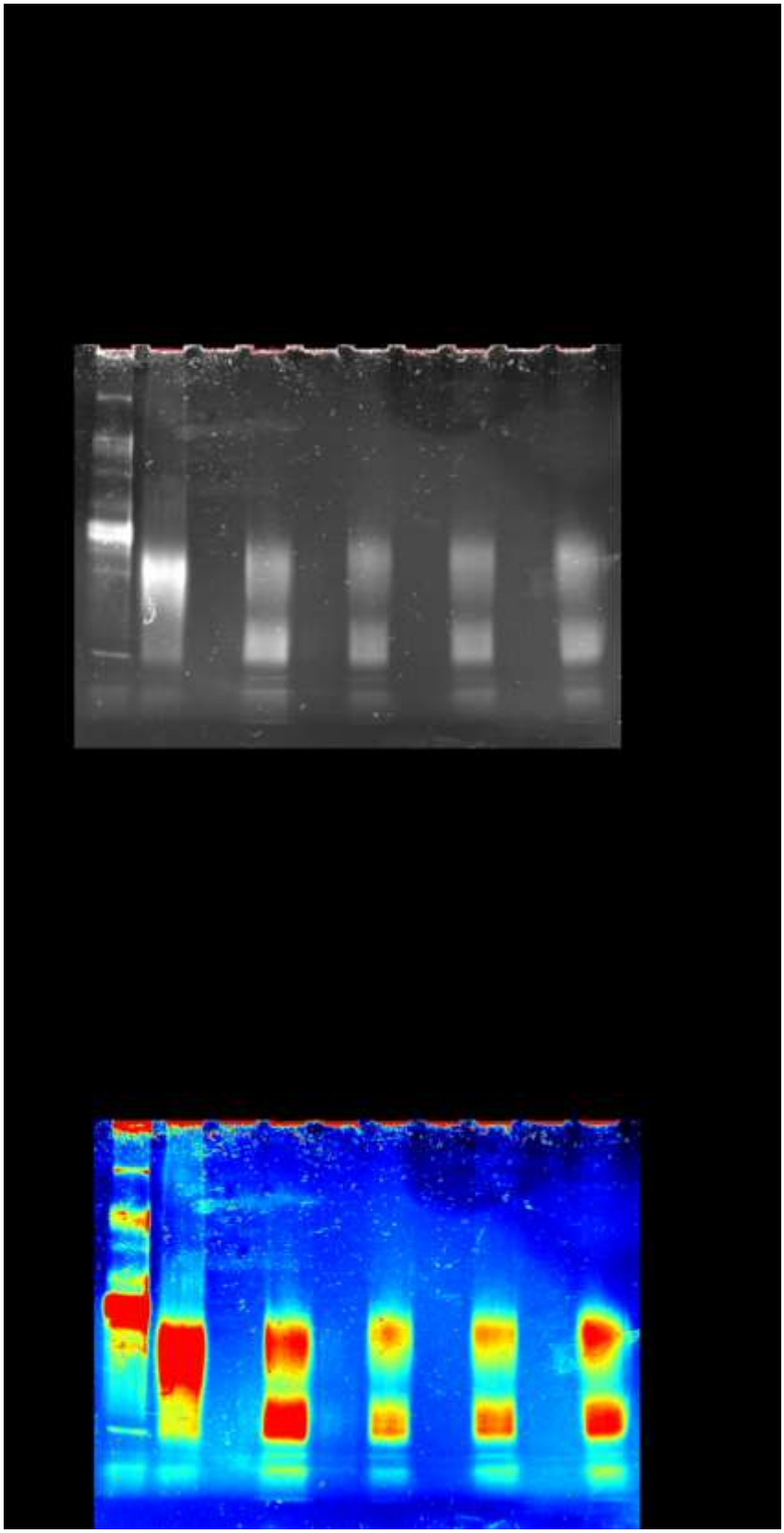

**Figure 3.4.1:** Analysis of planktonic control and triplicate biofilm *M. tuberculosis* carbohydrates of the cell wall. Non-covalently bound carbohydrate extracts from planktonic (pooled x3 biological replicates) and biofilm phenotype (x3 biological replicates) *M. tuberculosis* stained with Pro-Q Emerald 300, which binds to periodate-oxidized

carbohydrate groups. The image was taken using a Molecular Imager with Image-Lab software Gel Doc XRT (Bio-Rad, USA). Greyscale image (Top) and Spectrum image (Bottom) The spectrum highlights the intensity of staining with red indicating intense staining and blue unstained.

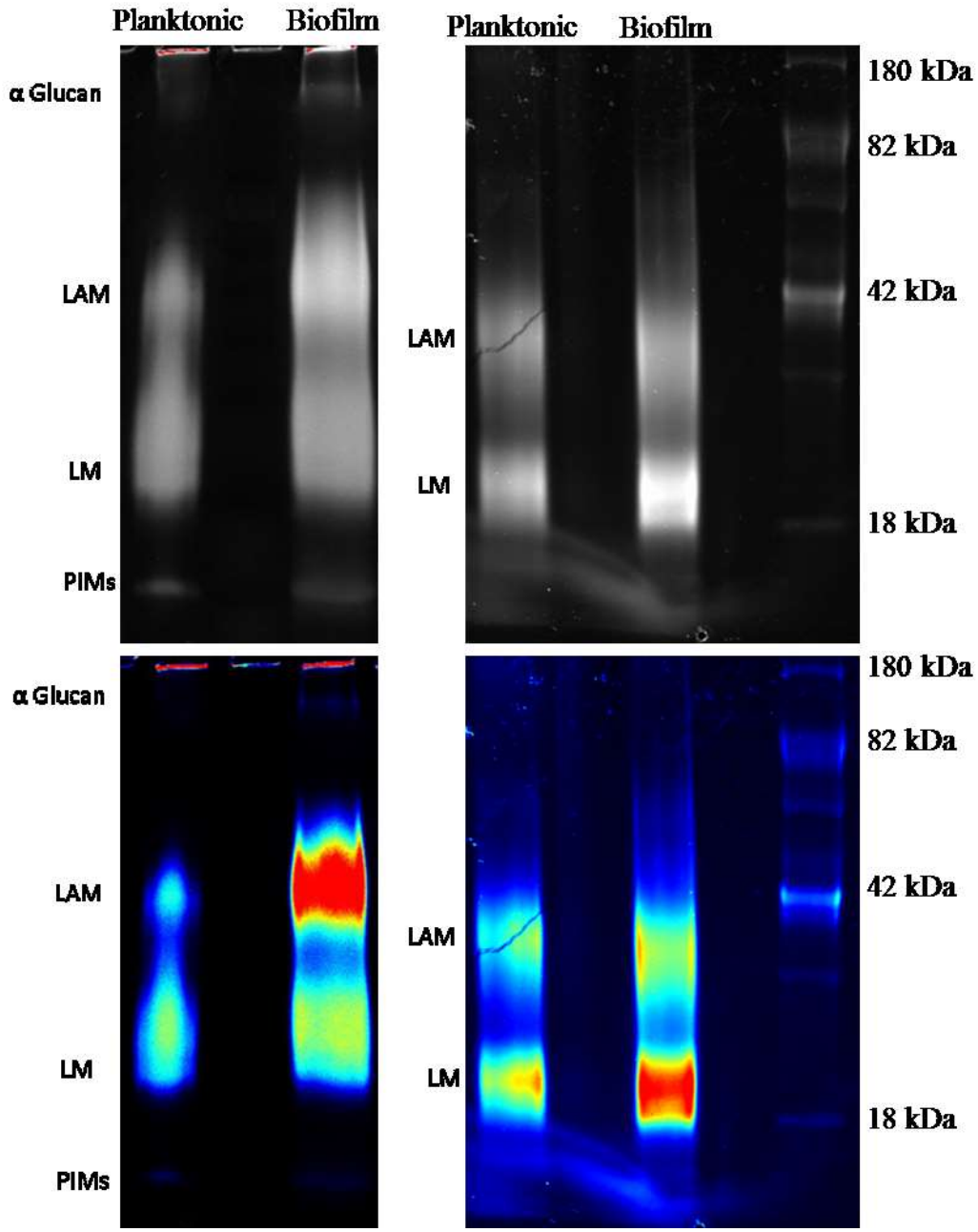


**Figure 3.4.2:** Carbohydrate/lipoglycan gels (extractions 1 and 2). Biological replicate planktonic (PK) and biofilm (BF) cultures *M. tuberculosis* stained with Pro Q Emerald 300 stain and viewed using Molecular Imager® Gel Doc™ XR System with Image Lab™ Software. Top panel - greyscale gel image. Bottom panel - spectrum gel image indicating band intensities.

To determine the relative proportions of the constituent sugars in *M. tuberculosis* planktonic and biofilm phenotype carbohydrate extracts and mAGP extracts, samples were hydrolysed and converted into alditol-acetate derivatives for gas chromatography analysis. Gas chromatography was performed by staff at the University of Birmingham. The relative proportions of arabinose, mannose and glucose from two independent total sugar analyses of planktonic carbohydrate extracts were 17.83±8.65 % (mean ± standard deviation), 33.75±0.39 % and 48.43±8.26 % respectively. The relative proportions of arabinose, mannose and glucose from two independent total sugar analyses of biofilm carbohydrate extracts were 34.89±0.65 %, 50.33±6.99 % and 14.78±6.34 % respectively.

These results indicated outermost carbohydrates were altered in *M. tuberculosis* biofilms compared to planktonic culture. To gain a clearer understanding of these constituent sugar changes that occur in *M. tuberculosis* biofilms compared to planktonic culture, sugar:sugar ratios were determined. The proportion of glucose, relative to both arabinose and mannose, was reduced in the biofilm phenotype compared to planktonic phenotype, while the proportion of arabinose relative to mannose was unchanged (**Figure 3.4.3a**). The relative proportions of sugars in cell wall arabinogalactan appeared unchanged due to phenotype (**Figure 3.4.3b**). These results suggest that there is a phenotype-specific reduction in glucose in the *M. tuberculosis* biofilm carbohydrate extract. Since glucose is the constituent sugar of capsular α-glucan, this suggests that the prevalence of α-glucan relative to other outermost carbohydrates may diminish during the formation of mycobacterial biofilms under the conditions described in this study.

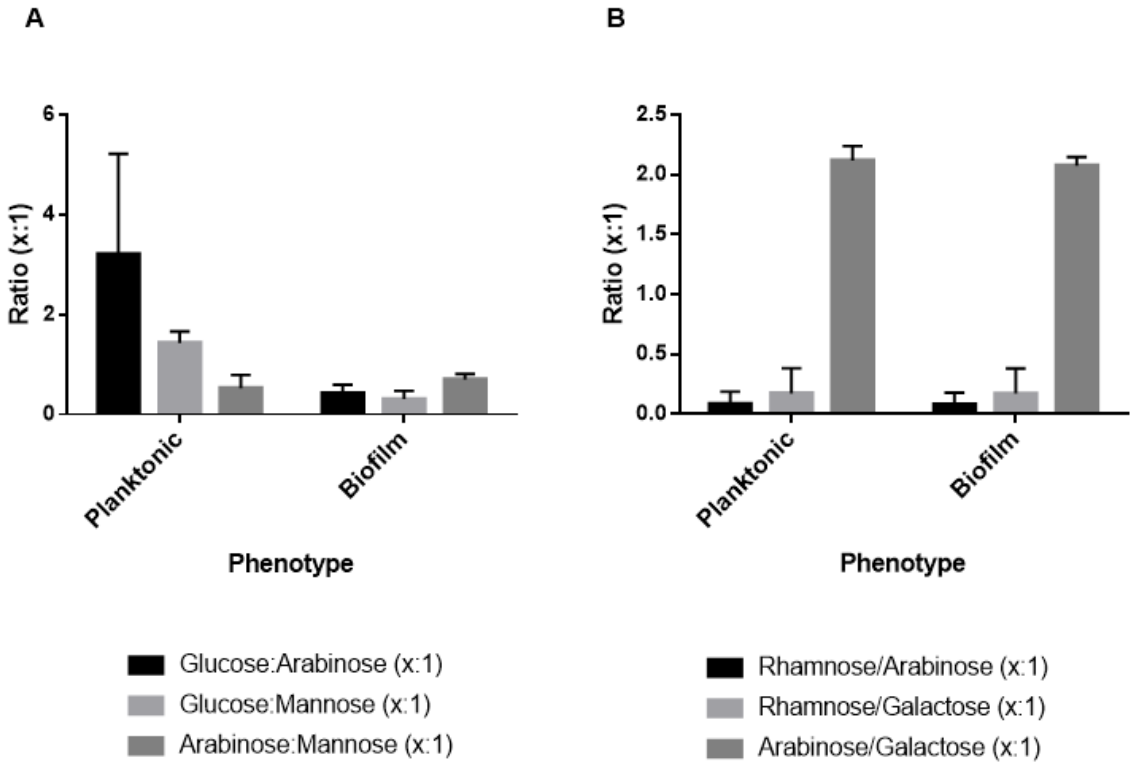


**Figure 3.4.3:** Sugar analysis of *M. tuberculosis* planktonic and biofilm phenotype carbohydrate and mAGP cell wall extracts. (A) Mean constituent sugar:sugar ratios of planktonic and biofilm phenotype *M. tuberculosis* carbohydrate extracts. (B) Mean constituent sugar:sugar ratios of planktonic and biofilm phenotype mAGP cell wall extracts. Error bars show standard deviation of x2 biological replicates.

### 3.5 Technical discussion

The results presented in this chapter suggest modification to the outermost lipids and carbohydrates of *M. tuberculosis* when it adopts a pellicle biofilm phenotype. To summarise the key findings, Solvent system A showed that *M. tuberculosis* biofilms have increased MK and an unidentified lipid ($?_1$) relative to planktonic samples. Solvent system B showed biofilm *M. tuberculosis* bacteria had increased FFA. System C revealed the biofilm phenotype had increased free mycolates in agreement with the findings of Ojha et al., (2008) who showed free mycolates were part of the mycobacterial biofilm EPS and were increased compared to the planktonic phenotype. System D showed biofilm lipid extracts had increased SL-I and solvent system E revealed no consistent changes in mycobacterial PIMs between planktonic and biofilm phenotypes. Sugar analysis of carbohydrate extracts revealed a reduction in glucose in the biofilm phenotype, which is most likely to be the constituent sugar of the exopolysaccharide α-glucan.

The culture of *M. tuberculosis* biofilms produced ample biomass for biochemical analyses. However, the culture of exponential phase planktonic *M. tuberculosis* in flasks produced a low yield of biomass. The yield could have been increased by setting up more flasks or by further optimising the planktonic control to increase the yield. Preliminary optimisation for planktonic growth showed that vented flasks produced a higher yield than sealed flasks and standard Sauton's medium, with ten-fold higher $KH_2PO_4$, produced a higher yield than modified Sauton's medium (data not shown). This suggests oxygen and $KH_2PO_4$ availability are important limiting factors for planktonic growth, as has been previously described in the literature: Gradual depletion of oxygen triggers nonreplicating persistence (Wayne and Hayes, 1996) and both potassium and phosphate depletion trigger *M. tuberculosis* to enter a non-replicative persistent growth state (Rifat et al., 2009; Salina et al., 2014). Furthermore, phosphate depletion causes elongation of *M. tuberculosis* bacterium over 28 days (Rifat et al.,

2009) similar to what was seen in 35 day pellicle biofilm *M. tuberculosis* (**Figure 2.4.1**). While the use of vented flasks was subsequently implemented, the use of modified Sauton's medium was continued for consistency, as it had been used previously for biofilm growth (Lethbridge 2013 pers. comm.). However, pellicles have been shown to grow sufficiently in 5 weeks with Sauton's medium (Kulka et al., 2012) and the benefit of a higher planktonic yield may have out-weighed any cost in reduced biofilm biomass for cell wall extractions and analyses.

Preliminary data showed that the addition of 0.05% Tween-80 to planktonic Sauton's cultures increased the yield of biomass (data not shown). The addition of detergent inhibits biofilm formation (Ojha and Hatfull, 2012) and therefore an ideal planktonic control would not use any detergent, and especially not Tween 80 because it can be used as a carbon source by *M. tuberculosis* (Bacon et al., 2014). However the detergent tyloxapol cannot be hydrolysed (de Carvalho et al., 2010) and therefore needn't be added to biofilm cultures to keep medium nutrient levels equivalent. If the addition of Tween-80 increases planktonic yield due to its detergent effects of greater dispersion of the bacteria and hence surface area for nutrient uptake and gas exchange, and not due to the hydrolysable nature of Tween-80, then one could consider the use of 0.05% tyloxapol in planktonic cultures to increase yield. However, it is not possible to separate *M. tuberculosis* lipids from the detergent in culture filtrates (Wheeler, 2009) and importantly, the addition of a detergent would cause shedding of lipids and carbohydrates into the medium (Sani et al., 2010). Therefore, it would be preferable to compare lipid and carbohydrate extracts from wildtype (WT) *M. tuberculosis* and a biofilm-deficient mutant, which grows amply as a dispersed culture under the same conditions that the WT grows as a biofilm, rather than utilise detergents.

The accuracy of quantitation of lipids could have been improved by incorporating $^{14}C$ labelled glycerol into the medium of the *M. tuberculosis* cultures, which would then be

incorporated into synthesised lipids. After polar and non-polar lipid extraction and TLC analyses, the quantity of label in each lipid spot could be measured using a PhosphorImager (Wheeler, 2009).

Separation of lipids in the biological replicate samples alongside one another in the same solvent system eliminated variations that might have been caused from making up the solvent system multiple times. There was an additional unannotated spot in the top-right corner of solvent system A TLCs that was not analysed by densitometry because it could not be separated from the solvent front and therefore it could have contained a mixture of lipids. Solvent system D TLC plates (**Figure 3.3.5**, **Figure 3.3.6** and **Figure 3.3.4**) showed faint spots in all replicates. Extraction from more initial biomass or loading more lipids onto the TLC plate to produce bolder spots could have made them amenable to densitometry analysis, however care must be taken not to overload the plates which can result in poor separation.

The quantity of lipid in the culture filtrates of the biofilm and planktonic cultures was not assessed. The turbulence created in shaken flasks may have caused the shedding of free lipids into the medium in planktonic cultures to a greater extent than in biofilm cultures. This could account for the presence of higher quantities of PDIMs, MK, unidentified lipid-$?_1$, FFA, FMA and SL-I seen in the biofilm extracts. Analyses of culture filtrates from both growth conditions would be required to ascertain if there was an upregulation in the synthesis of these lipids by *M. tuberculosis* during pellicle biofilm formation or whether these lipids are partially shed into the medium of the planktonic cultures because of shearing through shaking. Notably, shaken cultures without detergent still shed capsular polysaccharides, but to a lesser extent, suggesting that shearing effects do have an impact (Sani et al., 2010).

Gel analysis of non-covalently bound carbohydrates and lipoglycans showed disparate proportions of LM to LAM between planktonic and biofilm samples with initial extractions

(**Figure 3.4.1**, **Figure 3.4.2**). However, gel analyses of the third extraction (**Figure 3.4.1**), which was prepared from three biological replicates of *M. tuberculosis* biofilms and a pooled planktonic biological replicates (run in parallel) showed no differences between planktonic and biofilm LAM and LM in their relative quantities. The utilisation of additional replicates in this gel suggests it is likely to be more reliable than the single extractions 1 and 2 (**Figure 3.4.2**). As the culture method for *M. tuberculosis* was consistent for each extraction, it is possible that the efficiency of the extraction process was dependent on the reagents and equipment used on the day and/or human error.

Despite the variation in the results of the gel electrophoresis, there was a consistent decrease in the quantity of glucose relative to arabinose and mannose with extracts 1 and 2 from the total sugar analysis (**Figure 3.4.3**). Unfortunately, samples from the third extraction were contaminated during the derivatization process to prepare samples for gas chromatography (data not shown), since the gel of extraction 3 showed no contaminants (**Figure 3.4.1**). α-glucan could only be visualised on the gel in the biofilm extract of extraction 1 (**Figure 3.4.2**). This biofilm gel lane appeared to be more heavily loaded with carbohydrate extract compared to the planktonic lane in extraction 1 which could have been human error. This could account for the α-glucan band visible in the biofilm but not planktonic extract, despite total sugar analysis suggesting glucose prevalence was reduced on biofilm phenotype *M. tuberculosis*. It is possible that levels of α-glucan were below the limit of detection in most cases. The ProQ Emerald labelling kit can detect ≥0.5 ng of periodate-oxidized carbohydrate groups per band. This suggests there was less than 0.5 ng α-glucan extracted in the *M. tuberculosis* samples, with the exception of the biofilm sample from extraction 1 (**Figure 3.4.2**).

A third replication of the total sugar analysis to support the finding of reduced glucose constituent sugar in the carbohydrate extracts could have made the data amenable to

statistical analyses. However, there is good consistency in the findings from the replicate samples used. Further work could include linkage analysis through per-*O* methylation and GC/MS analysis of the carbohydrate extracts (Alderwick et al., 2005). This would allow confirmation that the glucose is derived from α-glucan, if α(1,4) glucopyranosyl and α(1,6) linked glucopyranosyl residues were identified (Angala et al., 2014). Alternatively, if β(1,4) linked glucopyranosyl units were identified, it would be indicative of cellulose, as has been found in surface attached *M. tuberculosis* biofilms (Trivedi et al., 2016). Until these analyses have been performed, the reduction in glucose constituent sugars from the results presented in this thesis could be due to a reduced prevalence of α-glucan, cellulose, or both. However, previous linkage analysis of *M. tuberculosis* H37Rv cultured in Sauton's medium as pellicle biofilms has only identified α-glucan (Ortalo-Magné et al., 1995) leading to the reasoning the glucose identified in the extracts here is also derived from α-glucan.

# 4 OPTIMISATION AND ANALYSIS OF DIFFERENENTIAL CYTOKINE/CHEMOKINE RELEASE IN WHOLE BLOOD STIMULATED WITH PLANKTONIC AND BIOFILM PHENOTYPE *M. TUBERCULOSIS* EXTRACTS

## 4.1 Introduction (Part 1)

Chapter 3 identified a novel change in *M. tuberculosis* carbohydrate extracts through total sugar analysis. *M. tuberculosis* biofilms possess reduced glucopyranose constituents compared to exponentially growing planktonic cultures in their outermost carbohydrates. Glucose is the constituent sugar of α-glucan, a capsular polysaccharide that represents a key component of the host-pathogen interface (Schwebach et al., 2002).

α-glucan has been shown to modulate the immune response in tuberculosis as it is required for virulence and affects phagocytosis. A genetic study used an *M. tuberculosis* strain deficient in two genes required for α-glucan synthesis. One gene, *glgC,* encodes an ADP-glucose pyrophosphorylase enzyme and the other, *treS*, encodes a trehalose synthase enzyme. The *M. tuberculosis* H37Rv Δ*glgC* Δ*treS* mutant was deficient in α-glucan and this resulted in reduced bacterial load in a BALB/c mouse infection model (Koliwer-Brandl et al., 2016). Complement receptor 3 (CR3), one of the many PRRs involved in the uptake of *M. tuberculosis,* binds to α-glucan without prior opsonisation (Cywes et al., 1997). Uptake via this receptor downregulates cell mediated immunity due to limited IL-12 secretion (Marth and Kelsall, 1997). However Stokes et al., (2004) used sonication to alter the exposed carbohydrate groups on *M. tuberculosis* capsules and showed increased binding to macrophages and snowdrop lectin (GNA) compared to control (not sonicated) bacteria. GNA specifically binds to mannopyranose units with preferential binding to terminal α(1-3)

mannose units but also to mannooligosaccharides with α(1-6) linkages (Shibuya et al., 1988). α(1-3) mannopyranose units have not been described in *M. tuberculosis* capsular polysaccharides however mannopyranose α(1-6) linkages are the backbone of capsular arabinomannans and mannans (Angala et al., 2014). This suggests α-glucan has antiphagocytic properties by covering capsular mannans and arabinomannans, which induce rapid phagocytosis when recognised by PRRs such as mannose receptors.

This raises the intriguing possibility that *in vivo* planktonic *M. tuberculosis* i.e. individual bacterium, non-replicating in areas of necrosis (Irwin et al., 2015), could be rich in α-glucan to limit phagocytosis and evade immune responses. While actively replicating *M. tuberculosis*, as a biofilm aggregate of increasing size, could downregulate capsular α-glucan synthesis; exposing arabinomannans to impair phagosome-lysosome fusion to promote serial phagocytosis-necrosis cycles, to drive *M. tuberculosis* pathogenesis (Mahamed et al., 2017).

To investigate whether the altered carbohydrate profile of biofilm phenotype *M. tuberculosis* affects the host innate immune response, a whole blood stimulation assay was optimised and developed to measure cytokine and chemokine secretion induced by the carbohydrate extracts. Cytokine secretion such as TNFα has been shown to be increased by *M. tuberculosis* LAM in numerous studies (Källenius et al., 2015) and changes to its structure, such as truncation or its arabinomannan domain, have been shown to increase proinflammatory responses through TLR2 activation (Birch et al., 2010).

Innate immunity can be sufficient to clear *M. tuberculosis* infection. Evidence for this is shown in studies where heavily exposed individuals fail to show signs of infection (Houk et al., 1968; Israel et al., 1941; Morrison et al., 2008). Cytokines and chemokines are essential for regulating innate killing mechanisms effective against *M. tuberculosis* (Khan et al., 2016). For example the release of reactive nitrogen intermediates (RNIs) which effectively control

*M. tuberculosis* growth, can be initiated by IFN-γ (Flesch and Kaufmann, 1991; Khan et al., 2016) secreted by natural killer (NK), NK T and γδ T cells in the early stages of infection (Feng et al., 2006; Ladel et al., 1995; Sada-Ovalle et al., 2008). Also activation of the NLRP3 inflammasome in THP-1 macrophages can be triggered by purified Man-LAM resulting in a nine-fold induction of caspase-1 activation, which cleaves pro-IL-1β into its activated form (Mishra et al., 2010). IL-1β initiates the maturation and clearance of *M, tuberculosis* containing phagosomes (Master et al., 2008) and has been shown to effectively control *M. tuberculosis* infection using knockout mice (Sugawara et al., 2001).

The reason for choosing a whole blood stimulation to measure innate cytokine responses instead of alternatives such as a cell line, peripheral blood mononuclear cells (PBMCs) or bronchoalveolar lavage fluid are as follows: Firstly immortal macrophage cell lines such as THP-1 cells in 2D-monolayers have undergone cancer-like mutations meaning they may not be representative of *in vivo* phagocytes in their cytokine and chemokine responses. Secondly primary cell lines, such as human alveolar macrophages, or PBMCs, while overcoming this issue, lack fundamental soluble factors present in serum and BAL fluid which may interact with *M. tuberculosis* carbohydrates, such as complement proteins (Ferguson et al., 2004). BAL fluid contains many of the primary cells that *M. tuberculosis* first encounters during infection while the cells present in whole blood must be recruited to the site of infection. This is because tuberculosis is rarely a disseminated disease in immunocompetent individuals but is instead isolated in the lung and lymph nodes. Furthermore, BAL fluid also contains sPRRs not present in whole blood that modulate cytokine secretion. For example, SP-A recognises *M. tuberculosis* LAM (Sidobre et al., 2000) triggering TNFα (Weikert et al., 2000) and IL-6 (Gold et al., 2004) production by macrophages.

Why then choose whole blood over BAL fluid? Primarily because the bronchoalveolar lavage procedure is invasive and requires hospitalisation, with limited yields, whereas whole blood

can be readily taken from donors by trained phlebotomists at PHE Porton. Although whole blood does not contain surfactant proteins, it does contains other important soluble factors not present in cell lines such as complement proteins which may be important in recognising *M. tuberculosis* PAMPs and triggering cytokine production and phagocyte recruitment through the release of anaphylatoxins C3a and C5a (Merle et al., 2015). Furthermore there is cross-talk between the complement system and inflammasome activation (Triantafilou et al., 2015). Complement proteins are present in both whole blood and the lung (Watford et al., 2000). Finally it may be unethical to expect donors to provide BAL fluid for early-stage methods development. In the absence of a fully optimised assay measuring specific cytokines and chemokines of interest secreted after stimulation of BAL fluid with planktonic and biofilm *M. tuberculosis* extracts with quantifiable potency, whole blood stimulation seems the most appropriate approach.

Whole blood has successfully been used to measure cytokine responses to *M. tuberculosis* culture filtrates (van Crevel et al., 1999). This study found that stimulation with 100 µg culture filtrate led to a dose dependent increase in TNFα in whole blood from three donors which peaked after 4 hours incubation. Furthemore, IFNγ responses were reported in whole blood from three tuberculin-skin-test positive individuals stimulated with 100 µg culture filtrate, peaking at 24 hours incubation.

*M. tuberculosis* culture filtrates will likely contain capsular components but also immunomodulatory proteins and lipids. The carbohydrate samples extracted for experimental use as described in this chapter are free of these proteins but contained lipids moieties in molecules such as LAM and PIMs and might therefore be more comparable to stimulation assays using purified *M.* tuberculosis LAM. There have been extensive stimulation studies assessing cytokine and chemokine responses to *M. tuberculosis* LAM which have differed wildly in their outcome, providing consistently conflicting results (Källenius et al., 2015).

The closest study to *M. tuberculosis* carbohydrate stimulation in whole blood is a study using primary human monocytes and *M. tuberculosis* ManLAM at 10 μg $mL^{-1}$ (Dahl et al., 1996). This study used ELISAs measuring TNFα, IL-1, IL-6, IL-10 and TGF secretion and the results suggested that ManLAM at this concentration was a poor inducer of all these cytokines bar TGF-β compared to LPS. Cytokine production by blood monocytes may be further enhanced by complement activation in whole blood and the release of complement anaphylatoxins, which have been shown to regulate cytokines and chemokines such as IL-12 and CCL2 (Actor et al., 2001)

To measure cytokine and chemokine induction in whole blood by *M. tuberculosis* planktonic and carbohydrate extracts, a Luminex Magpix multiplexing unit and a ProcartaPlex Th1/Th2 panel were used, which can assesses a broad range of secreted cytokines and chemokines with sensitivity in the picogram $mL^{-1}$ range.

The 20-plex panel of cytokine and chemokine analytes can be divided into three groups: Proinflammatory cytokines, anti-inflammatory cytokines and chemokines. The pro-inflammatory cytokines tested are IFN-γ, IL-12p70, IL-1β, IL-2, IL-6, TNF-α, GM-CSF, and IL-18. The anti-inflammatory cytokines tested are IL-4, IL-5, and IL-13 and the chemokines are CCL11 (Eotaxin), CXCL1 (GRO-α), CXCL8 (IL-8), CXCL10 (IP-10), CCL2 (MCP-1), CCL3 (MIP-1α), CCL4 (MIP-1β), CXCL12a (SDF-1α) and CCL5 (RANTES).

The reason for choosing these twenty analytes in a Th1/Th2 panel, despite not focussing on adaptive immunity was because these chemokines and cytokines may also be secreted after innate activation by PRRs and TLRs recognising mycobacterial carbohydrate and lipid PAMPS (see sections1.6 and 1.7). Especially since pellicle biofilm phenotype *M. tuberculosis* resemble *M. tuberculosis* found in sputum (Arora et al., 2016). Therefore pellicle

biofilm derived carbohydrate extracts may be a significant component of the host-pathogen interaction in newly infected individuals.

Results for each of the three donors were kept separate. Individual donor results allowed the variation in cytokine/chemokine response in each donor to be visualised in addition to the difference in response between planktonic and biofilm carbohydrate stimulants. This is important since the donors may different genetic and acquired immunological backgrounds that could influence responses. No donors had previously had tuberculosis and all donors had received the BCG vaccine earlier in their lives.

Analysis was performed as described in methods section (7.16). Briefly, carbohydrate extracts from biofilm and planktonic cultures dissolved in RPMI medium were added to undiluted whole blood to give final concentrations of 10 μg $mL^{-1}$ in triplicate and 25 μg $mL^{-1}$ in duplicate (**Table 4.1-1**). For a positive control, yeast cell wall extract zymosan was used at a final concentration of 10 μg $mL^{-1}$. Zymosan mostly comprises of α-D-mannans and β-D-glucans known to induce the production of inflammatory cytokine both *in vivo* and *in vitro* (Ohno, 2012). Negative controls were included comprising of unstimulated whole blood and whole blood stimulated with RPMI medium only. After 24 hours incubation, whole blood was pelleted and the plasma was filtered before being stored at -80$^{o}$C until required. The samples were then incorporated into a 20-plex eBioscience Procartaplex Human Th1/Th2 & Chemokine Panel 1 kit and run on a Luminex Magpix according to manufacturer's instructions.

| | Standards | | Donor1 | | | Donor2 | | | Donor3 | | | |
|---|---|---|---|---|---|---|---|---|---|---|---|---|
| | 1 | 2 | 3 | 4 | 5 | 6 | 7 | 8 | 9 | 10 | 11 | 12 |
| A | Std1 | Std1 | Unstim | PK2 | BF3 | Unstim | PK2 | BF3 | Unstim | PK2 | BF3 | BF1(25) |
| B | Std2 | Std2 | Unstim | PK2 | BF3 | Unstim | PK2 | BF3 | Unstim | PK2 | BF3 | BF1(25) |
| C | Std3 | Std3 | Unstim RPMI | PK3 | PK1(25) | Unstim RPMI | PK3 | PK1(25) | Unstim RPMI | PK3 | PK1(25) | BF1(25) |
| D | Std4 | Std4 | Unstim RPMI | PK3 | PK1(25) | Unstim RPMI | PK3 | PK1(25) | Unstim RPMI | PK3 | PK1(25) | BF1(25) |
| E | Std5 | Std5 | Zy | BF1 | PK2(25) | Zy | BF1 | PK2(25) | Zy | BF1 | PK2(25) | BF1(25) |
| F | Std6 | Std6 | Zy | BF1 | PK2(25) | Zy | BF1 | PK2(25) | Zy | BF1 | PK2(25) | BF1(25) |
| G | Std7 | Std7 | PK1 | BF2 | BF1(25) | PK1 | BF2 | BF1(25) | PK1 | BF2 | BF1(25) | |
| H | Std8 | Std8 | PK1 | BF2 | BF1(25) | PK1 | BF2 | BF1(25) | PK1 | BF2 | BF1(25) | |

**Table 4.1-1**: Whole blood carbohydrate stimulation plate layout. Std, standards; Unstim, unstimulated plasma; Unstim RPMI, plasma stimulated with RPMI 2mM L-glutamine only; Zy, zymosam 10 µg $mL^{-1}$; PK1-PK3, planktonic *M. tuberculosis* carbohydrate extracts 10 µg $mL^{-1}$; BF1-BF3 biofilm *M. tuberculosis* carbohydrate extracts 10 µg $mL^{-1}$; (25) 25 µg $mL^{-1}$.

## 4.2 Chapter 4 hypothesis I

The reduction in the constituent sugar glucose in the outermost carbohydrate extract of biofilm phenotype *M. tuberculosis* causes altered innate cytokine and chemokine secretion in whole blood compared to planktonic carbohydrate extracts.

## 4.3 Analysis of whole blood stimulated with carbohydrate/lipoglycan fractions from planktonic and biofilm phenotype *M. tuberculosis*

The upper limits and lower limits of quantitation for the 5-parameter logistic standard curves were determined using the recommended default bias of 30% (acceptable percentage variation form the ideal standard curve.) setting provided by Procartaplex Analyst software.

Total cytokine secretion by all stimulants, including the negative control RPMI response and positive control zymosan response was calculated from the standard curves.

Fold-change was calculated using the following formula:

$$Fold\ change = \left(\frac{\text{Response in stimulated whole blood}}{\text{Response in unstimulated RPMI whole blood}}\right) - 1$$

Multiple t-tests corrected for multiple comparisons by false discovery rate (Q=5%) determined there was no significant difference in any of the secreted cytokines/chemokines (pg $mL^{-1}$) induced by *M. tuberculosis* planktonic and biofilm carbohydrate extracts (stimulants) at both 10 µg $mL^{-1}$ and 25 µg $mL^{-1}$ concentrations, normalised to the RPMI only negative control.

Without correcting for multiple comparisons, more results were significant ($P<0.05$) a 25 µg $mL^{-1}$ compared to 10 µg $mL^{-1}$. The lowest uncorrected P values for stimulations at 25 µg $mL^{-1}$ are collated in **Table 4.3-1**.

| Planktonic vs Biofilm carbohydrate extracts | P Value | Significant after correction for multiple comparisons |
|---|---|---|
| Donor 2 CCL4 | 0.021183 | No |
| Donor 1 CCL2 | 0.022914 | No |
| Donor 2 CXCL8 | 0.032551 | No |
| Donor 2 CCL5 | 0.032892 | No |
| Donor 1 CXCL1 | 0.035933 | No |
| Donor 1 IL-6 | 0.045357 | No |

**Table 4.3-1:** P values of multiple planktonic vs biofilm carbohydrate t-tests. The lowest P values from multiple t-tests of Planktonic vs Biofilm carbohydrate stimulations at 25 µg $mL^{-1}$ where $P<0.05$. The P value shown is uncorrected for multiple comparisons using false discovery rate (Q=5%).

All results for the cytokines and chemokines are described below. Standard curves are shown in appendix section 9.1. Additionally, the corresponding figures for the cytokines and chemokines for which there was no consistent response above the lower limit of quantitation after incubation with any of the stimulants (IL-12p70, IL-4, IL-5, GM-CSF and IL-13) are shown in the appendix section 9.2 .

The CCL4 (MIP-1β) standard curve is shown in **Figure 9.1.4b**. A t-test corrected for multiple comparisons by false discovery rate (Q=5%) determined there was no significant difference in the total secreted CCL4 (pg $mL^{-1}$) induced by *M. tuberculosis* planktonic and biofilm carbohydrate extracts at both 10 μg $mL^{-1}$ and 25 μg $mL^{-1}$ concentrations (**Figure 4.3.1a,b**). Zymosan induced an ≈ 2 – 5-fold increase in CCL4 production dependent on donor. There was no discernible difference in CCL4 secretion induced by either planktonic and biofilm derived carbohydrates at both 10 μg $mL^{-1}$ and 25 μg $mL^{-1}$ with each extract inducing an ≈ 0 – 1 fold change in both planktonic and biofilm phenotype carbohydrate extracts (**Figure 4.3.1c,d**). Planktonic *M. tuberculosis* carbohydrate extracts induced on average higher CCL4 secretion than biofilm carbohydrate extracts in donor 1 and 2 at 25 μg $mL^{-1}$ stimulant concentration however this was not seen in donor 3

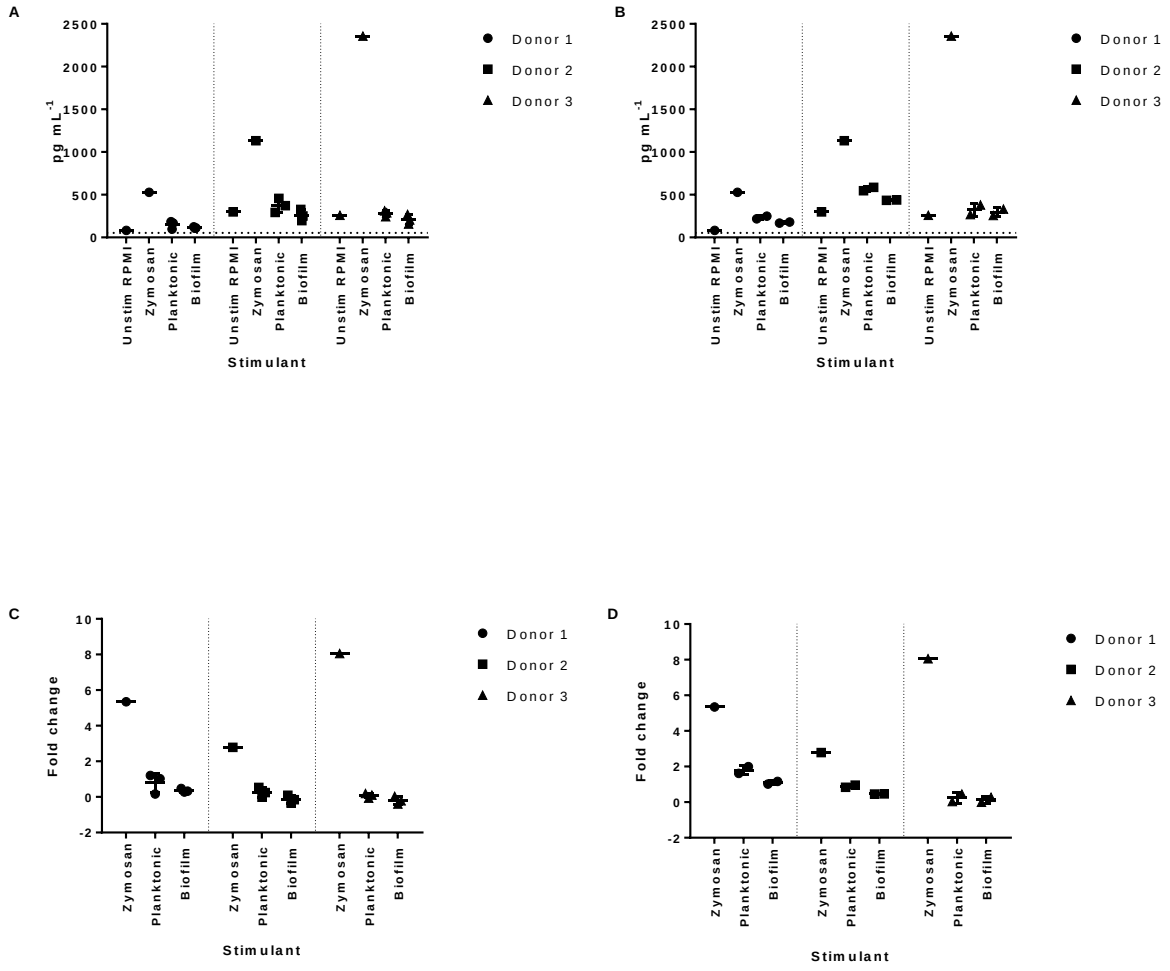


**Figure 4.3.1:** CCL4 (MIP-1β) response in whole blood stimulated with carbohydrate extracts from planktonic and biofilm phenotype *M. tuberculosis*. Total secreted CCL4 (A) and fold change ((stimulant response (pg $mL^{-1}$) / RPMI response (pg $mL^{-1}$) -1) (C) in whole blood after 24h stimulation with x3 biological replicate planktonic *M. tuberculosis* **carbohydrate extracts (10 µg $mL^{-1}$)** and x3 biological replicate biofilm *M. tuberculosis* **carbohydrate extracts (10 µg $mL^{-1}$)**. Total secreted CCL4 (B) and fold change (D) in whole blood after 24h stimulation with x2 biological replicate planktonic *M. tuberculosis* **carbohydrate extracts (25 µg $mL^{-1}$)** and x2 biological replicate biofilm *M. tuberculosis* **carbohydrate extracts (25 µg $mL^{-1}$)**. Negative control RPMI response (Unstim RPMI), Positive control Zymosan (10 µg $mL^{-1}$). The horizontal dotted line on each graph represents the lower limit of quantitation. Each donor blood stimulation is presented separately by vertical dotted lines. Error bars = standard deviation.

The CCL2 (MCP-1) standard curve is shown in **Figure 9.1.3e**. A t-test corrected for multiple comparisons by false discovery rate (Q=5%) determined there was no significant difference in the total secreted CCL2 (pg $mL^{-1}$) induced by *M. tuberculosis* planktonic and biofilm carbohydrate extracts at both 10 µg $mL^{-1}$ and 25 µg $mL^{-1}$ concentrations (**Figure 4.3.2a,b**). Zymosan induced a <1-fold change in CCL2 production dependent on donor. While planktonic and biofilm derived carbohydrates induced ≈0 – 1 fold change in CCL2 secretion (**Figure 4.3.2**). Biofilm *M. tuberculosis* carbohydrate extracts induced on average higher CCL2 secretion than planktonic carbohydrate extracts in donor 1 at 25 µg $mL^{-1}$ stimulant concentration however this was reversed in the other donors.

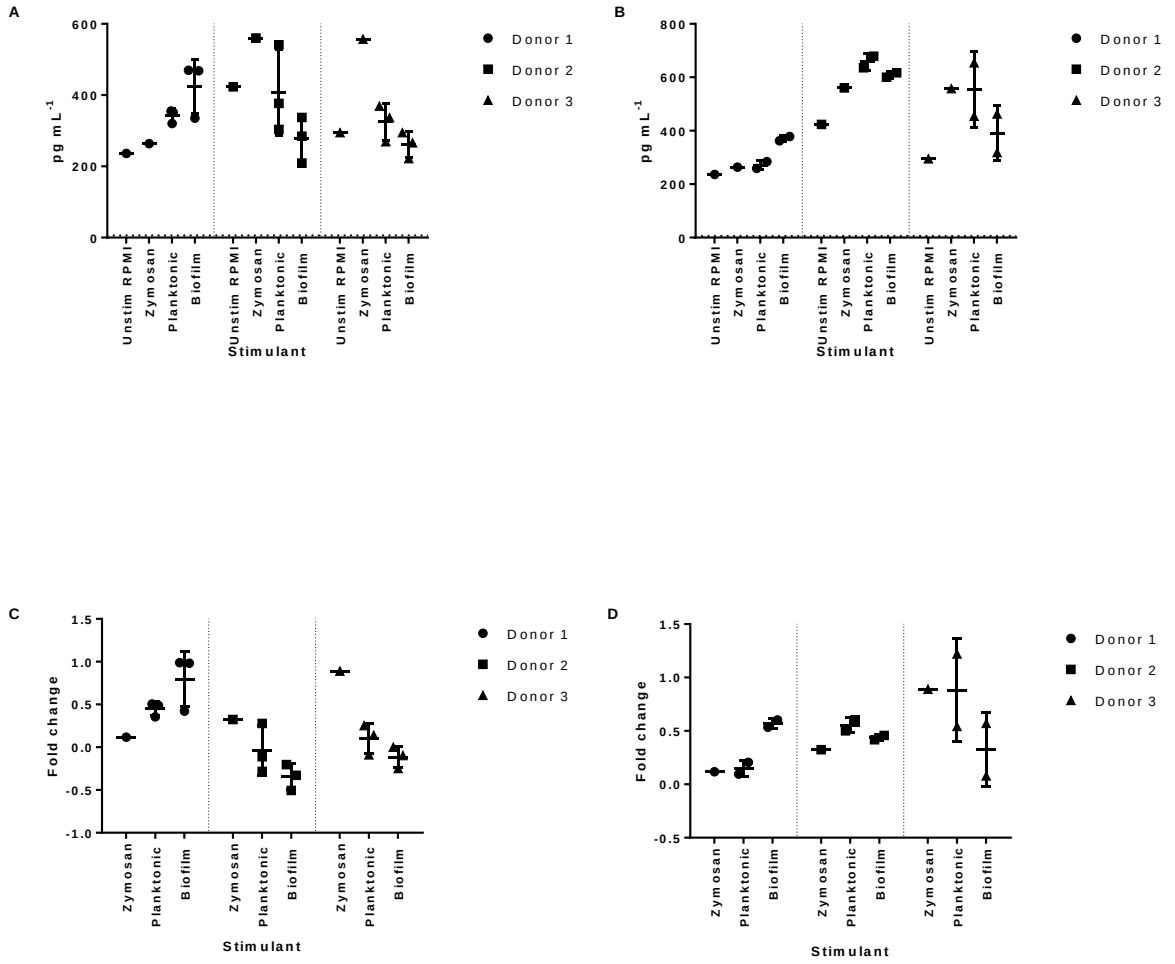


**Figure 4.3.2:** CCL2 (MCP-1) response in whole blood stimulated with carbohydrate extracts from planktonic and biofilm phenotype. Total secreted CCL2 (A) and fold change ((stimulant response (pg $mL^{-1}$) / RPMI response (pg $mL^{-1}$) -1) (C) in whole blood after 24h stimulation with x3 biological replicate planktonic *M. tuberculosis* **carbohydrate extracts (10 µg $mL^{-1}$)** and x3 biological replicate biofilm *M. tuberculosis* **carbohydrate extracts (10 µg $mL^{-1}$)**. Total secreted CCL2 (B) and fold change (D) in whole blood after 24h stimulation with x2 biological replicate planktonic *M. tuberculosis* **carbohydrate extracts (25 µg $mL^{-1}$)** and x2 biological replicate biofilm *M. tuberculosis* **carbohydrate extracts (25 µg $mL^{-1}$)**. Negative control RPMI response (Unstim RPMI), Positive control Zymosan (10 µg $mL^{-1}$). The horizontal dotted line on each graph represents the lower limit of quantitation. Each donor blood stimulation is presented separately by vertical dotted lines. Error bars = standard deviation.

The CXCL8 (IL-8) standard curve is shown in **Figure 9.1.3c**. A t-test corrected for multiple comparisons by false discovery rate (Q=5%) determined there was no significant difference in the total secreted CXCL8 (pg $mL^{-1}$) induced by *M. tuberculosis* planktonic and biofilm carbohydrate extracts at both 10 µg $mL^{-1}$ and 25 µg $mL^{-1}$ concentrations (**Figure 4.3.3a,b**). Zymosan induced an ≈ 0 – 1-fold increase in CXCL8 production dependent on donor. While planktonic and biofilm derived carbohydrates induced between 0 – 2 fold increase with the highest levels observed in donor 1 and <1-fold changes in donors 2 and 3. Planktonic *M. tuberculosis* carbohydrate extracts induced on average higher CXCL8 secretion than biofilm carbohydrate extracts in donors 1 and 2 at 25 µg $mL^{-1}$ stimulant concentration however this was not seen in donor 3.

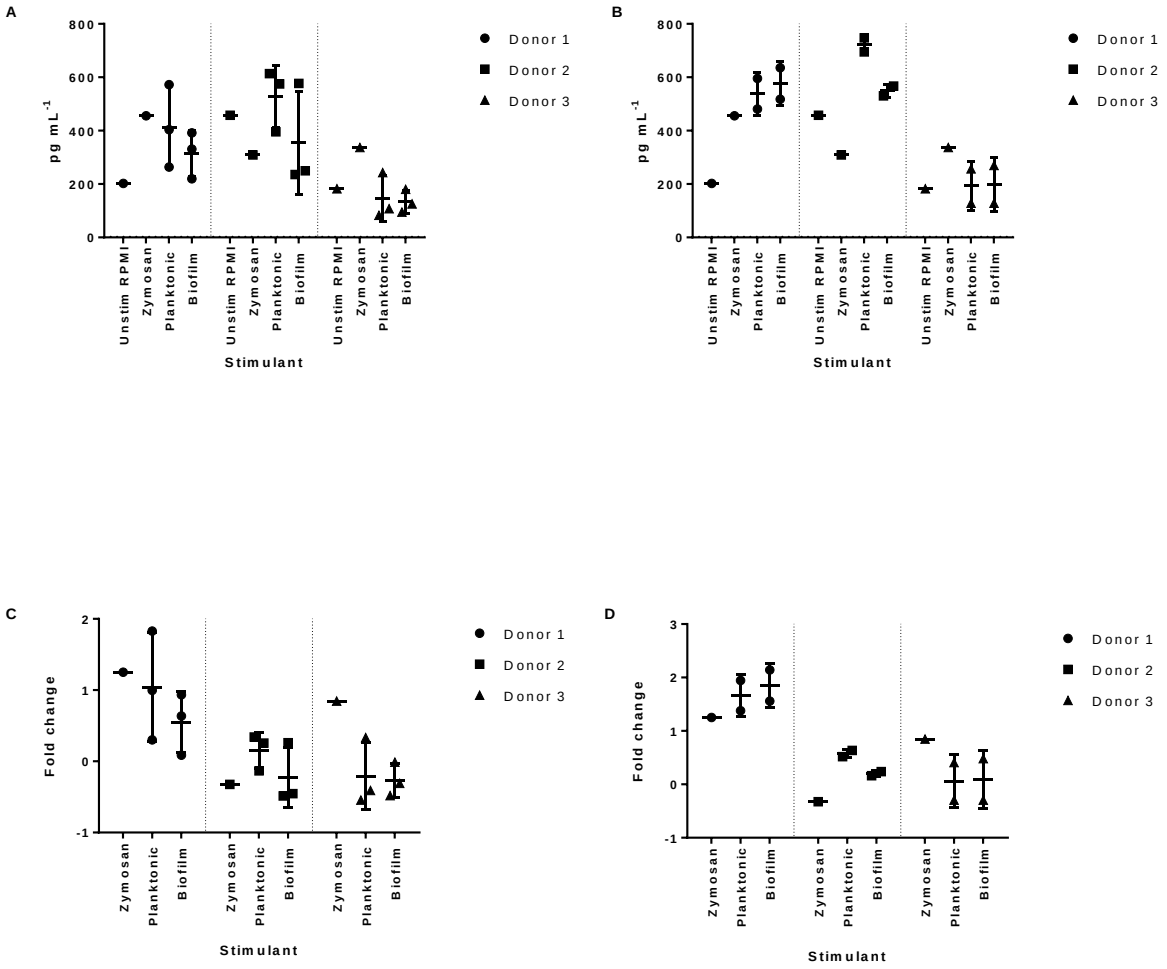


**Figure 4.3.3:** CXCL8 (IL-8) response in whole blood stimulated with carbohydrate extracts from planktonic and biofilm phenotype *M. tuberculosis*. Total secreted CXCL8 (A) and fold change ((stimulant response (pg $mL^{-1}$) / RPMI response (pg $mL^{-1}$) -1) (C) in whole blood after 24h stimulation with x3 biological replicate planktonic *M. tuberculosis* **carbohydrate extracts (10 µg $mL^{-1}$)** and x3 biological replicate biofilm *M. tuberculosis* **carbohydrate extracts (10 µg $mL^{-1}$)**. Total secreted CXCL8 (B) and fold change (D) in whole blood after 24h stimulation with x2 biological replicate planktonic *M. tuberculosis* **carbohydrate extracts (25 µg $mL^{-1}$)** and x2 biological replicate biofilm *M. tuberculosis* **carbohydrate extracts (25 µg $mL^{-1}$)**. Negative control RPMI response (Unstim RPMI), Positive control Zymosan (10 µg $mL^{-1}$). The horizontal dotted line on each graph represents the lower limit of quantitation. Each donor blood stimulation is presented separately by vertical dotted lines. Error bars = standard deviation.

The CCL5 (RANTES) standard curve is shown in **Figure 9.1.4e**. A t-test corrected for multiple comparisons by false discovery rate (Q=5%) determined there was no significant difference in the total secreted CCL5 (pg $mL^{-1}$) induced by *M. tuberculosis* planktonic and biofilm carbohydrate extracts at both 10 μg $mL^{-1}$ and 25 μg $mL^{-1}$ concentrations (**Figure 4.3.4a,b**). All stimulants including Zymosan induced a <1-fold change in CCL5 in each donor (**Figure 4.3.4c,d**). Planktonic *M. tuberculosis* carbohydrate extracts induced on average higher CCL5 secretion than biofilm carbohydrate extracts in donor 2 at 25 μg $mL^{-1}$ stimulant concentration however this was not seen in donors 1 and 3.

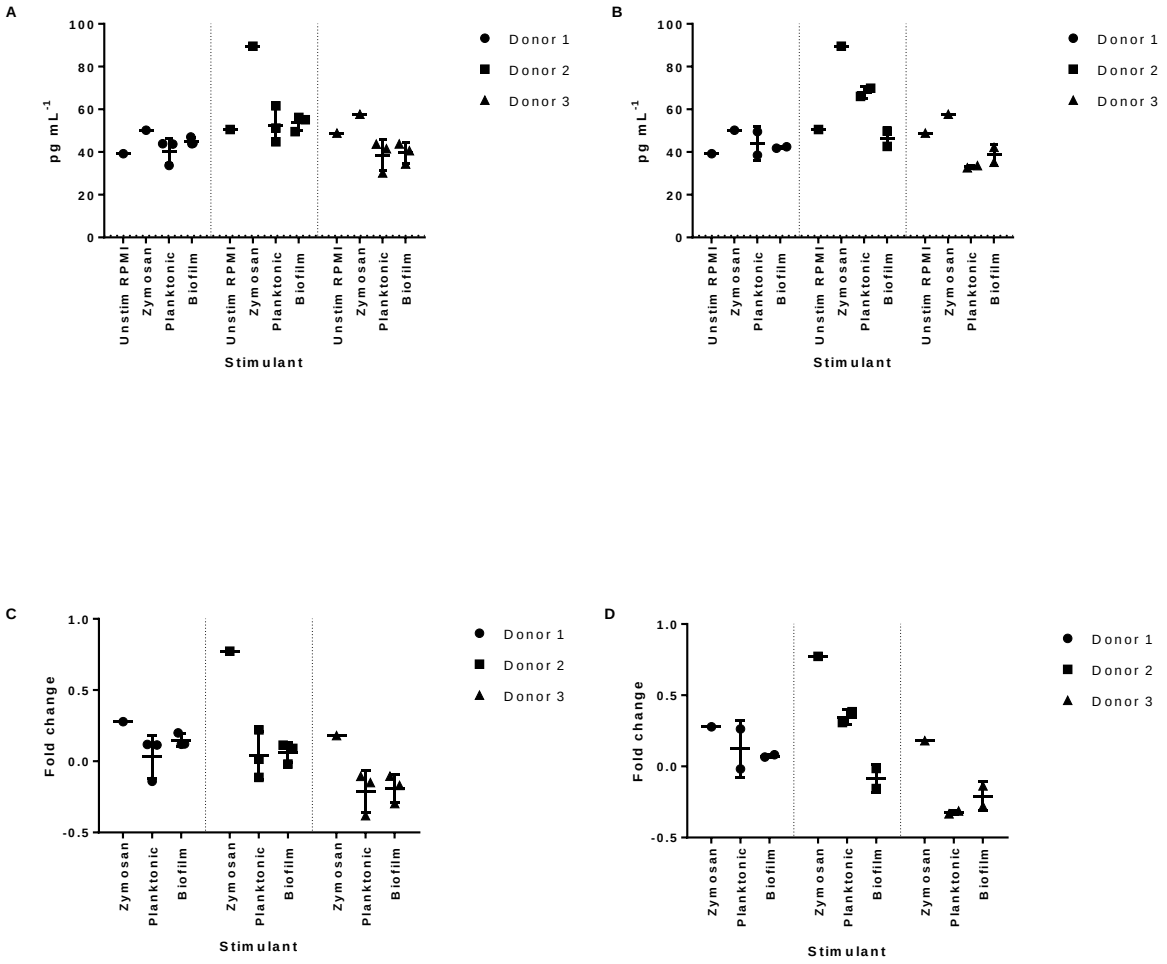


**Figure 4.3.4:** CCL5 (RANTES) response in whole blood stimulated with carbohydrate extracts from planktonic and biofilm phenotype *M. tuberculosis*. Total secreted CCL5 (A) and fold change ((stimulant response (pg $mL^{-1}$) / RPMI response (pg $mL^{-1}$) -1) (C) in whole blood after 24h stimulation with x3 biological replicate planktonic *M. tuberculosis* **carbohydrate extracts (10 µg $mL^{-1}$)** and x3 biological replicate biofilm *M. tuberculosis* **carbohydrate extracts (10 µg $mL^{-1}$)**. Total secreted CCL5 (B) and fold change (D) in whole blood after 24h stimulation with x2 biological replicate planktonic *M. tuberculosis* **carbohydrate extracts (25 µg $mL^{-1}$)** and x2 biological replicate biofilm *M. tuberculosis* **carbohydrate extracts (25 µg $mL^{-1}$)**. Negative control RPMI response (Unstim RPMI), Positive control Zymosan (10 µg $mL^{-1}$). The horizontal dotted line on each graph represents the lower limit of quantitation. Each donor blood stimulation is presented separately by vertical dotted lines. Error bars = standard deviation.

The CXCL1 (GRO-α) standard curve is shown in **Figure 9.1.3b**. A t-test corrected for multiple comparisons by false discovery rate (Q=5%) determined there was no significant difference in the total secreted CXCL1 (pg $mL^{-1}$) induced by *M. tuberculosis* planktonic and biofilm carbohydrate extracts at both 10 μg $mL^{-1}$ and 25 μg $mL^{-1}$ concentrations (**Figure 4.3.5a,b**). However, in donor 1 and donor 2 planktonic *M. tuberculosis* carbohydrates at 25 μg $mL^{-1}$ induced ≈ 1 – 2-fold increase in CXCL1 secretion compared to unstimulated controls while biofilm derived carbohydrates induced < 1-fold change. In donor 3 the planktonic and biofilm carbohydrates were close to or below the LLOQ. The increase in CXCL1 secretion was not observed at 10 μg $mL^{-1}$. Zymosan induced an ≈ 3 – 7-fold increase in CXCL1 secretion (**Figure 4.3.5c,d**). Planktonic *M. tuberculosis* carbohydrate extracts induced on average higher CXCL1 secretion than biofilm carbohydrate extracts in donors 1 and 2 at 25 μg $mL^{-1}$ stimulant concentration however this was not seen in donor 3.

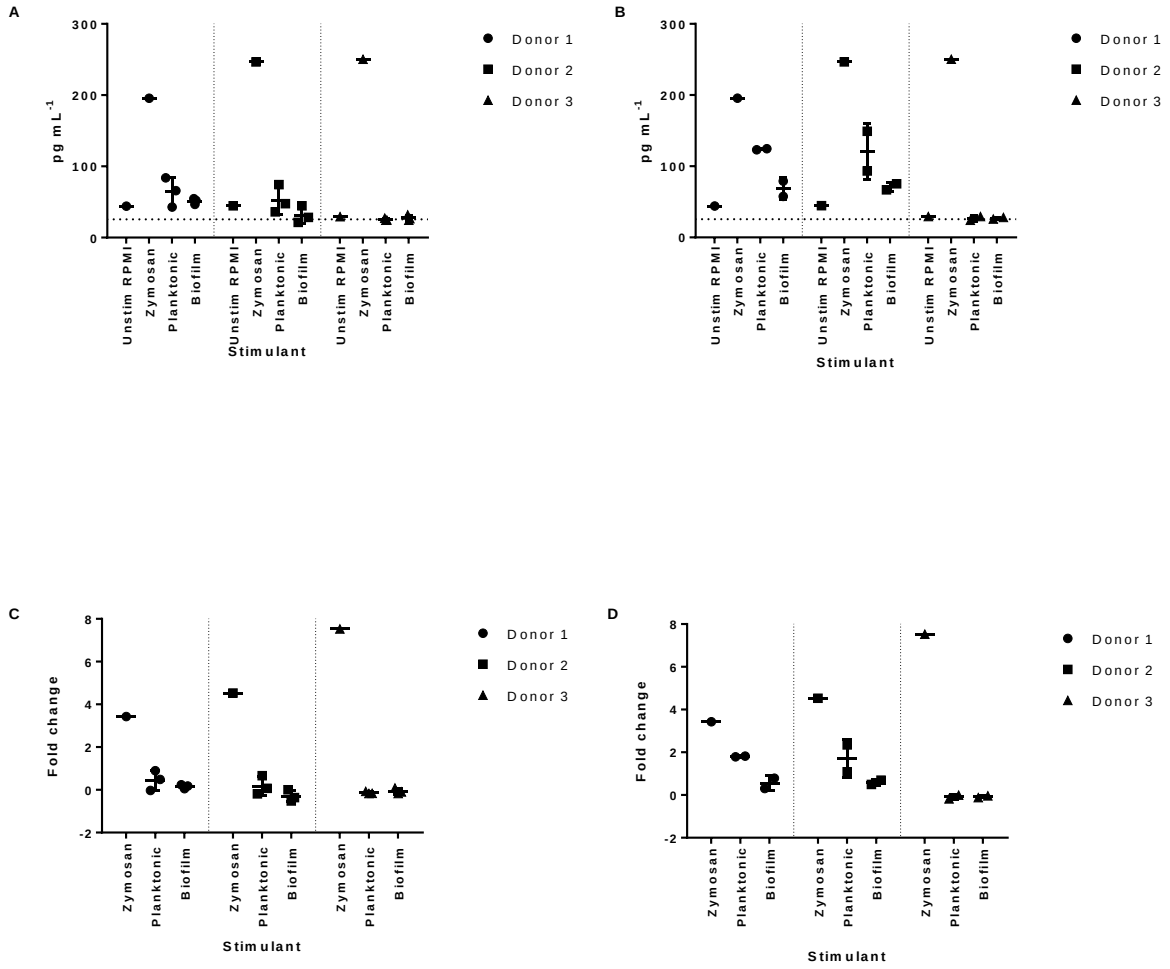


**Figure 4.3.5:** CXCL1 (GRO-α) response in whole blood stimulated with carbohydrate extracts from planktonic and biofilm phenotype *M. tuberculosis*. Total secreted CXCL1 (A) and fold change ((stimulant response (pg $mL^{-1}$) / RPMI response (pg $mL^{-1}$) -1) (C) in whole blood after 24h stimulation with x3 biological replicate planktonic *M. tuberculosis* **carbohydrate extracts (10 µg $mL^{-1}$)** and x3 biological replicate biofilm *M. tuberculosis* **carbohydrate extracts (10 µg $mL^{-1}$)**. Total secreted CXCL1 (B) and fold change (D) in whole blood after 24h stimulation with x2 biological replicate planktonic *M. tuberculosis* **carbohydrate extracts (25 µg $mL^{-1}$)** and x2 biological replicate biofilm *M. tuberculosis* **carbohydrate extracts (25 µg $mL^{-1}$)**. Negative control RPMI response (Unstim RPMI), Positive control Zymosan (10 µg $mL^{-1}$). The horizontal dotted line on each graph represents the lower limit of quantitation. Each donor blood stimulation is presented separately by vertical dotted lines. Error bars = standard deviation.

The IL-6 standard curve is shown in **Figure 9.1.2b**. A t-test corrected for multiple comparisons by false discovery rate (Q=5%) determined there was no significant difference in the total secreted IL-6 (pg $mL^{-1}$) induced by *M. tuberculosis* planktonic and biofilm carbohydrate extracts at both 10 µg $mL^{-1}$ and 25 µg $mL^{-1}$ concentrations (**Figure 4.3.6a,b**). Zymosan induced an IL-6 response between ≈ 45 – 69-fold above control levels in each donor. *M. tuberculosis* planktonic carbohydrates induced a ≈ 0 – 3-fold increase at 10 µg $mL^{-1}$ and a 0 – 24-fold increase in secreted IL-6, with the highest secretion observed in donor 1(**Figure 4.3.6c,d**). *M. tuberculosis* biofilm carbohydrates induced a <1-fold increase in secreted IL-6 at 10 µg $mL^{-1}$ and a 0 – 3-fold increase at 25 µg $mL^{-1}$ with the highest secretion observed in donor 1. The higher IL-6 production induced by stimulation of whole blood with planktonic carbohydrate extracts compared to biofilm carbohydrate extracts in donor 1 was not observed in the other two donors. Planktonic *M. tuberculosis* carbohydrate extracts induced on average higher IL-6 secretion than biofilm carbohydrate extracts in donor 1 at 25 µg $mL^{-1}$ stimulant concentration however this was not seen in donors 2 and 3.

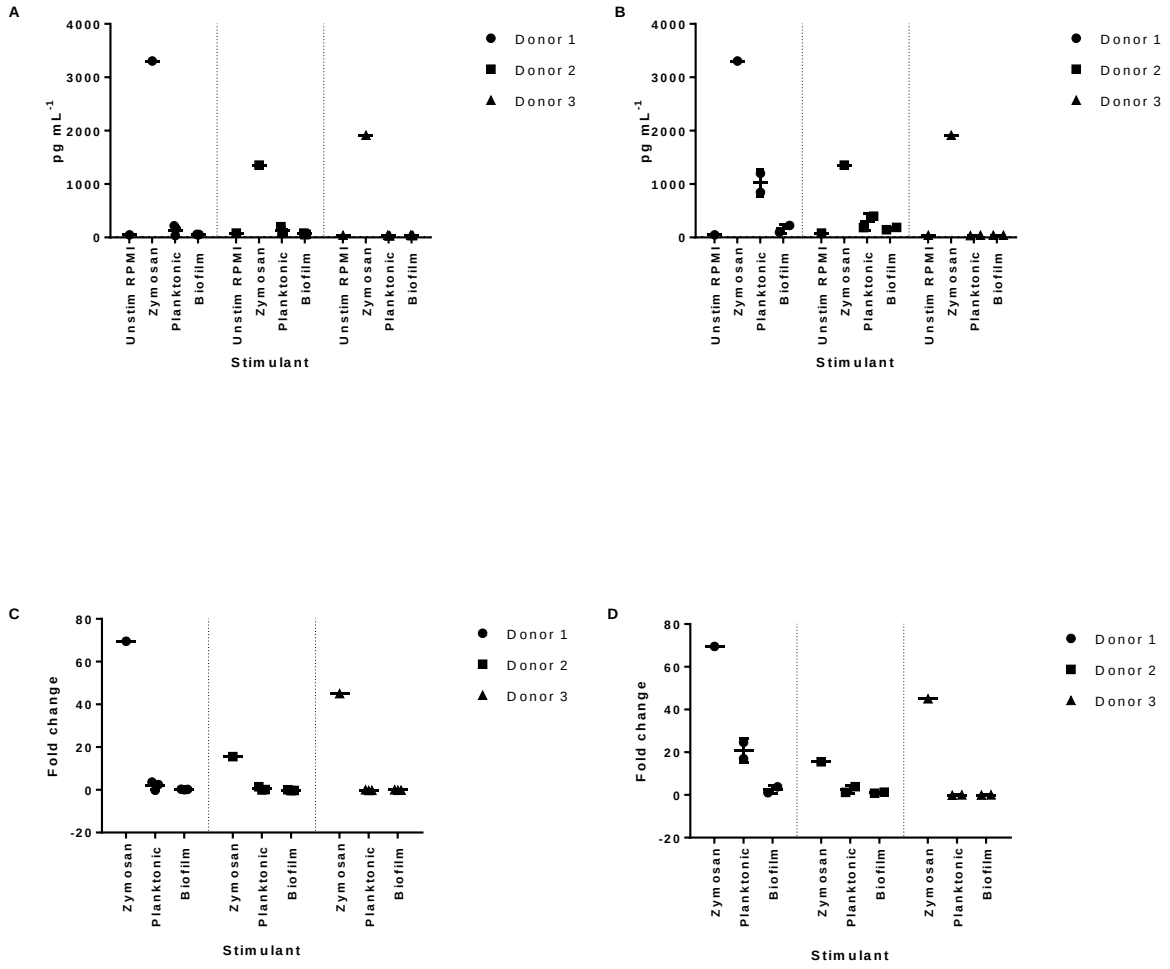


**Figure 4.3.6:** IL-6 response in whole blood stimulated with carbohydrate extracts from planktonic and biofilm phenotype *M. tuberculosis*. Total secreted IL-6 (A) and fold change ((stimulant response (pg $mL^{-1}$) / RPMI response (pg $mL^{-1}$) -1) (C) in whole blood after 24h stimulation with x3 biological replicate planktonic *M. tuberculosis* **carbohydrate extracts (10 µg $mL^{-1}$)** and x3 biological replicate biofilm *M. tuberculosis* **carbohydrate extracts (10 µg $mL^{-1}$)**. Total secreted IL-6 (B) and fold change (D) in whole blood after 24h stimulation with x2 biological replicate planktonic *M. tuberculosis* **carbohydrate extracts (25 µg $mL^{-1}$)** and x2 biological replicate biofilm *M. tuberculosis* **carbohydrate extracts (25 µg $mL^{-1}$)**. Negative control RPMI response (Unstim RPMI), Positive control Zymosan (10 µg $mL^{-1}$). The horizontal dotted line on each graph represents the lower limit of quantitation. Each donor blood stimulation is presented separately by vertical dotted lines. Error bars = standard deviation.

The IFN-γ standard curve is shown in **Figure 9.1.1a.** A t-test corrected for multiple comparisons by false discovery rate (Q=5%) determined there was no significant difference in the total secreted IFN-γ (pg $mL^{-1}$) induced by *M. tuberculosis* planktonic and biofilm carbohydrate extracts (stimulants) at both 10 µg $mL^{-1}$ and 25 µg $mL^{-1}$ concentrations (**Figure 4.3.7a,b**) Zymosan induced an IFN-γ response between ≈ 1 to 6-fold above control levels in each donor. *M. tuberculosis* carbohydrates induced a negligible < 1-fold change in secreted IFN-γ irrespective of the concentration used (**Figure 4.3.7c,d**).

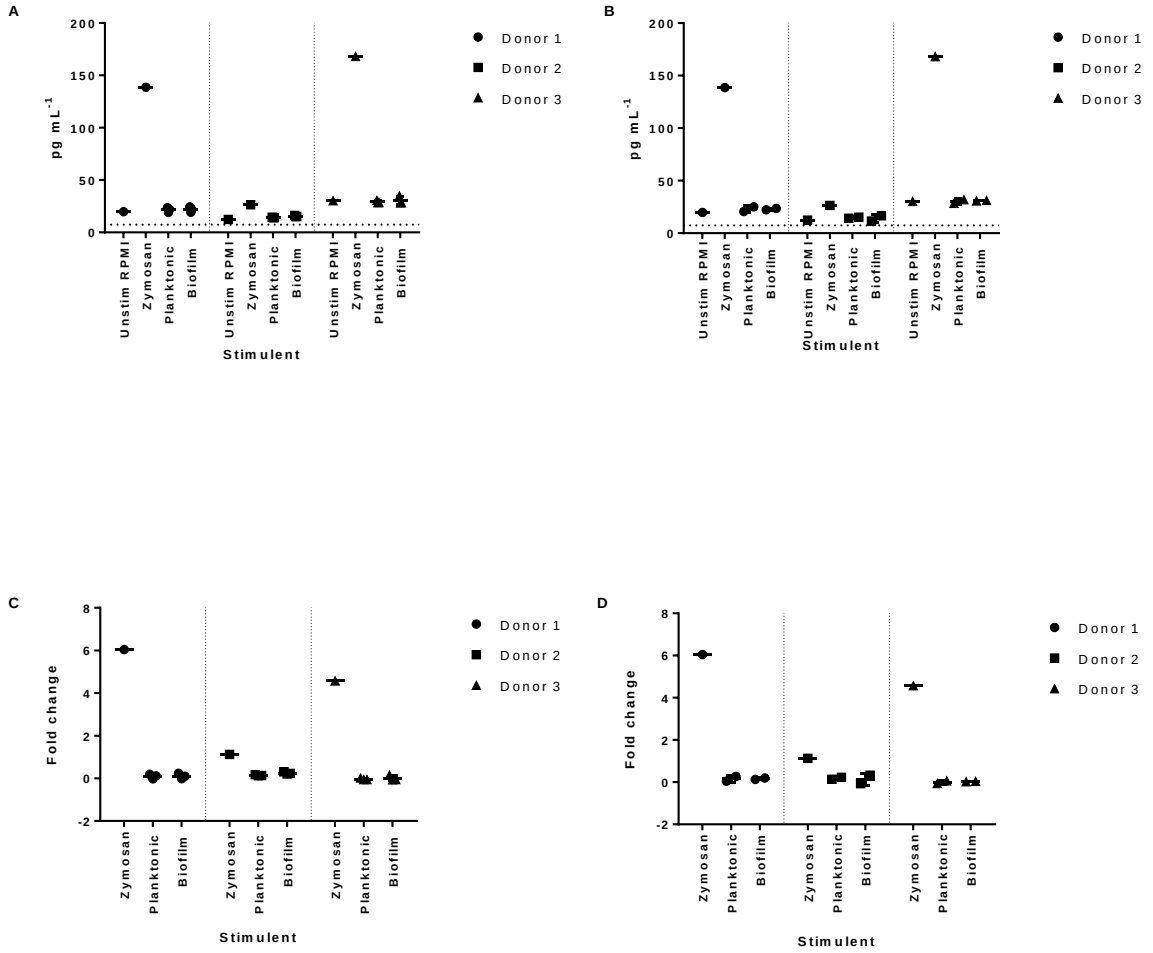


**Figure 4.3.7:** IFN-γ response in whole blood stimulated with carbohydrate extracts from planktonic and biofilm phenotype *M. tuberculosis*. Total secreted IFN-γ (A) and fold change ((stimulant response (pg $mL^{-1}$) / RPMI response (pg $mL^{-1}$) -1) (C) in whole blood after 24h stimulation with x3 biological replicate planktonic *M. tuberculosis* **carbohydrate extracts (10 µg $mL^{-1}$)** and x3 biological replicate biofilm *M. tuberculosis* **carbohydrate extracts (10 µg $mL^{-1}$)**. Total secreted IFN-γ (B) and fold change (D) in whole blood after 24h stimulation with x2 biological replicate planktonic *M. tuberculosis* **carbohydrate extracts (25 µg $mL^{-1}$)** and x2 biological replicate biofilm *M. tuberculosis* **carbohydrate extracts (25 µg $mL^{-1}$)**. Negative control RPMI response (Unstim RPMI), Positive control Zymosan (10 µg $mL^{-1}$). The horizontal dotted line on each graph represents the lower limit of quantitation. Each donor blood stimulation is presented separately by vertical dotted lines. Error bars = standard deviation.

The IL-1β standard curve is shown in **Figure 9.1.1c**. A t-test corrected for multiple comparisons by false discovery rate (Q=5%) determined there was no significant difference in the total secreted IL-1β (pg $mL^{-1}$) induced by *M. tuberculosis* planktonic and biofilm carbohydrate extracts at both 10 µg $mL^{-1}$ and 25 µg $mL^{-1}$ concentrations (**Figure 4.3.8a,b**). Zymosan induced an IL-1β response between ≈ 200 – 400-fold above control levels in each donor. *M. tuberculosis* planktonic carbohydrates induced a variable ≈ 0 – 12-fold increase at 10 µg $mL^{-1}$ and a 0 – 91-fold increase in secreted IL-1β, with the highest secretion observed in donor 1(**Figure 4.3.8c,d**). *M. tuberculosis* biofilm carbohydrates induced a 0 – 1-fold increase in secreted IL-1β at 10 µg $mL^{-1}$ and a 0 – 17-fold increase at 25 µg $mL^{-1}$ with the highest secretion observed in donor 1.

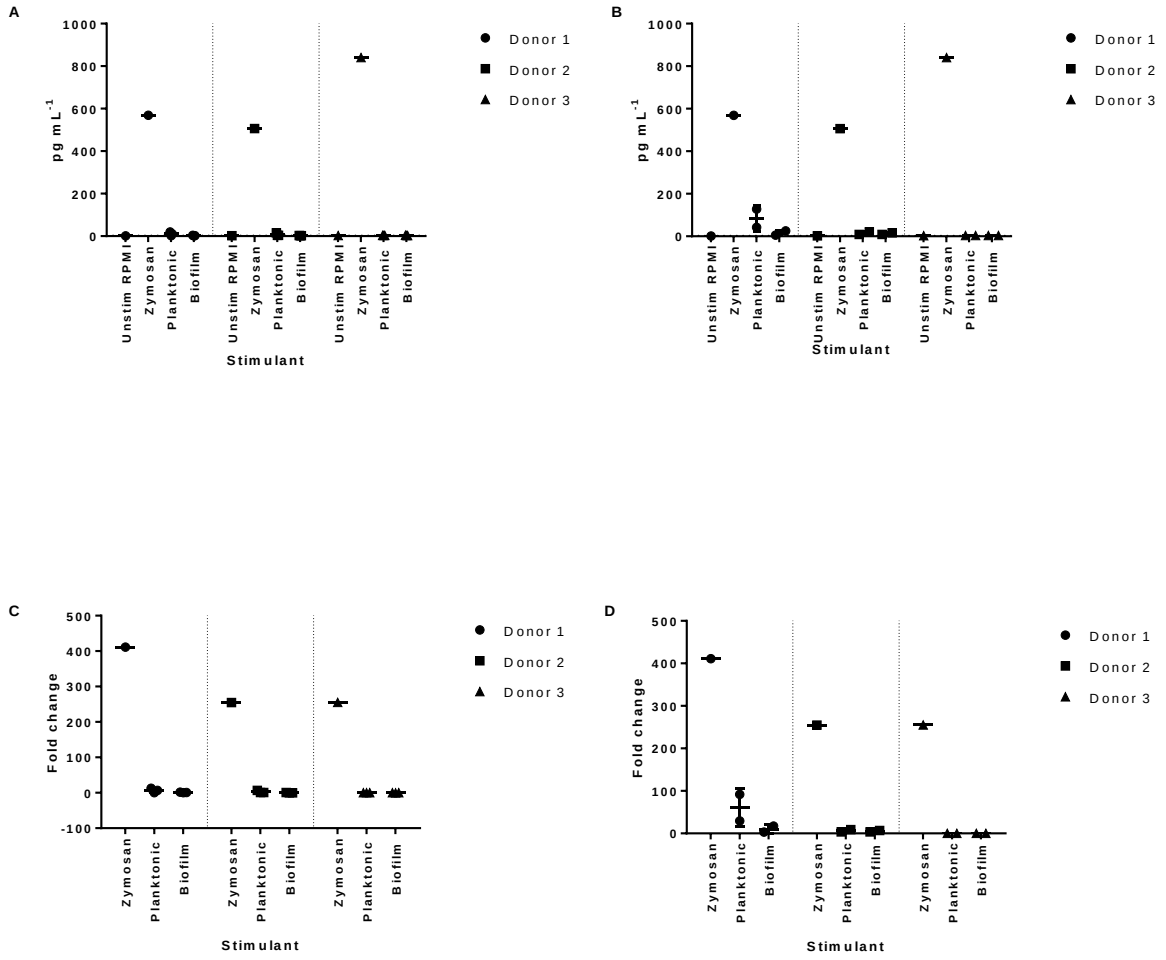


**Figure 4.3.8:** IL-1β response in whole blood stimulated with carbohydrate extracts from planktonic and biofilm phenotype *M. tuberculosis*. Total secreted IL-1β (A) and fold change ((stimulant response (pg $mL^{-1}$) / RPMI response (pg $mL^{-1}$) -1) (C) in whole blood after 24h stimulation with x3 biological replicate planktonic *M. tuberculosis* **carbohydrate extracts (10 µg $mL^{-1}$)** and x3 biological replicate biofilm *M. tuberculosis* **carbohydrate extracts (10 µg $mL^{-1}$)**. Total secreted IL-1β (B) and fold change (D) in whole blood after 24h stimulation with x2 biological replicate planktonic *M. tuberculosis* **carbohydrate extracts (25 µg $mL^{-1}$)** and x2 biological replicate biofilm *M. tuberculosis* **carbohydrate extracts (25 µg $mL^{-1}$)**. Negative control RPMI response (Unstim RPMI), Positive control Zymosan (10 µg $mL^{-1}$). The horizontal dotted line on each graph represents the lower limit of quantitation. Each donor blood stimulation is presented separately by vertical dotted lines. Error bars = standard deviation.

The IL-2 standard curve is shown in **Figure 9.1.1d**. A t-test corrected for multiple comparisons by false discovery rate (Q=5%) determined there was no significant difference in the total secreted IL-2 (pg $mL^{-1}$) induced by *M. tuberculosis* planktonic and biofilm carbohydrate extracts at both 10 µg $mL^{-1}$ and 25 µg $mL^{-1}$ concentrations (**Figure 4.3.9a,b**). All samples, including zymosan induced an IL-2 response between >1-fold above control levels in each donor (**Figure 4.3.9c,d**).

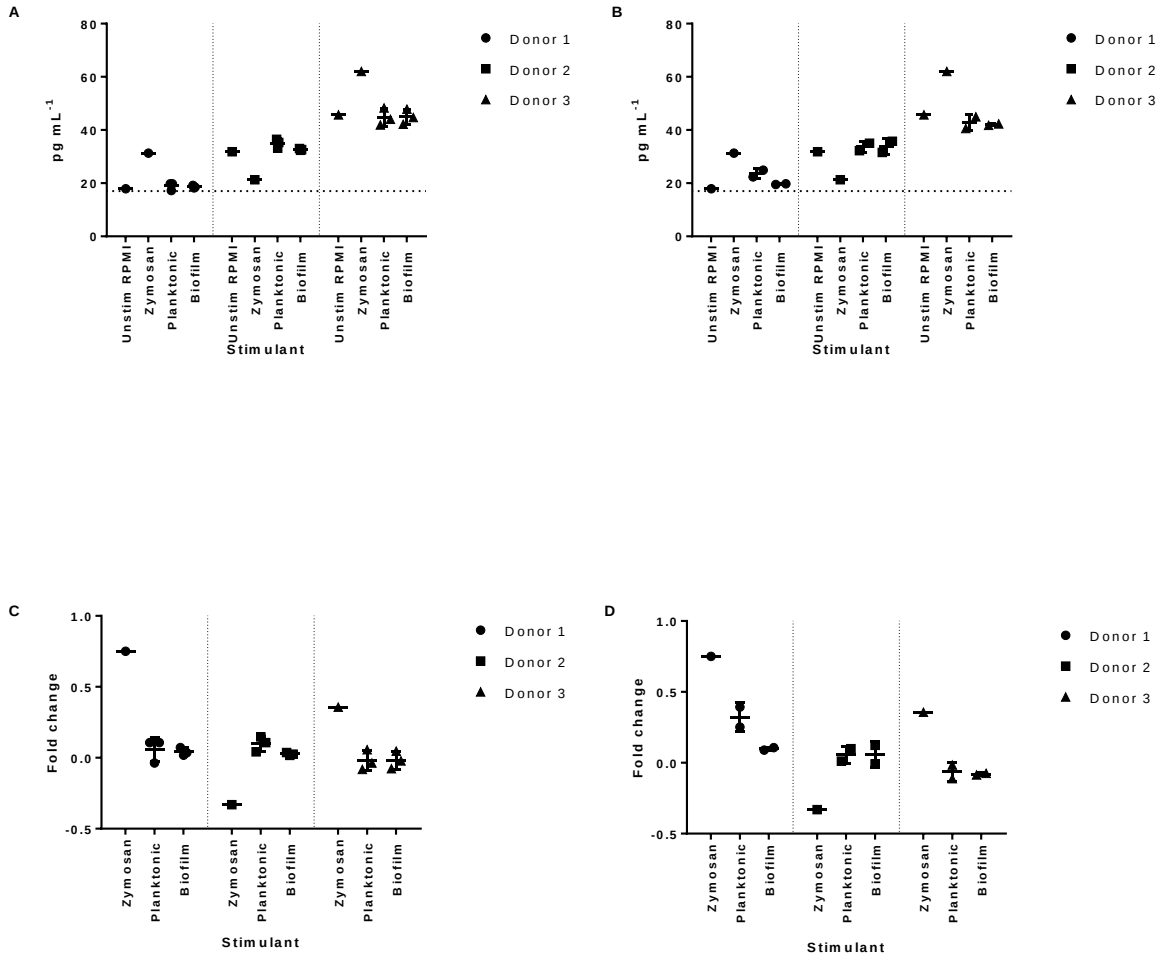


**Figure 4.3.9:** IL-2 response in whole blood stimulated with carbohydrate extracts from planktonic and biofilm phenotype *M. tuberculosis*. Total secreted IL-2 (A) and fold change ((stimulant response (pg $mL^{-1}$) / RPMI response (pg $mL^{-1}$) -1) (C) in whole blood after 24h stimulation with x3 biological replicate planktonic *M. tuberculosis* **carbohydrate extracts (10 µg $mL^{-1}$)** and x3 biological replicate biofilm *M. tuberculosis* **carbohydrate extracts (10 µg $mL^{-1}$)**. Total secreted IL-2 (B) and fold change (D) in whole blood after 24h stimulation with x2 biological replicate planktonic *M. tuberculosis* **carbohydrate extracts (25 µg $mL^{-1}$)** and x2 biological replicate biofilm *M. tuberculosis* **carbohydrate extracts (25 µg $mL^{-1}$)**. Negative control RPMI response (Unstim RPMI), Positive control Zymosan (10 µg $mL^{-1}$). The horizontal dotted line on each graph represents the lower limit of quantitation. Each donor blood stimulation is presented separately by vertical dotted lines. Error bars = standard deviation.

The TNFα standard curve is shown in **Figure 9.1.2c**. A t-test corrected for multiple comparisons by false discovery rate (Q=5%) determined there was no significant difference in the total secreted TNFα (pg $mL^{-1}$) induced by *M. tuberculosis* planktonic and biofilm carbohydrate extracts at both 10 µg $mL^{-1}$ and 25 µg $mL^{-1}$ concentrations (**Figure 4.3.10a,b**). Zymosan induced a TNFα response between ≈ 66 – 76-fold above control levels in each donor. *M. tuberculosis* planktonic carbohydrates induced a ≈ 0 – 2-fold increase at 10 µg $mL^{-1}$ and a 0 – 14-fold increase at 25 µg $mL^{-1}$ in secreted TNFα, with the highest secretion observed in donor 1(**Figure 4.3.10c,d**). *M. tuberculosis* biofilm carbohydrates induced a <1-fold increase in secreted IL-6 at 10 µg $mL^{-1}$ and a 0 – 11-fold increase at 25 µg $mL^{-1}$ with the highest secretion observed in donor 1.

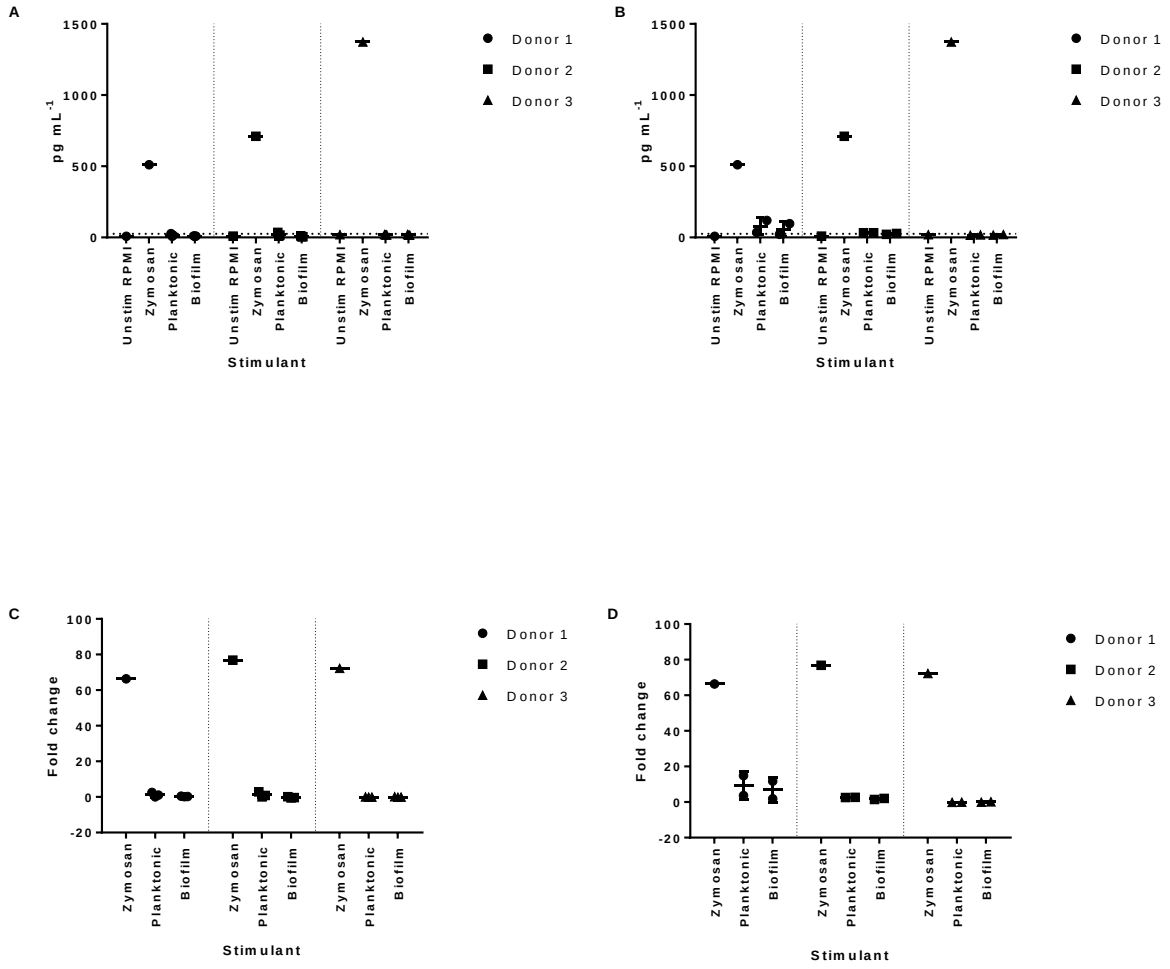


**Figure 4.3.10:** TNFα response in whole blood stimulated with carbohydrate extracts from planktonic and biofilm phenotype *M. tuberculosis*. Total secreted TNFα (A) and fold change ((stimulant response (pg $mL^{-1}$) / RPMI response (pg $mL^{-1}$) -1) (C) in whole blood after 24h stimulation with x3 biological replicate planktonic *M. tuberculosis* **carbohydrate extracts (10 µg $mL^{-1}$)** and x3 biological replicate biofilm *M. tuberculosis* **carbohydrate extracts (10 µg $mL^{-1}$)**. Total secreted TNFα (B) and fold change (D) in whole blood after 24h stimulation with x2 biological replicate planktonic *M. tuberculosis* **carbohydrate extracts (25 µg $mL^{-1}$)** and x2 biological replicate biofilm *M. tuberculosis* **carbohydrate extracts (25 µg $mL^{-1}$)**. Negative control RPMI response (Unstim RPMI), Positive control Zymosan (10 µg $mL^{-1}$). The horizontal dotted line on each graph represents the lower limit of quantitation. Each donor blood stimulation is presented separately by vertical dotted lines. Error bars = standard deviation.

The IL-18 standard curve is shown in **Figure 9.1.2e**. A t-test corrected for multiple comparisons by false discovery rate (Q=5%) determined there was no significant difference in the total secreted IL-18 (pg $mL^{-1}$) induced by *M. tuberculosis* planktonic and biofilm carbohydrate extracts at both 10 µg $mL^{-1}$ and 25 µg $mL^{-1}$ concentrations (**Figure 4.3.11a,b**). Zymosan induced an IL-18 response between ≈ 0 – 1-fold above control levels in each donor. All *M. tuberculosis* carbohydrate samples induce <1-fold change in IL-18 secretion (**Figure 4.3.11c,d**).

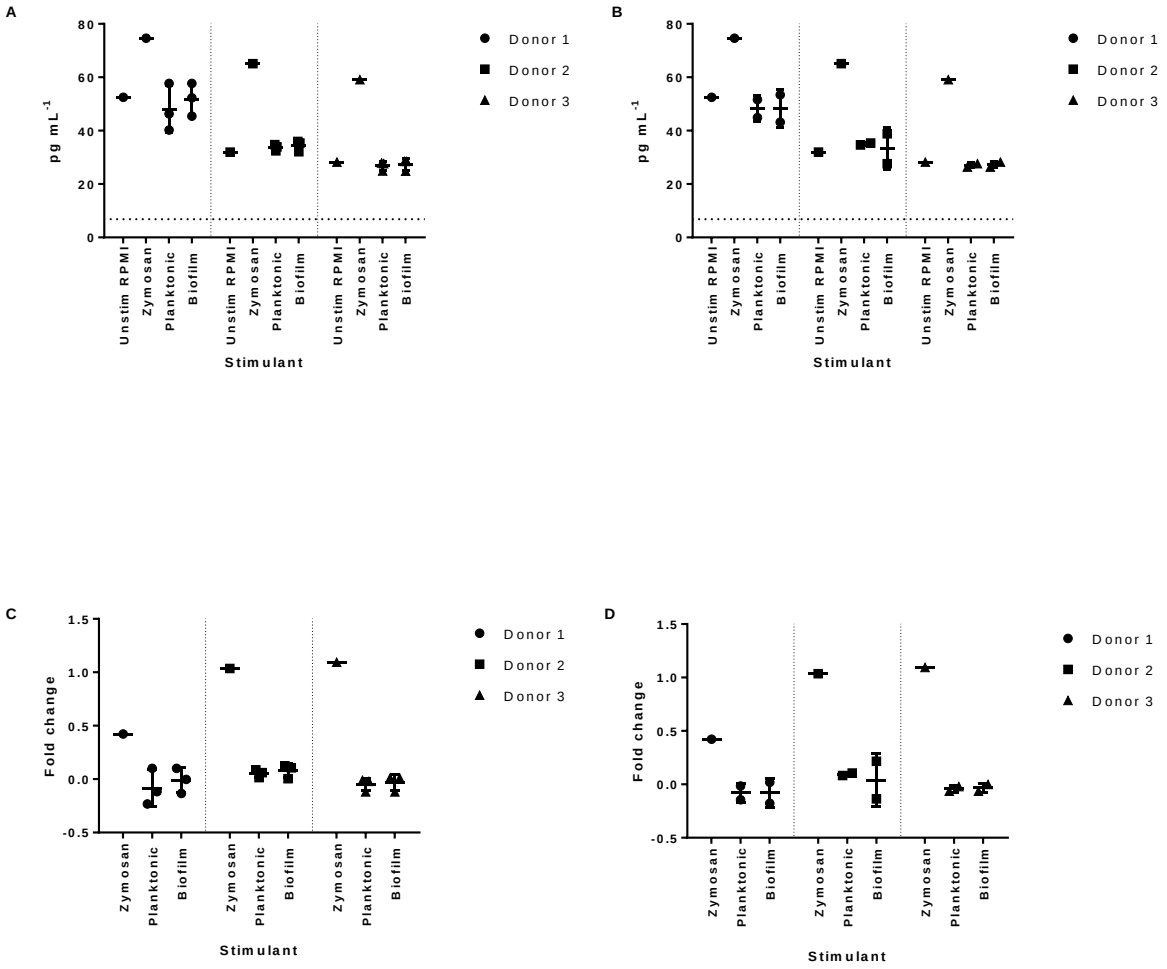


**Figure 4.3.11:** IL-18 response in whole blood stimulated with carbohydrate extracts from planktonic and biofilm phenotype *M. tuberculosis*. Total secreted IL-18 (A) and fold change ((stimulant response (pg $mL^{-1}$) / RPMI response (pg $mL^{-1}$) -1) (C) in whole blood after 24h stimulation with x3 biological replicate planktonic *M. tuberculosis* **carbohydrate extracts (10 µg $mL^{-1}$)** and x3 biological replicate biofilm *M. tuberculosis* **carbohydrate extracts (10 µg $mL^{-1}$)**. Total secreted IL-18 (B) and fold change (D) in whole blood after 24h stimulation with x2 biological replicate planktonic *M. tuberculosis* **carbohydrate extracts (25 µg $mL^{-1}$)** and x2 biological replicate biofilm *M. tuberculosis* **carbohydrate extracts (25 µg $mL^{-1}$)**. Negative control RPMI response (Unstim RPMI), Positive control Zymosan (10 µg $mL^{-1}$). The horizontal dotted line on each graph represents the lower limit of quantitation. Each donor blood stimulation is presented separately by vertical dotted lines. Error bars = standard deviation.

The CCL11 (Eotaxin) standard curve is shown in **Figure 9.1.3a**. A t-test corrected for multiple comparisons by false discovery rate (Q=5%) determined there was no significant difference in the total secreted CCL11 (pg $mL^{-1}$) induced by *M. tuberculosis* planktonic and biofilm carbohydrate extracts at both 10 μg $mL^{-1}$ and 25 μg $mL^{-1}$ concentrations (**Figure 4.3.12a,b**). All blood stimulants induced a <1-fold change in CCL11 secretion. (**Figure 4.3.12c,d**).

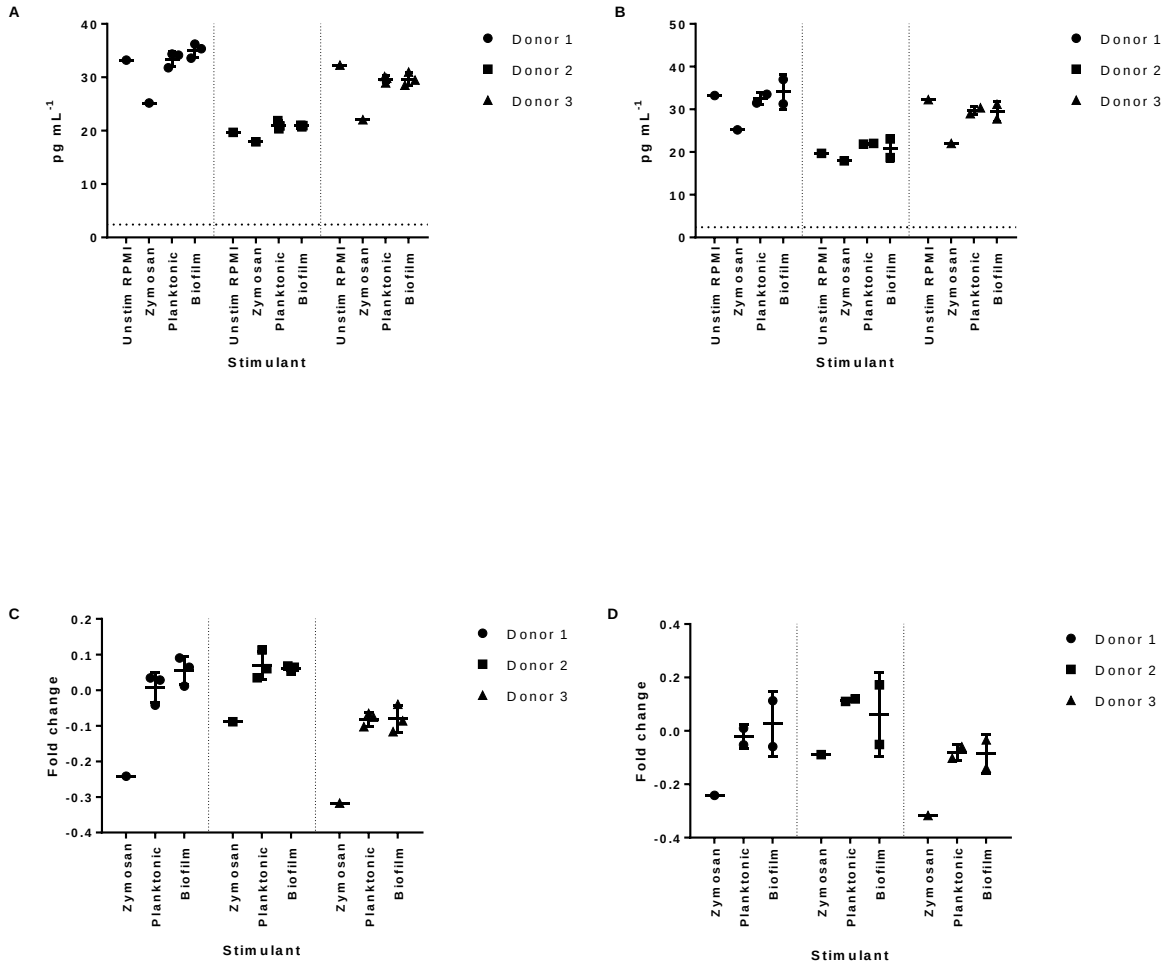


**Figure 4.3.12:** CCL11 (Eotaxin) response in whole blood stimulated with carbohydrate extracts from planktonic and biofilm phenotype *M. tuberculosis*. Total secreted CCL11 (A) and fold change ((stimulant response (pg $mL^{-1}$) / RPMI response (pg $mL^{-1}$) -1) (C) in whole blood after 24h stimulation with x3 biological replicate planktonic *M. tuberculosis* **carbohydrate extracts (10 µg $mL^{-1}$)** and x3 biological replicate biofilm *M. tuberculosis* **carbohydrate extracts (10 µg $mL^{-1}$)**. Total secreted CCL11 (B) and fold change (D) in whole blood after 24h stimulation with x2 biological replicate planktonic *M. tuberculosis* **carbohydrate extracts (25 µg $mL^{-1}$)** and x2 biological replicate biofilm *M. tuberculosis* **carbohydrate extracts (25 µg $mL^{-1}$)**. Negative control RPMI response (Unstim RPMI), Positive control Zymosan (10 µg $mL^{-1}$). The horizontal dotted line on each graph represents the lower limit of quantitation. Each donor blood stimulation is presented separately by vertical dotted lines. Error bars = standard deviation.

The CXCL10 (IP-10) standard curve is shown in **Figure 9.1.3d**. A t-test corrected for multiple comparisons by false discovery rate (Q=5%) determined there was no significant difference in the total secreted CXCL10 (pg $mL^{-1}$) induced by *M. tuberculosis* planktonic and biofilm carbohydrate extracts at both 10 μg $mL^{-1}$ and 25 μg $mL^{-1}$ concentrations (**Figure 4.3.13a,b**). Zymosan induced an ≈ 0 – 2-fold increase in CXCL10 production dependent on donor. While planktonic and biofilm derived carbohydrates induced between 0 – 2 fold increase with the highest level observed in donor 1 after stimulation with one of the biofilm extracts (**Figure 4.3.13c,d)**. Due to the large amount of variation, there was no discernible difference in CXCL10 levels secreted after stimulation with either *M. tuberculosis* planktonic or biofilm carbohydrate.

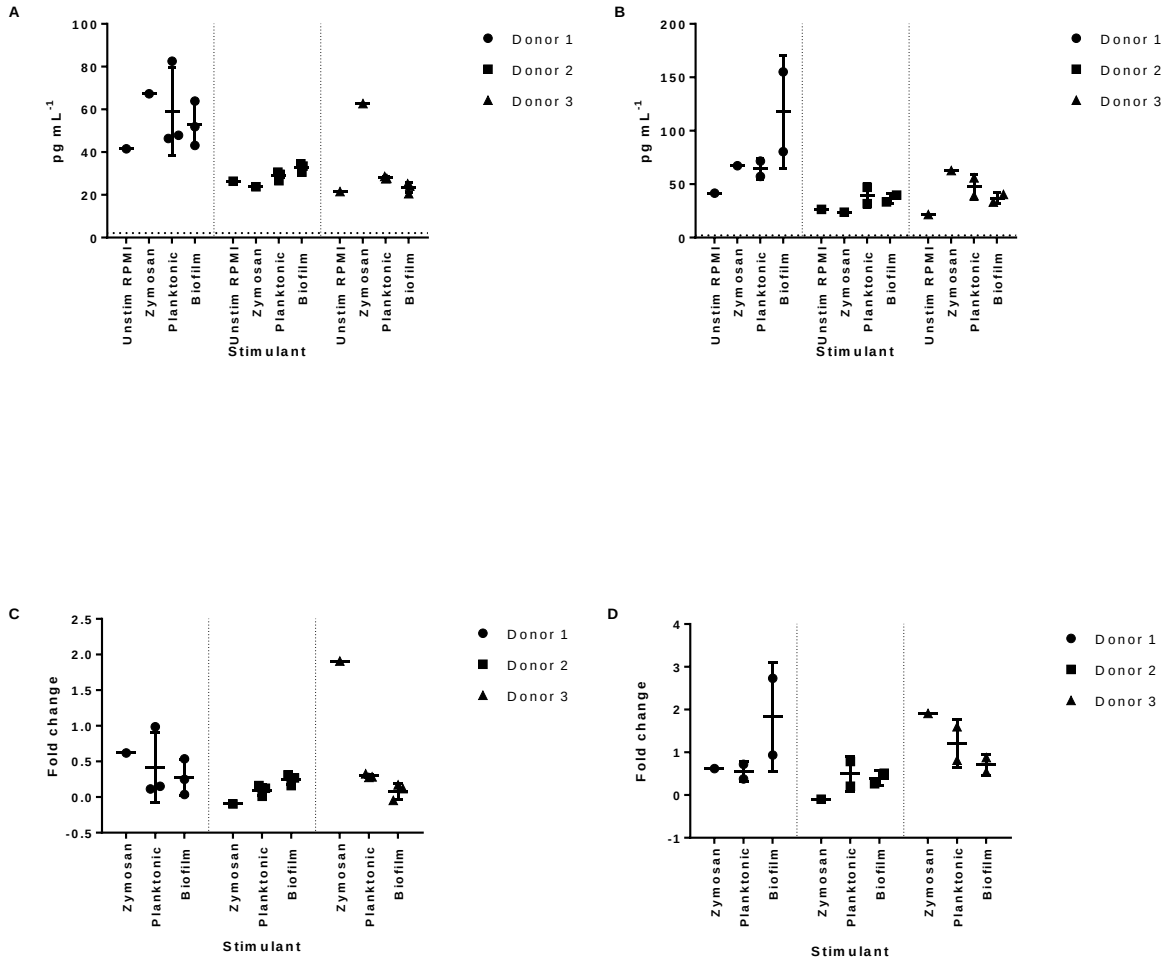


**Figure 4.3.13:** CXCL10 (IP-10) response in whole blood stimulated with carbohydrate extracts from planktonic and biofilm phenotype *M. tuberculosis*. Total secreted CXCL10 (A) and fold change ((stimulant response (pg $mL^{-1}$) / RPMI response (pg $mL^{-1}$) -1) (C) in whole blood after 24h stimulation with x3 biological replicate planktonic *M. tuberculosis* **carbohydrate extracts (10 µg $mL^{-1}$)** and x3 biological replicate biofilm *M. tuberculosis* **carbohydrate extracts (10 µg $mL^{-1}$)**. Total secreted CXCL10 (B) and fold change (D) in whole blood after 24h stimulation with x2 biological replicate planktonic *M. tuberculosis* **carbohydrate extracts (25 µg $mL^{-1}$)** and x2 biological replicate biofilm *M. tuberculosis* **carbohydrate extracts (25 µg $mL^{-1}$)**. Negative control RPMI response (Unstim RPMI), Positive control Zymosan (10 µg $mL^{-1}$). The horizontal dotted line on each graph represents the lower limit of quantitation. Each donor blood stimulation is presented separately by vertical dotted lines. Error bars = standard deviation.

The CCL3 (MIP-1α) standard curve is shown in **Figure 9.1.4a**. A t-test corrected for multiple comparisons by false discovery rate (Q=5%) determined there was no significant difference in the total secreted CCL3 (pg $mL^{-1}$) induced by *M. tuberculosis* planktonic and biofilm carbohydrate extracts at both 10 µg $mL^{-1}$ and 25 µg $mL^{-1}$ concentrations (**Figure 4.3.14a,b**). Zymosan induced an ≈ 6 – 7-fold increase in CCL3 production dependent on donor. There was no discernible difference in CCL3 secretion induced by either planktonic and biofilm derived carbohydrates at 10 µg $mL^{-1}$ with each extract inducing an ≈ 0 – 1 fold change (**Figure 4.3.14c**). This was also the case at the higher carbohydrate concentration (25 µg $mL^{-1}$) apart from in donor 1 where planktonic carbohydrate extracts induced an ≈ 3 – 4-fold increase in secreted CCL3 while biofilm derived carbohydrates induced an ≈ 0 – 2-fold increase (**Figure 4.3.14d**). This difference was not replicated in donors 2 and 3.

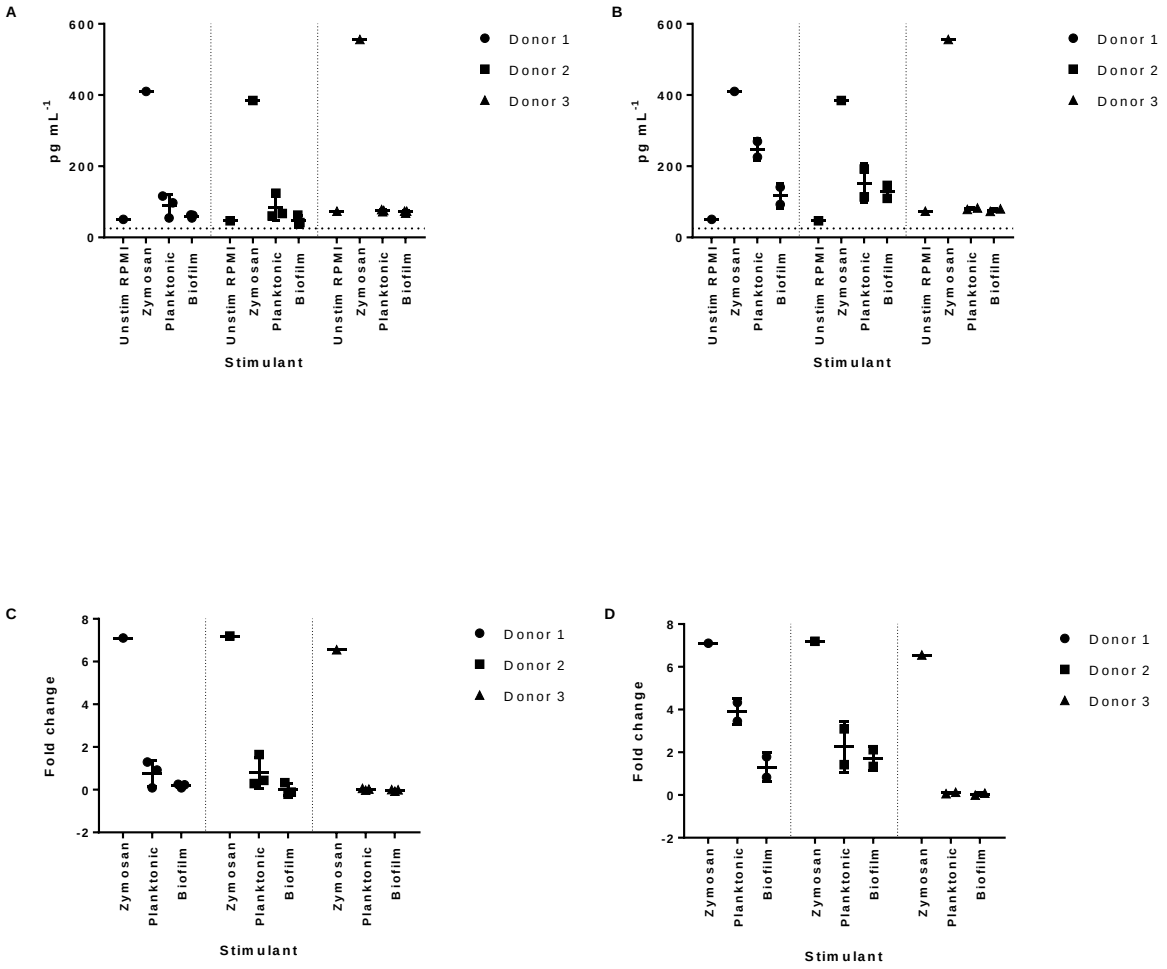


**Figure 4.3.14:** CCL3 (MIP-1α) response in whole blood stimulated with carbohydrate extracts from planktonic and biofilm phenotype *M. tuberculosis*. Total secreted CCL3 (A) and fold change ((stimulant response (pg $mL^{-1}$) / RPMI response (pg $mL^{-1}$) -1) (C) in whole blood after 24h stimulation with x3 biological replicate planktonic *M. tuberculosis* **carbohydrate extracts (10 µg $mL^{-1}$)** and x3 biological replicate biofilm *M. tuberculosis* **carbohydrate extracts (10 µg $mL^{-1}$)**. Total secreted CCL3 (B) and fold change (D) in whole blood after 24h stimulation with x2 biological replicate planktonic *M. tuberculosis* **carbohydrate extracts (25 µg $mL^{-1}$)** and x2 biological replicate biofilm *M. tuberculosis* **carbohydrate extracts (25 µg $mL^{-1}$)**. Negative control RPMI response (Unstim RPMI), Positive control Zymosan (10 µg $mL^{-1}$). The horizontal dotted line on each graph represents the lower limit of quantitation. Each donor blood stimulation is presented separately by vertical dotted lines. Error bars = standard deviation.

The CXCL12α (SDF-1α) standard curve is shown in **Figure 9.1.4c**. A t-test corrected for multiple comparisons by false discovery rate (Q=5%) determined there was no significant difference in the total secreted CXCL12α (pg $mL^{-1}$) induced by *M. tuberculosis* planktonic and biofilm carbohydrate extracts at both 10 µg $mL^{-1}$ and 25 µg $mL^{-1}$ concentrations (**Figure 4.3.15a,b**). All stimulants including Zymosan induced a <1-fold change in CXCL12α in each donor (**Figure 4.3.15c,d**).

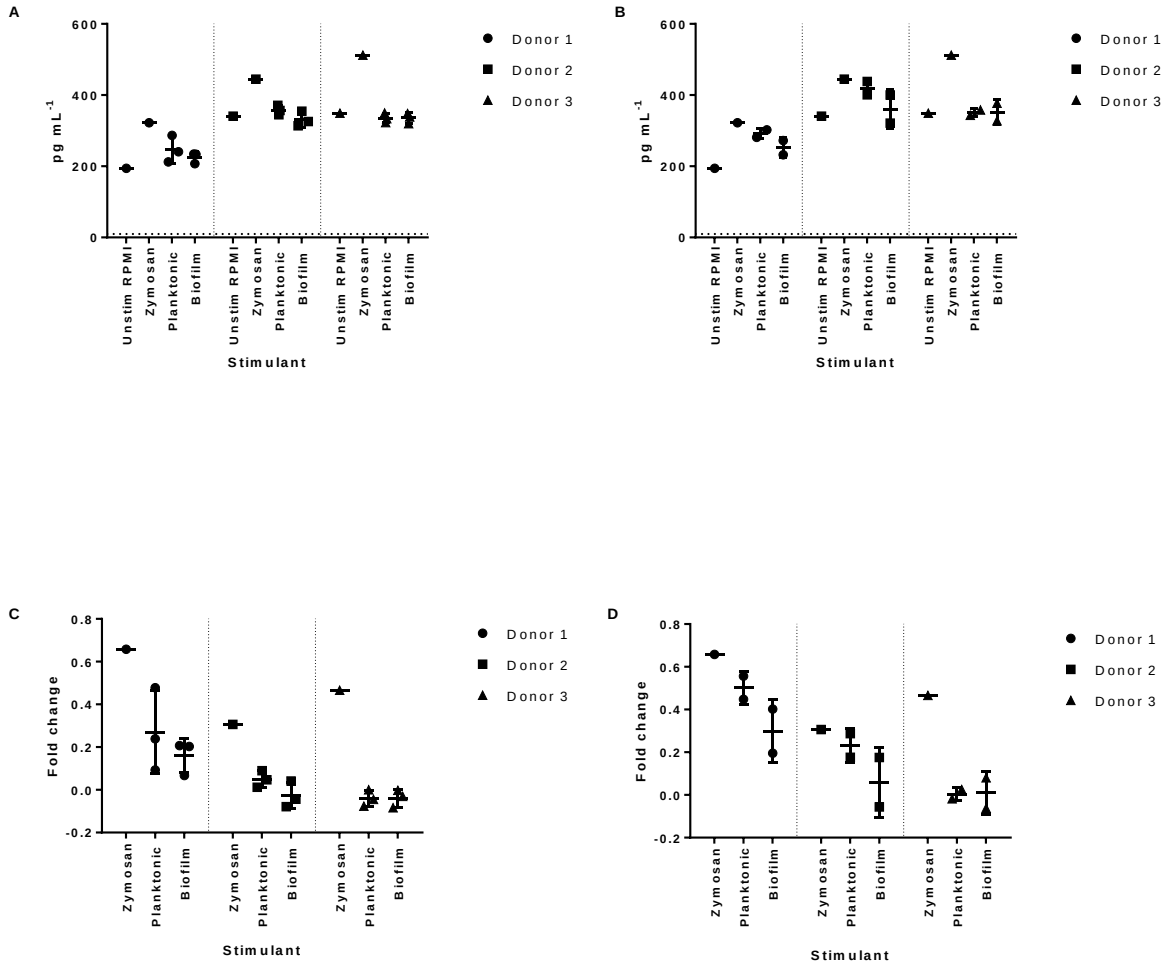


**Figure 4.3.15:** CXCL12α (SDF-1α) response in whole blood stimulated with carbohydrate extracts from planktonic and biofilm phenotype *M. tuberculosis*. Total secreted CXCL12α (A) and fold change ((stimulant response (pg $mL^{-1}$) / RPMI response (pg $mL^{-1}$) -1) (C) in whole blood after 24h stimulation with x3 biological replicate planktonic *M. tuberculosis* **carbohydrate extracts (10 µg $mL^{-1}$)** and x3 biological replicate biofilm *M. tuberculosis* **carbohydrate extracts (10 µg $mL^{-1}$)**. Total secreted CXCL12α (B) and fold change (D) in whole blood after 24h stimulation with x2 biological replicate planktonic *M. tuberculosis* **carbohydrate extracts (25 µg $mL^{-1}$)** and x2 biological replicate biofilm *M. tuberculosis* **carbohydrate extracts (25 µg $mL^{-1}$)**. Negative control RPMI response (Unstim RPMI), Positive control Zymosan (10 µg $mL^{-1}$). The horizontal dotted line on each graph represents the lower limit of quantitation. Each donor blood stimulation is presented separately by vertical dotted lines. Error bars = standard deviation.

The IL-12p70 standard curve is shown in **Figure 9.1.1b**. The 5-parameter logistic regression did not fit well with the observed values at the lower end of the curve resulting in a higher LLOQ. IL-12p70 secreted in blood stimulated with *M. tuberculosis* carbohydrate samples and was below the LLOQ (**Figure 9.2.1**). In addition detectable IL-12p70 induced by zymosan was only above the LLOQ in 1 donor.

The IL-4 standard curve is shown in **Figure 9.1.1e**. In donors 1 and 2 the quantity of secreted IL-4 was below the limit of detection and all stimulants including zymosan induced IL-4 levels <1-fold above control levels in donor 3 (**Figure 9.2.2**).

The IL-5 standard curve is shown in **Figure 9.1.2a**. Similarly to IL-4, IL-5 production was only above the LLOQ after 24h stimulation with Zymosan in donors 1 and 3 while other stimulants and unstimulated controls were below (donors 1 and 2) or clustered around the LLOQ in donor 3 (**Figure 9.2.3**).

The GM-CSF standard curve is shown in **Figure 9.1.2d**. In donors 1 and 2 the quantity of secreted GM-CSF was below the limit of detection for all stimulants. This was also the case for donor 3 apart from zymosan which induced detectable levels of GM-CSF (**Figure 9.2.4**).

The IL-13 standard curve is shown in **Figure 9.1.4d**. In donors 1 and 2 the unstimulated control and planktonic and biofilm stimulants were below the LLOQ. This was also the case for one of the planktonic replicates in donor 3 (**Figure 9.2.5**).

## 4.4 Introduction (Part 2)

The EPS of *M. tuberculosis* biofilms constitutes proteins and lipids in addition to carbohydrates. These may modulate innate immune responses. *M. tuberculosis* pellicle biofilms can be mechanically shaken with glass-beads and filtered to remove the outermost material, referred to as capsule extracts (Ortalo-Magné et al., 1995). This method was performed on planktonic and biofilm phenotype *M. tuberculosis* cultures to obtain the outermost material of both phenotypes. Rather than a broad 20-plex panel, a 4-plex panel measuring IFN-γ, IL-6, CCL-2, and MMP-1 (Matrix metalloproteinase-1) was used.

IFN-γ is essential for *M. tuberculosis* control (O'Garra et al., 2013). Therefore an *M. tuberculosis* phenotype which induced reduced innate IFN-γ secretion in uninfected hosts may be better adapted for establishing infection. IL-6 was chosen in the panel because it has been shown to inhibit IFN-γ secretion in macrophages (Nagabhushanam et al., 2003) and therefore induction of high levels may be beneficial to *M. tuberculosis*. A phenotype which was better able to induce high IL-6 secretion may be better able to establish infection in naïve hosts. CCL2 levels have been shown to correlate with disease severity (Hasan et al., 2009). It has been hypothesised that CCL2 promotes a non-protective response to TB involving inhibition of IL-12 (Flores-Villanueva et al., 2005) (required for induction of a protective IFN-γ response) and recruitment of permissive phagocyte providing *M. tuberculosis* replicative niche (Cambier et al., 2013). Thus an *M. tuberculosis* phenotype that could induce higher CCL2 may be more transmissible. MMP-1 the primary collagenolytic MMP in TB most likely to be responsible for triggering cavitation, which is essential for *M. tuberculosis* transmission (Elkington et al., 2011). Since pellicle biofilms are associated with *M. tuberculosis* cavities (Hunter, 2016), they may contribute to their formation. Therefore, biofilm capsule may also be more potent inducers of MMP-1 than planktonic capsule.

In this experiment, two donors for whole blood instead of three and whole blood was stimulated at a single, higher concentration of 200 μg $mL^{-1}$. This allowed space for extra capsule biological replicates and positive controls. A higher concentration of capsule compared to carbohydrate extract was possible because capsule could be harvested in much higher quantities in a shorter time-span than the carbohydrate extracts. Thus x6 biological replicates of both planktonic and biofilm phenotype *M. tuberculosis* capsule extracts derived from independent cultures, in addition to extra positive controls 12-O-Tetradecanoylphorbol-13-acetate (PMA)/Ionomycin and tuberculin purified protein derivative (PPD) protein were included in the experiment **Table 4.4-1**.

| | Standards | | Donor 1 PIP027 | | | | | Donor 2 PIP004 | | | | |
|---|---|---|---|---|---|---|---|---|---|---|---|---|
| | 1 | 2 | 3 | 4 | 5 | 6 | 7 | 8 | 9 | 10 | 11 | 12 |
| A | Std1 | Std1 | Unstim | PPD | PK4 | BF2 | BF6 | Unstim | PPD | PK4 | BF2 | BF6 |
| B | Std2 | Std2 | Unstim | PPD | PK4 | BF2 | BF6 | Unstim | PPD | PK4 | BF2 | BF6 |
| C | Std3 | Std3 | Unstim RPMI | PK1 | PK5 | BF3 | | Unstim RPMI | PK1 | PK5 | BF3 | |
| D | Std4 | Std4 | Unstim RPMI | PK1 | PK5 | BF3 | | Unstim RPMI | PK1 | PK5 | BF3 | |
| E | Std5 | Std5 | Zy | PK2 | PK6 | BF4 | | Zy | PK2 | PK6 | BF4 | |
| F | Std6 | Std6 | Zy | PK2 | PK6 | BF4 | | Zy | PK2 | PK6 | BF4 | |
| G | Std7 | Std7 | PMA | PK3 | BF1 | BF5 | | PMA | PK3 | BF1 | BF5 | |
| H | Std8 | Std8 | PMA | PK3 | BF1 | BF5 | | PMA | PK3 | BF1 | BF5 | |

**Table 4.4-1:** Whole blood capsule stimulation plate layout. Std, standards; Unstim, unstimulated plasma; Unstim RPMI, plasma stimulated with RPMI 2mM L-glutamine only; Zy, zymosam 50 µg $mL^{-1}$; PMA, 12-O-Tetradecanoylphorbol-13-acetate 4.8 µg $mL^{-1}$ combined with Ionomycin 95 µg $mL^{-1}$; PK1-PK6, planktonic *M. tuberculosis* capsule extracts 200 µg $mL^{-1}$; BF1-BF6 biofilm *M. tuberculosis* carbohydrate extracts 200 µg $mL^{-1}$;

## 4.5 Chapter 4 hypothesis II

Capsule extracts (defined as the *M. tuberculosis* outermost material, which included EPS and was extracted using agitation with glass beads and filtration) of biofilm phenotype *M. tuberculosis* alter innate cytokine (IFN-γ and IL-6), chemokine (CCL2) and MMP-1 protease secretion in whole blood compared to capsule extracts from exponential phase shaken flask planktonic phenotype *M. tuberculosis* cultured in identical medium.

## 4.6 Whole blood stimulation with outermost material extracts from planktonic and biofilm phenotype *M. tuberculosis*.

Capsule extractions from x6 biological replicate *M. tuberculosis* planktonic and biofilm cultures were performed as described in methods section 7.17 and the whole blood stimulation was performed as described in methods section 7.18. Briefly, whole blood from two healthy donors was stimulated for 24 hours with RPMI 2mM L-glutamine only, zymosam (50 μg $mL^{-1}$), PMA/ionomycin (4.8 μg $mL^{-1}$/95 μg $mL^{-1}$); purified protein derivative (PPD) (200 μg $mL^{-1}$) x6 biological replicate planktonic *M. tuberculosis* capsule extracts or x6 biological replicate biofilm *M. tuberculosis* capsule extracts (200 μg $mL^{-1}$).

The standard curve for IFN-γ is given shown in **Figure 9.3.1a** Unstimulated RPMI only controls were below the LLOQ and therefore it was not possible to calculate fold-change in IFN-γ secretion of the stimulants to unstimulated controls level. Instead, since unstimulated controls = ≤ LLOQ, the fold-change to LLOQ (10.8 pg $mL^{-1}$) was calculated. There was no significant difference in the amount of IFN-γ secretion induced by planktonic *M. tuberculosis* capsule extracts compared to biofilm *M. tuberculosis* extracts (t-test corrected for multiple comparisons by false discovery rate (Q=5%). **Figure 4.6.1a** and **Figure 4.6.1c** show the amount of secreted IFN-γ secreted by each stimulant tested (**a),** and with PMA/ionomicin

excluded (**c**). Unlike the previous whole blood stimulation with carbohydrate extracts, Zymosan induced a <1 fold IFN-γ response. PMA/ionomycin induced a 325-fold and 119-fold increase in IFN-γ secretion in donors 1 and 2 respectively. PPD induced a <1-fold and 4-fold increase in IFN-γ secretion in donors 1 and 2. Planktonic *M. tuberculosis* capsule extracts induced a 0 – 20-fold increase with the highest levels in donor 2. Biofilm *M. tuberculosis* capsule extracts induced a 0 – 21 fold increase in IFN-γ secretion with the highest levels also in donor 2. **Figure 4.6.1b** and **Figure 4.6.1d** show fold change induced by all stimulants (**b**) and with PMA/Ionomycin excluded (**d**).

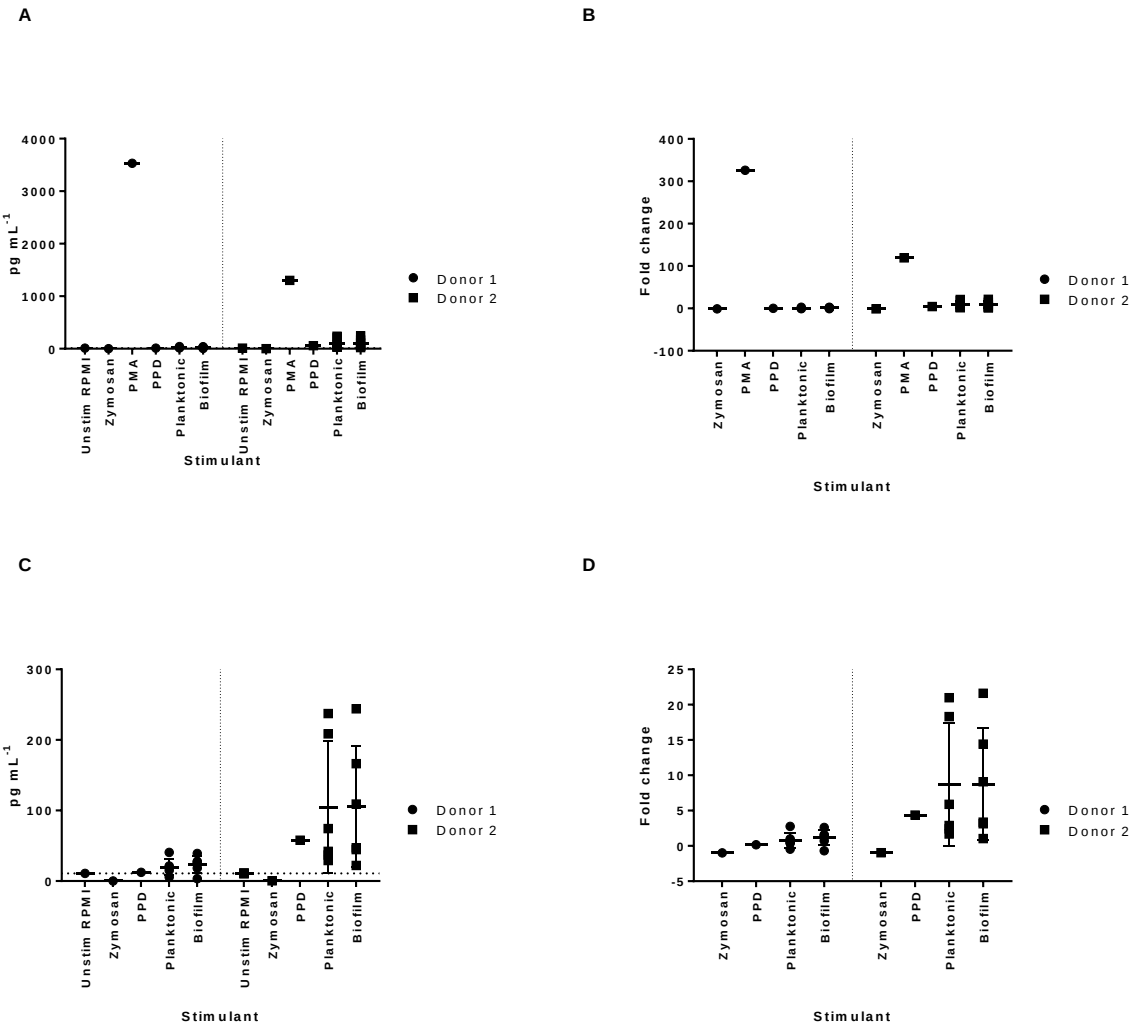


**Figure 4.6.1:** IFN-γ response in whole blood stimulated with capsule extracts from planktonic and biofilm phenotype *M. tuberculosis*. IFN-γ response in whole blood stimulated with capsule extracts from planktonic and biofilm phenotype *M. tuberculosis*. Total secreted IFN-γ (A) and fold change ((stimulant response (pg $mL^{-1}$) / RPMI response (pg $mL^{-1}$) -1) (B) in whole blood after 24h stimulation with medium only (Unstim RPMI), Zymosan (50 µg $mL^{-1}$), PMA/Ionomycin (4.8 µg $mL^{-1}$/95 µg $mL^{-1}$), PPD (200 µg $mL^{-1}$), x6 biological replicate planktonic *M. tuberculosis* capsule extracts (200 µg $mL^{-1}$) and x6 biological replicate biofilm *M. tuberculosis* carbohydrate extracts (200 µg $mL^{-1}$). Total secreted IFN-γ (C) and fold change (D) with PMA/Ionomycin excluded. The horizontal dotted line on each graph represents the lower limit of quantitation. Each donor blood stimulation is presented separately by vertical dotted lines. Error bars are standard deviation.

The standard curve for IL-6 is shown in **Figure 9.3.1b.** There was no significant difference in the amount of IL-6 secretion induced by planktonic *M. tuberculosis* capsule extracts compared to biofilm *M. tuberculosis* extracts (t-test corrected for multiple comparisons by false discovery rate (Q=5%). **Figure 4.6.2a** shows the amount of IL-6 secreted by each stimulant tested. Zymosan induced a 3-fold and 12-fold IL-6 response in donors 1 and 2 respectively. PMA/ionomycin induced a 133-fold and 143-fold increase in IL-6 secretion in donors 1 and 2 respectively. PPD induced a 7-fold and 4-fold increase in IL-6 secretion in donors 1 and 2. Planktonic *M. tuberculosis* capsule extracts induced a 9 – 90-fold increase with the highest levels in donor 2. Biofilm *M. tuberculosis* capsule extracts induced a 10 – 165-fold increase in IL-6 secretion with the highest levels also in donor 2. **Figure 4.6.2b** shows fold change induced by all stimulants.

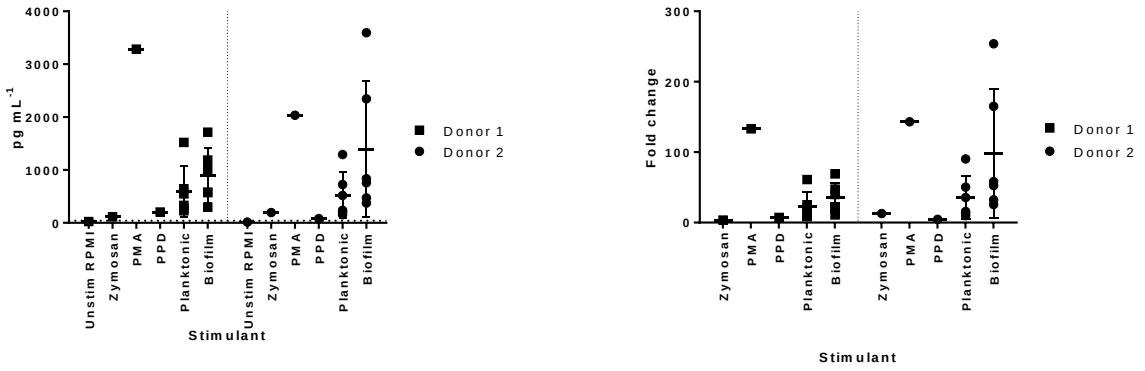


**Figure 4.6.2:** IL-6 response in whole blood stimulated with capsule extracts from planktonic and biofilm phenotype *M. tuberculosis*. Total secreted IL-6 (A) and fold change ((stimulant response (pg $mL^{-1}$) / RPMI response (pg $mL^{-1}$) -1) (B) in whole blood after 24h stimulation with medium only (Unstim RPMI), Zymosan (50 µg $mL^{-1}$), PMA/Ionomycin (4.8 µg $mL^{-1}$/95 µg $mL^{-1}$), PPD (200 µg $mL^{-1}$), x6 biological replicate planktonic *M. tuberculosis* capsule extracts (200 µg $mL^{-1}$) and x6 biological replicate biofilm *M. tuberculosis* carbohydrate extracts (200 µg $mL^{-1}$). The horizontal dotted line on each graph represents the lower limit of quantitation. Each donor blood stimulation is presented separately by vertical dotted lines. Error bars are standard deviation.

The standard curve for CCL2 (MCP-1) is shown in **Figure 9.3.1c.** There was no significant difference in the amount of CCL2 secretion induced by planktonic *M. tuberculosis* capsule extracts compared to biofilm *M. tuberculosis* extracts (t-test corrected for multiple comparisons by false discovery rate (Q=5%). **Figure 4.6.3a** shows the amount of CCl2 secreted by each stimulant tested. Zymosan induced a <1-fold CCL2 response in donors 1 and 2. Likewise PMA/ionomycin induced a <1-fold increase in CCL2 secretion in donors 1 and 2. PPD induced a <1-fold and 1-fold increase in CCL2 secretion in donors 1 and 2 respectively. Planktonic *M. tuberculosis* capsule extracts induced a 0 – 3-fold increase in CCL2 with the highest levels in donor 2. Biofilm *M. tuberculosis* capsule extracts induced a 0 – 1-fold increase in CCL2 secretion with the highest levels also in donor 2. **Figure 4.6.3b** shows fold change induced by all stimulants.

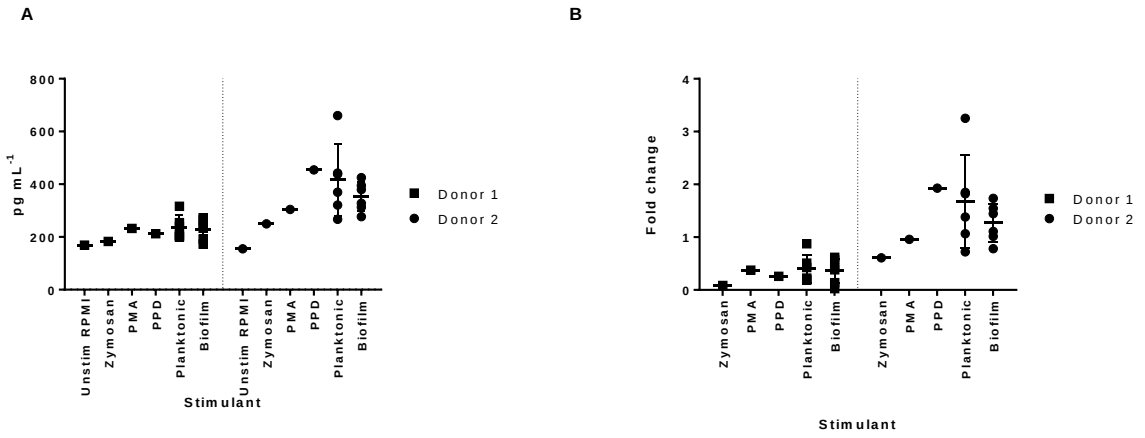


**Figure 4.6.3:** CCL2 (MCP-1) response in whole blood stimulated with capsule extracts from planktonic and biofilm phenotype *M. tuberculosis*. Total secreted CCL2 (A) and fold change ((stimulant response (pg $mL^{-1}$) / RPMI response (pg $mL^{-1}$) -1) (B) in whole blood after 24h stimulation with medium only (Unstim RPMI), Zymosan (50 µg $mL^{-1}$), PMA/Ionomycin (4.8 µg $mL^{-1}$/95 µg $mL^{-1}$), PPD (200 µg $mL^{-1}$), x6 biological replicate planktonic *M. tuberculosis* capsule extracts (200 µg $mL^{-1}$) and x6 biological replicate biofilm *M. tuberculosis* carbohydrate extracts (200 µg $mL^{-1}$). The horizontal dotted line on each graph represents the lower limit of quantitation. Each donor blood stimulation is presented separately by vertical dotted lines. Error bars are standard deviation.

The standard curve for MMP-1 is shown in **Figure 9.3.1d.** There was no significant difference in the amount of MMP-1 secretion induced by planktonic *M. tuberculosis* capsule extracts compared to biofilm *M. tuberculosis* extracts (t-test corrected for multiple comparisons by false discovery rate (Q=5%). **Figure 4.6.4a** and **Figure 4.6.4c** show the amount of secreted IFN-γ secreted by each stimulant tested (**a**)**,** and with PMA/ionomycin excluded (**c**). Zymosan induced a <1 fold MMP-1 response in both donors. PMA/ionomycin induced a 3-fold and 7-fold increase in MMP-1 secretion in donors 1 and 2 respectively. PPD induced a <1-fold increase in MMP-1 secretion in donors 1 and 2. Both planktonic and biofilm *M. tuberculosis* capsule extracts induced a <1-fold increase in both donors. **Figure 4.6.4b** and **Figure 4.6.4d** show fold change induced by all stimulants (**b**) and with PMA/ionomycin excluded (**d**).

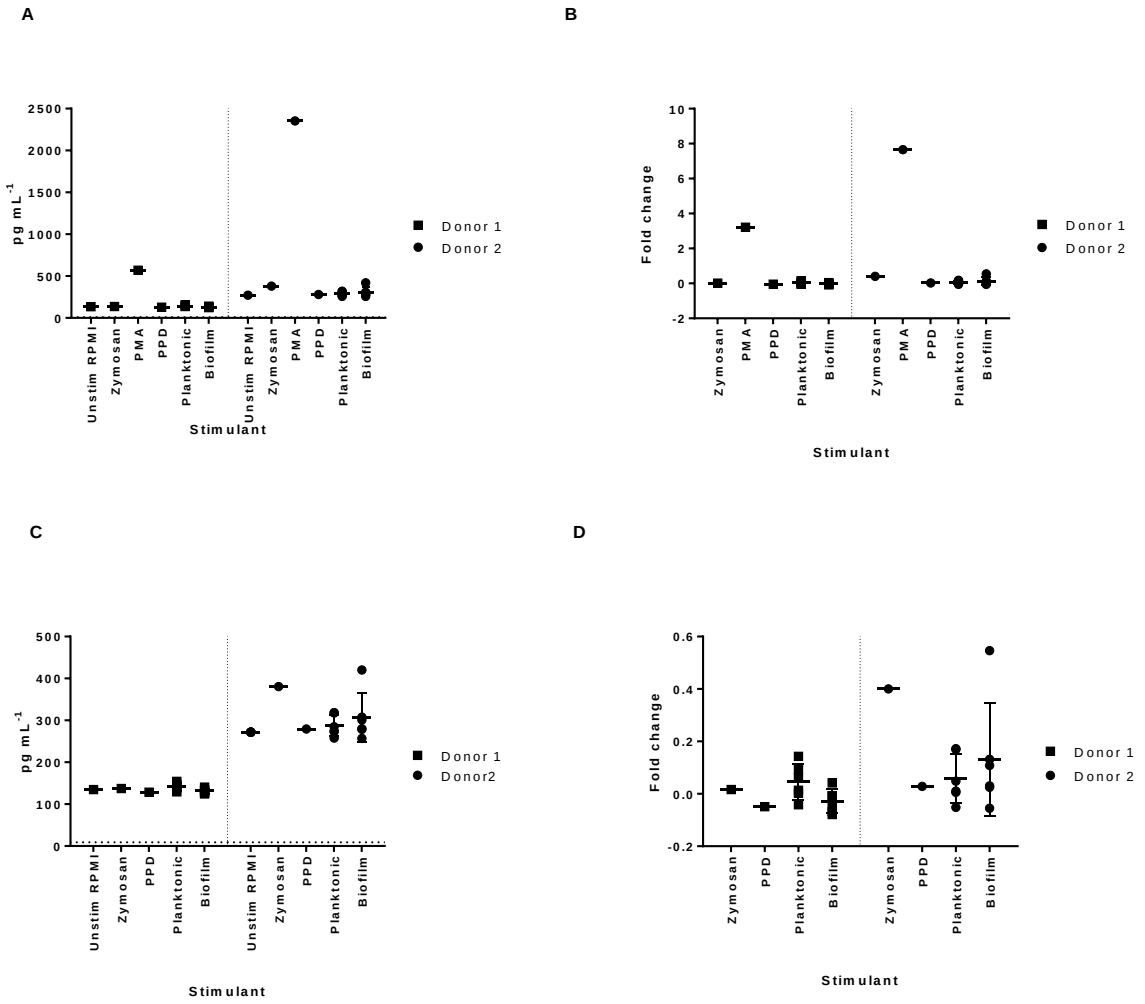


**Figure 4.6.4:** MMP-1 response in whole blood stimulated with capsule extracts from planktonic and biofilm phenotype *M. tuberculosis*. Total secreted MMP-1 (A) and fold change ((stimulant response (pg $mL^{-1}$) / RPMI response (pg $mL^{-1}$) -1) (B) in whole blood after 24h stimulation with medium only (Unstim RPMI), Zymosan (50 µg $mL^{-1}$), PMA/Ionomycin (4.8 µg $mL^{-1}$/95 µg $mL^{-1}$), PPD (200 µg $mL^{-1}$), x6 biological replicate planktonic *M. tuberculosis* capsule extracts (200 µg $mL^{-1}$) and x6 biological replicate biofilm *M. tuberculosis* carbohydrate extracts (200 µg $mL^{-1}$). Total secreted MMP-1 (C) and fold change (D) with PMA/Ionomycin excluded. The horizontal dotted line on each graph represents the lower limit of quantitation. Each donor blood stimulation is presented separately by vertical dotted lines. Error bars are standard deviation.

## 4.7 Technical discussion

To summarise the results presented in this chapter, there were no significant differences in cytokine and chemokine responses to planktonic and biofilm phenotype *M. tuberculosis* carbohydrate/lipoglycan extracts. Generally, the higher carbohydrate concentration was the greater the cytokine/chemokine responses. The cytokines that showed the most consistent high expression above control levels when stimulated with the highest concentration of carbohydrate extract (25 μg $mL^{-1}$) were IL-1β, TNFα and IL-6 yet none of these cytokines showed a >1-fold change across all replicates and donors. 25 μg $mL^{-1}$ planktonic *M. tuberculosis* carbohydrate extract induced the highest response measured in the experiment, which was IL-1β (92-fold) yet this magnitude of response was not consistently seen between biological replicates or donors. Capsule extracts were used to stimulate whole blood at a higher concentration than the carbohydrate extracts (200 μg $mL^{-1}$) but no significant differences were found in the amount of secreted IFN-γ, IL-6, CCL2 and MMP-1 between planktonic and biofilm phenotypes. Only IL-6 secretion was induced by *M. tuberculosis* capsule extracts consistently in both donors at >1-fold above control levels, with the highest response (254-fold) induced by biofilm capsule in whole blood from donor 2.

Despite the evidence presented in chapter 3 of an altered carbohydrate profile of biofilm phenotype *M. tuberculosis* compared to planktonic *M. tuberculosis*, the results of the whole blood stimulation using carbohydrate extracts described in section 4.3 showed no evidence that these different phenotypes alter the innate immune response in whole blood. Analyses of 20 different cytokines and chemokines in three different healthy BCG vaccinated donor blood samples were measured. The variation between donors was more apparent than any variation in innate response due to *M tuberculosis* phenotype. This could be due potential confounding factors such as the length of time between BCG vaccination and the whole blood stimulation, recent exposure to environmental mycobacteria or polymorphisms in genes responsible

expression of baseline levels of cytokines/chemokines. *M. tuberculosis* carbohydrates behaved markedly similar in all analytes tested, with no significant differences between planktonic and biofilm phenotypes after correcting for multiple comparisons with a 5% false discovery rate. In several cytokines: IL-12p70, IL-4, IL-5, GM-CSF and IL-13 the response generated was below the LLOQ in most donors. This could be because *M. tuberculosis* carbohydrate extract do not trigger secretion of these cytokines or because the concentration of carbohydrate extract was sub-optimal to maximise the response. In many cases the amount of secreted cytokine/chemokine was greater at the higher concentration (25 $\mu g\ mL^{-1}$) than the lower concentration (10 $\mu g\ mL^{-1}$). If the response generated is linear in relation to stimulant concentration then stimulating whole blood with carbohydrate extracts at higher concentrations may permit greater discrimination between phenotype.

The whole blood stimulations could be optimised by harvesting a larger sample size of biological replicate carbohydrate extracts and stimulating whole blood with a broader range of concentrations. The gel analyses of lipoglycan extractions showed variation in the proportions of LAM and LM (**Figure 3.4.1** and **Figure 3.4.2**) which could have a larger impact on immunomodulation than the changes in α-glucan which couldn't be detected on the gel, given the immunomodulatory properties of these lipoglycans (Mishra et al., 2011).

The whole blood stimulation was based on an established protocol (Thurm and Halsey, 2005). For multiplex analysis, harvested plasma was filtered before running the assay since past experience revealed that unfiltered plasma blocked the instrument. This approach has been recommended in a paper published on immunoassay prerequisites for optimised multiplex analysis for clinical trials (de Jager et al., 2009). Given the sub-optimal response of some cytokines measured, further work is required to identify a positive control for the carbohydrate experiment. A good candidate would be PMA/ionomycin, which produced strong responses in all conditions tested with capsule extracts (see section 4.6). Multiple

optimisation experiments could be set-up to determine incubation period and titres of carbohydrate extract required for a measurable response. To perform this further work using multiplex kits would be prohibitively expensive however, kits for single cytokines or chemokines are available commercially and this approach could be coupled with use of a cell line instead of whole blood, such as THP-1 monocytes for preliminary work. However, optimal concentrations and incubation times for one cytokine/chemokine may be sub-optimal for another, and the response generated by a cell line may vary considerably from the response with whole blood. Additionally performing multiple optimisation experiments would require regular donation of blood and therefore if whole blood was used, experiments would need to test many conditions in a single experiment to reduce the number of donations required.

The results of the whole blood stimulation assays showed significant variation in cytokine response between donors and highlights the importance of measuring cytokine responses from multiple donors. Commercial pooled human whole blood is available for purchase and would be a useful alternative to testing separate donors, especially if the pool was large. It would also permit a greater proportion of tests to be dedicated to comparing planktonic and biofilm extract biological replicates and/or additional concentrations of carbohydrate samples instead of different donors. Finally, the results may be more reproducible if stimulations were performed on large pools of healthy donors available from a specified supplier.

Following optimisation with an immortal cell line or pooled whole blood, a primary cell line such as human lung alveolar macrophages or brochoalveolar lavage may better recapitulate the *in vivo* environment to which biofilm phenotype *M. tuberculosis* may encounter after expectoration from tuberculosis cavities and would therefore be the logical choice for optimised *ex vivo* stimulations in future.

Notably the Zymosan control was used to stimulate whole blood at different concentrations in the carbohydrate whole blood stimulation (10 μg $mL^{-1}$) and capsule whole blood stimulations (50 μg $mL^{-1}$). Yet paradoxically, larger responses were seen in IFN-γ, and IL-6 at the lower concentration in the whole blood stimulation with carbohydrate extracts. With hindsight, the zymosan concentration should have been kept consistent in both experiments after an initial preliminary experiment to determine the optimal concentration for maximum cytokine responses. Preliminary work showed 50 μg $mL^{-1}$ to be optimal (data not shown) and despite how the results are presented in this chapter, the capsule experiment was performed first. This was because the capsule samples were much faster/easier to obtain in larger yields and therefore not as precious. However, for the subsequent carbohydrate whole blood stimulation, the decision was then made to keep the zymosan control at the same concentration as the carbohydrate samples. This allowed for relative comparison of the *M. tuberculosis* carbohydrates to a known proinflammatory stimulant (zymosan) at the same concentration. There was insufficient carbohydrate sample to stimulate with 50 μg $mL^{-1}$. Yet this does not explain why responses were higher for zymosan at the lower concentration. One possibility is that the difference is due to the different blood donors used in the respective experiments and could be addressed by using pooled whole blood. Replicate data with zymosan at a range of concentrations using pooled whole blood would determine the relationship between concentration and response and validate the results for zymosan in both experiments.

The PPD positive control for the capsule stimulation experiment was kept at the same concentration as the capsule extracts and induced broadly similar magnitude responses in IFN-γ, CCL2 and MMP-1 compared to the capsule extracts. Yet it did not induce a large IL-6 response unlike the capsule extracts suggesting it does not share the mycobacterial component responsible for triggering IL-6 secretion **Figure 4.6.2**. Potential candidates for the IL-6 inducing component are evaluated in the general discussion (1).

In chapter 3 changes in the quantities of lipids PDIMs, MK, FFA, FMA and SL-I were found in addition to the changes in carbohydrate extracts. Therefore it would have been a good idea to perform whole blood stimulations with the non-polar and polar planktonic and biofilm *M. tuberculosis* extracts. One issue with these extracts is their solubility in RPMI medium. This could be addressed by performing serial dilutions in the solvent used for TLC analysis e.g. dichloromethane for non-polar lipids. Care should be taken to ensure the vessel is compatible with the solvent. The solvent could then be evaporated-off leaving known quantities of lipid seeded on the bottom of tubes to which pooled whole blood could be added. There would not be a risk of blocking the MAGPIX instrument since after stimulation the plasma would be filtered.

The whole blood stimulation of planktonic and biofilm *M. tuberculosis* capsule extracts utilised a larger number of biological replicates since the extraction method was simply double filtration of bead-treated biomass. There is a possibility that bead treatment ruptured the cell walls of *M. tuberculosis* bacteria leading to the leakage of intracellular material. Notably this has been shown to not be the case with glass bead treated *M. tuberculosis* cells (Ortalo-Magné et al., 1995). To confirm this is not the case with the capsule samples, a commercial glucose-6-phosphate dehydrogenase G6HDH detection assay could be used. The assay would need to compare capsule extracts to lysed *M. tuberculosis*, since G6PDH is an intracellular enzyme often used to confirm the absence of intracellular material from EPS extractions (Nielsen and Jahn, 1999). Some capsule material may also have been retained on the Minisart cellulose acetate filters during extraction. Since both planktonic and biofilms capsule extracts undergo the same treatment this should not significantly skew the results, however a range of filters could be compared by carbohydrate/lipoglycan gel analysis, total sugar analysis and lipid analysis to determine the filter that retains the least capsular material.

Notably cellulose acetate filters are described by suppliers as the most appropriate filters for biological aqueous solutions (Corning, 2011).

Despite the larger sample size and simplified extraction method of capsule extraction, there was a large amount variation in the sample responses within each donor. This is most clearly seen when measuring IL-6 secretion after stimulation with capsule extracts, which produced the largest response compared to other analytes (**Figure 4.6.2**). The source of this variation may be due to the intrinsic heterogeneity of biofilms (Stewart and Franklin, 2008). It is important to bear in mind that even the planktonic cultures clumps may have oxygen/nutrient gradients (Islam et al., 2012). In addition, mycobacteria replicate asymmetrically to produce heterogeneous populations (Kieser and Rubin, 2014). The constituents of the outermost capsular material and EPS surrounding each bacterium may vary dependent on the position of the bacteria within the biofilm. Hence, minor variations in biofilm morphology between replicates could result in differential expression of immunomodulatory macromolecules.

# 5 ANALYSIS OF COMPLEMENT ACTIVATION BY PLANKTONIC AND BIOFILM PHENOTYPE *M. TUBERCULOSIS*

## 5.1 Introduction

In chapter 2 *M. tuberculosis* biofilm EPS was identified by measuring the density of the bacterial population (CFU $g^{-1}$) over time and by direct visualisation using SEM. Furthermore, immuno-gold EM labelling identified this outermost material to contain α(1,2) mannopyranose residues, although there was no significant difference in labelling between planktonic and biofilm phenotype samples. Chapter 3 extended the biochemical analyses and a reduction in the constituent sugar glucose in the non-covalently bound carbohydrate fraction of pellicle biofilm phenotype *M. tuberculosis* was identified. This indicated that the prevalence of exopolysaccharide α-glucan was reduced in pellicle biofilm phenotype *M. tuberculosis* compared to planktonic phenotype *M. tuberculosis*. Chapter 4 investigated whether the carbohydrate changes affected the innate immune response by stimulating whole blood with the extracts for 24 hours and measuring cytokine/chemokine responses. The experiment did not reveal significant difference in cytokine/chemokine response. However, changes to *M. tuberculosis* carbohydrates may directly influence human complement activation via the lectin pathway and the binding of C1q. The complement system is essentially an innate immune surveillance system involved in pathogen defence, modulation of inflammation and homeostasis (Merle et al., 2015). Activation of this signalling cascade affects tuberculosis pathogenesis, as will be discussed below, and may be modulated by *M. tuberculosis* biofilm formation, as shown with other bacteria such as *Streptococcus pneumoniae* (Domenech et al., 2013).

Complement activation by *M. tuberculosis* can be triggered by the alternative pathway, classical pathway, lectin pathway and C2 pathway (Bartlomiejczyk et al., 2014; Ferguson et al., 2004; Schlesinger et al., 1990; Schorey et al., 1997). In the lung, the alternative pathway is not significantly activated due to low levels of factor B (Watford et al., 2000).

Previous studies have suggested C3b/iC3b deposition onto *M. tuberculosis* is one of a number of mechanisms utilised by the pathogen to gain access to its intracellular niche. Complement opsonisation with nonimmune serum enhances adherence to monocytes predominantly via complement receptor 3 (CR3) (Schlesinger et al., 1990). Furthermore entry via complement receptors of viable complement-opsonised *M. tuberculosis* does not lead to $Ca^{2+}$ signalling associated with phagosome-lysosome fusion (Malik et al., 2000).

A study measuring levels of complement component C3d (the end product from the cleavage of C3) anaphylatoxins C3a, C4a and C5a, and C5b-9 in circulating immune complexes showed these components were all significantly higher in untreated tuberculosis patients compared to treated and heathy controls. Furthermore immune complexes showed decreased solubilisation, which prevents complement activation, in TB patients, suggesting excessive complement activation in TB patients (Senbagavalli et al., 2009).

Downstream components of the complement system may be involved in modulation of tuberculosis pathogenesis. While C5b-9 assembly onto the *M. tuberculosis* cell surface may not result in direct lytic activity, as observed with some gram negative bacteria, a study utilising congenic C5 sufficient and C5 deficient mouse strains showed decreased IL-12p40 transcription in lung tissue of C5-deficient mice. Additionally, C5-deficiency enhanced bacterial growth in the lung and was required for granulomatous inflammation (Actor et al., 2001). Subsequent studies which utilised C5 and C5aR deficient mice also showed that C5 mediated events were essential for generation of a granulomatous response against

mycobacterial trehalose dimycolate (TDM) (Borders et al., 2005; Welsh et al., 2008). During *M. tuberculosis* infection C5a also affects IFNγ production in T cells, since C5-deficient T cells produce less IFNγ (Mashruwala et al., 2011). The extent of C5/C5aR induced IFNγ production may be *M. tuberculosis* strain dependent since M strain but not H37Rv has been shown to induce higher IFNγ production in healthy donors and TB patients when C5aR is blocked (Sabio y García et al., 2017). C7-deficient mice infected with *M. tuberculosis* showed decreased lung immunopathology with reduced macrophages and smaller granulomas (Welsh et al., 2012)..

Biofilm phenotype *M. tuberculosis* may induce altered levels of complement activation due to the changes in its outermost carbohydrates, specifically reduced α-glucan prevalence. These changes may directly impact the binding of lectin pathway activators such as MBL, which binds to glucose residues (Weis et al., 1992). MBL but not ficolin-3 has been shown to bind to *M. tuberculosis* LAM (Bartlomiejczyk et al., 2014; Świerzko et al., 2016). Interestingly both lectin pathway activators can bind to recombinant antigen 85 protein complex; proteins without posttranslational modification or acetylation (Świerzko et al., 2016). Antigen 85 is a secreted complex of mycolyl transferases involved in the addition of mycolic acids to arabinogalactan and TDM (Huygen, 2014).

Biofilm formation of the Gram-positive bacteria *Streptococcus pneumoniae* has been shown to reduce C3b/iC3b deposition and C1q binding (Domenech et al., 2013). Biofilm formation has also been shown to modulate complement deposition on *Staphylococcus epidermidis* and *Mycoplasma pulmonis* (Kristian et al., 2008; Simmons and Dybvig, 2007). Although the cell wall and EPS of mycobacteria varies considerably from these species, the reduced constituent glucose in *M. tuberculosis* biofilm carbohydrate extracts compared to planktonic extracts (section 3.4) may modulate the extent of C3b/iC3b and C5b-9 deposition via altered binding of complement activators. Furthermore the *M. tuberculosis* cell surface contains a unique but

currently unidentified C2a binding protein which together with C2a forms a functioning C3 convertase (Schorey et al., 1997). It is possible that the expression of this protein is affected by *M. tuberculosis* biofilm formation.

Prior to measuring C3b/iC3b and C5b-9 deposition on planktonic and biofilm phenotype *M. tuberculosis* cells, the disaggregation of clumpy 'planktonic' and biofilm *M. tuberculosis* samples was optimised in order to measure complement deposition directly on live *M. tuberculosis* planktonic and biofilm phenotypes, by flow cytometry. With the use of live, dispersed planktonic and biofilm phenotype *M. tuberculosis* bacteria, the relative contributions of each known complement activation pathway in this deposition; the classical pathway, the alternative pathway, the lectin pathway and the C2a pathway was investigated. Finally, enzyme linked immunosorbent assays (ELISAs) were developed to interrogate whether complement deposition is altered on *M. tuberculosis* biofilm carbohydrate extracts compared to planktonic carbohydrate extracts. C3b/iC3b deposition, C5b-9 deposition and MBL deposition were measured.

## 5.2 Chapter 5 hypotheses

1) Live biofilm phenotype *M. tuberculosis* cells show altered complement deposition (C3b/iC3b and C5b-9) compared to planktonic phenotype.
2) The relative contribution of the known complement activation pathways that trigger C3b/iC3b and C5b-9 deposition are altered in biofilm phenotype *M. tuberculosis* compared to planktonic phenotype.
3) C3b/iC3b and C5b-9 deposition is altered on biofilm *M. tuberculosis* carbohydrate extracts compared to planktonic extracts

4) MBL deposition is altered on biofilm *M. tuberculosis* carbohydrate extracts compared to planktonic extracts.

## 5.3 Optimisation of planktonic and biofilm phenotype *M. tuberculosis* samples for flow cytometry

To gain an understanding of how *M. tuberculosis* phenotype effects complement activation, complement deposition onto live *M. tuberculosis* cells was measured using flow cytometry. In order to use flow cytometry to study mycobacteria, let alone biofilms, the cells must be efficiently dispersed. This was achieved by following a method previously described in several papers using agitation with glass beads without damaging the bacterial cells (N'Diaye et al., 1998; Ortalo-Magné et al., 1995; Villeneuve et al., 2003). To investigate the effect of agitation with glass beads on mycobacteria, a viable count using fast-growing *M. smegamtis* biofilms before and after agitation with glass beads was performed. In addition, glass-bead treated and untreated *M. tuberculosis* samples were sent to the University of Amsterdam for immune-gold EM mannosyl labelling to determine the extent of shedding of the outermost carbohydrates.

Pre and post bead treatment viable counts were performed as described in the method (sections 7.23). Briefly, x3 biological replicate *M. smegmatis* pellicle biofilm cultures were set up in separate plates. After 7 days incubation the biofilms were scraped into pre-weighed falcon tubes. Prior to glass bead treatment *M. smegmatis* samples were suspended in 10 mL PBS and plated. The serial dilutions were performed in PBS 1% Tween 80 to disperse clumps before spreading. Glass beads were added at ≈x5 the volume of the pellet. This step was skipped for control untreated cultures. Samples were vortexed with glass beads for 30

seconds and resuspended in 10 mL PBS and plated. Viable counts (CFU $g^{-1}$) were performed on pre and post treatment and control plates after 7 days incubation **Figure 5.3.1a**. Welch's t-test showed there was no significant difference in viable count after glass bead agitation or compared to control untreated cultures. This shows that agitation with glass beads does not appear to effect mycobacterial viability.

To assess to what extent agitation with glass beads shed outermost carbohydrates, *M. tuberculosis* planktonic cultures which had been dispersed using glass beads as described in methods section 7.22 or untreated controls, were resuspended in PBS 4%-formaldehyde and sent to Dr. Nicole N van der Wel, University of Amsterdam. Analysis of immuno gold labelling was performed as described in section 7.6 using anti-PIM/LAM antibody which binds to α(1-2) mannosyl residues, the mannose caps of PIM, LM and LAM and their non-lipdated counterparts. A sample of ≥38 glass bead treated and untreated individual bacterium were imaged. **Figure 5.3.1b** shows a representative bead-treated *M. tuberculosis* bacterium. The length and number of gold particles and each bacterium was calculated using Image J software (Schindelin et al., 2012). Welch's t-test confirmed there was a significant 60% reduction in the extent of α(1-2) mannosyl residues present on the mycobacterial cell surface after glass bead treatment **Figure 5.3.1c**. However, this meant that 40% of the outermost material remained associated with the dispersed bacteria.

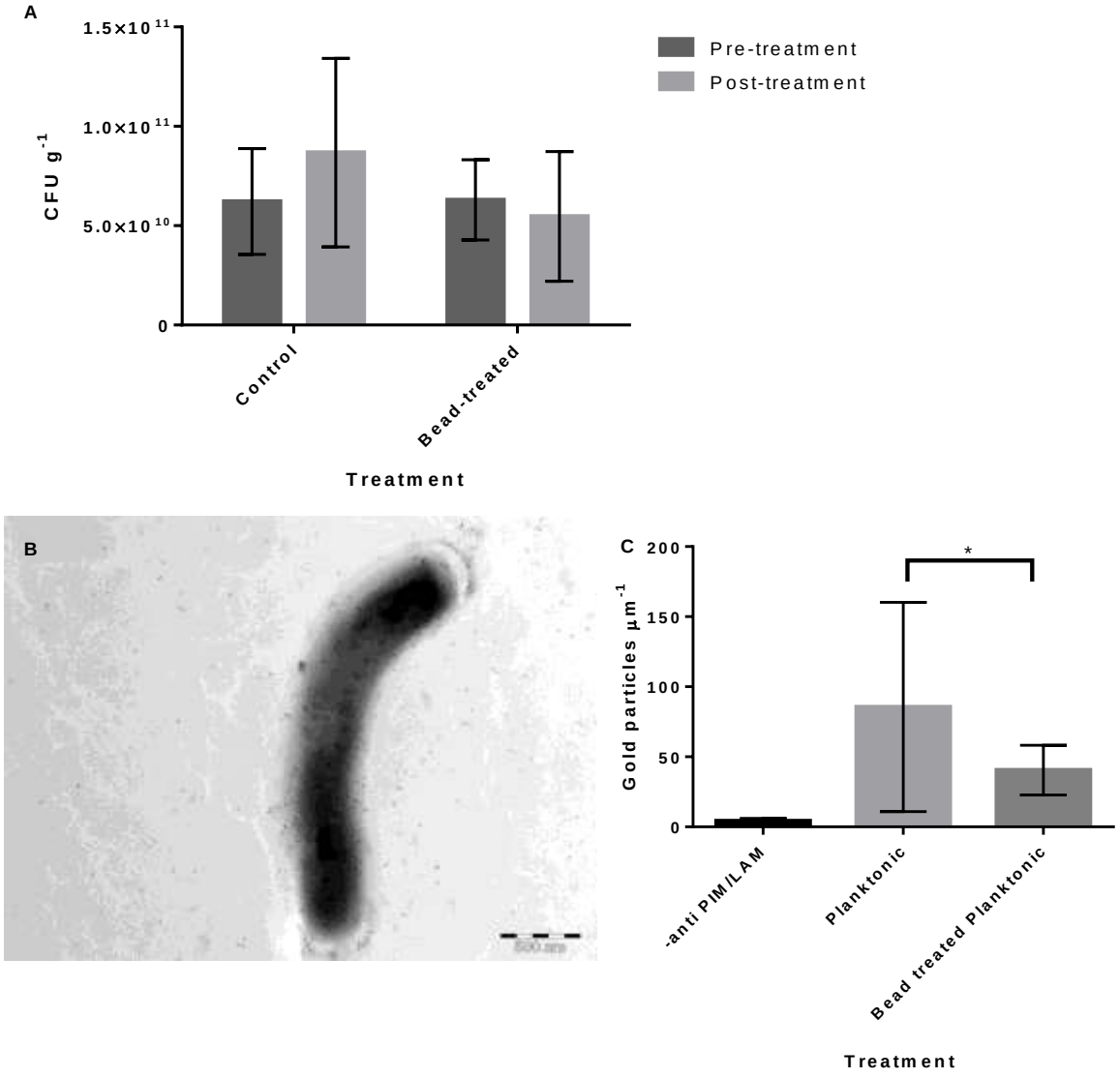


**Figure 5.3.1:** The effect of glass bead dispersion on viability and capsule shedding. (A) Viable counts of *M. smegmatis* biofilms before and after glass bead treatment x3biological replicates Error bars = standard deviation. (B) Representative *M. tuberculosis* planktonic bacterium immuno gold labelled with anti PIM/LAM antibody. (C) Quantification of immuno gold anti-PIM/LAM dots visible on each micrograph associated with a bacterium/length of bacterium. Number of samples ≥38 Error bars = standard deviation.

x4 biological replicate planktonic and biofilm *M. tuberculosis* cultures were set up, harvested and dispersed using glass beads followed by low-speed centrifugation and frozen in PBS aliquots at -80$^{o}$C until required for flow cytometry experiments. The gating strategy for flow cytometry experiments is shown in **Figure 5.3.2**. Mycobacteria and positive controls zymosan and *S. agalactiae* were identified using a forward scatter / side scatter gating strategy constantly applied for all flow cytometry experiments **Figure 5.3.2a**. After labelling with the appropriate fluorescent antibodies, events with fluorescence intensities higher than the negative control samples (bacteria + conjugate without complement) were deemed positive (**Figure 5.3.2b**). The magnitude of deposition was determined by multiplying the median fluorescence intensity (MFI) by % positive cells to calculate the integrated median fluorescence intensity iMFI (Darrah et al., 2007).

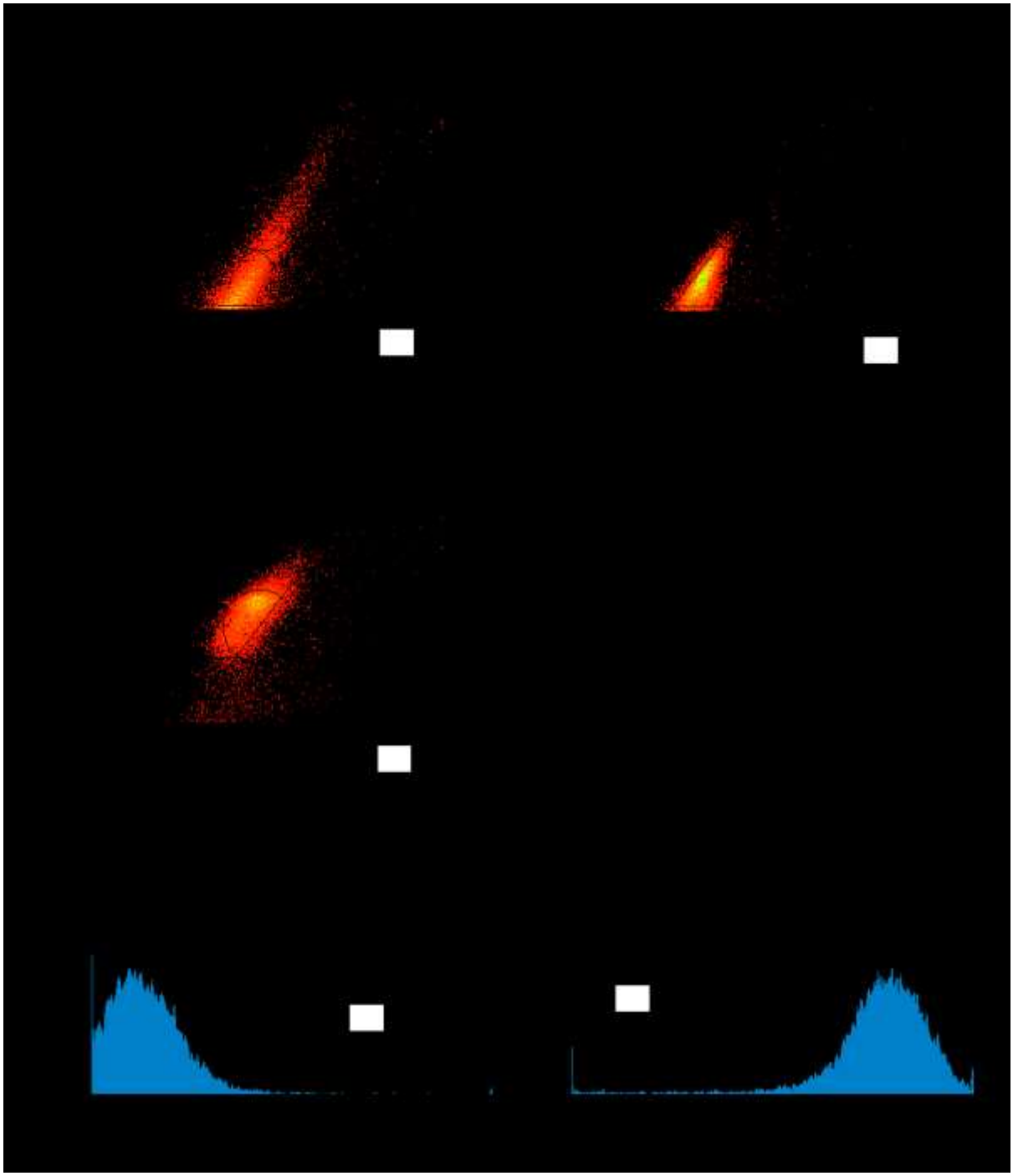

**Figure 5.3.2:** Gating strategy for flow cytometry experiments. (A) Forward scatter and side scatter gates for *M. tuberculosis* (top left) and controls *S. agalactiae* (top right) and Zymosan (bottom left). (B) Example negative control sample *M. tuberculosis* with conjugate only (Mouse anti-human MBL and Goat anti-mouse FITC secondary antibody) (left panel) *M. tuberculosis* + recombinant MBL + conjugate (right panel).

For flow cytometry experiments, the x4 biological replicates of planktonic and biofilm phenotype dispersed bacteria were thawed and their concentrations were equalised to an absorbance of 0.09 $OD_{540\ nm}$ *M. tuberculosis,* equivalent to 2 x $10^5$ CFU $mL^{-1}$.

## 5.4 Analysis of C3b/iC3b and C5b-9 deposition on planktonic and biofilm phenotype *M. tuberculosis* with additional positive controls.

The magnitude of C3b/iC3b and C5b-9 deposition on the surface of live planktonic and biofilm phenotype was assessed to determine the relative contribution of each of the major complement activation pathways; lectin, classical and alternative. The assay method was performed as described in section 7.24. Briefly *M. tuberculosis* x4 planktonic and x4 biofilm bead-treated biological replicate *M. tuberculosis* samples, *S. agalactiae* and Zymosan were incubated with complement under the following conditions: IgG-depleted complement was either pre-incubated with anti-C1q mAb or PBS control to interrogate the role of the classical pathway. Also, samples were incubated with either 2% or 10% complement concentrations as all three pathways are active at 10% complement concentration but the alternative pathway is inhibited at 2% complement concentration (Ferguson et al., 2004; Nilsson and Nilsson, 1984) (**Table 5.4-1)**.

| Reference | Complement pre-incubation | Complement concentration | Outcome |
|---|---|---|---|
| i | 1/5 anti-C1q mAb | 2% | Classical and alternative pathway inhibited |
| ii | 1/5 anti-C1q mAb | 10% | Classical pathway inhibited |
| iii | 1/5 PBS | 2% | Alternative pathway inhibited |
| iv | 1/5 PBS | 10% | All pathways active |

**Table 5.4-1:** Experimental conditions for C3b/iC3b and C5b-9 deposition assay.

Following incubation, samples were labelled with rabbit anti-human C3c FITC pAb and mouse anti-human C5b-9 Alexafluor 647 mAb. Samples were fixed in 4% formaldehyde and run on a flow cytometer to 10 000 events per sample using the gating strategy shown in **Figure 5.3.2**. Net iMFI above negative control levels was calculated under all test conditions (**Figure 5.4.1**).

In the absence of classical pathway blocking (**Table 5.4-1iii and iv)** C3b/iC3b deposition was highest in zymosan followed by planktonic *M. tuberculosis,* biofilm *M. tuberculosis*, planktonic *M. smegmatis* and planktonic *S. agalactiae*. This was the case at both 2% and 10% complement concentrations. Inhibition of the alternative pathway (2%) partially reduced C3b/iC3b deposition onto each sample **Figure 5.4.1a**.

Blocking the classical pathway completely abolished C3b/iC3b deposition in *S. agalactiae* even when the alternative pathway was active at 10% concentration, suggesting deposition was entirely dependent on the classical pathway. *M. smegmatis* showed minimal C3b/iC3b deposition at 10% complement concentration after blocking the classical pathway and no deposition at 2% complement concentration suggesting roles for the classical pathway and a minor role for the alternative pathway. C3b/iC3b deposition was still present on Zymosan even when the alternative and classical pathways were inhibited suggesting the lectin pathway was also involved in deposition. Similarly, C3b/iC3b deposition was still present on *M. tuberculosis* phenotypes after inhibition of the classical and alternative pathways suggesting the lectin and/or C2 pathway contribute to C3b/iC3b deposition on *M. tuberculosis* **Figure 5.4.1a**.

In the absence of classical pathway blocking but when the alternative pathway was active (**Table 5.4-1iv)** C5b-9 deposition was highest in zymosan. This deposition was greatly reduced in comparison to the other samples when the alternative pathway was inhibited. *M. tuberculosis* phenotypes showed only partial inhibition of C5b-9 deposition when the alternative pathway was inhibited and all other pathways were active. *M. smegmatis* followed by *S. agalactiae* showed less C5b-9 deposition than *M. tuberculosis* phenotypes when all three pathways were active. C5b-9 was diminished further in *M. smegmatis* and *S. agalactiae* when the alternative pathway was inhibited **Figure 5.4.1b**.

Blocking the classical pathway completely abolished C5b-9 deposition in *S. agalactiae* even when the alternative pathway was active at 10% concentration suggesting deposition was entirely dependent on the classical pathway. *M. smegmatis* showed minimal C5b-9 deposition at 10% complement concentration after blocking the classical pathway and no deposition at 2% complement concentration suggesting roles for the classical pathway and a minor role for the alternative pathway. Despite the predominant role of the alternative pathway in the deposition of C5b-9 on Zymosan, C5b-9 deposition was still present on Zymosan even when the alternative and classical pathways were inhibited suggesting the lectin pathway is also partially involved in deposition. C5b-9 deposition was still present on *M. tuberculosis* phenotypes after inhibition of the classical and alternative pathways suggesting the lectin and/or C2 pathway contribute to C5b-9 deposition on *M. tuberculosis* **Figure 5.4.1b**.

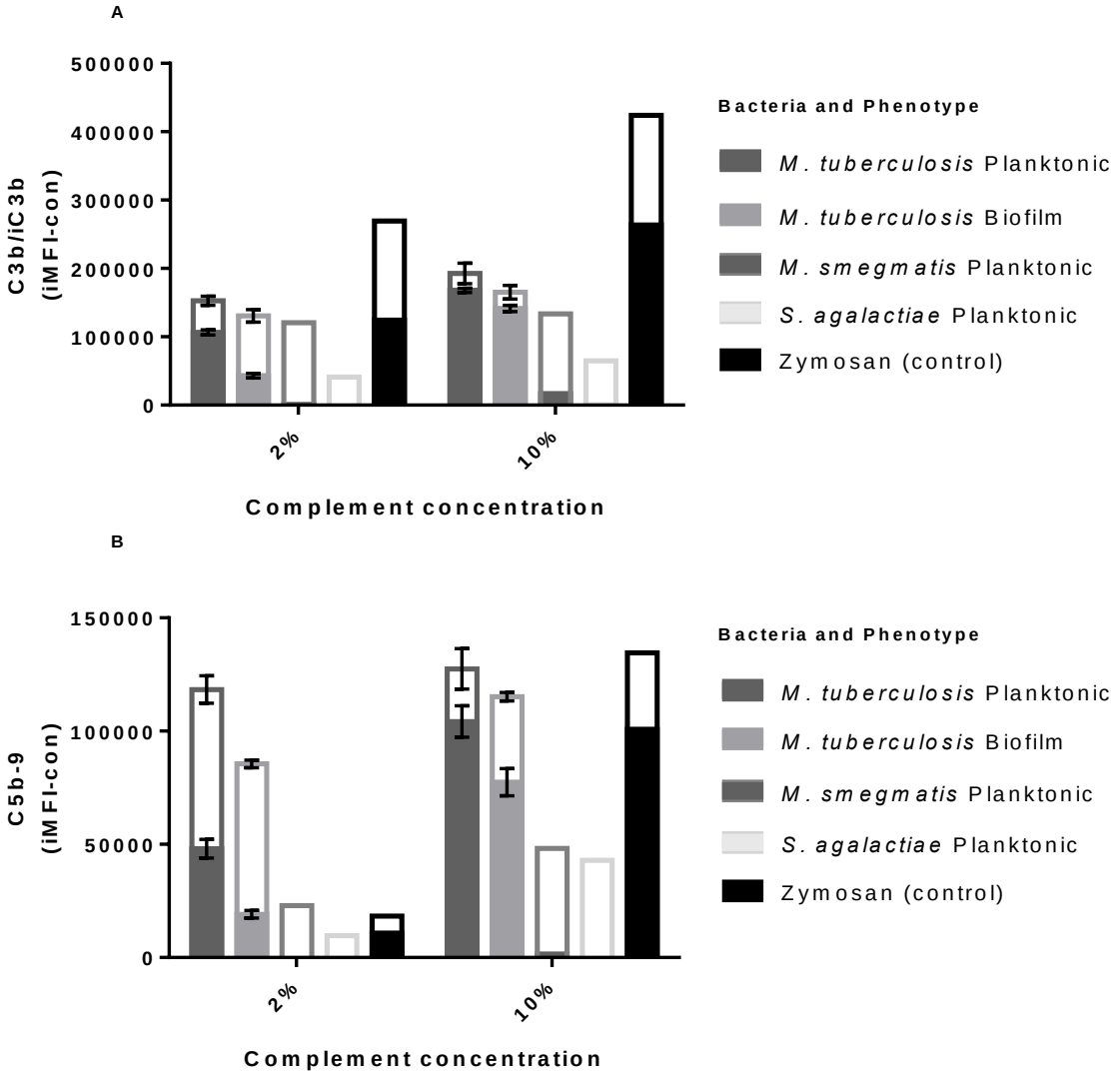


**Figure 5.4.1:** Complement deposition on planktonic and biofilm phenotype *M. tuberculosis* relative to planktonic *M. smegmatis* and planktonic *S. agalactiae* and Zymosan. (A) Net mean C3b/iC3b deposition (integrated median fluorescence intensity - iMFI) of samples after pre-incubation of complement with mAb anti-C1q (shaded bars) or pre-incubation with PBS (clear bars) and labelling with anti-C3c FITC pAb. (B) Net mean C5b-9 deposition (iMFI) onto samples after pre-incubation of complement with mAb anti-C1q (shaded bars) or pre-incubation with PBS (clear bars) labelled with anti-C5b-9 Alexafluor 647. Error bars show standard deviation of x4 biological replicates.

A t-test corrected for multiple comparisons by false discovery rate (Q=5%)showed that C3b/iC3b (**Figure 5.4.2a**) and C5b-9 (**Figure 5.4.2b**) deposition were significantly reduced on biofilm phenotype *M. tuberculosis* compared to planktonic phenotype *M. tuberculosis* at both 2% concentration when the alternative pathway is inhibited and 10% concentration when all three major pathways are active. C3b/iC3b showed on average 14% less deposition in biofilm phenotype *M. tuberculosis* compared to planktonic phenotype at both 2% and 10% complement concentrations. C5b-9 showed on average 27% less deposition at 2% complement concentration and 6% less deposition at 10% complement concentration. There remained a significant difference in C3b/iC3b deposition when the classical pathway was inhibited and when both the classical and alternative pathways were inhibited (**Figure 5.4.2c**). Furthermore, in the absence of the classical and alternative pathways the effect size was much larger. C3b/iC3b deposition after C1q blocking showed on average 60% less deposition in biofilm phenotype *M. tuberculosis* compared to planktonic phenotype *M. tuberculosis* at 2% complement concentration and 16% at 10% complement concentration. Likewise there remained a significant difference in C5b-9 deposition after C1q blocking with a much larger effect size with the classical and alternative pathways inhibited together **Figure 5.4.2d**. At 2% complement concentration after C1q blocking, biofilm phenotype *M. tuberculosis* showed 60% less C5b-9 deposition compared to planktonic phenotype *M. tuberculosis*. At 10% complement concentration with C1q blocking, biofilm phenotype showed 26% less deposition compared planktonic phenotype **Figure 5.4.2c**.

The percentage of C3b/iC3b deposition and C5b-9 deposition that was classical pathway dependent (C1q-dependent) was calculated by determining the percentage change in deposition before and after C1q blocking. C3b/iC3b deposition onto biofilm phenotype *M. tuberculosis* was significantly more dependent on the classical pathway (67%) compared to

planktonic *M. tuberculosis* (30%) in the absence of alternative pathway activity (2% complement). This difference was abolished when the alternative pathway was active (10% complement concentration) where 12% of C3b/iC3b deposition was classical pathway dependent on planktonic *M. tuberculosis* compared to 14% classical pathway dependence on biofilm *M. tuberculosis* (**Figure 5.4.2e**). C5b-9 deposition onto biofilm phenotype *M. tuberculosis* was significantly more dependent on the classical pathway (78%) compared to planktonic *M. tuberculosis* (60%) in the absence of alternative pathway activity (2% complement concentration) although the effect size was smaller than seen with C3b/iC3b deposition. Furthermore, unlike with C3b/iC3b deposition there was also a significant difference when the alternative pathway was active (10% complement concentration) where biofilm phenotype *M. tuberculosis* showed 33% classical pathway dependence compared to 18% classical pathway dependence on C5b-9 deposition onto planktonic *M. tuberculosis* (**Figure 5.4.2f**).

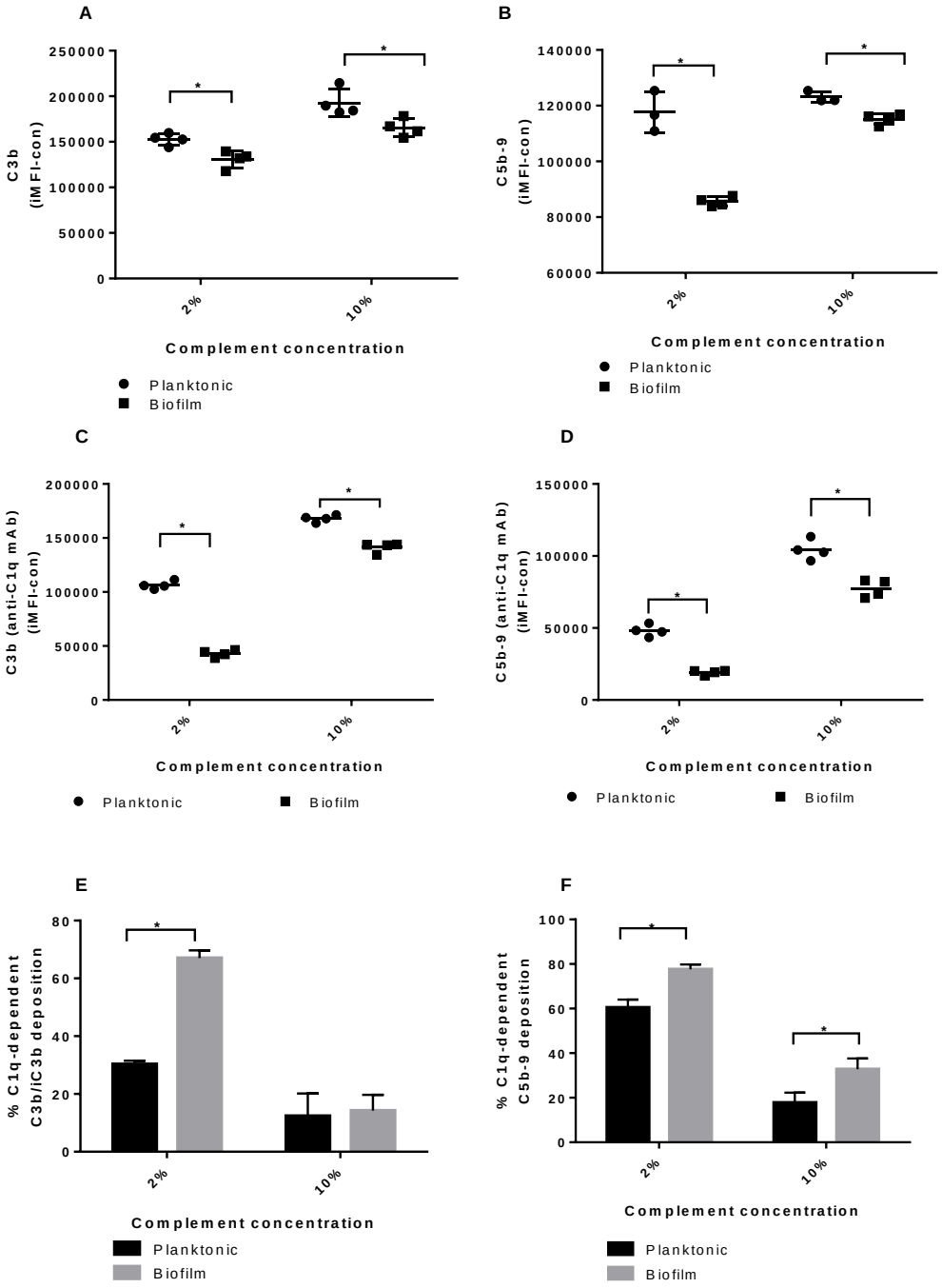


**Figure 5.4.2:** Complement activation by planktonic and biofilm phenotype *M. tuberculosis*. (A) Net mean C3b/iC3b deposition (iMFI) of samples after pre-incubation of complement with PBS and labelling with anti-C3c FITC pAb. (B) Net mean C5b-9 deposition (iMFI) onto samples after pre-incubation of complement with PBS, labelled with anti-C5b-9 Alexafluor 647. (C) Net mean C3b/iC3b deposition (iMFI) of samples after pre-incubation of complement with anti-C1q and labelling with anti-C3c FITC pAb. (D) Net mean C5b-9 deposition (iMFI) of samples after pre-incubation of complement with anti-C1q and labelling with anti-C3c FITC pAb. (E) Net mean % C1q-dependent C3b/iC3b deposition onto planktonic and biofilm phenotype *M. tuberculosis*. (F) Net mean % C1q-dependent C5b-9

deposition onto planktonic and biofilm phenotype *M. tuberculosis*. Error bars = standard deviation of ≥3 biological replicates. * = P<0.05 corrected t-tests by false discovery rate Q=5%.

## 5.5 Analysis of complement activator binding to planktonic and biofilm phenotype *M. tuberculosis*

The direct binding onto planktonic and biofilm phenotype *M. tuberculosis* of two lectin pathway activators, mannose binding lectin (MBL) and ficolin-3 in addition to classical pathway activator C1q were investigated using flow cytometry using the methods described in section 7.25.

As with the C3b/iC3B and C5b-9 experiment, for each complement activator a final concentration of 0.09 $OD_{540\ nm}$ x4 *M. tuberculosis* planktonic biological replicates, x4 *M. tuberculosis* biofilm biological replicates, *M. smegmatis, S. agalactiae* and Zymosan were added to respective wells. In separate experiments, purified human C1q, recombinant human MBL and recombinant human ficolin-3 were each incubated directly with live *M. tuberculosis*, labelled with primary and fluorescent secondary antibodies. Mycobacteria were identified in 10 000 events using a forward scatter side scatter gating strategy constantly applied for all flow cytometry experiments (**Figure 5.3.2**). The net magnitude of deposition was determined by multiplying the median fluorescence intensity (MFI) by % positive cells to calculate the integrated median fluorescence intensity iMFI (Darrah et al., 2007) and subtracting the negative controls (sample + complement activator + conjugate).

MBL deposition was highest on *M. tuberculosis* planktonic samples, followed by zymosan and *M. tuberculosis* biofilm samples, with no deposition seen on *M. smegmatis* or *S. agalactiae* (**Figure 5.5.1a**). This result was consistent with the observation from the C3b/iC3b and C5b-9 deposition assay that complement deposition onto *M. smegamatis* and *S. agalactiae* was dependent on the classical pathway. C1q deposition was highest on *M. tuberculosis* planktonic samples, followed by *M. tuberculosis* biofilm samples followed by *M. smegmatis* and Zymosan (**Figure 5.5.1b**). Interestingly despite the C3b/iC3b and C5b-9 deposition assay showing classical pathway dependent complement deposition on *S.*

*agalactiae* (**Figure 5.4.1**), **Figure 5.5.1**b suggests this does not appear to be dependent on direct C1q binding and therefore presumably C3b/iC3b and C5b-9 deposition is dependent on C1q via interaction with anti-*S. agalactiae* natural antibodies in the pooled IgG-depleted complement source. Ficolin-3 deposition was highest in planktonic *M. tuberculosis* followed by *M. smegmatis,* biofilm *M. tuberculosis* Zymosan and *S. agalactiae* **Figure 5.5.1c**.

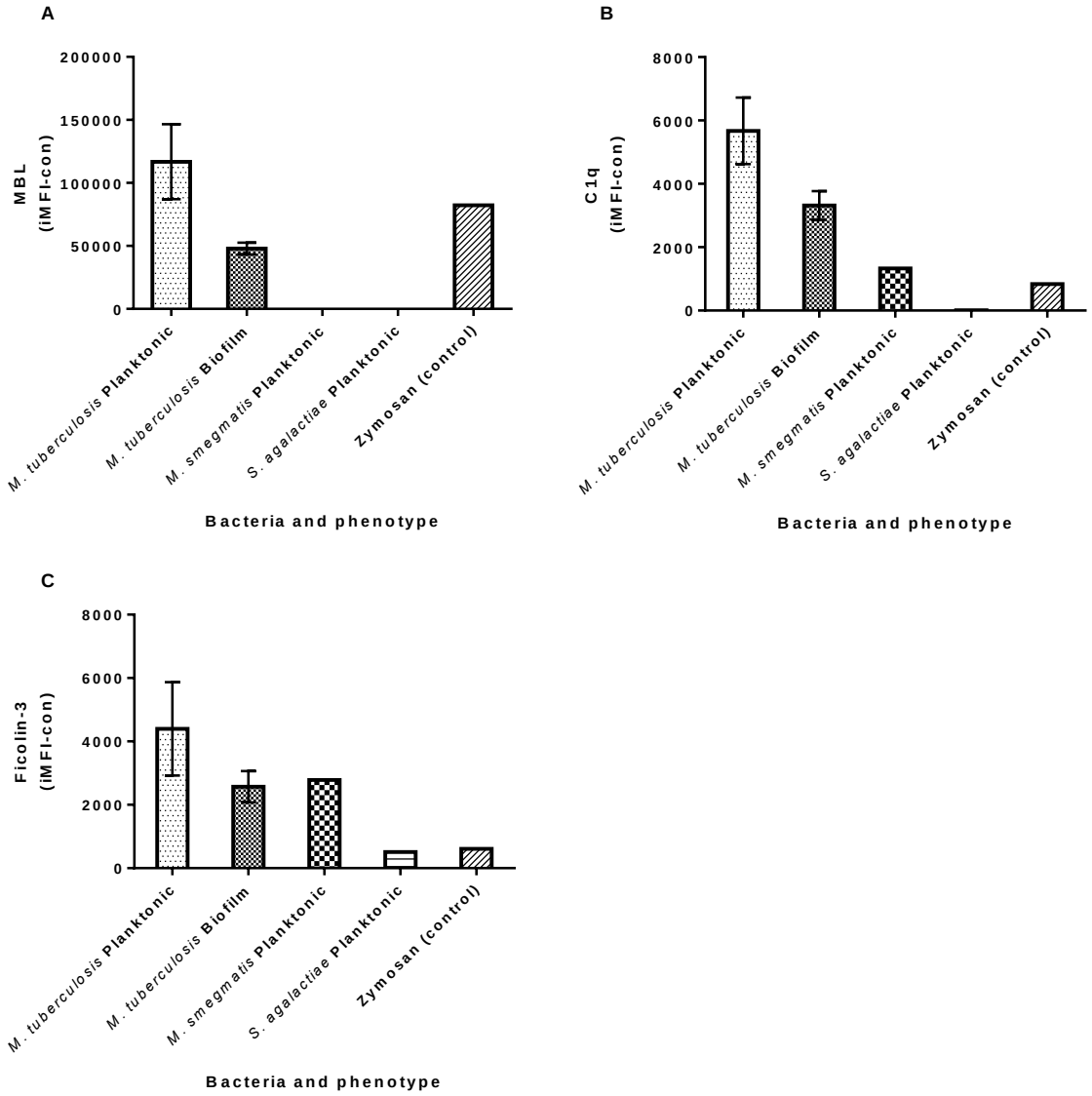


**Figure 5.5.1:** Complement activator binding to planktonic and biofilm phenotype *M. tuberculosis r*elative to planktonic *M. smegmatis* and planktonic *S. agalactiae* and Zymosan. (A) Net mean binding of MBL to samples (iMFI) after incubation with recombinant MBL and labelling with anti-MBL primary and anti mouse IgG (H+L) $F(ab')_2$ Fragment FITC. (B) Net mean binding of C1q to samples (iMFI) after incubation with purified C1q and labelling with anti-C1q primary and anti-mouse IgG (H+L) $F(ab')_2$ Fragment FITC. (C) Net mean binding of ficolin-3 to samples (iMFI) after incubation with recombinant ficolin-3 and labelling with anti-ficonin-3 primary and anti-mouse IgG (H+L) $F(ab')_2$ Fragment FITC. Error bars = standard deviation of ≥3 biological replicates.

Welch's t-tests revealed MBL deposition was significantly reduced on biofilm phenotype *M. tuberculosis* compared to planktonic phenotype ($P<0.05$), showing a 59% knockdown in binding (**Figure 5.5.2a**). Similarly, direct binding of C1q was also significantly reduced in the biofilm phenotype and the effect size was slightly smaller showing a 42% knockdown ($P<0.05$) (**Figure 5.5.2b**). Notably despite the C3b/iC3b and C5b-9 deposition assay suggesting deposition onto biofilm phenotype *M. tuberculosis* was more dependent on the classical pathway, the total direct binding of C1q to biofilm phenotype compared to planktonic phenotype was reduced. Ficolin-3 was incubated with planktonic or biofilm phenotype *M. tuberculosis* and was reduced on the biofilm phenotype but this was not a statistically significant difference (**Figure 5.5.2c**).

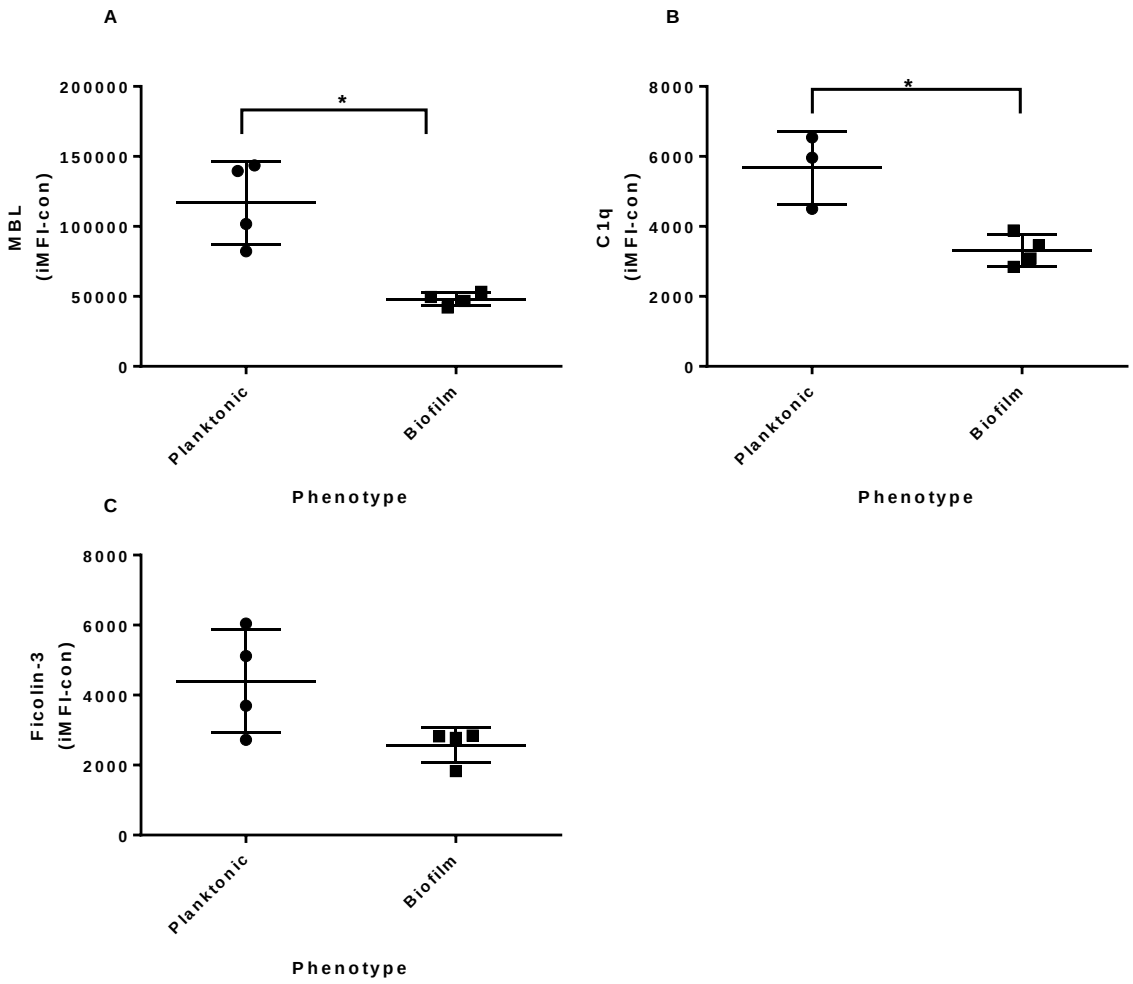


**Figure 5.5.2:** Binding of complement activators to planktonic and biofilm phenotype *M. tuberculosis.* (A) Net mean binding of MBL to samples (iMFI) after incubation with recombinant MBL and labelling with anti-MBL primary and anti-mouse IgG (H+L) $F(ab')_2$ Fragment FITC. (B) Net mean binding of C1q to samples (iMFI) after incubation with purified C1q and labelling with anti-C1q primary and anti-mouse IgG (H+L) $F(ab')_2$ Fragment FITC. (C) Net mean binding of ficolin-3 to samples (iMFI) after incubation with recombinant ficolin-3 and labelling with anti-ficonin-3 primary and anti-mouse IgG (H+L) $F(ab')_2$ Fragment FITC. Error bars = standard deviation ≥3 biological replicates. * = $P<0.05$ Welch's t-test.

## 5.6 Investigation of the C2-pathway of complement deposition onto planktonic and biofilm phenotype *M. tuberculosis*.

The C3b/iC3b and C5b-9 deposition assay inhibited both the classical and alternative pathways of complement deposition. With most bacterial species, this would leave any remaining deposition attributable to the lectin pathway. However, *M. tuberculosis* has a little-studied fourth pathway of complement activation that relies on the capture of C2a after its cleavage from component C2 by an unidentified surface expressed protein to form a functioning C3 convertase. This pathway is unique to pathogenic mycobacteria (Schorey et al., 1997). C2 can be cleaved by MBL-associated serine protease 2 (MASP-2) which forms part of the complex of complement activating collectins and ficolins of the lectin pathway. It can also be cleaved by C1s which associates with C1q after it binds either directly or via antibodies to the bacterial surface (Murphy, 2012). Therefore when both the classical and alternative pathway were inhibited in C3b/iC3b and C5b-9 deposition experiment, the C2a pathway may have acted via MASP-2 to amplify lectin pathway complement deposition through C2a capture to create additional functioning C3 covertases. To investigate the C2a pathway of complement deposition, an experiment was planned to demonstrate C2 pathway activity by *M. tuberculosis* planktonic and biofilm phenotypes in the absence of the lectin, classical and alternative pathway activity.

To demonstrate C2a binding to *M. tuberculosis* an experiment was performed as described in methods sections 7.26. Briefly, live planktonic and biofilm *M. tuberculosis*, in addition to negative controls *M. smegmatis, S. agalactiae* and zymosan was incubated with purified human C2 with or without pre-incubation with activated purified human C1s enzyme, which cleaves C2 into C2a and C2b. The samples were then washed and labelled with Rabbit anti-human C2a FITC pAb and fixed with formaldehyde before measuring FITC fluorescence on

bacteria by flow cytometry. FITC channel iMFI values would be indicative of C2a binding in the absence of other complement components. The plate layout is shown in **Table 5.6-1**.

| | 1 | 2 | 3 | 4 | 5 | 6 | 7 | 8 | 9 | 10 | 11 | 12 |
|---|---|---|---|---|---|---|---|---|---|---|---|---|
| A | PKA | PKB | PKC | PKD | BFA | BFB | BFC | BFD | Smeg | GBS | Zy | Zy |
| B | PKAcon | PKB con | PKC con | PKD con | BFAcon | BFB con | BFC con | BFD con | Smeg con | GBS con | Zy con | Zy con |
| C | PKA con | PKB con | PKC con | PKD con | BFA con | BFB con | BFC con | BFD con | Smeg con | GBS con | Zy con | Zy con |
| D | PKA C2 | PKB C2 | PKC C2 | PKD C2 | BFA C2 | BFB C2 | BFC C2 | BFD C2 | Smeg C2 | GBS C2 | Zy C2 | Zy C2 |
| E | PKA C2 | PKB C2 | PKCC2 | PKD C2 | BFA C2 | BFB C2 | BFCC2 | BFD C2 | Smeg C2 | GBS C2 | Zy C2 | Zy C2 |
| F | PKA C2a/b | PKB C2a/b | PKC C2a/b | PKD C2a/b | BFA C2a/b | BFB C2a/b | BFC C2a/b | BFD C2a/b | Smeg C2a/b | GBS C2a/b | Zy C2a/b | Zy C2a/b |
| G | PKA C2a/b | PKB C2a/b | PKC C2a/b | PKD C2a/b | BFA C2a/b | BFB C2a/b | BFC C2a/b | BFD C2a/b | Smeg C2a/b | GBSC2a/b | Zy C2a/b | Zy C2a/b |
| H | PKA | PKB | PKC | PKD | PKA | BFB | BFC | BFD | Smeg | GBS | Zy | Zy |

**Table 5.6-1:** Plate layout of the C2 pathway experiment. C2 wells contain PBS-C2, C2a/b wells contain C2 cleaved by enzyme activated C1s into components C2a and C2. PKA – PKD, x4 biological replicate planktonic *M. tuberculosis* samples; BFA – BFD, x4 biological replicate biofilm *M. tuberculosis* samples; Smeg, *M. smegmatis;* GBS, *S agalactiae*; Zy, Zymosan.

The experiment did not show specific C2a binding to *M. tuberculosis*, as shown in **Figure 5.6.1**d. Histograms showed no shift in fluorescence between *M. tuberculosis* sample incubated with conjugate only, conjugate + uncleaved C2 and conjugate in the presence of C2a. **Figure 5.6.1**c,d and e. However, there was a shift in fluorescence that was seen between 'mycobacteria only' negative controls and 'mycobacteria + rabbit-anti-human C2a pAb conjugate' negative controls (**Figure 5.6.1**b and c). Since the shift was also seen with *M. smegmatis* it was not specific to pathogenic mycobacteria. Additional negative controls *S. agalactiae* and Zymosan did not show C2a binding (**Figure 5.6.1**d). Furthermore, *S. agalactiae* did not show a shift in fluorescence after incubation with Rabbit-anti-human C2a pAb conjugate while Zymosan showed a marginal shift (**Figure 5.6.1**b and c). These results suggest that mycobacteria may harbour epitopes on their surface with affinity to anti-human C2a pAb.

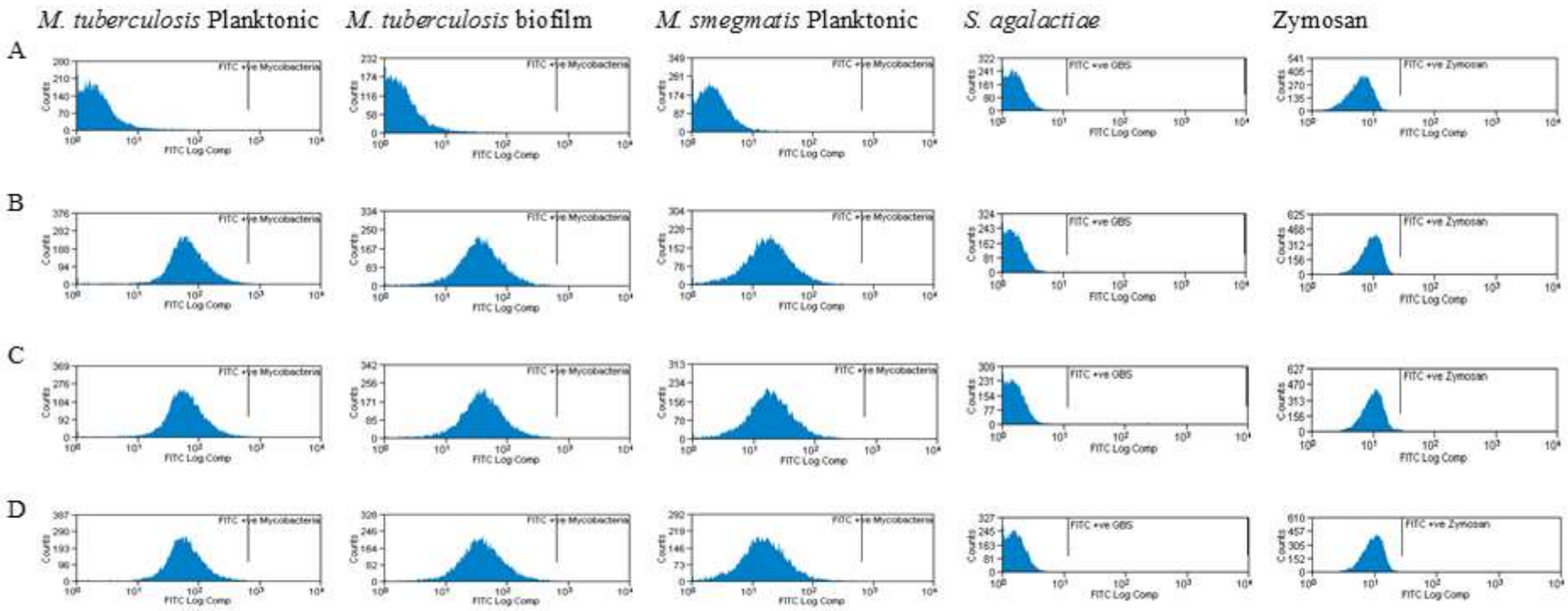


**Figure 5.6.1**: Assessment of C2-pathway deposition onto planktonic and biofilm phenotype *M. tuberculosis* with additional controls. Columns from left to right are representative fluorescence histograms from samples as indicated in the top row. Samples were incubated without rabbit anti-human C2a FITC pAb (a), with rabbit anti-human C2a FITC pAb only (b), with rabbit anti-human C2a FITC pAb and C2 (c) and with rabbit anti-human C2a FITC pAb and pre-incubated C2/C1s (d).

The extent of direct binding of Rabbit anti-human C2a pAb to bacteria and zymosan is shown in **Figure 5.6.2**a. *M. tuberculosis* planktonic samples showed the greatest magnitude of binding followed by *M. tuberculosis* biofilm samples and *M. smegmatis* planktonic samples which showed a similar magnitude of binding. There was minimal binding of rabbit anti-human C2a pAb to zymosan and *S. agalactiae.* A Welch's corrected t-test (for unequal variances) showed there was no statistically significant difference in the magnitude of binding between planktonic and biofilm phenotypes ($P>0.05$). This was likely to be due the large variation in the magnitude of fluorescence in the planktonic samples between biological replicates.

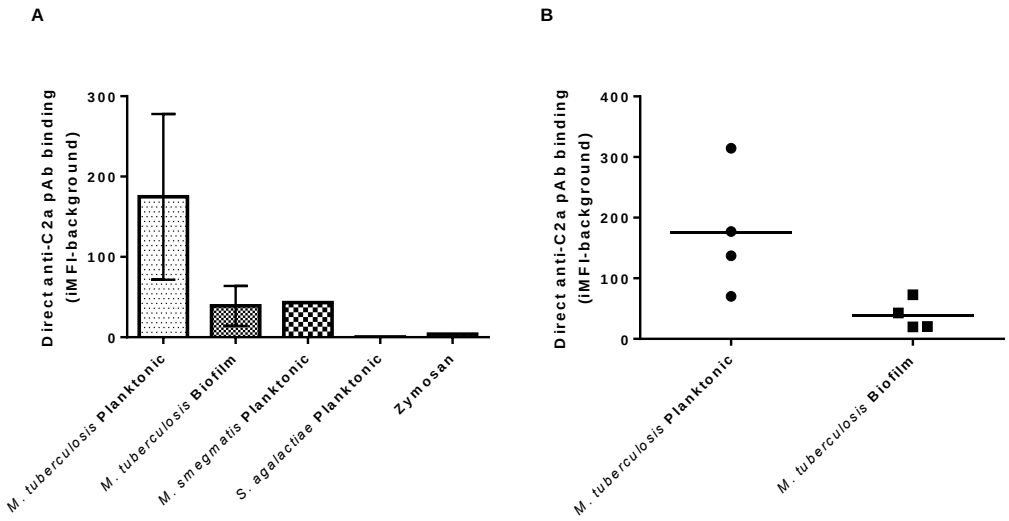


**Figure 5.6.2**: Direct binding of Rabbit anti-human C2a polyclonal antibody to bacteria and zymosan. (A) Binding anti human-C2a pAb to x4 biological replicate *M. tuberculosis* planktonic and biofilm phenotype samples, *M. smegmatis* planktonic, *S. agalactiae* planktonic and zymosan samples. (B) Binding anti human-C2a pAb to x4 biological replicate *M. tuberculosis* planktonic and biofilm phenotype samples only. iMFI-background, iMFI of samples incubated with antibody minus iMFI of control samples incubated without antibody.

## 5.7 Optimisation and analysis of complement deposition on to *M. tuberculosis* carbohydrate extracts

To investigate the extent of complement pathway activation by planktonic and biofilm phenotype *M. tuberculosis* carbohydrates extracts, A method by Bahia El Idrissi et al., (2015) was modified to include a standard curve. Carbohydrate extractions and C3b/iC3b, C5b-9 and MBL ELISAs were performed as described in methods sections 7.13, 7.19, 7.20 and 7.21 respectively.

To investigate C3b/iC3b deposition onto planktonic and biofilm *M. tuberculosis* carbohydrate extracts, Briefly 2.5 µg of x3 biological replicate planktonic and biofilm carbohydrate extract was coated onto wells and incubated with 2% and 10% IgG-depleted human complement. In addition to the x3 biological replicate planktonic and biofilm samples, known concentrations of purified human C3 were labelled with pAb anti-C3c HRP and incubated. Plates were developed by the addition of TMB substrate and quenched after 10 minutes. The absorbance was read and a 5-parameter logistic standard curve was generated with the absorbance readings of known quantities of human purified C3 (**Figure 5.7.1a**). Due to the large difference in C3 quantity at 2% and 10% complement concentrations, a second standard curve of higher C3 concentrations was required to quantify C3 deposition after incubation of carbohydrate extracts with 10% complement, shown in **Figure 5.7.1b.** The net amount (sample + complement + conjugate pg $mL^{-1}$ minus sample + conjugate only negative controls pg $mL^{-1}$) of C3b/iC3b deposition on x3 biological replicate planktonic and biofilm phenotype *M. tuberculosis* carbohydrate samples was calculated by interpolating absorbance values into the standard curve **Figure 5.7.2a**. Welch's t-test revealed C3b/iC3b deposition was significantly reduced on biofilm phenotype *M. tuberculosis* carbohydrate extracts compared to planktonic carbohydrate extracts at physiologically relevant 2% complement concentration (**Figure 5.7.2a**) but not at 10% complement concentration (**Figure 5.7.2b**).

To investigate C5b-9 deposition onto planktonic and biofilm *M. tuberculosis*, carbohydrate extracts plates were prepared in the same manner as with the C3 ELISA and incubated with 2% and 10% complement. Carbohydrate extracts and known concentrations of purified human C5b-9 were then labelled with mouse anti-human C5b-9 followed by goat anti mouse-HRP secondary antibody and incubated. Plates were developed by the addition of TMB substrate and quenched after 10 minutes. The absorbance was read and a 5-parameter logistic standard curve was generated with the absorbance readings of known quantities of human purified C5b-9 **Figure 5.7.1c**. The net amount of C5b-9 deposition on x3 biological replicate planktonic and biofilm phenotype *M. tuberculosis* carbohydrate samples was calculated by interpolating absorbance values into the standard curve **Figure 5.7.2b**. C5b-9 deposition was on average higher on planktonic *M. tuberculosis* carbohydrate extracts, however Welch's t-test showed no significant difference in C5b-9 deposition on planktonic and biofilm phenotype *M. tuberculosis* carbohydrate extracts at both 2% complement concentration (**Figure 5.7.2c**) and 10% complement concentration (**Figure 5.7.2d**).

To investigate MBL deposition onto planktonic and biofilm *M. tuberculosis* carbohydrate extracts plates were prepared in the same manner as with the C3 ELISA and incubated with 10 mg $mL^{-1}$ recombinant MBL. Carbohydrate extracts and known concentrations of recombinant human MBL were then labelled with mouse anti-human MBL followed by goat anti mouse-HRP secondary antibody and incubated and the standard curve was generated with absorbance readings of known quantities of recombinant human MBL (**Figure 5.7.1d**). The net amount of MBL deposition on x3 biological replicate planktonic and biofilm phenotype *M. tuberculosis* carbohydrate samples was calculated by interpolating absorbance values into the standard curve **Figure 5.7.2e**. MBL deposition onto planktonic carbohydrate extracts was on average higher than on biofilm carbohydrates. However, Welch's t-test

showed no significant difference in C5b-9 deposition on planktonic and biofilm phenotype *M. tuberculosis* carbohydrate extracts (**Figure 5.7.2e**)

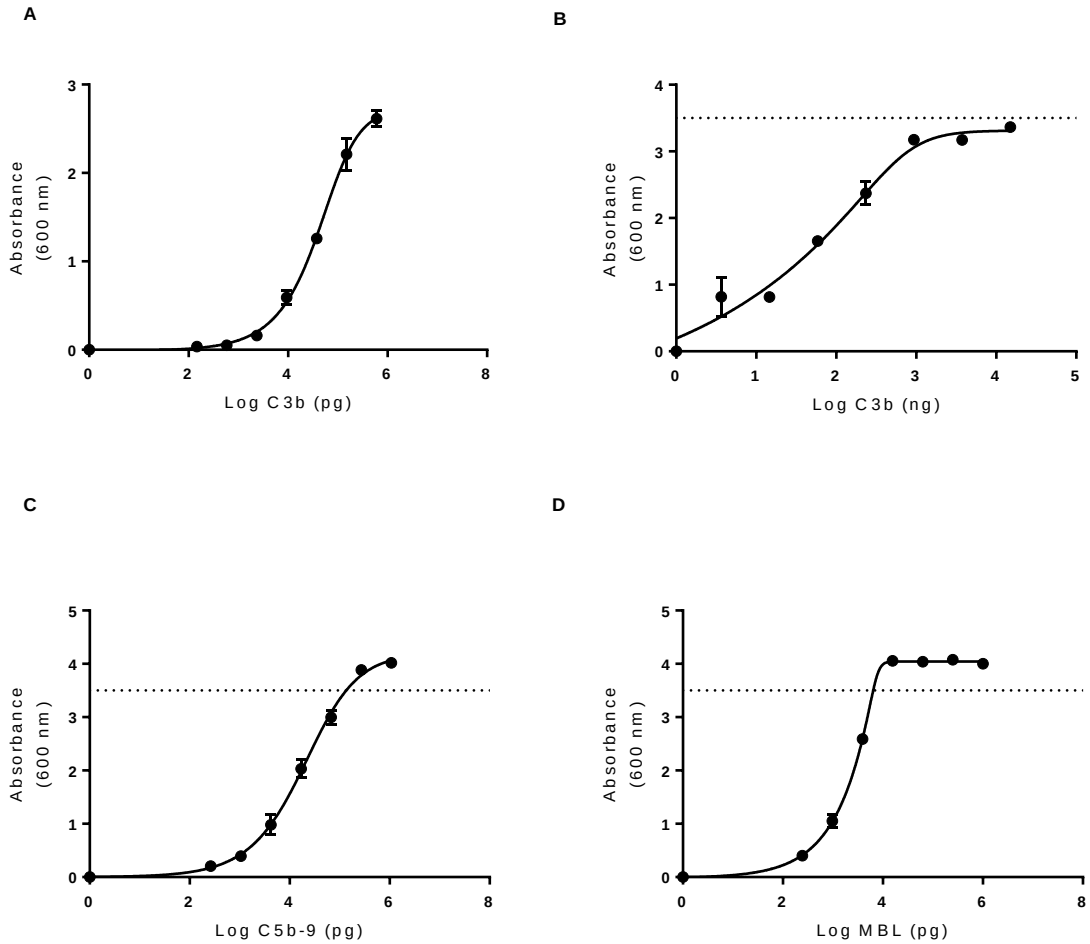


**Figure 5.7.1:** Standard curves for quantification of C3b, C5b-9 and MBL deposition on carbohydrate extracts. (A) 7 point ¼ standard curve of well-bound C3 starting at 600 ng purified C3. (B) 7 point ¼ standard curve of well-bound C3 starting at 15 000 ng purified C3. (C) 7 ¼ point standard curve of well-bound C5b-9 starting at 1080 ng purified C5b-9. (D) 7 point ¼ standard curve of well-bound MBL starting at 1000 ng recombinant MBL. Horizontal dotted-lines indicate ULOQ, Error bars = standard deviation of two replicate curves.

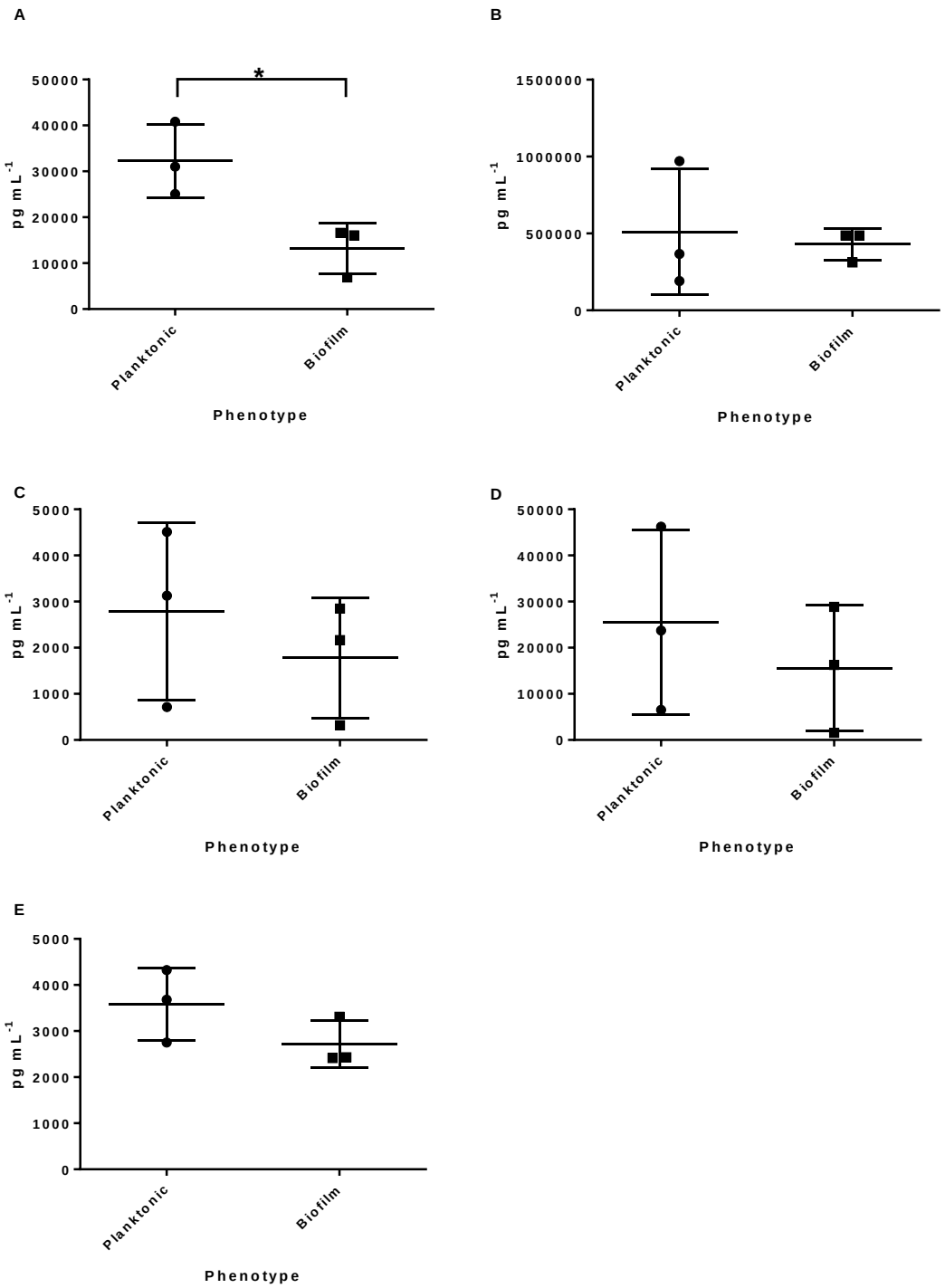


**Figure 5.7.2:** ELISAs measuring complement deposition on planktonic and biofilm phenotype *M. tuberculosis* carbohydrate extracts. (A) C3b/iC3b deposition on planktonic and biofilm carbohydrate extracts incubated with 2% complement. (B) C3b/iC3b deposition on planktonic and biofilm carbohydrate extracts incubated with 10% complement. (C) C5b-9 deposition on planktonic and biofilm carbohydrate extracts incubated with 2% complement. (D) C5b-9 deposition on planktonic and biofilm carbohydrate extracts incubated with 10% complement. (E) MBL deposition on planktonic and biofilm carbohydrate extracts incubated with 10 mg $mL^{-1}$ MBL. Error bars = standard deviation of 3 biological replicates. * = $P<0.05$ Welch's t-test.

## 5.8 Technical discussion

To summarise the final results chapter, *M. tuberculosis* biofilm carbohydrate extracts showed significantly reduced C3b/iC3b deposition compared to planktonic carbohydrate extracts when the alternative pathway was inhibited at 2% complement concentration. This effect was not seen with C5b-9 deposition or MBL binding. Analysis of whole live cell deposition on *M. tuberculosis* planktonic and biofilm phenotypes showed reduced C3b/iC3b deposition and C5b-9 deposition on biofilm phenotype cells and greater importance of the classical pathway in triggering this deposition. Biofilm phenotype *M. tuberculosis* also showed reduced direct C1q binding and MBL binding compared to planktonic phenotype *M. tuberculosis.*

For flow cytometry experiments it was decided that dispersion of planktonic and biofilm cultures followed by low-speed centrifugation was the best way to prepare *M. tuberculosis* cultures. Clumping has been shown to cause issues with flow cytometry assay involving mycobacteria (Hartmann et al., 2001; Lowe et al., 2013). Methods such as dispersal using a vortex alone fail to declump mycobacteria and therefore vortexing samples followed by low speed centrifugation or filtration would be unfeasible due to the large amount of sample loss. As the yields from planktonic cultures were very low, it was not possible to obtain enough dispersed cells without prior mechanical disaggregation of mycobacterial clumps with glass beads. Dispersal using detergents has been shown to alter innate immune responses (Sani et al., 2010) and therefore would not be appropriate for these experiments. Dispersal using glass beads reduced the extent of capsular polysaccharides on the surface of the bacterium (**Figure 5.3.1**), the effect was partial as α(1-2) mannosyl residues on the surface of glass bead treated bacteria could still be labelled. Furthermore, the viability of mycobacteria had been shown to be not significantly reduced after dispersion with glass beads ($P>0.05$).

An ideal measurement of innate complement deposition on *M. tuberculosis* would need to recapture the aerosolised expectorated cells that cause transmission. These are a

heterogeneous population including aerobically growing bacteria and persisters with lipid bodies, as seen in sputum samples (Garton et al., 2008). The aerosolisation of bacteria shed from *in vivo* pellicle biofilms would disperse the bacteria as they are forced upwards and outwards from lung cavities into the air since typical infectious droplet sizes are less than 5 μm in diameter (Fennelly and Jones-López, 2015). As EPS and capsule material are likely to be associated with bacteria in these aerosols, studying dispersed *M. tuberculosis* biofilms may have more *in vivo* relevance than deposition onto whole intact biofilms when studying innate immunity and the establishment of infection.

Absorbance was used to equalise the planktonic and biofilm samples instead of viable counts to compare deposition on equal amounts of biomass. Pellicle biofilm cultures consisted of significant amounts of EPS that was not present in planktonic cultures (**Figure 2.3.1**). In addition, mature 5 week pellicle biofilm cultures may harbour increased viable but non-culturable bacteria that may activate complement. Therefore, adjustment for viability may overcorrect the available surface area for complement interactions in biofilm cells compared to planktonic cells. Thus absorbance was used to keep the available surface area in the samples for complement deposition equal.

Previous studies suggest lowering the complement concentration to ≈2% (1/50 dilution) inhibits the alternative pathway to a far greater extent than the classical pathway due to low availability of factor D, which cleaves factor B (Ferguson et al., 2004; Nilsson and Nilsson, 1984). While alternative pathway activity is greatly restored at 10% concentration (1/10 dilution) (Nilsson and Nilsson, 1984). Additional experimental evidence for the activity of all three pathways at 10% concentration and inhibition of the alternative pathway at 2% concentration, can be gleaned from the results C3b/iC3b and C5b-9 deposition on *M. smegmatis* using complement pre-incubated with C1q (**Figure 5.4.1**). *M. smegmatis* showed no deposition at 2% complement concentration with the classical pathway inhibited but

showed deposition at 10% complement concentration with the classical pathway inhibited. *M. smegmatis* only weakly triggers lectin pathway activation (Bartlomiejczyk et al., 2014). Therefore this suggests the remaining deposition at 10% complement concentration when the classical pathway was inhibited with C1q was attributable to the alternative pathway. The absence of this deposition at 2% complement concentration shows the alternative pathway was inhibited at this concentration.

The C2a binding experiment did not show C2a binding to *M. tuberculosis* but there was direct binding of the anti-human C2a pAb to mycobacteria (**Figure 5.6.2**). The reason for this binding is unclear. However, the most likely answer is that the antibodies were raised in rabbits using human C2a in Freund's complete adjuvant (FCA), which contains mycobacteria proteins (Leenaars et al., 2005). If this were the case it would explain the binding to mycobacteria and a different anti-C2a antibody that was not raised using FCA should be used in this assay. Were direct anti-C2a binding still to be shown in mycobacteria using an antibody confirmed to be raised without FCA, this could suggest a novel host modulation mechanism. The IgG antibodies are unlikely to bind to mycobacteria via their Fc domains, as seen in pathogenic bacteria such as *Streptococcus pyogenes* (Nordenfelt et al., 2012) since this has not been previously reported in the literature. Pathogenic mycobacteria are suggested to have a C4b-like protein that binds with free C2a to create a functioning convertase (Lachmann, 1998; Schorey et al., 1997). If a C2a-like protein is also present on the surface of mycobacteria, could mycobacteria also bind C4b to create functioning convertases? Alternatively could pathogenic mycobacteria secrete fully functioning C3 convertases? Prior to further investigation, an anti-C2a antibody confirmed not to have been raised using FCA should be sourced. Also SDS-PAGE of the purified C1s, C2 and C2-C1s combination could be performed to confirm that the purified C1s enzyme cleaves C2. The experiment could then be repeated.

The biological replicates of the carbohydrates used in the complement ELISAs showed wide-ranging variability in the amount of C5b-9 and MBL deposition (**Figure 5.7.2**). As mentioned during the technical discussion of whole blood stimulation with carbohydrate extracts, this variability could have been reduced by obtaining additional biological replicates. The *M. tuberculosis* planktonic carbohydrate extracts functioned as the control to the biofilm carbohydrate extracts. Yet it would have been preferable to include a positive control such as zymosan, known for its induction of complement activity, to assess whether the levels of complement deposition induced by *M. tuberculosis* carbohydrate extracts were high, as seen with dispersed live whole cells (**Figure 5.4.1**).

In most of the standard curves generated for the ELISAs, and especially for the MBL standard curves, the highest levels of well-bound standard were above the limit of detection of the plate reader. Therefore, for further optimisation of the assay, standard curves should be generated starting from lower concentrations of standard. If for example MBL binding to *M. tuberculosis* carbohydrate was then above the new standard curve range, lower concentrations of MBL could be incubated with the carbohydrate samples. For the ELISAs using 2% and 10% complement incubation, instead of altering complement concentration, the amount of carbohydrate bound to the bottom of each well could be reduced to ensure plate readings were within the range of the instrument.

# 6 DISCUSSION

## 6.1 Biofilm and planktonic growth of bacteria *in vivo*

Biofilms represent the predominant lifestyle of microbes (Watnick and Kolter, 2000) and there is strong evidence that biofilm formation is a key factor in many diseases, including chronic bacterial infections of the cystic fibrosis lung, in which *Pseudomonas aeruginosa* and *Burkholderia cenocepacia* biofilms can cause significant lung damage and increased mortality (Tomlin et al., 2001). Aggregates of bacteria in chronic infections are types of biofilms with increased antibiotic tolerance and resistance to host defences compared to dispersed planktonic bacteria (Bjarnsholt, 2013). There are numerous advantages to bacteria in chronic infections adopting a biofilm phenotype. Firstly the size of the biofilm can lead to 'frustrated phagocytosis' where failure of phagocytes such as neutrophils to engulf the biofilm result in their release of proteolytic enzymes and cytotoxic effectors (Wagner et al., 2003) which drives host tissue damage, releasing nutrients for bacterial growth. Secondly the oxygen/nutrient gradients in the biofilm slow the metabolism of bacteria located in the core turning them into persisters, which can survive antimicrobial therapy and reactivate, resulting in treatment failure as seen with *P. aeruginosa* biofilms (Walters et al., 2003). Thirdly extracellular DNA in the EPS of *P. aeruginosa* biofilms has been shown to sequester cations and inhibit the effectiveness of cationic antimicrobial peptides (Mulcahy et al., 2008). *M. tuberculosis* biofilms in tuberculosis cavities, isolated from adaptive immune responses through fibrosis of the cavity rim (Hunter, 2011) may not require such mechanisms to persist. However, pellicles are easily dislodged from their surface and may be the predominant phenotype of expectorated bacteria during transmission in untreated cavitary tuberculosis cases, as sputum samples suggest similarities between the transmissible bacteria and *in vitro*

pellicles (Arora et al., 2016). Following transmission, mechanisms similar to those described above, may allow *M. tuberculosis* to resist host defences and establish infection.

*M. tuberculosis* replication is asymmetric, with faster growth at the old pole creating two daughter cells of different sizes (Kieser and Rubin, 2014) . Asymmetric division may promote directional interlocking growth of mycobacteria as serpentine cords. The spontaneous tendency of *M. tuberculosis* to form a biofilm in addition to the absence of any non-passive motility mechanism begs the question, is there any point during *M. tuberculosis* pathogenesis when the bacteria do not aggregate as some type of biofilm?

Planktonic *M. tuberculosis* can be observed *in vivo.* Extracellular bacteria within the caseum of granulomas of infected C3HeB/FeJ mice have been shown to be more dispersed than intracellular aggregates at the rim of granulomas (Irwin et al., 2015). As previously mentioned in section 1.3, aerosols of expectorated *M. tuberculosis* can harbour single cells during transmission (Fennelly and Jones-López, 2015). These may be shed from pellicle-like biofilms growing in *M. tuberculosis* cavities (Hunter, 2011) and therefore share similar phenotypic characteristics to dispersed *in vitro* pellicle biofilm cultures. Planktonic intracellular *M. tuberculosis* may only occur in phagocytes able to control infection and prevent replication. *M. tuberculosis* H37Rv requires a multiplicity of infection >10 bacteria to replicate in macrophages (Welin et al., 2011) implying only *M. tuberculosis* bacteria in close proximity, such as biofilms, may be able to induce disease progression. Thus *M. tuberculosis* exists in heterogeneous growth states, since intracellular, extracellular planktonic and biofilm (aggregates) phenotypes have been documented *in vivo* using animal models (Driver, 2014; Hoff et al., 2011; Irwin et al., 2015; Lenaerts et al., 2007; Ryan et al., 2010). *In vivo* planktonic *M. tuberculosis* might be most prevalent when replication is prevented through lack of nutrients/oxygen or via host bacteriostatic immune mechanisms

and the action of pulmonary surfactants. The source of these bacteria could be shed from actively replicating biofilms at the focal site of infection.

### 6.2 Biofilm culture

The comparison of *in vitro* shaken cultures and pellicles is useful principally because the specific type of biofilm being assessed for its immunological effects (pellicles) consists of bacteria encased in a type of EPS which is not present until week 4 of pellicle culture (**Figure 2.3.1e**). SEM of intact pellicles provided evidence that the pellicles are in an organised structure (**Figure 2.4.1**). Historically, pellicle formation has been dismissed as a benign process of aggregation by mycobacterial cell wall hydrophobicity (Ojha and Hatfull, 2012). While hydrophobicity is an obvious pre-requisite to biofilm formation on a liquid surface, if pellicles are merely disorganised aggregations on liquid surface, one would expect a confluent spread of bacteria with no discernible macrostructural features. Whereas true biofilm formation would have distinct morphology and three-dimensional architecture, such as filaments or mushroom-shaped macrocolonies (Flemming and Wingender, 2010). The results presented in this thesis show that *M. tuberculosis* replication in non-perturbed cultures produces organised biofilms with serpentine cords encased in copious quantities of EPS (**Figure 2.4.1**). The delay to pellicle EPS production was until around week four of culture (**Figure 2.3.1**) and could be due to unrestrictive replication of *M. tuberculosis* until confluence is reached on the surface of the medium. The pellicle biofilms contained regions of confluence speckled with cording regions (**Figure 2.4.2**, **Figure 2.4.3**). Within the cords, *M. tuberculosis* bacteria were oriented pole to pole which may provide a much greater surface area to volume ratio than a confluent mass of cells, possibly improving diffusion efficiency during mycobacterial respiration, as gases may be able to penetrate deep into the 3D structure.

Cording is an innate phenomena seen in *M. tuberculosis* and other mycobacteria (Caceres et al., 2013; Julián et al., 2010). *M. tuberculosis* cords enhance macrophage extracellular trap formation (Kalsum et al., 2017). Extracellular trap formation is a controlled cell-death process where the phagocyte releases its chromatin lined with antimicrobial proteins (Boe et al., 2015). But their formation does not affect intracellular mycobacterial growth (Wong et al., 2013). It is now becoming clear that *M. tuberculosis* biofilm formation is an important tuberculosis disease driver involved in all stages of the disease, including intracellular replication. *M. tuberculosis* replication within macrophages aggregate via an ESX-1 dependent process, which is further enhanced by IFN-γ (Wong et al., 2013). After infected macrophage necrosis, the *M. tuberculosis* aggregate may continue to grow, increasing its cytotoxicity to facilitate serial phagocytosis and necrosis and disease progression (Mahamed et al., 2017). Since large aggregates are more cytotoxic than multiple smaller phagocytosis events of the same quantity of bacteria, this suggests that the EPS binding the aggregates plays an important role in cytotoxicity.

Immuno gold EM labelling of α(1,2) mannospyranose residues using anti-PIM/LAM antibody revealed the capsule of *M. tuberculosis* (**Figure 2.4.1c,d**) as has been previously observed (Sani et al., 2010). Furthermore, labelling of the planktonic and biofilm culture aggregates showed EPS also has α(1,2) mannospyranose residues (**Figure 2.4.4**), found in *M. tuberculosis* PIMs, LM, and LAM (Mishra et al., 2011). While these lipoglycans are thought to be anchored to the inner and outer mycobacterial membranes, hydrolysis of the lipid anchor of LM and LAM allows export of mannans and arabinomannans to form the capsule (Angala et al., 2014). It is therefore likely that these polysaccharides are also constituents of EPS. The distinction between capsule and EPS becomes more challenging because *M. tuberculosis* pellicle biofilm cultures have been used to characterise the capsule surrounding each bacterium (Ortalo-Magné et al., 1995). This study utilised the mechanical force of

agitation with glass beads to extract extracellular material without lysing cells but did not acknowledge that a pellicle is a biofilm. Therefore the extracellular material extracted was classed as 'capsule' regardless of whether it was a distinct layer encompassing each bacterium or EPS. Ortalo-Magné et al., (1995) determined the 'outermost cellular material' hereto referred to as EPS, was comprised of 1 – 6% lipids with the remaining 94-99% being a mixture of carbohydrates (arabinomannan, mannan and α-glucan) and proteins.

*M. tuberculosis* pellicle biofilm cells were significantly longer that planktonic cells (**Figure 2.4.1e**). This contrasts with observations made during *M. smegmatis* biofilm formation, in which the bacteria became smaller over time as the pellicle matures (Sochorová et al., 2014). Increased cell size is indicative of arrested cell division but continued cell elongation. It could be indicate of changes to the cell wall components during phenotypic adaptation to pellicle biofilm-conducive conditions. Such conditions may include depletion of phosphate which has been shown to cause cell elongation (Rifat et al., 2009). It would be interesting to investigate whether there is a relationship between cell length and location within the biofilm using microscopy. In addition, to look at how the average cell length of *M. tuberculosis* in biofilms changes over time in relation to alterations to the environment.

The EPS constituents of *M. tuberculosis* could be further characterised by labelling with fluorescent dyes, lectins and antibodies to look for extracellular DNA, specific polysaccharides and proteins respectively (Flemming and Wingender, 2010). Extracellular DNA, a key component of biofilms in many bacterial species, such as *Pseudomonas aeruginosa* (Montanaro et al., 2011), and *M. avium* (Rose et al., 2015) where it contributes to the stability of the biofilm, could be identified on *M. tuberculosis* pellicles following DNase treatment and a crystal violet assay. Alternatively EPS extracted from pellicles (without lysis of the bacteria and leakage of intracellular material) (Ortalo-Magné et al., 1995) could be subjected to additional biochemical analyses to what has already been performed here, such

as liquid chromatography-mass spectrometry, to identify proteins by peptide sequencing and linkage analysis of carbohydrates for accurate identification. It is possible that *M. tuberculosis* pellicle EPS contains ESX-1 secreted proteins, such as the ESAT6 as seen in studies of the capsule of *M. marinum* (Sani et al., 2010). ESAT6 is an immunodominant antigen that directly modulates the immune responses since it has been implicated in *M. tuberculosis* phagosomal escape into the cytosol of infected phagocytes (Houben et al., 2012),

### 6.3 *M. tuberculosis* biofilm phenotype lipid alterations

The growth state *M. tuberculosis* directly modulates the anabolism of carbohydrates and lipids, influencing the quantities expressed, as shown in this thesis, and can also modulate the structure of the macromolecules, as seen with the increased arabinosylation of LAM in NRP *M. tuberculosis* cultures (Bacon et al., 2014). Such alterations are phenotypic adaptations to the environment, sensed by mechanisms such as two component systems to detect oxygen availability (Honaker et al., 2010) and influenced by levels of secondary messengers such as c-di-GMP (Hengge, 2009). *M. tuberculosis* is able to colonise and survive in a wide array of heterogeneous host environments from cavities to necrotising and non-necrotising granulomas (Lenaerts et al., 2015). Large scale changes to the pathogen surface PAMPs in turn alter host immune responses, as seen clearly in other bacteria such as *Neisseria meningitides*, which regulates expression of its virulence factor capsule via the *MisS/R* two component system (Tzeng et al., 2016). The synthesis of capsule imparts anti-adherence and anti-opsonophagocytic properties to *N. meningitides* cells, and also enhances its intracellular survival (Tzeng et al., 2016). While *M. tuberculosis* doesn't show simple switching from highly virulent capsulated and commensal non-capsulated forms, its complex cell wall has numerous components shown to influence the immune response (Angala et al., 2014; Lopez-Marin, 2012; Mishra et al., 2011).

While the EPS of *M. tuberculosis* biofilm and planktonic cultures described in this thesis were not separated from the bacteria for biochemical analysis, lipoglycans and carbohydrates were separated from the mycolyl-arabinogalactan-peptidoglycan cell wall core. These would include carbohydrates located in EPS. Organic soluble lipids were also extracted from the cell envelope and EPS of *M. tuberculosis*. These techniques are well established and are applied to total dried biomass (Besra, 1998). Accurate analysis of EPS would depend on high extraction efficiency, whereas analysis of cell wall extracts include total EPS. However, a drawback of this approach is that the location of specific changes seen in carbohydrates and lipids cannot be delineated between the cell envelope or EPS. It would be preferable in future to optimise EPS extraction efficiency without contamination of intracellular or cell envelope constituents using established techniques (Nielsen and Jahn, 1999). However, since the cell envelope contains free lipids of the outer membrane outer leaflet (predominately TAG, glycopeptidolipids, TDM and diacyl gycerols in *M. smegmatis*) (Bansal-Mutalik and Nikaido, 2014) and capsular carbohydrates (Daffé and Etienne, 1999), complete extraction of EPS without cell envelope contamination may not be achievable.

Triacylglycerol (TAG) was seen as a smear in the biofilm lipid extract, which was reduced to a faint spot in the planktonic lipid extract (**Figure 3.3.1**). Ojha et al., (2008) has previously identified alterations to the lipid profiles of *M. tuberculosis* biofilms compared to planktonic cultures. Specifically, it was shown that biofilms have reduced TAG and increased free mycolic acids. However, Ojha et al., cultured biofilms with Sauton's medium and planktonic *M. tuberculosis* using Middlebrook 7H9+OADC 0.05% Tween 80 and therefore differences in extractable lipids may be due to available nutrients and not specific to pellicle biofilm formation. Furthermore the use of detergent sheds lipids into the culture filtrate (Wheeler, 2009). Notably an increase in TAG can be seen when comparing *M. tuberculosis* cultured in

Sauton's and Middlebrook 7H9 (Dobson et al., 1985). TAG may have been reduced in planktonic lipid extracts cultured for this thesis due to the shedding of lipid into the medium by the shearing forces of the shaken flask. Alternatively TAG could be a constituent of biofilm EPS. TAG has been shown to be in the outer membrane (OM) of *M. smegmatis* (Bansal-Mutalik and Nikaido, 2014). If the *M. tuberculosis* OM also contains TAG, the proportion of OM comprising of TAG may increase under biofilm culture conditions. The increased TAG could also be from increased intracellular lipid bodies or extracellular vesicles used for storage (Garton et al., 2002; Rastogi et al., 2017).

Menaquinones (MK) are a group of mycobacterial lipids present in the plasma membrane and central to the electron transport chain, which have been found to decrease during oxygen limitation (Honaker et al., 2010). The biofilm cultures used in this thesis were in sealed boxes with limited oxygen, yet MK was increased in the biofilm phenotype (**Figure 3.3.1**). This suggests that the available oxygen may not have been fully used up in the biofilm culture. Alternatively the conditions for biofilm formation may also trigger increase biosynthesis of MK. MK may also be shed into the culture medium of planktonic *M. tuberculosis* accounting for the reduction in planktonic cells compared to biofilm cells.

The unidentified lipid $?_1$ and an additional spot at the solvent front (**Figure 3.3.1**) are also not annotated in older reviews of mycobacterial lipid analysis (Besra, 1998; Dobson et al., 1985). The most recent review labels these spots as cholesterol esters (Wheeler, 2009). While *M. tuberculosis* has been shown to be able to metabolise host cholesterol (Pandey and Sassetti, 2008), it was not present in the medium of the cultures used in this thesis. *M. tuberculosis*, like all other prokaryotes, does not synthesise cholesterol (Mouritsen and Zuckermann, 2004). Therefore the identity of this apolar lipids remains to be determined.

Solvent system B revealed free fatty acid (FFA) to be increased in the biofilm phenotype (**Figure 3.3.2**). This spot is also annotated in Besra et al., (2008) in solvent system C which was later identified as free mycolate overlapping FFA (Ojha et al., 2008). Unidentified lipid $?_3$ was present just to the right of FFA in system B. Another unidentified lipid $?_2$ was only seen on 2/3 of the biofilm replicates. The reason why it did not show up on a simultaneous extraction and TLC analysis of a biological replicate is unclear. It is worth repeating the lipid analysis of *M. tuberculosis* biofilms to determine whether the presence/absence of $?_3$ is an artefact or a novel unidentified lipid unique to the biofilm phenotype. Notably there was no reduction in free lipid trehalose mycolipenates (TMPs) between planktonic and biofilm phenotype, suggesting that the shedding of mycobacterial lipids into the medium may not be a significant issue in the shaken planktonic cultures.

Free mycolates are a major component of *M. tuberculosis* pellicle biofilm EPS (Ojha et al., 2008) and were increased in *M. tuberculosis* biofilm cultures compared to planktonic cultures (**Figure 3.3.3**) as previously described by (Ojha et al., 2008). The effect size did not appear as significant as the earlier publication and this may be due to the absence of detergent in the planktonic medium of cultures used in this thesis compared to Ojha et al., (2008). Free mycolate is thought to be a major constituent of the pellicle biofilm matrix (Zambrano and Kolter, 2005), with keto mycolic acids essential for its formation (Sambandan et al., 2013). Mycolic acids introduced into the airways of mice have been shown to induce foamy-like macrophages similar to those found in tuberculosis granulomas and modulate cytokine expression (Korf et al., 2005). This suggests that *in vitro* infection of macrophages with biofilm phenotype *M. tuberculosis* may better reflect the *in vivo* transformation of alveolar macrophages into foam cells during tuberculosis infection compared to infection with planktonic *M. tuberculosis*.

Additional unidentified lipids were present in solvent system C, ?$_4$, ?$_5$ and ?$_6$ (**Figure 3.3.3**). These have not been annotated in systematic *M. tuberculosis* lipid reviews (Besra, 1998; Wheeler, 2009).Wheeler annotated phenolic glycolipids in solvent system C but the additional spots in the system C TLCs presented in this thesis are not phenolic glycolipids as the H37Rv strain does not synthesise phenolic glycolipids (Pang et al., 2012). ?$_6$ appeared in 2/3 biofilm replicates and could be an artefact or a biofilm phenotype specific lipid, whereas ?$_4$ and ?$_5$ were present in all planktonic and biofilm *M. tuberculosis* replicates.

System D can be used to analyse both polar and apolar lipids (Besra, 1998). Recently an improved system D has been developed (Wheeler, 2009) which allows visualisation of glycolipids trehalose dimycolate (TDM), trehalose monomycolate (TMM) and sulfolipid (SL-I) in apolar lipid mycobacterial extracts. TDM and TMM have also been seen in the polar extract of *M. bovis* (Pirson et al., 2012). There was no obvious trend of increased or decreased TMM or TDM between planktonic and biofilm samples in apolar lipid extracts (**Figure 3.3.4**) or polar lipid extracts (**Figure 3.3.5**). Total levels were surprisingly low considering that TDM is a major component of *M. tuberculosis* pellicles (Robert Lee Hunter et al., 2006). SL-I was increased in biofilm phenotype *M. tuberculosis*. Regarding innate immunity, one study showed a genetic *M. tuberculosis* mutant that couldn't produce SL-I had increased intracellular growth and survival and was more resistant to antimicrobial peptide LL-37 (Gilmore et al., 2012). The reason why *M. tuberculosis* evolution has conserved a lipid that negatively regulates growth and survival is unclear, yet it may be involved in phenotypic change into non-replicating persisters, as seen with the upregulation of TAG containing extracellular vesicles in low iron medium (Rastogi et al., 2017). Further studies are required to elucidate the localisation and role of SL-I during infection. There remains a possibility that the lipids in system D have been incorrectly annotated. For example, SL-I could be TDM. To

confirm the identity of the spot labelled SL-I, H-NMR could be performed as described for the identification of free mycolates by Ojah et al., (2008).

No differences were seen between planktonic and biofilm phenotype *M. tuberculosis* in system E (**Figure 3.3.7**) Annotations were based on Pirson et al., (2012) who were able to discriminate not only between dimannoside and hexamannoside PIMs but also the mono and diacyl derivatives. Diphosphatidylglycerol can be seen in MPA stained system E. However the system E TLCs in this thesis were stained with α-napthol for glycolipids. Therefore the identities of glycolipids $?_6$ and $?_7$, which can be seen in planktonic and biofilm phenotype *M. tuberculosis* remain to be elucidated. All unidentified lipids could potentially be identified using comprehensive lipidomics analysis by separation simplification (CLASS) or shotgun lipidomics mass spectrometry approaches (Harkewicz and Dennis, 2011). Mass spectrometry could also be used to investigate potential structural differences, such as proximal cyclopropanation (Glickman et al., 2000) in the cell wall mycolic acids from biofilm and planktonic extracts (MAMES).

### 6.4 *M. tuberculosis* biofilm phenotype carbohydrate alterations

Non-replicating *M. tuberculosis* in batch cultures have previously been shown to gradually extend LAM through arabinosylisation visible over the course of >200 days and with visible extension during late stationary phase compared to exponential phase (Bacon et al., 2014). Extension of LAM in the 35 day mature biofilm cultures was not seen compared to 7 day exponential phase planktonic cultures (**Figure 3.4.1**). This suggests the pellicle model of biofilm phenotype differs from the biofilms produced by NRP *M. tuberculosis* and may therefore have a different infectivity profile in the guinea pig infection model.

The reduced constituent sugar glucose in the carbohydrate extracts of biofilm *M. tuberculosis* (**Figure 3.4.3**) suggest either *M. tuberculosis* α-glucan (Ortalo-Magné et al., 1995) or

cellulose (Trivedi et al., 2016) or both are less prevalent in biofilm phenotype *M. tuberculosis*. Future analysis of biofilm phenotype carbohydrates should include linkage studies to determine from which carbohydrate the sugar is derived from. This approach was unsuccessfully attempted with one of the extracts produced for this thesis. However it can be inferred that the most likely carbohydrate is α-glucan since Ortalo-Magné et al., (1995) used Sauton's medium pellicle biofilms in their linkage study and only identified α-glucan, while cellulose has only been observed in surface attached biofilms induced by exposure to dithiothreitol (Trivedi et al., 2016).

If α-glucan and/or cellulose prevalence depletes during *M. tuberculosis* biofilm maturation, it is worth discussing how this may occur. One possibility is the upregulation of glucoside hydrolases to recycle glucose residues stored in carbohydrates. *M. tuberculosis* has been shown to harbour β-glucanases (Varrot et al., 2005) which could be upregulated if cellulose is metabolised during biofilm maturation. Also *M. tuberculosis* harbours the gene *treX* which encodes a malto-oligosyltrehalose synthase thought to target the α(1-6) branch linkages of α-glucans. While TreYZ acts on linear α(1-4) glucans to convert them into trehalose, and can be further hydrolysed to glucose by Rv2402. Additionally gene *Rv2471* encodes a putative α-glucosidase which may target terminal α(1,4) residues of α-glucans (Van Wyk et al., 2017). Another possibility is the downregulation of genes involved in the synthesis of α-glucan via the GlgC-GlgA, the Rv3032 and the TreS-Pep2-GlgE pathways (Koliwer-Brandl et al., 2016). The expression of glucose metabolism genes during biofilm formation and maturation could be assessed using RNA-Seq at specific time points in conjunction with corresponding carbohydrate/lipoglycan extractions to reveal the pathways responsible for the reduction in glucose in *M. tuberculosis* biofilm carbohydrate extracts.

## 6.5 Cytokines and chemokines involved in tuberculosis

Cytokines and chemokines direct much of the host response to pathogens by regulating inflammation and recruiting immune cells to the site of infection. Modulation of cytokine and chemokine responses can have a profound effect on the immune responses in tuberculosis (Hossain and Norazmi, 2013), as outlined in the paragraphs below. The subversion of immune signalling mechanisms by *M. tuberculosis* through dynamic changes in pathogen PAMPs and host PRRs at the host pathogen interface in the tuberculosis lung can result ultimately in cavitation and the transmission of the bacteria from an immunocompetent, ambulatory individual (Orme et al., 2014). Should biofilm formation be a key factor in tuberculosis pathogenesis, the functional result of biofilm-specific cytokine and chemokine responses may help elucidate those that offer protection and those that contribute to pathology.

IFN-γ release is the hallmark of a Th1 adaptive immune response, thought to be fundamental for a control of *M. tuberculosis* infection (Torrado and Cooper, 2013). However it can also be secreted after recognition by innate immune cells. Natural killer T cell (NKT) expressing Valpha19-Jalpha33 T cell receptor alpha chain circulate in blood and recognise MHC-related protein 1 (MR1) presented α-mannosyl phosphatidyl inositols, which form part of the structure of mycobacterial PIMs, LAM and LM and induce IFN-γ secretion (Shimamura, 2008). The carbohydrate extracts contained these lipoglycans and therefore could conceivably induce IFN-γ secretion after whole blood stimulation. NKT cell activation has been shown to produce IFN-γ, recognise *M. tuberculosis* infected macrophages, and reduce bacterial load (Sada-Ovalle et al., 2008). In addition, natural killer (NK) cells produce IFN-γ rapidly in response to *M. tuberculosis* exposure (Feng et al., 2006). TLR4 and TLR2 recognise mycobacterial lipoglycans (Jones et al., 2001) and both of these receptors are expressed by NK cells (Adib-Conquy et al., 2014). Finally γδ T Cells recognise CD1b

presented lipoglycans (Sieling et al., 1995) and also produce IFN-γ in response to TB infection (Gioia et al., 2003). **Figure 4.3.7** showed IFN-γ was not induced by *M. tuberculosis* carbohydrate extracts. This suggests NK, specific NKT and γδ T cells may have been present in whole blood at levels too low to allow detection of their activation. Another possibility is that the process of the loading lipoglycan fragments for antigen presentation and innate t-cell activation required more than 24 hours stimulation. Zymosan strongly induced IFN-γ in all three donors suggesting that there were sufficient populations of innate cells in whole blood capable of inducing IFN-γ secretion.

Paradoxically, the experiment stimulating whole blood with capsule extracts suggested Zymosan did not induce an IFN-γ response **Figure 4.6.1**. This difference may be due to the higher concentration of Zymosan used, which could be a sub-optimal concentration for measuring IFN-γ response after cytokine stimulation. Alternatively, donor blood responses to Zymosan stimulation may depend on previous exposure to the substance and/or their genetic background. *M. tuberculosis* capsule extracts induced an IFN-γ response, the extent of which varied widely between biological replicates. The crude method of material extraction using glass beads and filtration may account for this variability as the extracts could contain varying proportions of lipids, proteins and carbohydrates. Secondly the response was much larger in one of the donors and this could be due to recent exposure to environmental mycobacteria in the high responder, as seen in false positive tuberculin skin tests (O'Garra et al., 2013).

None of the stimulants induced IL-12p70 (**Figure 9.2.1**) above the lower limit of detection (25 pg $mL^{-1}$). The standard curve fit was only 90% with the lowest dilution excluded from the curve and this may have contributed to IL-12p70 results below the LLOQ. IL12p70 comprises of two subunits IL12p40 and IL12p35 and this cytokine is thought to be vital for inducing the generation of IFN-γ producing in T cells (Torrado and Cooper, 2013) and NK

cells (Ye et al., 1995). Although there have been conflicting studies, in general studies have shown that Man-LAM causes no change in IL-12 secretion in monocyte/macrophage cell cultures while LM has been found to increase IL-12 production and PIMs cause no change (Källenius et al., 2015). The carbohydrate samples used in this thesis were a mixture of these compounds, with varying proportions (**Figure 3.4.1**, **Figure 3.4.2**) and additionally α-glucan. The variability between samples complicates interpretation of the complex interplay between the *M. tuberculosis* carbohydrate extracts and the immune response in whole blood and may have masked phenotype-specific changes in the relative proportions of constituent glucose.

Some but not all *M. tuberculosis* carbohydrate extracts induced an IL-1β response with the highest levels induced by planktonic *M. tuberculosis* in donor 1, although this was not statistically higher than the level induced by *M. tuberculosis* biofilm carbohydrate extracts (**Figure 4.3.8**). It is possibly that with a larger number of biological replicates a significant difference would be seen however the biological significance of this difference would remain unclear. The amount of IL-1β secretion induced by *M. tuberculosis* carbohydrate extracts was considerably less than the zymosan positive control. Since *M. tuberculosis* is an obligate human pathogen and IL-1β has been shown to direct killing of *M. tuberculosis* (Master et al., 2008) there would be a strong selection pressure for *M. tuberculosis* carbohydrate synthesising enzymes and exporting proteins to create outermost carbohydrates which induce minimal IL-1β. The ability of *M. tuberculosis* carbohydrates to induce IL-1β *in vivo* may be masked by the action of proteins such as zmp1, which inhibits inflammasome activation (Master et al., 2008). In addition, excessive IL-1β production induces pyroptosis, which *M. tuberculosis* is able to subvert via secretion of Rv3365c, which inhibits downstream activation of caspase-1 required for IL-1β production (Danelishvili et al., 2011).

IL-2 is secreted by activated $CD4^+$ T cells (Nelson, 2004) but can also be produced by naïve dendritic cells (Granucci et al., 2001) and naïve $CD8^+$ T cells (Cheng et al., 2002) and

primarily acts to induce the proliferation of T cells. Dendritic cells and naïve $CD8^+$ T cells make up <1% and <3% of leukocytes in whole blood respectively (Technologies, 2010). Concerning innate immunity, presumably early secretion of IL-2 would be beneficial to the host since it may promote the rapid onset of $CD4^+$ T cell mediated immunity (Nelson, 2004) for *M. tuberculosis* control. Within the 24 hour stimulation period there was no significant change in IL-2 secretion (**Figure 4.3.9**) implying that none of the donors had active adaptive immunity to tuberculosis with $CD4^+$ T cells secreting IL-2 and endogenous innate expression of IL-2 in naïve whole blood does not respond to PRR recognition of *M. tuberculosis* carbohydrate extracts.

IL-4 is a key Th2 cytokine often associated with the response generated in hosts after chronic infection by large parasites such as helminths (van Panhuys et al., 2011). It has anti-inflammatory effect and inhibits IFN-γ production (Powrie et al., 1993). IL-4 secretion by $CD4^+$ and $CD8^+$ T cells is higher in tuberculosis patients, especially those with cavitary tuberculosis compared to controls. Tuberculosis cavities are where pellicle-like biofilms are thought to exist (Hunter, 2011; Hunter et al., 2014). NKT cells and basophils in whole blood are able to produce IL-4 after stimulation (Seder et al., 1991; Yoshimoto and Paul, 1994). The experiment measuring IL-4 response after 24 hour stimulation with carbohydrate extracts showed levels of IL-4 were only clearly above the LLOQ in one of the 3 donors. This suggests the variation between donors has a larger effect on IL-4 secretion compared to carbohydrate stimulation. Furthermore, even with donor 3, zymosan and *M. tuberculosis* stimulated whole blood induced a less than 1-fold response suggesting innate IL-4 producing cells e.g. basophils rely on different pathogen associated molecular patterns (PAMPS) than those present on the carbohydrate extracts in this assay.

IL-5 is a Th2 cytokine which stimulates the activation and proliferation of eosinophils and primarily expressed by T cells and mast cells (Matthaei et al., 1997; Murphy, 2012). One

study looking at SIV and TB coinfection in the cynomologus macaque model showed SIV-induced IL-5 production in monocytes reduced the frequency of *M. tuberculosis* specific CD4 T cells (Diedrich et al., 2013). If biofilm *M. tuberculosis* carbohydrates promoted a Th2 like response similar to large organism parasitic infections then IL-5 could be a biomarker. However no evidence was seen for this after whole blood stimulation with biofilm carbohydrate extracts.

IL-6 was one of the cytokines which showed the largest responses after exposure to planktonic and biofilm *M. tuberculosis* capsule and carbohydrate extracts. IL-6 has been shown to be the only consistent cytokine biomarker of *M. tuberculosis* infected murine peritoneal macrophages (Singh and Goyal, 2013). IL-6 has also been shown to inhibit effective IFN-γ dependent macrophage activation, which may contribute to impaired mycobacterial clearance (Nagabhushanam et al., 2003). Since capsule extracts induced far greater IL-6 production than carbohydrate extracts, the major source of IL-6 induction could be mycobacterial EPS lipids or proteins.

TNFα is secreted after exposure of macrophages to *M. tuberculosis* LAM (Källenius et al., 2015). The release of TNFα can trigger IFNγ dependent reactive nitrogen intermediate production and mycobacterial killing (Chan et al., 1992). Yet TNFα production in alveolar macrophages has been shown to permit *M. tuberculosis* growth (Engele et al., 2002) Tuberculosis diseased mice that cannot produce TNFα receptors have reduced survival (Flynn et al., 1995) showing TNFα production to be a broadly protective. The results in this thesis do not suggest carbohydrates from *M. tuberculosis* biofilm phenotype modulate TNFα secretion any differently to planktonic phenotype. However removal of capsular polysaccharides using Tween 80 has been shown to modulate TNFα production (Sani et al., 2010). It is therefore possible that TNFα induction is primarily caused by arabinomannans and mannans, which are not altered between planktonic and biofilm phenotypes.

GM-CSF is constitutively expressed in the lung and has been shown to enhance protection against tuberculosis in mice and improves the effectiveness of tuberculosis vaccines (Chroneos and Jagannath, 2012). Over expression of Th2 cytokine IL-13 in mice infected with *M. tuberculosis* produced necrotizing granulomas similar to human pathology which would otherwise be absent in mice (Heitmann et al., 2014). Since these cytokines modulate disease progression in tuberculosis their induction by *M. tuberculosis* warrant further study. However the whole blood stimulation technique used in this thesis failed to show detectable levels of GM-CSF and IL-13 suggesting it may not be an appropriate assay for detection of these cytokines. IL-18 enhances the protective Th1 response against tuberculosis in mice (Schneider et al., 2010) yet its production in *M. tuberculosis* carbohydrate stimulated whole blood does not appear to be affected by phenotype.

CCL11 is increased in *M. tuberculosis* patients (Sharifabadi et al., 2014), CXCL1 is secreted early on in the *M. tuberculosis* mouse infection model (Kang et al., 2011). CXCL8 can directly bind to *M. tuberculosis* and enhance phagocytosis and *M. tuberculosis* killing (Krupa et al., 2015). CXCL10 has been touted as a potential biomarker for *M. tuberculosis* infection (Ruhwald et al., 2012). Humans with *CCL2*-2518 (A/G) polymorphisms which increases expression of CCL2 are more susceptible to active TB (Feng et al., 2012) . While a similar type of study found no association with CCL3 and CCL4 with susceptibility to pulmonary TB (Singh et al., 2014), they may still be involved in orchestrating innate immune responses to tuberculosis (Monin and Khader, 2014). CXCL12 is another potential biomarker of tuberculosis disease (Kohmo et al., 2012). Finally CCL5 knockout mice have been shown to have delayed IFNγ responses and poor control of *M. tuberculosis* growth indicating a role in innate immunity to tuberculosis (Vesosky et al., 2010). Despite these the involvement of these chemokines in tuberculosis disease, their expression appears broadly generic when comparing the responses generated between planktonic and biofilm phenotype *M.*

*tuberculosis*. An alternative complementary approach to the one taken in this thesis could utilise *M. tuberculosis* mutants with completely inhibited biofilm formation grown under the same conditions. This approach taken with titration of a broader range of carbohydrate stimulant concentrations may highlight interesting biofilm-specific innate responses not seen in the data presented in this thesis. Undoubtedly, comparison of planktonic and biofilm lipid extracts, EPS extract and whole biomass would also be of interest.

MMP-1 the primary collagenolytic MMP in TB, is the most likely protease to be responsible for triggering cavitation, which is essential for *M. tuberculosis* transmission (Elkington et al., 2011). Since pellicle biofilms are associated with tuberculosis cavities, biofilm capsule may also be a more potent inducer of MMP-1 than planktonic capsule. The results presented in this study suggest that neither planktonic or biofilm capsule were able to trigger MMP-1 secretion. Since cavitation can appear suddenly after years of control, it may be that MMP-1 secretion at levels significant enough to form a lung cavity is only triggered in a hypersensitivity reaction once a threshold in the accumulation of mycobacterial antigens has been reached (Hunter et al., 2014). The data presented in this thesis suggests that MMP-1 secretion may not be involved in the establishment of infection. However, it cannot be ruled out because it would be preferable to observe MMP-1 secretion in human alveolar macrophages or BAL fluid after stimulation with *M. tuberculosis* extracts to better model the establishment of infection.

### 6.6 Biofilm formation and the complement system

The complement system is an innate immune surveillance system as well as regulating the clearance of apoptotic host cells (Merle et al., 2015). There are three primary immunologic outcomes from complement activation are opsonisation by covalent attachment of C3b to the surface of bacteria, deposition of the C5b-9 membrane attack complex and the release of anaphylatoxins C3a and C5a to regulate inflammation (Murphy, 2012). There is also cross-

talk with adaptive immunity via antibody-dependent activation of complement via the classical pathway and C3aR and C5aR expressed on the surface of activated T cells, contributing to recruitment and development of a Th1 response (Merle et al., 2015). Complement deposition and activity has been shown to be modulated by biofilm formation compared to the planktonic growth state in many species of bacteria. For instance, *Streptococcus pneumoniae* biofilms impair C3b and C1q deposition with increased factor H recruitment, which downregulates the alternative pathway (Domenech et al., 2013). While *Mycoplasma pulmonis* biofilms are more resistant to complement killing (Simmons and Dybvig, 2007). *Staphylococcus epidermidis* biofilms promote more C3 cleavage than planktonic cells yet less C3b binds to the bacteria embedded in the biofilm (Kristian et al., 2008). Also, *Acinetobacter baumannii* strains that produce more biofilm are more resistant to complement mediated killing than strains that produce less biofilm (King et al., 2009). Similarly the EPS of *M. tuberculosis* pellicle biofilms could modulate complement deposition. Furthermore, the changes seen in *M. tuberculosis* carbohydrate extracts may directly influence the affinity of lectin pathway complement activators.

The results from this thesis agreed with the published literature that complement deposition on *M. tuberculosis* complex can be activated by direct binding of C1q, MBL and ficolin-3 to *M. tuberculosis* (**Figure 5.5.1**) (Bartlomiejczyk et al., 2014; Carroll et al., 2009), and by the three major complement pathways (**Figure 5.4.2**) (Bartlomiejczyk et al., 2014; Ferguson et al., 2004; Schlesinger et al., 1990). However, the *M. tuberculosis* C2 pathway of complement deposition was not observed (**Figure 5.6.1**)

Flow cytometry revealed a significantly reduced magnitude of C3b/iC3b and C5b-9 deposition on *M. tuberculosis* biofilm cells compared to planktonic cells (**Figure 5.4.2**), yet quantitative ELISA of sugar extracts only showed significantly reduced C3b/iC3b deposition at 2% complement concentration (**Figure 5.7.2**). There are several possible reasons which

may explain why. Firstly, the method of quantification for ELISAs differed to the flow cytometry experiments, although there is evidence that there may be a linear correlation from other studies (Shooshtari et al., 2010). Secondly, whole cells contain lipids and proteins, which are also modified in the biofilm phenotype, and may result in altered affinity to complement activators. For example, surface expressed proteins and free lipids may provide additional direct binding sites for C1q. C1q has been shown to bind to bacterial proteins, lipopolysaccharide and phospholipids (Kishore et al., 2004). Additionally the as yet unidentified C4b-like protein present on surface of pathogenic mycobacteria that is able to form a convertase with host C2a (Schorey et al., 1997), may have altered expression on biofilm phenotype cells. The C5b-9 complex only forms where C3b has already bound. The availability of C5 convertases on 2% complement incubated biofilm *M. tuberculosis* may not be a rate limiting factor for C5b-9 assembly, accounting for similar quantities of C5b-9 deposition on planktonic and biofilm carbohydrate extracts. The phenotype dependent interference of lipids and proteins on C5b-9 deposition may account for reduced deposition on biofilm whole cells. Thus the absence of the full spectrum of complement activator epitopes in the planktonic and biofilm *M. tuberculosis* carbohydrate extracts is the most likely reason why there was no significant reduction in C5b-9 deposition at 2% and 10% complement concentration and C3b/iC3b deposition at 10% concentration on biofilm *M. tuberculosis* carbohydrate extracts. Additionally the alternative pathway, which is a positive feedback loop that amplifies complement deposition, may mask any differences in complement activation triggered by the lectin pathway on the planktonic and biofilm carbohydrate extracts incubated with 10% complement concentration.

A significant reduction in C3b/iC3b deposition onto biofilm *M. tuberculosis* carbohydrate extract was observed when the alternative pathway was inactive (**Figure 5.7.2a**). This is physiologically relevant as the alternative pathway is not active in the human lung (Watford

et al., 2000). The reason why biofilm carbohydrate extracts showed reduced C3b/iC3b deposition at 2% concentration is unlikely to be due to reduced affinity to MBL, since MBL deposition on biofilm phenotype carbohydrate extracts is not significantly different from planktonic MBL deposition (**Figure 5.7.2e)**. Reduced affinity of other complement activators in the IgG-depleted complement source, such as C1q or serum ficolin-2 (Ren et al., 2014) to biofilm carbohydrate extracts are more likely to account for the reduced C3b/iC3b deposition seen on biofilm carbohydrate extracts at 2% complement concentration.

Since there is redundancy in the mechanisms *M. tuberculosis* utilises to enter cells (Schlesinger, 1996), it may be that reduced complement activation would have little effect on phagocytosis efficiency. This could be assessed using a macrophage infection assay. However the cleavage of C3 also releases anaphylatoxin C3a. C3a is an inflammatory modulator and is proinflammatory in chronic inflammation where monocytes and macrophages predominate, inducing the production of IL-1β, TNF-a and IL-6 (Coulthard and Woodruff, 2015). C3a induced IL-1β production and subsequent inflammasome activation (Asgari et al., 2013) may enhance early clearance of *M. tuberculosis* bacteria (Master et al., 2008). Since the sight of establishment of infection is the alveoli, rich in alveolar macrophages, it may be advantageous for the establishment of tuberculosis infection if C3a activation was low. C3a release after incubation of carbohydrate extracts with complement could be measured directly with a fluorescent anti-C3a antibody following aspiration of the supernatant. A study utilising C3aR deficient mice has shown C3aR enhances early clearance of intracellular pathogen *Chlamydia psittaci* in the mouse lung and increases recruitment and proliferation of $CD4^+$ T cells (Dutow et al., 2014).

Notably direct C1q binding to biofilm phenotype *M. tuberculosis* was reduced (**Figure 5.5.2b**) despite the C3b/iC3b and C5b-9 deposition assay suggesting greater dependence on the classical (C1q) pathway for C3b/iC3b and C5b-9 deposition onto biofilm cells (**Figure**

**5.4.2e,f**). This could be due to a number of reasons. Firstly natural antibodies in the complement source may have interacted to a greater extent with *M. tuberculosis* biofilm phenotype compared to planktonic phenotype and C1q bound via these secondary sites. Conversely, another explanation is that this discrepancy is due to the lectin pathway and/or C2 pathway. **Figure 5.5.2a** shows that MBL deposition is increased on planktonic bacteria compared to biofilm bacteria. The effect size is also greater than with C1q. MBL that is present in the complement source would interact to a greater extent with planktonic *M. tuberculosis* compared to biofilm grown bacteria and therefore reduce the relative contribution of the classical pathway in C3b/iC3b deposition in planktonic phenotype compared to biofilm phenotype.

MBL binds to mannose and glucose residues (Weis et al., 1992) and therefore the reduced α-glucan prevalence on biofilm phenotype *M. tuberculosis* may be the reason why deposition is higher on planktonic bacteria. However, although MBL deposition is higher on average on *M. tuberculosis* planktonic carbohydrate extracts compared to biofilm carbohydrate extracts, the difference was not statistically significant (**Figure 5.7.2e**). A potential reason why no statistical significance was seen could be because a relative reduction in the proportion of glucose coincides with a relative increase in the proportion of mannose in the biofilm extracts compared to planktonic extracts (see results section 3.4).

The complement deposition experiments on live bacteria also included positive controls to guide interpretation of the results; specifically the inclusion of *M. smegmatis*, which is an environmental bacterium and would be less likely to have evolved complement evasion mechanisms. Whereas *S. agalactiae* evades complement activation *in vivo* (Jarva, 2003). *S. agalactiae* serotype Ia has been shown to recruit the negative regulator of complement activation Factor H to its surface protein Bac in order to avoid C3b deposition (Areschoug et al., 2002). Notably even *M. tuberculosis* biofilm phenotype bacteria show greater deposition

of C3b/iC3b and C5b-9 compared to *M. smegmatis* (**Figure 5.4.1**). The functional implications of the biofilm phenotype specific reduction in complement activation have not yet been assessed. It would be necessary to assess *M. tuberculosis* survival and replication and immunological parameters in a macrophage infection model using non-opsonised and complement opsonised planktonic and biofilm cells to determine this in future.

The biological implications differential C3b/iC3b binding between planktonic and biofilm phenotypes may not be in the subsequent efficiency of phagocytosis and intracellular fate of the bacteria, since *M. tuberculosis* uptake and intracellular survival is efficient with or without complement activation (Schlesinger, 1996). Equally C5b-9 deposition to lyse the bacterial membrane is considered to be a useless host defence against Gram positive bacteria, yet shows distinct localisation in a controlled manner on Gram positive bacteria such as *Streptococcus pyogenes* and *Bacillus subtilis*, implying other immunological roles for the C5b-9 complex (Berends et al., 2013). While the function of localised binding to either the septum or poles respectively of these bacteria remain undefined, the localisation of C5b-9 deposition on planktonic and biofilm phenotype could be similarly investigated. The effects of complement activation are not limited to opsonisation and lysis of Gram negative bacteria. Complement acts as an extracellular surveillance and alarm system which interacts with innate and adaptive elements and regulates inflammation (Triantafilou et al., 2015). The effect of C5b-9 deposition on *M. tuberculosis* viability could not be found in a literature search although its deposition may be beneficial to the pathogen since the lungs of C7 deficient mice show reduced pathology (Welsh et al., 2012). C5b-9 has been shown to deposit onto *M. leprae* LAM to a far greater extent than *M. tuberculosis* LAM and it is postulated that C5b-9 assembly and complement activation is associated with nerve damage (Bahia El Idrissi et al., 2015). Therefore C5b-9 deposition on *M. tuberculosis* may be associated with other components of the *M. tuberculosis* cell envelope and EPS.

In tandem with complement deposition is the release of anaphylatoxins C3a and C5a. While little work has been published on C3a and tuberculosis, gene expression and serum levels of C3 have been shown to be higher in wild boars without active bovine tuberculosis (Naranjo et al., 2006a, 2006b). There have been extensive studies about the protective role of C5a. A/J mice deficient in C5 showed enhanced *M. tuberculosis* growth in the lungs and reduced TNFα, IL-1β, IL-6, IL-12 CXCL1, CXCL2 and CCL3 compared to C5 sufficient B10 mice (Jagannath et al., 2000). Congenic C5 sufficient and deficient mice were then tested and C5 deficient mice were found to have decreased IL-12p40 transcription and reduced CXCL1, CXCL2, CXCL10 and CCL2 transcription as well as increased bacterial load in the lung (Actor et al., 2001). TDM injection into C5aR deficient mice were unable to form granulomas and showed excessive inflammation with, contrary to the Actor et al., study, increased CCL3, CXCL1, IL-β and TNF-α secretion (Borders et al., 2005). Interestingly, viable delipidated and TDM reconstituted *M. tuberculosis* have been introduced into C5a sufficient and deficient macrophages. Wild type *M. tuberculosis* and TDM reconstituted *M. tuberculosis* showed greater TNFα and IL-6 production compared to delipidated *M, tuberculosis* and the response was always greater in C5a sufficient macrophages compared to C5a deficient macrophages (Welsh et al., 2008). Finally regarding adaptive immunity, purified C5 deficient mouse T cells secrete less IFNγ after exposure to *M. tuberculosis* infected macrophages (Mashruwala et al., 2011).

Levels of C3 and C4 do not correlate with TST status in populations with TB high disease burden (Araujo et al., 2006), yet TST status is often not indicative of *M. tuberculosis* infection (O'Garra et al., 2013). While ficolin-2, ficolin 3 and MASP-2 serum levels do not correlate with TB incidence, MBL levels are increased (Chalmers et al., 2015). Similarly C1q levels are also increased in patients with active TB (Cai et al., 2014). Taken together with the

comprehensive analysis of C5 in mice, the complement system clearly interacts and modulates the host-pathogen interaction in tuberculosis disease.

Therefore in the context of TB pathogenesis, excessive complement-driven inflammation may be detrimental to the pathogen during the establishment of infection, but also contribute towards disease progression during its chronic phase, augmenting granuloma formation and perhaps contributing towards cavitation. Inhaled pellicle biofilm phenotype *M. tuberculosis* that enter a new host lung environment where the alternative pathway is not active (Ferguson et al., 2004; Watford et al., 2000) may therefore induce less inflammation and be more infectious than inhalation of equivalent quantities of planktonic phenotype bacteria from shaken flasks. The results presented in this thesis suggest the presence of pellicle EPS, high in arabinomannans, mannans and free mycolates but low in α-glucan may partially shield the bacteria complement activation predominantly initiated by modulation of direct C1q and MBL binding. This may impair early clearance of the establishing infection by reducing the release of immunomodulatory C5a and the formation of C5b-9 at the site of infection.

## 6.7 Future work

The results presented in this thesis point to a new hypothesis that *M. tuberculosis* biofilms limit complement activation (compared to planktonic phenotype), which contributes to the establishment of infection (**Figure 6.7.1**). To test this hypothesis in future, researchers could utilise both EPS extraction techniques and/or mutant *M. tuberculosis* strains with inhibited biofilm formation.

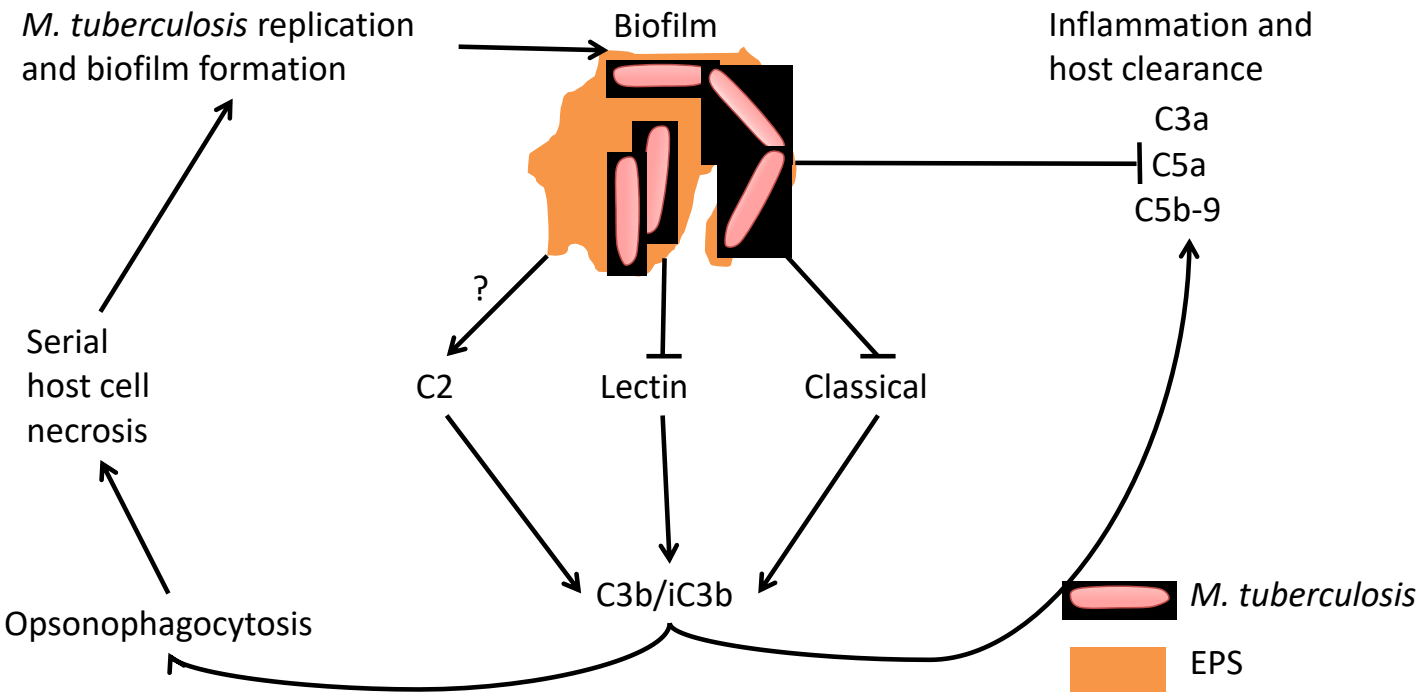


**Figure 6.7.1:** Hypothesis: *M. tuberculosis* biofilm formation reduces complement activation, which aids in the establishment of infection. Biofilm phenotype *M. tuberculosis* (expectorated from tuberculosis cavities (Arora et al., 2016)) enters the lung of a new host, where the alternative pathway of complement activation is absent (Watford et al., 2000). Results from this thesis suggest that biofilm phenotype *M. tuberculosis* shows reduced complement deposition via the, lectin and classical pathways. Biofilm formation may also affect the C2 pathway (Schorey et al., 1997). This reduces the release of anaphylatoxins C3a and C5a and also the formation of the C5b-9 complex, which all modulate inflammation (Bahia El Idrissi et al., 2015; Merle et al., 2015) and may promote early clearance of the infection. Despite the overall reduction in complement activation, there is still sufficient C3b/iC3b deposition (in addition to non-C3b/iC3b mediated pathogen recognition) to promote phagocytosis (Schlesinger, 1996). *M. tuberculosis* biofilms enter cells and escape into the cytosol leading to necrosis (Simeone et al., 2012). Biofilms grow and trigger serial phagocytosis-necrosis cycles to establish infection (Mahamed et al., 2017). The cycle of *M. tuberculosis* biofilm growth, phagocyte necrosis and low-level complement activation continues until the onset of adaptive immunity controls the infection.

EPS could be extracted by utilising petroleum ether extraction to remove lipids such as TDM from *M. tuberculosis* biofilms without affecting viability (Bloch, 1950) followed by extraction with a cation exchange resin to extract carbohydrates and proteins (Frølund et al., 1996). The viability and intracellular leakage of EPS depleted *M. tuberculosis* could be assessed through viable counts and glucose-6-phophate dehydrogenase assays respectively (Nielsen and Jahn, 1999). The extracted EPS components could be identified and *M. tuberculosis* pellicle biofilm, EPS-depleted and EPS reconstituted bacteria could be used in *in vitro* innate immunoassays to assess EPS effects.

Alternatively, genetic manipulation of c-di-GMP synthesis in *M. tuberculosis* may inhibit pellicle biofilm formation. For example, the culture of wild type *M. tuberculosis* H37Rv as pellicle biofilms, *M. tuberculosis* H37RvΔ *Rv1354c* with a truncated GGDEF domain (the only known diguanylate cyclase encoding gene in *M. tuberculosis*) and the complemented strain (Hong et al., 2013). Since deletion of this gene eliminates c-di-GMP synthesis, and high c-di-GMP levels are associated with biofilms (Hengge, 2009) it may inhibit pellicle biofilm formation.

If either approach was successful, all cultures could be grown in pellicle biofilm-promoting conditions. Furthermore, the humidified cultures could be aerated in 5% $CO_2$ chambers to better resemble human cavities. Dispersal of bacteria for experiments could be performed by light agitation using a vortex and low-speed centrifugation since the use of glass beads should be avoided to reduce EPS shedding of the EPS associated bacteria. Equal absorbance/CFU cultures could be opsonised with human complement at 2% and 10% concentrations and complement deposition could be assessed by labelling with fluorescent antibodies and flow cytometry as described in this thesis.

In addition, using an *in vitro* granuloma model of healthy donor human peripheral blood mononuclear cells (Guirado et al., 2015) and exogenous IgG-depleted human complement, the survival and proliferation of complement opsonised *M. tuberculosis* biofilm cells versus complement opsonised *M. tuberculosis*Δ*Rv1354c/*EPS-depleted planktonic cells could be assessed. The location, aggregation and proliferation of *M. tuberculosis* bacteria could be measured by acid-fast SYBR Gold staining (Ryan et al., 2014) and microscopy at specific time points. Furthermore, secreted levels of anaphylatoxins C3a and C5a could be measured using ELISAs.

Significantly greater proliferation of complement opsonised biofilm *M. tuberculosis* compared to complement opsonised planktonic *M. tuberculosis* within *in vitro* granulomas, in conjunction with reduced anaphylatoxin release and complement deposition on biofilm bacteria would suggest biofilm formation by *M. tuberculosis* reduces complement activation and enhances the ability of *M. tuberculosis* to establish infection. It may even suggest adjuvant therapies which target biofilm formation and/or complement activation at the site of infection could assist host clearance and shorten the lengthy treatment regimen required for tuberculosis patients.

Regarding the generation of an improved tuberculosis vaccine compared to the current BCG vaccine (itself mostly manufactured as a pellicle biofilms), novel vaccines containing attenuated *M. tuberculosis* complex biofilm phenotype bacteria or their components have been suggested (Flores-Valdez, 2016). Furthermore an *M. bovis* BCG strain that shows enhanced pellicle production, due to accumulation of c-di-GMP by deletion of the phosphodiesterase encoding gene *BCG1419c*, has shown improved efficacy in a mouse model (Pedroza-Roldán et al., 2016). Such developments suggest that understanding how the immune response is altered by *M. tuberculosis* biofilm formation may be a key factor to

developing better vaccines and drug regimens to significantly reduce tuberculosis disease prevalence and mortality worldwide.

# 7 MATERIALS AND METHODS

## 7.1 Mycobacterial culture

All mycobacterial strains were cultured in Sauton's medium (Parish et al., 2009; Sauton, 1912) with a 1/10 reduction in $KH_2PO_4$ hereafter referred to as Modified Sauton's medium. *M. tuberculosis* H37Rv was inoculated at 0.05 $OD_{540\ nm}$ from steady state chemostat cultures grown in Mod2 medium (Bacon and Hatch, 2009). *M. smegmatis* ATCC 700084/$mc^2$155 cultures were inoculated from 24 hour cultures grown in Middlebrook 7H9 + OADC + 0.05% Tween 80 or Tryptic Soy Broth + 0.05% Tween 80 at 0.05 $OD_{540\ nm}$. Planktonic cultures were grown in aerated flasks shaken at 200 rpm at 37$^{o}$C for 24 hours (*M. smegmatis*) or 7 days (*M. tuberculosis*). Biofilms were grown as pellicles in 24-well microplates, static at 37$^{o}$C in an airtight 5.5L plastic box for large batches of 8-12 plates or a 550mL box for smaller batches (1 plate) (Lock & Lock HPL836 and HPL815 respectively). Cultures were grown 7 days (*M. smegmatis*) or 5 weeks (*M. tuberculosis*). *Streptococcus agalactiae* serotype Ia was grown in aerated flasks in Todd Hewitt broth at 37$^{o}$C 180 rpm for 2 hours after suspending seed stock plates in PBS and inoculating at 0.1 $OD_{540\ nm}$.

## 7.2 Biofilm viable counts

Replicate donor chemostats were used to inoculate two independent cultures A and B in modified Sauton's medium at 0.05 $OD_{540\ nm}$. These cultures were used to seed biofilms in 24 well plates. x12 1 mL A cultures and x12 1 mL B cultures were aliquoted per plate for a total of 5 plates. These were placed in separate Lock & Lock HPL815 550 mL containers and incubated statically at 37$^{o}$C. One plate was used for sampling on weeks 3, 4, 5, 6 and 7.

Viable counts were performed by removing the medium from the wells minimising disruption of the biofilms by using a P200 pipette tip. Biofilms were then scraped from the bottom of the wells into pre-weighed 1.7 mL cryotubes within universal containers (double contained)

using sterile disposable spatulas. For each sample point, x6 technical replicates per biological replicate were scraped into cryotubes. Universals were sprayed out of the CL3 cabinet and weighed in a CL3 lab to allow for calculation of wet-weight biomass. Samples were placed back in the cabinet and suspended in 1mL of filter-sterilised PBS-1% Tween 80 and vortexed for 30 seconds to attempt to disperse the biofilms as much as possible. Samples were then serial diluted to $10^{-6}$ and dilutions $10^{-2}$ to $10^{-6}$ were plated using the spread plate method onto Middlebrook 7H10 + OADC plates. The viable count of the inoculum was determined by pipetting 1 mL of innoculum into pre-weighed tubes within Universals, pelleted and weighed again to calculate biomass. After weighing, the samples were re-suspended in PBS 1% Tween 80 and plating was performed as described for the biofilm samples. Plates were incubated at 37$^{o}$C for 3 weeks before counting colonies. Data was analysed using Microsoft Excel 2010 and Graph Pad Prism 6.

### 7.3 Biofilm crystal violet assay

Replicate donor chemostats A and B were used to inoculate two independent cultures A and B in modified Sauton's medium at 0.05 $OD_{540\ nm}$. These cultures were used to seed biofilms in 24 well plates. x12 1 mL A cultures and x12 1 mL B cultures were aliquoted per plate for a total of 5 plates. These were placed in separate Lock & Lock HPL815 550 mL containers and incubated statically at 37$^{o}$C. One plate was used for sampling on weeks 3, 4, 5, 6 and 7.

The crystal violet assay was performed by removing the medium from the wells minimising disruption of the biofilms by using a P200 pipette. For each sample point 6 technical replicates per biological replicate per plate were air dried overnight in a CL3 cabinet. Samples were immersed in 1mL of 1% crystal violet solution (Sigma, V5265) for 10 minutes. The crystal violet was removed using a P1000 pipette (air-dried biofilms stayed on the base of the wells.) Samples were washed x3 times in 1 mL of sterile water which was swilled before removing. Wells were then immersed in 95% ethanol to de-stain for 10 minutes.

Samples were then pipetted into empty bijous and serial diluted in 95% ethanol to $10^{-3}$. Serial dilutions and neat samples were read on a spectrophotometer and $OD_{600}$ values were recorded. For the T0 initial time point, samples were centrifuged to pellet bacteria at 3060g for 5 minutes at each step. Finally the $OD_{600}$ of blank wells treated the same as the biofilm samples (negative control) was calculated and subtracted from each biofilm sample. Data was analysed using Microsoft Excel 2010 and Graph Pad Prism 6.

### 7.4 *M. tuberculosis* planktonic growth curve

Three independent cultures (12 mL) in universal containers were fitted with a sampling line and vent and incubated at 37$^{o}$C 200 rpm for 14 days. Approximately 1mL of culture was sampled. Viable counts were taken on day 0, 4, 10 and 14. Serial dilutions of the cultures in PBS-Tween 0.05% were made and plated using the spread plate method (100 µL on each plate). Plates were incubated and counted after 3 weeks. Data was analysed using Microsoft Excel 2010 and Graph Pad Prism. Generation time was calculated using the equations $n = 3.3(\log N - \log N_0)$, where n is the number of generations during the period of exponential growth, N is the final cell number and $N_0$ is the initial cell number. $g = t/n$ where g is the generation time and t is the duration of exponential growth (time) (Madigan et al., 2010).

### 7.5 SEM of intact *M. tuberculosis* biofilms

*M. tuberculosis* biofilms were cultured in 24-well plates containing 70% ethanol sterilised plastic coverslips (VWR, 48376-049) cut to size and placed into each well were set up and fixed with 4% formaldehyde. X6 samples were taken to the Electron Microscopy department at Public Health England where they were prepared using the following 2 methods:

Ethanol/solvent dehydration: Formaldehyde was carefully removed and replaced with 2% Osmium tetroxide for 2 hours at room temperature for secondary fixation. Biofilms were then dehydrated through graded ethanol solutions for 15 min at room temperature sequentially at

25%, 50%, 75%  and 100% concentration. Next the coverslips were dehydrated with 100% Hexamethyldisilazane for 15 min at room temperature and this step was repeated. Coverslips were then air dried. Coverslips were mounted on to SEM stubs using double sided adhesive carbon discs. The mounted coverslips/pellicles were then conductive coated with approximately 10nm thickness of gold using an ion beam sputter coater (AtomTech 700 series Ultra Fine Grain Coating Unit).

Air drying method: Coverslips were removed from wells using forceps, placed on absorbent tissue and allowed to air-dry. The coverslips were then mounted on to SEM stubs and gold coated as described above. Samples were then examined in a Philips XL30 FEG SEM.

### 7.6 Immuno gold α(1-2) mannosyl residue labelling of *M. tuberculosis*

*M. tuberculosis* planktonic and biofilm phenotypes were cultured as described in section 7.1. The samples were split into non-treated and glass bead treated sub-groups. Dispersion with glass beads followed by low speed centrifugation was performed as described in section 7.22. 1 mL Samples were diluted or concentrated to absorbance 0.5 $OD_{540\,nm}$. EM grade formaldehyde was added to the x4 samples to a final concentration of 4%. Samples were stored at room temperature and sent to Dr. Nicole N van der Wel, University of Amsterdam. Samples were immuno gold labelled with anti-PIM/LAM antibody which binds to α(1-2) mannosyl residues and individual bacilli were imaged using electron microscopy by Zehui Zhang. The images were retuned and analysed using FIJI (Schindelin et al., 2012). Images of large bacilli were stitched using MosaicJ plugin, the length of each bacilli was measured as well as the number of gold particles present on the bacilli. Data analysis was performed with GraphPad Prism 6.

### 7.7 Preparation of heat-inactivated planktonic and biofilm *M. tuberculosis* biomass

Biofilms were scraped using sterilised disposable spatulas into glass universals, planktonic cultures were spun at 3060g for 10 minutes, consolidated and pelleted into glass universals. Samples were inactivated by autoclaving at 126$^{o}$C for 30 minutes, evaporated to dryness using a Genevac EZ-2 Plus evaporator (Genevac Ltd, UK) and frozen at -80$^{o}$C until required.

### 7.8 *M. tuberculosis* polar and apolar lipid extractions

Apolar and polar lipids were extracted from planktonic and biofilm heat-inactivated *M. tuberculosis* biomass according to the method described in (Besra 1998). Briefly, 50 mg of biomass was resuspended in 2mL methanol-0.3% NaCl (100:10) and 1 mL or Petroleum Ether was added. Samples were mixed overnight. The upper petroleum layer was removed and 1 mL of petroleum ether was added again, mixed for 15 minutes and combined. These were evaporated to yield apolar lipids which were re-suspended in 250µL dichloromethane. 2.3 mL of chloroform-methanol-0.3% NaCl (9:10:3) was added to the methanolic saline extract and mixed for an hour, spun for 15 minutes at 3500g and the supernatant was retained. The pellet was further extracted with 0.75 mL of chloroform-methanol-0.3% NaCl (5:10:4) for 1 hour, spun and combined with the previous supernatant. 1.3mL of chloroform and 1.3 mL of 0.3% NaCl was added and mixed for 2 hours until a biphase had formed. Samples were centrifuged and the lower organic layer was evaporated to yield polar lipids. These were suspended in 300µL chloroform-methanol (2:1).

### 7.9 Analysis of *M. tuberculosis* planktonic and biofilm phenotype polar and apolar lipids

Apolar and polar lipids were analysed by two-dimensional thin-layer chromatography (2d-TLC) using the solvent systems described in (Besra, 1998) (Systems A- C) and (Wheeler, 2009) (systems D and E). Aluminium backed silicon TLC sheets were divided into 9 squares each 6.6 cm by 6.6 cm. Solvent systems A-E were set-up as described in **Table 3.3-1**.

Solvent mixtures were agitated and left to form an atmosphere in TLC developing tanks for 5 minutes before TLC analysis. 20µL of lipids were spotted on TLC plates 1cm X 1cm from the bottom left corner using a capillary tube, allowed to dry and placed in the correct orientation into developing tanks. Once completed the plates was dried using a heat gun (lowest setting) and run in direction 2 at the correct orientation. After a second period of drying the TLCs were sprayed with 5% ethanolic molybdophosphoric acid (MPA) and charred with a heat-gun to visualise the lipids. Alternatively they were sprayed with α-naphthol-sulphuric acid to visualise glycolipids.

### 7.10 Imaging and analysis of apolar and polar TLC plates

TLC plates were scanned into TIFF images in sets relating to solvent system and stain applied. For preparation of figures, the brightness and contrast of each image was uniformly optimised for each set and the plates were cropped, rotated and compiled using GIMP 2.8 software. For densitometry analysis, raw scanned image sets were analysed using FIJI software (Schindelin et al., 2012). Images were converted to greyscale and the background was subtracted. The image was inverted and the integrated density was measured in equal size circular selections over each spot replicate. Raw integrated density data was imported to Microsoft Excel and for each biological replicate, the relative density of planktonic and biofilm lipid spots was calculated. Statistical analysis was performed using Graph Pad Prism 6 software.

### 7.11 mAGP extraction

2% SDS in PBS was added to planktonic and biofilm pellets left over from the ethanol reflux step of the carbohydrate and lipoglycan extraction (see section 7.13). This was heated under reflux at 95$^{o}$C overnight. The following day the samples were washed with water, pelleted, washed with 80% acetone, pelleted and washed with 100% acetone and dried.

## 7.12 Extraction and analysis of fatty acid and mycolic acid methyl esters (FAMES and MAMES)

As described in (Besra, 1998). 2mL of 15% Tetrabutylammonium hydroxide (TABH) was added to 50mg of planktonic and biofilm mAGP extracts. Samples were heated at 95$^{o}$C overnight and allowed to cool. 2 mL of water was added to the samples followed by 1 mL of dichloromethane and 250 µL of idomethane and mixed for 1 hour. The samples were centrifuged at 3000g for 10 minutes. The lower layer was retained and 3ml of water was added. These were mixed and centrifuged again and the water wash step was repeated another 2 times. Samples were suspended in 0.5 mL dichloromethane and evaporated. 0.2 mL toluene and 0.3 mL acetonitrile were added and the samples were left for an hour. FAMES and MAMES were centrifuged at 3000g for 15 minutes and resuspended in dichloromethane. FAMES and MAMES were analysed by spotting 20µL and running in 1 direction in a solvent system of hexane.ethyl acetate (95:5) three times and charred using a heat gun after spraying with 5% MPA.

## 7.13 Extraction of carbohydrate and lipoglycan extracts

As described in (Besra, 1998). Equal biomass samples of planktonic or biofilm heat-inactivated biomass were heated under reflux with 10mL ethanol-water (1:1) at 75$^{o}$C for 4 hours. Samples were then left to cool to room temperature, spun at 3000g for 15 minutes and the supernatant was removed into fresh tubes. The pellet was topped up to with 10mL ethanol-water (1:1) and the heating step and centrifugation was repeated. The supernatants were vacuum dried overnight in an EZ-2 personal evaporator to give dried pellets. The remaining pellet from the ethanol reflux was used for mAGP extraction (section 7.11). To the dried supernatants, 1 mL PBS was added to the smaller pellet which was resuspended by sonicating for 10 minutes. The suspensions were pipetted into the tubes containing the larger pellet and sonicated again for another 10 minutes. An equal volume of phenol saturated with

PBS was added to the tubes. The tubes were heated at 75$^{o}$C for 30 minutes. The tubes were left to stand and cool to room temperature. The phenol and aqueous layers were separated by centrifugation at 3000g. The aqueous layer was removed into a semi-permeable dialysis membrane (MWCO 3500) which was wetted and sealed at one end with a mediclip using a plastic Pasteur pipette. The samples were dialysed overnight with running tap water and left in distilled water for 1 hour to remove salts from the tap water. Samples were transferred into clean pre-weighed glass tubes and were subsequently vacuum dried using the aqueous setting on the EZ-2 overnight. The tubes were weighed again and the biomass of the crude lipoglycan fraction was calculated.

### 7.14 Carbohydrate and lipoglycan gel

Planktonic and biofilm carbohydrate/lipoglycan extracts were suspended in water at 15 µg mL$^{-1}$. 150µg (10 µL) was added to Eppendorf tubes along with 10 µL *M. smegmatis* LAM standard. Subsequently 10µL of x2 concentrated SDS loading buffer was added. Samples were added to a Mini Protean TGX Precast Gel (Bio-Rad, USA) submerged in 1% SDS buffer (National diagnostics Ultra-pure 10X Tris, Glycine, SDS diluted 1/10) and the samples were run with PageRuler pre-stained protein ladder and CandyCane molecular weight standards (Life Technologies, USA). The gel was run for 45 minutes 200V 30mA. The gel was stained to visualise lipoglycans using Pro-Q emerald stain kit (P21857) and the gel was processed according to the manufacturer's instructions (Life Technologies, USA). The gel was viewed on a Molecular imager with image-lab software Gel Doc XRT (Bio-Rad, USA).

### 7.15 Total sugar analysis

Planktonic and biofilm phenotype carbohydrate/lipoglycan extracts and mAGP fractions were treated with 2M trifluoroacetic acid (TFA). 200µL of 2M TFA was added to 0.5 mg mAGP extracts and 3µg of carbohydrate/lipoglycans. Samples were heated to 120$^{o}$C for 1.5 hours under reflux and allowed to cool to room temperature. The acid was evaporated using a

sample concentrator. 100 µL of 10 mg mL-1 NaBH4 in 1:1 ethanol:NH4OH (1M) was added to each sample and left capped at room temperature overnight. 3 drops of glacial acetic acid were added to each sample and evaporated. 3 drops of 10% glacial acetic acid in methanol were added then evaporated. This step was repeated once. Next 3 drops of 100% methanol was added and evaporated. This step was repeated once. 100µL acetic anhydride was added and this was heated at 120$^{o}$C for 1 hour. After allowing the sample to cool to room temperature, 100 µL of toluene was added to the samples and was evaporated. 2 mL of chloroform and 2 mL of $H_2O$ was added to each sample. The lower organic layer of each sample was transferred into a fresh tube using a glass pipette and dried using a sample concentrator, ready for gas chromatography analysis. Gas chromatography was carried out by the University of Birmingham Chemistry department. Percentage of constituent sugars was determined after identifying arabinose, mannose, glucose peaks for carbohydrate/lipoglycan fraction and rhamnose, arabinose and galactose peaks for mAGP extract from planktonic and biofilm cultures.

### 7.16 Whole blood stimulation with *M. tuberculosis* planktonic and biofilm phenotype carbohydrate extracts

x3 planktonic and x3 biofilm *M. tuberculosis* carbohydrate extracts were resuspended in RPMI 2mM L-glutamine at 1000 and 2500 µg mL$^{-1}$ and zymosan at 1000 µg mL$^{-1}$. 5µL of stock solutions was added to 495 µL of blood from x3 donors (PIP039, PIP027 and PIP004) for final concentrations of 10 µg mL$^{-1}$ and 25 µg mL$^{-1}$. After 24 hours incubation at 37$^{o}$C 5% $CO_2$, plasma was collected after centrifugation of the samples at 1000g for 10 minutes. Samples were either stored at -80$^{o}$C until required or filtered using 0.2 µm spin-X centrifuge tube filters (Sigma, CLS8160) and analysed for cytokine secretion using a 20-plex eBioscience Procartaplex Human Th1/Th2 & Chemokine Panel 1 (EPX200-12173-901) kit which detected secreted IL-12p70, CCL2 (MCP-1), CCL5 (RANTES), CXCL1 (GRO α),

CXCL12 α (SDF-1 α), CXCL10 (IP-10), CCL11 (Eotaxin), GM-CSF, IFN gamma, IL-1 β, IL-13, IL-18, IL-2, IL-4, IL-5, IL-6, IL-8, CCL3 (MIP-1 α), and CCL4 (MIP-1 β) and TNF α. The kit was used according to manufacturer's instructions using the plate layout in **Table 7.16-1**. The kit was run on a MAGPIX instrument and standard curves were developed using Procartaplex analyst software to calculate the amount of secreted cytokines in each sample in pg $mL^{-1}$.

| | Standards | | Donor1 | | | Donor2 | | | Donor3 | | | |
|---|---|---|---|---|---|---|---|---|---|---|---|---|
| | 1 | 2 | | | | | | | 9 | 10 | 11 | 12 |
| A | Std1 | Std1 | Unstim | PK2 | BF3 | Unstim | PK2 | BF3 | Unstim | PK2 | BF3 | BF1(25) |
| B | Std2 | Std2 | Unstim | PK2 | BF3 | Unstim | PK2 | BF3 | Unstim | PK2 | BF3 | BF1(25) |
| C | Std3 | Std3 | Unstim RPMI | PK3 | PK1(25) | Unstim RPMI | PK3 | PK1(25) | Unstim RPMI | PK3 | PK1(25) | BF1(25) |
| D | Std4 | Std4 | Unstim RPMI | PK3 | PK1(25) | Unstim RPMI | PK3 | PK1(25) | Unstim RPMI | PK3 | PK1(25) | BF1(25) |
| E | Std5 | Std5 | Zy | BF1 | PK2(25) | Zy | BF1 | PK2(25) | Zy | BF1 | PK2(25) | BF1(25) |
| F | Std6 | Std6 | Zy | BF1 | PK2(25) | Zy | BF1 | PK2(25) | Zy | BF1 | PK2(25) | BF1(25) |
| G | Std7 | Std7 | PK1 | BF2 | BF1(25) | PK1 | BF2 | BF1(25) | PK1 | BF2 | BF1(25) | |
| H | Std8 | Std8 | PK1 | BF2 | BF1(25) | PK1 | BF2 | BF1(25) | PK1 | BF2 | BF1(25) | |

**Table 7.16-1:** Plate layout *M. tuberculosis* whole blood stimulation with carbohydrate extracts. Std, standards; Unstim, unstimulated plasma; Unstim RPMI, plasma stimulated with RPMI 2mM L-glutamine only; Zy, zymosam 10 µg $mL^{-1}$; PK1-PK3, planktonic *M. tuberculosis* carbohydrate extracts 10 µg $mL^{-1}$; BF1-BF3 biofilm *M. tuberculosis* carbohydrate extracts 10 µg $mL^{-1}$; (25) 25 µg $mL^{-1}$.

### 7.17 Generation of *M. tuberculosis* planktonic capsule and biofilm extracts

x6 planktonic capsule extracts were prepared from biological replicate planktonic cultures set-up as described in methods section (7.1). To harvest, each culture was spun at 3060g for 10 min in x2 50 mL tubes, the supernatants were discarded and pellets combined resulting in x6 planktonic pellets. x6 biofilm capsule extracts were prepared from biological replicate *M. tuberculosis* biofilm cultures as described in methods section (7.1) with x4 24-well plate technical replicates per biological replicate. To harvest, biofilms were scraped off the surface of the wells into x6 50 mL falcon tubes.

Approximately x5 pellet volume sterilised 4mm glass beads were added to the wet cells and vortexed for 1 minute. 3 mL of distilled water was added to each bead-treated sample and briefly vortexed and passed through a 0.2µm sterile filter using a syringe. The filtrates were transported to a non-toxic CL3 cabinet and filtered a second time to ensure the contents were sterile, into pre-weighed glass tubes. Capsule extracts were dried down using the aqueous setting on a Genevac EZ-2 personal evaporator and dried capsule biomass was calculated. Dried capsule extracts were frozen at -80$^{o}$C until required.

### 7.18 Whole blood stimulation with capsule extracts

x6 planktonic and x6 biofilm dried capsule extracts were suspended in distilled water to 10mg/mL and heavily vortexed until sufficiently dissolved. The samples were then added to RPMI 2mM L-glutamine to give a final concentration of 200µg/mL. Additional controls were also dissolved in RPMI 2mM L-glutamine at the following concentrations: pre-activated Zymosan (CompTech, B400) 50 µg mL$^{-1}$ and Tuberculin PPD RT 23 (Statens Serum Institut) 200 µg mL$^{-1}$. 12-O-Tetradecanoylphorbol-13-acetate (PMA) (4.8 µg mL$^{-1}$) combined with Ionomycin (95 µg mL$^{-1}$) dissolved in DMSO was also used as a positive control. 5 µL of capsule or controls were added to 495 µL of fresh heparinised human blood from 2 donors

PIP004 and PIP027 in 5mL dual- position capped sterile tubes. Additionally 5 µL of RPMI 2mM L-glutamine without antigen was added to one sample as a negative control and 500µL of unstimulated blood were also included as an additional negative control. Tubes (caps in loose position to allow ventilation) were incubated statically at 37$^{o}$C 5% $CO_2$ for 24 hours. After incubation, tubes were spun at 1000g for 10 min and the plasma was collected into cryovials which were frozen at -80$^{o}$C until required.

A Procartaplex custom kit (eBiosciences) measuring human IFN-γ, IL-6, CCL2 and MMP-1 was set up with the plate layout shown in **Table 7.18-1**. The assay was performed as described in the multiplex instruction manual. However, prior to their addition, the plasma samples were thawed and pipetted into 0.2µm Spin-X centrifuge tube filters which were spun at a 2000g for 10 minutes to remove aggregates. The plasma samples were incubated with the beads overnight and analysed on a MAGPIX (Luminex). The .csv results file was exported and imported on to ProcartaPlex Analyst 1.0 software. The standards and lot numbers were added and the software was used to generate standard curves and results for each secreted cytokine/chemokine/enzyme in pg/mL. Standard curves were exported as well as the re-analysed results in a .csv file into Microsoft Excel to generate graphs.

| | Standards | | Donor 1 PIP027 | | | | | Donor 2 PIP004 | | | | |
|---|---|---|---|---|---|---|---|---|---|---|---|---|
| | 1 | 2 | 3 | 4 | 5 | 6 | 7 | 8 | 9 | 10 | 11 | 12 |
| A | Std1 | Std1 | Unstim | PPD | PKD | BFB | BFF | Unstim | PPD | PKD | BFB | BFF |
| B | Std2 | Std2 | Unstim | PPD | PKD | BFB | BFF | Unstim | PPD | PKD | BFB | BFF |
| C | Std3 | Std3 | Unstim RPMI | PKA | PKE | BFC | | Unstim RPMI | PKA | PKE | BFC | |
| D | Std4 | Std4 | Unstim RPMI | PKA | PKE | BFC | | Unstim RPMI | PKA | PKE | BFC | |
| E | Std5 | Std5 | Zy | PKB | PKF | BFD | | Zy | PKB | PKF | BFD | |
| F | Std6 | Std6 | Zy | PKB | PKF | BFD | | Zy | PKB | PKF | BFD | |
| G | Std7 | Std7 | PMA | PKC | BFA | BFE | | PMA | PKC | BFA | BFE | |
| H | Std8 | Std8 | PMA | PKC | BFA | BFE | | PMA | PKC | BFA | BFE | |

**Table 7.18-1:** Whole blood stimulation with *M. tuberculosis* capsule extracts. Std, standards; Unstim, unstimulated plasma; Unstim RPMI, plasma stimulated with RPMI 2mM L-glutamine only; Zy, zymosam 10 µg $mL^{-1}$; PK1-PK3, planktonic *M. tuberculosis* carbohydrate extracts 10 µg $mL^{-1}$; BF1-BF3 biofilm *M. tuberculosis* carbohydrate extracts 10 µg $mL^{-1}$; (25) 25 µg $mL^{-1}$.

### 7.19 C3b/iC3b ELISA

x3 planktonic and x3 biofilm phenotype carbohydrate extracts were diluted in 1 mL carbonate/bicarbonate buffer capsule (Sigma, C3041) in 100 mL distilled water to a final concentration of 25 μg $mL^{-1}$. 100 μL was added to to ensure 2.5 μg of carbohydrate per well in Microlon high-affinity binding plates (Sigma, M4561). A 7 point standard curve of human purified C3 (CompTech, A113) was generated after diluting neat purified human C3 in to 12 μg $mL^{-1}$ in carbonate buffer before serial diluting 1/4. Likewise a second 7-point standard curve was generated after diluting C3 to 300 μg $mL^{-1}$ in carbonate buffer followed by 1/4 serial dilutions. 50 μL of standards was placed in respective wells.

The plate was sealed and left in the fridge overnight to bind the carbohydrate extracts to the bottom of the plate. The buffer was removed by inverting the plate over the sink and dabbing the plate with paper towels. The plate was blocked by adding 100 μL of 10% BSA in PBS to each well and incubating for 1 hour. The plate was washed by inverting the plate over the sink and dabbing the plate with paper towels, 100 μL PBS 0.05% Tween 20 was added to each well and the plate was inverted over the sink and dabbed with paper towels. Exogenous IgG depleted human complement (In house PHE) was thawed. Complement binding buffer (CBB) was made by dissolving a complement fixation diluent tablet (Thermo Scientific, BR0016) in 2% bovine serum albumen. CBB contained 1.76 mM MgCl2, 0.25 mM CaCl2, 145.4mM NaCl. 2% complement in CBB, and 10% complement in CBB, or control CBB only was added to respective wells and incubated for 1 hour at 37$^{o}$C.

For labelling, the plate was washed as previously described and 100 μL of (1:500) pAb anti-C3c HRP (Abcam, ab4212) in CBB or CBB control was added to respective wells.

The plate was sealed and incubated for 1 hour at room temperature. The plate was washed x3 times and developed by adding 100 μL of tetramethylbenzidine (TMB) (Abcam, ab171527)

to each well for 15 minutes. The reaction was stopped by adding 100 µL of stop solution (Abcam, ab171529). After 10 minutes to ensure equal diffusion of colour throughout the well, the plate was read using a Multiskan EX plate reader at 450 nm with Ascent software.

### 7.20 C5b-9 ELISA

x3 planktonic and x3 biofilm phenotype carbohydrate extracts were seeded to ensure 2.5 µg of carbohydrate per well as described in section 7.19. A seven point standard curve was generated by diluting neat purified human C5b-9 (CompTech) in carbonate buffer to 10.8 µg $mL^{-1}$ before serial diluting ¼**.** A second 7 point standard curve was generated by diluting neat human C5b-9 in carbonate buffer to 270 µg $mL^{-1}$ and performing ¼ serial dilutions**.** 100 µL of standards was placed into respective wells. The plate was sealed and left in the fridge overnight to bind the carbohydrate extracts to the bottom of the plate.

The ELISA was performed as described in section 7.19 until labelling. For labelling, the plate was washed and 100 µL of (1:100) pAb Mouse anti-Human C5b-9 Clone aE11 (DAKO, M0777) in CBB was added to each well. The plate was sealed and incubated for 1 hour at room temperature. The plate was washed as previously described and 100 µL of (1:2000) pAb Goat anti Mouse HRP (DAKO, P0447) in CBB was added to each well. Following labelling, the ELISA was continued as described in section 7.19

### 7.21 MBL ELISA

x3 planktonic and x3 biofilm phenotype carbohydrate extracts were seeded to ensure 2.5 µg of carbohydrate per well as described in section 7.19. A seven point standard curves was generated by serial diluting ¼ starting from 10 µg $mL^{-1}$ recombinant human MBL (R&D systems, 2307-MB) in in carbonate buffer. 100 µL of standards were added to respective wells. The plate was sealed and left in the fridge overnight to bind the carbohydrate extracts

to the bottom of the plate. The buffer was removed by inverting the plate over the sink and dabbing the plate with paper towels. The plate was blocked by adding 100 µL of 10% BSA in PBS to each well and incubating for 1 hour. The plate was washed by inverting the plate over the sink and dabbing the plate with paper towels, 100 µL PBS 0.05% Tween 20 was added to each well and the plate was inverted over the sink and dabbed with paper towels. 100 µL of 10 µg $mL^{-1}$ MBL in CBB, or control CBB only was added to respective wells and incubated for 1 hour at 37$^{o}$C.

For labelling, the plate was washed as previously described and 100 µL of mouse anti-human MBL mAb 3E7 (Hycult, HM2061) (1:100) in CBB or CBB only was added to respective wells. The plate was sealed and incubated for 1 hour at room temperature. The plate was washed as previously described and 100 µL of (1:2000) pAb Goat anti Mouse HRP (DAKO, P0447) in CBB was added to each well. Following labelling, the ELISA was continued as described in section 7.19

### 7.22 Dispersal of *M. tuberculosis* using glass beads.

Agitation with 4 mm glass beads was performed similarly to as described in published studies (N'Diaye et al., 1998; Villeneuve et al., 2003). Live *M. tuberculosis* planktonic pellets or scraped biofilms were agitated with sterile 4 mm glass beads which had been added at a ratio of approximately 5:1 bead volume:pellet volume. The samples were vortexed for 30 seconds, suspended in PBS and left to sediment for 10 minutes. The liquid was poured into fresh tubes and the suspension was spun at 200g. The supernatant (dispersed whole cell fraction) was aliquoted into cryovials and frozen at -80$^{o}$C until required.

### 7.23 Assessment of *M. smegmatis* viability before and after dispersal using glass beads.

7 day biofilms were cultured as previously described (7.1). These were weighed and dispersed non-mechanically by suspending in PBS-0.1% Tween 80 at 100 mg $mL^{-1}$ (wet

weight) and vortexing. Serial dilutions to $10^{-6}$ in PBS-0.1% Tween 80 and viable counts were performed using the spread plate method. Subsequently *M. smegmatis* Tween-80-dispersed fractions were pelleted and treated by vortexing for 30 seconds with or without beads (5g beads for every 1g wet weight) and re-suspended in PBS-0.1% Tween-80 to 100 mg $mL^{-1}$. Samples were serial diluted again and viable counts were performed. Middlebrook 7H10 + OADC plates were counted after 3 days incubation at 37°C.

### 7.24 C3b/iC3b and C5b-9 deposition ± mAb C1q assay

Viable, thawed planktonic and biofilm phenotype *M. tuberculosis* from glass-bead treated stocks, were diluted to 0.2 OD540 nm Complement binding buffer (CBB). IgG-depleted exogenous pooled human complement was pre-incubated for 20 minutes at 4°C with PBS (control) or mouse anti-human C1q mAb JL-1 (Hycult, HM1096) at 1/5 dilution. To bacteria/zymosan control wells, 55 µL of CBB was added. To 2% complement wells, 2.5 µL of IgG-depleted exogenous pooled human complement-PBS/mAb anti C1q (4:1) was added along with 52.5 µL of CBB. To 10% complement wells, 12.5 µL of IgG-depleted exogenous pooled human complement-PBS/mAb anti C1q (4:1) was added along with 42.5 µL CBB.

The plate was incubated at 37°C for 45 mins 900 rpm. The plate was centrifuged at 3060g for 5min and each well was washed with 200 µL CBB. The plate was spun again at 3060g and re-suspended in 4% PBS-formaldehyde. The plate was sealed and left in a fumigating cabinet overnight to inactivate *M. tuberculosis*. The following day at containment level 2 the plate was spun and re-suspended in CBB. The plate was spun again at 3060g and re-suspended in 200 µL of CBB containing rabbit anti-human C3c pAb FITC (Abcam, ab4212) and Alexafluor 647 nm conjugated mouse anti-human SC5b-9 (Quidel, A239) at 1/500 and 1/4000 dilutions respectively. The plate was incubated at 4°C for 20mins, centrifuged at

3060g for 5min and washed with 200µl PBS twice before being analysed on a CyAN ADP Analyzer flow cytometer (Beckman-Coulter, USA) using the gating strategy described in **Figure 5.3.2**.

After running the plate, compensation was performed using Summit 4.3 software (Beckman-Coulter, USA) from single conjugate sample FCS files and the magnitude of either C3b/iC3b or C5b-9 deposition was measured by calculating integrated median fluorescence intensity (iMFI) (Darrah et al., 2007) (median fluorescence*% positive cells) for each sample. The iMFI of bacteria + conjugate only negative control wells were subtracted from each sample to remove the contribution of background fluorescence to net iMFI values. For statistical analysis, ≥3 biological replicate planktonic and biofilm samples were compared by performing t-tests corrected for multiple comparisons by false discovery rate (Benjamini et al., 2006) with Q = 5% using GraphPad Prism software.

### 7.25 MBL, C1q and Ficolin-3 binding assay

Viable, thawed planktonic and biofilm phenotype *M. tuberculosis* from glass-bead treated stocks, were diluted to 0.2 $OD_{540\ nm}$ in CBB. 55 µL of CBB was added to control wells and 54 µL added to MBL/C1q/Ficolin-3 wells. 45 µL of bacteria was added to designated wells. In separate experiments, recombinant (R&D systems, 2307-MB) (100 µg $mL^{-1}$) or recombinant ficolin-3 (R&D systems, 2367-FC-050) or human purified C1q (Comp Tech, A099) was added to designated wells to give a final concentration of 1µg $mL^{-1}$ in 100 µL. Plates were incubated at 900 rpm 37$^{o}$C for 45 min. Plates were spun at 3060g for 5min and washed with 200 µL CBB per well. Plates were spun at 3060g for 5 min and re-suspended in either 1:100 mouse anti-human MBL 3E7 (Hycult, HM2061), 1:500 mouse anti-human C1q JL-1 (Hycult, HM1096) or 1:100 mouse anti-human Ficolin-3 4H5 (Hycult, HM2089) in CBB or CBB only and incubated for 20 min at room temperature. Plates were spun at 3060g 5 min and washed with 200 µL CBB per well. Plates were spun at 3060g 5min and re-suspended in 1:500 Goat

Anti-Mouse IgG (H+L) Fluorescein (FITC)-AffiniPure F(ab')2 Fragment antibody (Stratech, 115-096-062-JIR) in CBB or CBB only and incubated for 20 min at room temperature. Plates were spun at 3060g 5min and washed with 200 µL filter sterilised PBS per well and this step was repeated. Plates were spun at 3060g for 5 min and re-suspended in 200 µL 4% formaldehyde in PBS per well and sealed with 70% ethanol-soaked plate sealers. Plates were sprayed with 70% ethanol and incubated at room temperature for 1 hour to inactivate the bacteria in the wells. For statistical analyses of the MBL, C1q and ficolin-3 experiments, ≥3 biological replicate *M. tuberculosis* planktonic and biofilm samples were compared by performing two-tailed Welch's t-tests using GraphPad Prism software.

### 7.26 C2a binding assay

Live bead-treated *M. tuberculosis* planktonic, biofilm, *M. smegmatis*, *S. agalactiae* and Zymosan stocks were diluted to 0.2 $OD_{540\ nm}$ in CBB. 55 µL of CBB was added to control wells and 52 µL was added to C2 and C2a wells. Human purified C2 (Comp Tech, A112) and activated C1s (CompTech, A104) were fast thawed to 37$^{o}$C. 44 µL of 1/10 diluted activated C1s or PBS was added to 55 µL of C2. The x2 vials were vortexed and incubated at 37$^{o}$C for 20 min. 3 µL of PBS-C2 or C1s-C2 was added to designated wells and the plate was incubated for 45 minutes 900 rpm. The plate was spun at 3060g for 5 min and washed with 200 µL CBB per well. The plate was resuspended in 1:200 Rabbit anti-human C2a FITC pAb (Bioss Antibodies, bs-10428R-FITC) and incubated at room temp for 20 min. The plate was washed x2 with 200 µL PBS per well and resuspended a final time in PBS-4% formaldehyde. An ethanol sprayed plate sealer was placed over the plate and it was incubated for 1 hour at room temp to inactivate bacteria. The plate was sprayed out the cabinet and run on the flow cytometer.

# 8 LIST OF REFERENCES


Actor, J.K., Breij, E., Wetsel, R.A., Hoffmann, H., Hunter, R.L., Jagannath, C., 2001. A role for complement C5 in organism containment and granulomatous response during murine tuberculosis. Scand. J. Immunol. 53, 464–474. doi:10.1046/j.1365-3083.2001.00902.x

Adib-Conquy, M., Scott-Algara, D., Cavaillon, J.-M., Souza-Fonseca-Guimaraes, F., 2014. TLR-mediated activation of NK cells and their role in bacterial/viral immune responses in mammals. Immunol. Cell Biol. 92, 256–262. doi:10.1038/icb.2013.99

Alderwick, L.J., Radmacher, E., Seidel, M., Gande, R., Hitchen, P.G., Morris, H.R., Dell, A., Sahm, H., Eggeling, L., Besra, G.S., 2005. Deletion of Cg-emb in corynebacterianeae leads to a novel truncated cell wall arabinogalactan, whereas inactivation of Cg-ubiA results in an Arabinan-deficient mutant with a cell wall galactan core. J. Biol. Chem. 280, 32362–32371. doi:10.1074/jbc.M506339200

Alteri, C.J., 2005. Novel pili of Mycobacterium tuberculosis.

Alteri, C.J., Xicohténcatl-Cortes, J., Hess, S., Caballero-Olín, G., Girón, J.A., Friedman, R.L., 2007. Mycobacterium tuberculosis produces pili during human infection. Proc. Natl. Acad. Sci. U. S. A. 104, 5145–50. doi:10.1073/pnas.0602304104

Andersen, P., Doherty, T.M., 2005. The success and failure of BCG - implications for a novel tuberculosis vaccine. Nat. Rev. Microbiol. 3, 656–662. doi:10.1038/nrmicro1211

Anderson, L., Dias, H.M., Fal- zon, D., Baena, I.G., Gilpin, C., Glaziou, P., Hamada, Y., Kanchar, A., Law, I., Lienhardt, C., Siroka, A., Sis- manidis, C., Syed, L., Timimi, H., van Gemert, W., Weil, D., Zignol, M., Floyd, K., 2016. WHO | Global tuberculosis report 2016, WHO. World Health Organization.

Angala, S.K., Belardinelli, J.M., Huc-Claustre, E., Wheat, W.H., Jackson, M., 2014. The cell envelope glycoconjugates of Mycobacterium tuberculosis. Crit. Rev. Biochem. Mol. Biol. 49, 361–99. doi:10.3109/10409238.2014.925420

Araujo, Z., González, N., Cubeddu, L. de, Ziegler, R.C., Waard, J.H. de, Giampietro, F., Garzaro, D., Pujol, F.H., Serrano, N.C. de, Saboin, A.G. de, 2006. Levels of complement C3 and C4 components in Amerindians living in an area with high prevalence of tuberculosis. Mem. Inst. Oswaldo Cruz 101, 359–364. doi:10.1590/S0074-02762006000400003

Areschoug, T., Stålhammar-Carlemalm, M., Karlsson, I., Lindahl, G., 2002. Streptococcal beta protein has separate binding sites for human factor H and IgA-Fc. J. Biol. Chem. 277, 12642–8. doi:10.1074/jbc.M112072200

Arora, R., Armitige, L., Wanger, A., Hunter, R.L., Hwang, S.-A.A., 2016. Association of pellicle growth morphological characteristics and clinical presentation of Mycobacterium tuberculosis isolates. Tuberculosis 101, S63–S68. doi:10.1016/j.tube.2016.09.015

Asgari, E., Le Friec, G., Yamamoto, H., Perucha, E., Sacks, S.S., Kohl, J., Cook, H.T., Kemper, C., Köhl, J., Cook, H.T., Kemper, C., 2013. C3a modulates IL-1β secretion in human monocytes by regulating ATP efflux and subsequent NLRP3 inflammasome activation. Blood 122, 3473–81. doi:10.1182/blood-2013-05-502229

Bacon, J., Alderwick, L.J., Allnutt, J.A., Gabasova, E., Watson, R., Hatch, K.A., Clark, S.O., Jeeves, R.E., Marriott, A., Rayner, E., Tolley, H., Pearson, G., Hall, G., Besra, G.S., Wernisch, L., Williams, A., Marsh, P.D., 2014. Non-Replicating Mycobacterium tuberculosis Elicits a Reduced Infectivity Profile with Corresponding Modifications to the Cell Wall and Extracellular Matrix. PLoS One 9, e87329. doi:10.1371/journal.pone.0087329

Bacon, J., Hatch, K.A., 2009. Continuous culture of mycobacteria., in: Mycobacteria

Protocols Methods in Molecular Biology (Clifton, N.J.). pp. 153–71. doi:10.1007/978-1-59745-207-6_10
Baddeley, A., Dean, A., Dias, H.M., Falzon, D., Floyd, K., Garcia, I., Glaziou, P., Hiatt, T., Law, I., Lienhardt, C., Nguyen, L., Sismanidis, C., Timimi, H., van Gemert, W., Zignol, M., Baena, I.G., Gilpin, C., Glaziou, P., Hiatt, T., Law, I., Lienhardt, C., Likhite, N., Nguyen, L., Siroka, A., Sismanidis, C., Timimi, H., van Gemert, W., Zignol, M., 2013. WHO | Global tuberculosis report 2013. World Health Organization. doi:WHO/HTM/TB/2014.08
Baena, a., Porcelli, S. a., 2009. Evasion and subversion of antigen presentation by Mycobacterium tuberculosis. Tissue Antigens 74, 189–204. doi:10.1111/j.1399-0039.2009.01301.x
Bahia El Idrissi, N., Das, P.K., Fluiter, K., Rosa, P.S., Vreijling, J., Troost, D., Morgan, B.P., Baas, F., Ramaglia, V., 2015. M. leprae components induce nerve damage by complement activation: identification of lipoarabinomannan as the dominant complement activator. Acta Neuropathol. 129, 653–67. doi:10.1007/s00401-015-1404-5
Bals, R., Wang, X., Zasloff, M., Wilson, J.M., 1998. The peptide antibiotic LL-37/hCAP-18 is expressed in epithelia of the human lung where it has broad antimicrobial activity at the airway surface. Proc. Natl. Acad. Sci. U. S. A. 95, 9541–6.
Bansal-Mutalik, R., Nikaido, H., 2014. Mycobacterial outer membrane is a lipid bilayer and the inner membrane is unusually rich in diacyl phosphatidylinositol dimannosides. Proc. Natl. Acad. Sci. U. S. A. 111, 4958–63. doi:10.1073/pnas.1403078111
Bansal-Mutalik, R., Nikaido, H., 2011. Quantitative lipid composition of cell envelopes of Corynebacterium glutamicum elucidated through reverse micelle extraction. Proc. Natl. Acad. Sci. U. S. A. 108, 15360–5. doi:10.1073/pnas.1112572108
Bartlomiejczyk, M. a, Swierzko, A.S., Brzostek, A., Dziadek, J., Cedzynski, M., 2014. Interaction of lectin pathway of complement-activating pattern recognition molecules with Mycobacteria. Clin. Exp. Immunol. doi:10.1111/cei.12416
Basaraba, R.J., Ojha, A.K., 2017. Mycobacterial Biofilms: Revisiting Tuberculosis Bacilli in Extracellular Necrotizing Lesions 1–7. doi:10.1128/microbiolspec.TBTB2-0024-2016
Behler, F., Steinwede, K., Balboa, L., Ueberberg, B., Maus, R., Kirchhof, G., Yamasaki, S., Welte, T., Maus, U.A., 2012. Role of Mincle in alveolar macrophage-dependent innate immunity against mycobacterial infections in mice. J. Immunol. 189, 3121–9. doi:10.4049/jimmunol.1201399
Behr, M.A., 2013. Evolution of Mycobacterium tuberculosis. Adv. Exp. Med. Biol. 783, 81–91. doi:10.1007/978-1-4614-6111-1_4
Benjamini, Y., Krieger, A.M., Yekutieli, D., 2006. Adaptive linear step-up procedures that control the false discovery rate. Biometrika 93, 491–507. doi:10.1093/biomet/93.3.491
Berends, E.T.M., Dekkers, J.F., Nijland, R., Kuipers, A., Soppe, J.A., van Strijp, J.A.G., Rooijakkers, S.H.M., 2013. Distinct localization of the complement C5b-9 complex on Gram-positive bacteria. Cell. Microbiol. 15, 1955–1968. doi:10.1111/cmi.12170
Bernhard, W., 2016. Lung surfactant: Function and composition in the context of development and respiratory physiology. Ann. Anat. - Anat. Anzeiger 208, 146–150. doi:10.1016/j.aanat.2016.08.003
Besra, G.S., 1998. Preparation of cell-wall fractions from mycobacteria. Methods Mol. Biol. 101, 91–107. doi:10.1385/0-89603-471-2:91
Birch, H.L., Alderwick, L.J., Appelmelk, B.J., Maaskant, J., Bhatt, A., Singh, A., Nigou, J., Eggeling, L., Geurtsen, J., Besra, G.S., 2010. A truncated lipoglycan from mycobacteria with altered immunological properties. Proc. Natl. Acad. Sci. U. S. A. 107, 2634–9. doi:10.1073/pnas.0915082107
Bjarnsholt, T., 2013. The role of bacterial biofilms in chronic infections. APMIS. Suppl. 1–

51. doi:10.1111/apm.12099
Bloch, H., 1950. Studies on The Virulence of Tubercule Bacilli: Isolation and Biological Properties of A Constituent of Virulent Organisms. J. Exp. Med. 91, 197–218. doi:10.1084/jem.91.2.197
Boe, D.M., Curtis, B.J., Chen, M.M., Ippolito, J.A., Kovacs, E.J., 2015. Extracellular traps and macrophages: new roles for the versatile phagocyte. J. Leukoc. Biol. 97, 1023–35. doi:10.1189/jlb.4RI1014-521R
Borders, C.W., Courtney, A., Ronen, K., Laborde-Lahoz, M.P., Guidry, T. V., Hwang, S.A., Olsen, M., Hunter, R.L., Hollmann, T.J., Wetsel, R.A., Actor, J.K., 2005. Requisite role for complement C5 and the C5a receptor in granulomatous response to mycobacterial glycolipid trehalose 6,6′-dimycolate. Scand. J. Immunol. 62, 123–130. doi:10.1111/j.1365-3083.2005.01643.x
Bowdish, D.M.E., Sakamoto, K., Kim, M.-J., Kroos, M., Mukhopadhyay, S., Leifer, C.A., Tryggvason, K., Gordon, S., Russell, D.G., 2009. MARCO, TLR2, and CD14 are required for macrophage cytokine responses to mycobacterial trehalose dimycolate and Mycobacterium tuberculosis. PLoS Pathog. 5, e1000474. doi:10.1371/journal.ppat.1000474
Brennan, P.., 2003. Structure, function, and biogenesis of the cell wall of Mycobacterium tuberculosis. Tuberculosis 83, 91–97.
Brennan, P.J., Nikaido, H., 1995. The envelope of mycobacteria. Annu. Rev. Biochem. 64, 29–63. doi:10.1146/annurev.bi.64.070195.000333
Bulut, Y., Michelsen, K.S., Hayrapetian, L., Naiki, Y., Spallek, R., Singh, M., Arditi, M., 2005. Mycobacterium tuberculosis heat shock proteins use diverse Toll-like receptor pathways to activate pro-inflammatory signals. J. Biol. Chem. 280, 20961–7. doi:10.1074/jbc.M411379200
Burmølle, M., Thomsen, T.R., Fazli, M., Dige, I., Christensen, L., Homøe, P., Tvede, M., Nyvad, B., Tolker-Nielsen, T., Givskov, M., Moser, C., Kirketerp-Møller, K., Johansen, H.K., Høiby, N., Jensen, P.Ø., Sørensen, S.J., Bjarnsholt, T., 2010. Biofilms in chronic infections - a matter of opportunity - monospecies biofilms in multispecies infections. FEMS Immunol. Med. Microbiol. 59, 324–36. doi:10.1111/j.1574-695X.2010.00714.x
Caceres, N., Vilaplana, C., Prats, C., Marzo, E., Llopis, I., Valls, J., Lopez, D., Cardona, P.-J., 2013. Evolution and role of corded cell aggregation in M. tuberculosis cultures. Tuberculosis 93, 1–9. doi:10.1016/j.tube.2013.08.003
Cai, Y., Yang, Q., Tang, Y., Zhang, M., Liu, H., Zhang, G., Deng, Q., Huang, J., Gao, Z., Zhou, B., Feng, C.G., Chen, X., 2014. Increased complement C1q level marks active disease in human tuberculosis. PLoS One 9, e92340. doi:10.1371/journal.pone.0092340
Cambier, C.J., Takaki, K.K., Larson, R.P., Hernandez, R.E., Tobin, D.M., Urdahl, K.B., Cosma, C.L., Ramakrishnan, L., 2013. Mycobacteria manipulate macrophage recruitment through coordinated use of membrane lipids. Nature 505, 218–222. doi:10.1038/nature12799
Canetti, G., 1965. Present aspects of bacterial resistance in tuberculosis. Am. Rev. Respir. Dis. 92, 687–703.
Carroll, M. V, Lack, N., Sim, E., Krarup, A., Sim, R.B., 2009. Multiple routes of complement activation by Mycobacterium bovis BCG. Mol. Immunol. 46, 3367–78. doi:10.1016/j.molimm.2009.07.015
Chalmers, J.D., Matsushita, M., Kilpatrick, D.C., Hill, A.T., 2015. No Strong Relationship Between Components of the Lectin Pathway of Complement and Susceptibility to Pulmonary Tuberculosis. Inflammation 38, 1731–7. doi:10.1007/s10753-015-0150-0
Chan, J., Xing, Y., Magliozzo, R.S., Bloom, B.R., 1992. Killing of virulent Mycobacterium tuberculosis by reactive nitrogen intermediates produced by activated murine

macrophages. J. Exp. Med. 175, 1111–22.
Chandra, H., Basir, S.F., Gupta, M., Banerjee, N., 2010. Glutamine synthetase encoded by glnA-1 is necessary for cell wall resistance and pathogenicity of Mycobacterium bovis. Microbiology 156, 3669–3677. doi:10.1099/mic.0.043828-0
Chen, P., Bishai, W.R., 1998. Novel selection for isoniazid (INH) resistance genes supports a role for NAD+-binding proteins in mycobacterial INH resistance. Infect. Immun. 66, 5099–106.
Cheng, L.E., Ohlén, C., Nelson, B.H., Greenberg, P.D., 2002. Enhanced signaling through the IL-2 receptor in CD8+ T cells regulated by antigen recognition results in preferential proliferation and expansion of responding CD8+ T cells rather than promotion of cell death. Proc. Natl. Acad. Sci. U. S. A. 99, 3001–6. doi:10.1073/pnas.052676899
Cholo, M.C., Boshoff, H.I., Steel, H.C., Cockeran, R., Matlola, N.M., Downing, K.J., Mizrahi, V., Anderson, R., 2006. Effects of clofazimine on potassium uptake by a Trk-deletion mutant of Mycobacterium tuberculosis. J. Antimicrob. Chemother. 57, 79–84. doi:10.1093/jac/dki409
Chroneos, Z., Jagannath, C., 2012. Immunoregulatory Role of GM-CSF in Pulmonary Tuberculosis. Underst. Tuberc. - Anal. Orig. Mycobacterium Tuberc. Pathog. 1–5. doi:10.5772/30003
Comas, I., Chakravartti, J., Small, P.M., Galagan, J., Niemann, S., Kremer, K., Ernst, J.D., Gagneux, S., 2010. Human T cell epitopes of Mycobacterium tuberculosis are evolutionarily hyperconserved. Nat. Genet. 42, 498–503. doi:10.1038/ng.590
Corning, 2011. Corning Filtration Guide: Innovative Products for Filtration and Ultrafiltration 2.
Coulthard, L.G., Woodruff, T.M., 2015. Is the complement activation product C3a a proinflammatory molecule? Re-evaluating the evidence and the myth. J. Immunol. 194, 3542–8. doi:10.4049/jimmunol.1403068
Cywes, C., Hoppe, H.C., Daffé, M., Ehlers, M.R., 1997. Nonopsonic binding of Mycobacterium tuberculosis to complement receptor type 3 is mediated by capsular polysaccharides and is strain dependent. Infect. Immun. 65, 4258–66.
Daffé, M., Etienne, G., 1999. The capsule of Mycobacterium tuberculosis and its implications for pathogenicity. Tuber. Lung Dis. 79, 153–169.
Dahl, K.E., Shiratsuchi, H., Hamilton, B.D., Ellner, J.J., Toossi, Z., 1996. Selective induction of transforming growth factor β in human monocytes by lipoarabinomannan of Mycobacterium tuberculosis. Infect. Immun. 64, 399–405.
Danelishvili, L., Everman, J.L., McNamara, M.J., Bermudez, L.E., 2011. Inhibition of the Plasma-Membrane-Associated Serine Protease Cathepsin G by Mycobacterium tuberculosis Rv3364c Suppresses Caspase-1 and Pyroptosis in Macrophages. Front. Microbiol. 2, 281. doi:10.3389/fmicb.2011.00281
Dannenberg, A.M., 1994. Roles of cytotoxic delayed-type hypersensitivity and macrophage-activating cell-mediated immunity in the pathogenesis of tuberculosis. Immunobiology 191, 461–73. doi:10.1016/S0171-2985(11)80452-3
Dao, D.N., Kremer, L., Guerardel, Y., Molano, A., Jacobs, W.R., Porcelli, S.A., Briken, V., Guérardel, Y., 2004. Mycobacterium tuberculosis Lipomannan Induces Apoptosis and Interleukin-12 Production in Macrophages. Infect. Immun. 72, 2067–2074. doi:10.1128/IAI.72.4.2067-2074.2004
Darrah, P.A., Patel, D.T., De Luca, P.M., Lindsay, R.W.B., Davey, D.F., Flynn, B.J., Hoff, S.T., Andersen, P., Reed, S.G., Morris, S.L., Roederer, M., Seder, R.A., 2007. Multifunctional TH1 cells define a correlate of vaccine-mediated protection against Leishmania major. Nat. Med. 13, 843–50. doi:10.1038/nm1592
de Carvalho, L.P.S., Fischer, S.M., Marrero, J., Nathan, C., Ehrt, S., Rhee, K.Y., 2010.

Metabolomics of Mycobacterium tuberculosis reveals compartmentalized co-catabolism of carbon substrates. Chem. Biol. 17, 1122–31. doi:10.1016/j.chembiol.2010.08.009
de Jager, W., Bourcier, K., Rijkers, G.T., Prakken, B.J., Seyfert-Margolis, V., 2009. Prerequisites for cytokine measurements in clinical trials with multiplex immunoassays. BMC Immunol. 10, 52. doi:10.1186/1471-2172-10-52
Diedrich, C.R., Mattila, J.T., Flynn, J.L., 2013. Monocyte-Derived IL-5 Reduces TNF Production by Mycobacterium tuberculosis–specific CD4 T Cells during SIV/M. tuberculosis Coinfection. J. Immunol. 190.
Dobson, G., Minnikin, D.E., Minnikin, S.., Parlett, J.H., Goodfellow, M., Ridell, M., Magnusson, M., 1985. Systematic Analysis of Complex Mycobacterial Lipids, in: Minnikin, D.E., Goodfellow, M. (Eds.), Chemical Methods in Bacterial Systematics. Society for Applied Bacteriology, London, pp. 237–262.
Domenech, M., Ramos-Sevillano, E., García, E., Moscoso, M., Yuste, J., 2013. Biofilm formation avoids complement immunity and phagocytosis of Streptococcus pneumoniae. Infect. Immun. 81, 2606–15. doi:10.1128/IAI.00491-13
Donlan, R.M., 2002. Biofilms: microbial life on surfaces. Emerg. Infect. Dis. 8, 881–90. doi:10.3201/eid0809.020063
Downing, J.F., Pasula, R., Wright, J.R., Twigg, H.L., Martin, W.J., Martin, W.J., 2nd, 1995. Surfactant protein a promotes attachment of Mycobacterium tuberculosis to alveolar macrophages during infection with human immunodeficiency virus. Proc. Natl. Acad. Sci. U. S. A. 92, 4848–52.
Driver, E.R., 2014. The C3HeB/FeJ mice as a novel preclinical mouse model for Mycobacterium tuberculosis : an analysis of the host pathogenesis and the in vivo environment of the necrotic granuloma. Colorado State University.
Dutow, P., Fehlhaber, B., Bode, J., Laudeley, R., Rheinheimer, C., Glage, S., Wetsel, R.A., Pabst, O., Klos, A., 2014. The complement C3a receptor is critical in defense against Chlamydia psittaci in mouse lung infection and required for antibody and optimal T cell response. J. Infect. Dis. 209, 1269–78. doi:10.1093/infdis/jit640
Elkington, P.T., Ugarte-Gil, C.A., Friedland, J.S., 2011. Matrix metalloproteinases in tuberculosis. Eur. Respir. J. 38, 456–464. doi:10.1183/09031936.00015411
Engele, M., Castiglione, K., Schwerdtner, N., Wagner, M., Bölcskei, P., Röllinghoff, M., Stenger, S., 2002. Induction of TNF in Human Alveolar Macrophages As a Potential Evasion Mechanism of Virulent Mycobacterium tuberculosis. J. Immunol. 168, 1328–1337. doi:10.4049/jimmunol.168.3.1328
Eum, S.-Y., Kong, J.-H., Hong, M.-S., Lee, Y.-J., Kim, J.-H., Hwang, S.-H., Cho, S.-N., Via, L.E., Barry, C.E., 2010. Neutrophils are the predominant infected phagocytic cells in the airways of patients with active pulmonary TB. Chest 137, 122–8. doi:10.1378/chest.09-0903
Fattorini, L., Gennaro, R., Zanetti, M., Tan, D., Brunori, L., Giannoni, F., Pardini, M., Orefici, G., 2004. In vitro activity of protegrin-1 and beta-defensin-1, alone and in combination with isoniazid, against Mycobacterium tuberculosis. Peptides 25, 1075–1077. doi:10.1016/j.peptides.2004.04.003
Feng, C.G., Kaviratne, M., Rothfuchs, A.G., Cheever, A., Hieny, S., Young, H.A., Wynn, T.A., Sher, A., 2006. NK cell-derived IFN-gamma differentially regulates innate resistance and neutrophil response in T cell-deficient hosts infected with Mycobacterium tuberculosis. J. Immunol. 177, 7086–93.
Feng, W.-X., Flores-Villanueva, P.O., Mokrousov, I., Wu, X.-R., Xiao, J., Jiao, W.-W., Sun, L., Miao, Q., Shen, C., Shen, D., Liu, F., Jia, Z.-W., Shen, A., 2012. <I>CCL2</I>−2518 (A/G) polymorphisms and tuberculosis susceptibility: a meta-analysis [Review article]. Int. J. Tuberc. Lung Dis. 16, 150–156.

doi:10.5588/ijtld.11.0205
Fennelly, K.P., Jones-López, E.C., 2015. Quantity and Quality of Inhaled Dose Predicts Immunopathology in Tuberculosis. Front. Immunol. 6, 313. doi:10.3389/fimmu.2015.00313
Fennelly, K.P., Martyny, J.W., Fulton, K.E., Orme, I.M., Cave, D.M., Heifets, L.B., 2004. Cough-generated Aerosols of *Mycobacterium tuberculosis*. Am. J. Respir. Crit. Care Med. 169, 604–609. doi:10.1164/rccm.200308-1101OC
Ferguson, J.S., Voelker, D.R., McCormack, F.X., Schlesinger, L.S., 1999. Surfactant protein D binds to Mycobacterium tuberculosis bacilli and lipoarabinomannan via carbohydrate-lectin interactions resulting in reduced phagocytosis of the bacteria by macrophages. J. Immunol. 163, 312–21.
Ferguson, J.S., Voelker, D.R., Ufnar, J.A., Dawson, A.J., Schlesinger, L.S., 2002. Surfactant Protein D Inhibition of Human Macrophage Uptake of Mycobacterium tuberculosis Is Independent of Bacterial Agglutination. J. Immunol. 168, 1309–1314. doi:10.4049/jimmunol.168.3.1309
Ferguson, J.S., Weis, J.J., Martin, J.L., Schlesinger, L.S., 2004. Complement Protein C3 Binding to Mycobacterium tuberculosis Is Initiated by the Classical Pathway in Human Bronchoalveolar Lavage Fluid. Infect. Immun. 72, 2564–2573. doi:10.1128/IAI.72.5.2564-2573.2004
Fidler, K.J., Hilliard, T.N., Bush, A., Johnson, M., Geddes, D.M., Turner, M.W., Alton, E.W.F.W., Klein, N.J., Davies, J.C., 2009. Mannose-binding lectin is present in the infected airway: a possible pulmonary defence mechanism. Thorax 64, 150–5. doi:10.1136/thx.2008.100073
Fleming, A., 1922. On a Remarkable Bacteriolytic Element Found in Tissues and Secretions. Proc. R. Soc. London B Biol. Sci. 93.
Flemming, H.-C., Wingender, J., 2010. The biofilm matrix. Nat. Rev. Microbiol. 8, 623–33. doi:10.1038/nrmicro2415
Flesch, I.E., Kaufmann, S.H., 1991. Mechanisms involved in mycobacterial growth inhibition by gamma interferon-activated bone marrow macrophages: role of reactive nitrogen intermediates. Infect. Immun. 59, 3213–8.
Flores-Valdez, M.A., 2016. Vaccines Directed Against Microorganisms or Their Products Present During Biofilm Lifestyle: Can We Make a Translation as a Broad Biological Model to Tuberculosis? Front. Microbiol. 7, 14. doi:10.3389/fmicb.2016.00014
Flores-Valdez, M.A., de Jesús Aceves-Sánchez, M., Pedroza-Roldán, C., Vega-Domínguez, P.J., Prado-Montes de Oca, E., Bravo-Madrigal, J., Laval, F., Daffé, M., Koestler, B., Waters, C.M., 2015. The cyclic di-GMP phosphodiesterase gene Rv1357c/BCG1419c affects BCG Pellicle production and In Vivo maintenance. IUBMB Life 67, 129–38. doi:10.1002/iub.1353
Flores-Villanueva, P.O., Ruiz-Morales, J.A., Song, C.-H., Flores, L.M., Jo, E.-K., Montaño, M., Barnes, P.F., Selman, M., Granados, J., 2005. A functional promoter polymorphism in monocyte chemoattractant protein-1 is associated with increased susceptibility to pulmonary tuberculosis. J. Exp. Med. 202, 1649–58. doi:10.1084/jem.20050126
Flynn, J.L., Goldstein, M.M., Chan, J., Triebold, K.J., Pfeffer, K., Lowenstein, C.J., Schreiber, R., Mak, T.W., Bloom, B.R., 1995. Tumor necrosis factor-alpha is required in the protective immune response against Mycobacterium tuberculosis in mice. Immunity 2, 561–72.
Fratti, R.A., Backer, J.M., Gruenberg, J., Corvera, S., Deretic, V., 2001. Role of phosphatidylinositol 3-kinase and Rab5 effectors in phagosomal biogenesis and mycobacterial phagosome maturation arrest. J. Cell Biol. 154, 631–44. doi:10.1083/jcb.200106049

Fratti, R.A., Chua, J., Vergne, I., Deretic, V., 2003. Mycobacterium tuberculosis glycosylated phosphatidylinositol causes phagosome maturation arrest. Proc. Natl. Acad. Sci. U. S. A. 100, 5437–42. doi:10.1073/pnas.0737613100

Frølund, B., Palmgren, R., Keiding, K., Nielsen, P.H., 1996. Extraction of extracellular polymers from activated sludge using a cation exchange resin. Water Res. 30, 1749–1758. doi:10.1016/0043-1354(95)00323-1

Furuya, T., Hirose, S., Semba, H., Kino, K., 2011. Identification of the regulator gene responsible for the acetone-responsive expression of the binuclear iron monooxygenase gene cluster in mycobacteria. J. Bacteriol. 193, 5817–23. doi:10.1128/JB.05525-11

Garton, N.J., Christensen, H., Minnikin, D.E., Adegbola, R.A., Barer, M.R., 2002. Intracellular lipophilic inclusions of mycobacteria in vitro and in sputum. Microbiology 148, 2951–8.

Garton, N.J., Waddell, S.J., Sherratt, A.L., Lee, S.-M., Smith, R.J., Senner, C., Hinds, J., Rajakumar, K., Adegbola, R.A., Besra, G.S., Butcher, P.D., Barer, M.R., 2008. Cytological and transcript analyses reveal fat and lazy persister-like bacilli in tuberculous sputum. PLoS Med. 5, e75. doi:10.1371/journal.pmed.0050075

Gee, C.L., Papavinasasundaram, K.G., Blair, S.R., Baer, C.E., Falick, A.M., King, D.S., Griffin, J.E., Venghatakrishnan, H., Zukauskas, A., Wei, J.-R., Dhiman, R.K., Crick, D.C., Rubin, E.J., Sassetti, C.M., Alber, T., 2012. A phosphorylated pseudokinase complex controls cell wall synthesis in mycobacteria. Sci. Signal. 5, ra7. doi:10.1126/scisignal.2002525

Geijtenbeek, T.B.H., van Vliet, S.J., Koppel, E.A., Sanchez-Hernandez, M., Vandenbroucke-Grauls, C.M.J.E., Appelmelk, B., van Kooyk, Y., 2002. Mycobacteria Target DC-SIGN to Suppress Dendritic Cell Function. J. Exp. Med. 197, 7–17. doi:10.1084/jem.20021229

Gilmore, S.A., Schelle, M.W., Holsclaw, C.M., Leigh, C.D., Jain, M., Cox, J.S., Leary, J.A., Bertozzi, C.R., 2012. Sulfolipid-1 biosynthesis restricts Mycobacterium tuberculosis growth in human macrophages. ACS Chem. Biol. 7, 863–70. doi:10.1021/cb200311s

Gioia, C., Agrati, C., Goletti, D., Vincenti, D., Carrara, S., Amicosante, M., Casarinp, M., Giosue, S., Puglisi, G., Rossi, A., Colizzi, V., Pucillo, L.P., Poccia, F., 2003. Different Cytokine Production and Effector/Memory Dynamics of αβ+ or γδ+ T-Cell Subsets in the Peripheral Blood of Patients with Active Pulmonary Tuberculosis. Int. J. Immunopathol. Pharmacol. 16, 247–252. doi:10.1177/039463200301600310

Glickman, M.S., Cox, J.S., Jacobs, W.R., 2000. A Novel Mycolic Acid Cyclopropane Synthetase Is Required for Cording, Persistence, and Virulence of Mycobacterium tuberculosis. Mol. Cell 5, 717–727. doi:10.1016/S1097-2765(00)80250-6

Gold, J.A., Hoshino, Y., Tanaka, N., Rom, W.N., Raju, B., Condos, R., Weiden, M.D., 2004. Surfactant protein A modulates the inflammatory response in macrophages during tuberculosis. Infect. Immun. 72, 645–50. doi:10.1128/IAI.72.2.645-650.2004

Granucci, F., Vizzardelli, C., Pavelka, N., Feau, S., Persico, M., Virzi, E., Rescigno, M., Moro, G., Ricciardi-Castagnoli, P., 2001. Inducible IL-2 production by dendritic cells revealed by global gene expression analysis. Nat. Immunol. 2, 882–888. doi:10.1038/ni0901-882

Guirado, E., Mbawuike, U., Keiser, T.L., Arcos, J., Azad, A.K., Wang, S.-H.H., Schlesinger, L.S., 2015. Characterization of host and microbial determinants in individuals with latent tuberculosis infection using a human granuloma model. MBio 6, 1–13. doi:10.1128/mBio.02537-14

Gupta, K., Kumar, P., Chatterji, D., 2010. Identification, activity and disulfide connectivity of C-di- GMP regulating proteins in Mycobacterium tuberculosis. PLoS One 5, e15072. doi:10.1371/journal.pone.0015072

Hall-Stoodley, L., Stoodley, P., 2009. Evolving concepts in biofilm infections. Cell.

Microbiol. 11, 1034–43. doi:10.1111/j.1462-5822.2009.01323.x
Harkewicz, R., Dennis, E.A., 2011. Applications of mass spectrometry to lipids and membranes. Annu. Rev. Biochem. 80, 301–25. doi:10.1146/annurev-biochem-060409-092612
Hartmann, P., Becker, R., Franzen, C., Schell-Frederick, E., Romer, J., Jacobs, M., Fatkenheuer, G., Plum, G., 2001. Phagocytosis and killing of Mycobacterium avium complex by human neutrophils. J. Leukoc. Biol. 69, 397–404.
Hasan, Z., Cliff, J.M., Dockrell, H.M., Jamil, B., Irfan, M., Ashraf, M., Hussain, R., 2009. CCL2 responses to Mycobacterium tuberculosis are associated with disease severity in tuberculosis. PLoS One 4, e8459. doi:10.1371/journal.pone.0008459
Heitmann, L., Dar, M.A., Schreiber, T., Erdmann, H., Behrends, J., Mckenzie, A.N.J., Brombacher, F., Ehlers, S., Hölscher, C., 2014. The IL-13/IL-4Rα axis is involved in tuberculosis-associated pathology. J. Pathol. 234, 338–350. doi:10.1002/path.4399
Hengge, R., 2009. Principles of c-di-GMP signalling in bacteria. Nat. Rev. Microbiol. 7, 263–273. doi:10.1038/nrmicro2109
Henrichsen, J., 1972. Bacterial surface translocation: a survey and a classification. Bacteriol. Rev. 36, 478–503.
Hesper Rego, E., Audette, R.E., Rubin, E.J., 2017. Deletion of a mycobacterial divisome factor collapses single-cell phenotypic heterogeneity. Nature 546, 153–157. doi:10.1038/nature22361
Hirsch, C.S., Ellner, J.J., Russell, D.G., Rich, E.A., 1994. Complement receptor-mediated uptake and tumor necrosis factor-alpha-mediated growth inhibition of Mycobacterium tuberculosis by human alveolar macrophages. J. Immunol. 152, 743–53.
Hoff, D.R., Ryan, G.J., Driver, E.R., Ssemakulu, C.C., de Groote, M.A., Basaraba, R.J., Lenaerts, A.J., 2011. Location of intra- and extracellular M. tuberculosis populations in lungs of mice and guinea pigs during disease progression and after drug treatment. PLoS One 6, e17550. doi:10.1371/journal.pone.0017550
Hoffmann, C., Leis, A., Niederweis, M., Plitzko, J.M., Engelhardt, H., 2008. Disclosure of the mycobacterial outer membrane: cryo-electron tomography and vitreous sections reveal the lipid bilayer structure. Proc. Natl. Acad. Sci. U. S. A. 105, 3963–7. doi:10.1073/pnas.0709530105
Honaker, R.W., Dhiman, R.K., Narayanasamy, P., Crick, D.C., Voskuil, M.I., 2010. DosS responds to a reduced electron transport system to induce the Mycobacterium tuberculosis DosR regulon. J. Bacteriol. 192, 6447–55. doi:10.1128/JB.00978-10
Hong, Y., Zhou, X., Fang, H., Yu, D., Li, C., Sun, B., 2013. Cyclic di-GMP mediates Mycobacterium tuberculosis dormancy and pathogenecity. Tuberculosis 93, 625–634. doi:10.1016/j.tube.2013.09.002
Hoppe, H.C., de Wet, B.J., Cywes, C., Daffé, M., Ehlers, M.R., 1997. Identification of phosphatidylinositol mannoside as a mycobacterial adhesin mediating both direct and opsonic binding to nonphagocytic mammalian cells. Infect. Immun. 65, 3896–905.
Horsburgh, C.R., 2004. Priorities for the treatment of latent tuberculosis infection in the United States. N. Engl. J. Med. 350, 2060–7. doi:10.1056/NEJMsa031667
Hossain, M.M., Norazmi, M.-N., 2013. Pattern recognition receptors and cytokines in Mycobacterium tuberculosis infection--the double-edged sword? Biomed Res. Int. 2013, 179174. doi:10.1155/2013/179174
Houben, D., Demangel, C., van Ingen, J., Perez, J., Baldeón, L., Abdallah, A.M., Caleechurn, L., Bottai, D., van Zon, M., de Punder, K., van der Laan, T., Kant, A., Bossers-de Vries, R., Willemsen, P., Bitter, W., van Soolingen, D., Brosch, R., van der Wel, N., Peters, P.J., 2012. ESX-1-mediated translocation to the cytosol controls virulence of mycobacteria. Cell. Microbiol. 14, 1287–1298. doi:10.1111/j.1462-5822.2012.01799.x

Houk, V.N., Baker, J.H., Sorensen, K., Kent, D.C., 1968. The Epidemiology of Tuberculosis Infection in a Closed Environment. Arch. Environ. Heal. An Int. J. 16, 26–35. doi:10.1080/00039896.1968.10665011
Hu, C., Mayadas-Norton, T., Tanaka, K., Chan, J., Salgame, P., 2000. Mycobacterium tuberculosis Infection in Complement Receptor 3-Deficient Mice. J. Immunol. 165, 2596–2602. doi:10.4049/jimmunol.165.5.2596
Hunter, R.L., 2016. Tuberculosis as a three-act play: A new paradigm for the pathogenesis of pulmonary tuberculosis. Tuberculosis 97, 8–17. doi:10.1016/j.tube.2015.11.010
Hunter, R.L., 2011. Pathology of post primary tuberculosis of the lung: An illustrated critical review. Tuberculosis 91, 497–509.
Hunter, R.L., Actor, J.K., Hwang, S.-A., Karev, V., Jagannath, C., 2014. Pathogenesis of Post Primary Tuberculosis: Immunity and Hypersensitivity in the Development of Cavities. Ann. Clin. Lab. Sci. 44, 365–387.
Hunter, R.L., Olsen, M.M.R., Jagannath, C., Actor, J.K., 2006. Multiple roles of cord factor in the pathogenesis of primary, secondary, and cavitary tuberculosis, including a revised description of the pathology of secondary disease. Ann. Clin. … 36, 371–386.
Hunter, R.L., Venkataprasad, N., Olsen, M.R., 2006. The role of trehalose dimycolate (cord factor) on morphology of virulent M. tuberculosis in vitro. Tuberculosis (Edinb). 86, 349–356. doi:10.1016/j.tube.2005.08.017
Hussell, T., Bell, T.J., 2014. Alveolar macrophages: plasticity in a tissue-specific context. Nat. Rev. Immunol. 14, 81–93. doi:10.1038/nri3600
Huygen, K., 2014. The immunodominant T-cell epitopes of the mycolyl-transferases of the antigen 85 complex of M. tuberculosis. Front. Immunol. doi:10.3389/fimmu.2014.00321
Ingram, L.O., 1990. Ethanol tolerance in bacteria. Crit. Rev. Biotechnol. 9, 305–319. doi:10.3109/07388558909036741
Irwin, S.M., Driver, E., Lyon, E., Schrupp, C., Ryan, G., Gonzalez-Juarrero, M., Basaraba, R.J., Nuermberger, E.L., Lenaerts, A.J., 2015. Presence of multiple lesion types with vastly different microenvironments in C3HeB/FeJ mice following aerosol infection with Mycobacterium tuberculosis. Dis. Model. Mech. 8, 591–602. doi:10.1242/dmm.019570
Islam, M.S.M., Richards, J.J.P., Ojha, A.K.A., 2012. Targeting drug tolerance in mycobacteria: a perspective from mycobacterial biofilms. Expert Rev. Anti. Infect. Ther. 10, 1055–66. doi:10.1586/eri.12.88
Israel, H.L., Hetherington, H.W., Ord, J.G., 1941. A Study of Tuberculosis Among Students of Nursing. J. Am. Med. Assoc 117, 839–843. doi:10.1001/jama.1941.02820360021007
Jagannath, C., Hoffmann, H., Sepulveda, E., Actor, J.K., Wetsel, R.A., Hunter, R.L., 2000. Hypersusceptibility of A/J mice to tuberculosis is in part due to a deficiency of the fifth complement component (C5). Scand. J. Immunol. 52, 369–379. doi:10.1046/j.1365-3083.2000.00770.x
Jakel, A., Qaseem, A.S., Kishore, U., Sim, R.B., 2013. Ligands and receptors of lung surfactant proteins SP-A and SP-D. Front. Biosci. (Landmark Ed. 18, 1129–40.
James, B.W., Williams, A., Marsh, P.D., 2000. The physiology and pathogenicity of Mycobacterium tuberculosis grown under controlled conditions in a defined medium. J. Appl. Microbiol. 88, 669–77.
Jarva, H., 2003. Complement resistance mechanisms of streptococci. Mol. Immunol. 40, 95–107. doi:10.1016/S0161-5890(03)00108-1
Jiang, Z., Higgins, M.P., Whitehurst, J., Kisich, K.O., Voskuil, M.I., Hodges, R.S., 2011. Anti-tuberculosis activity of α-helical antimicrobial peptides: de novo designed L- and D-enantiomers versus L- and D-LL-37. Protein Pept. Lett. 18, 241–52. doi:10.2174/092986611794578288
Jones, B.W., Means, T.K., Heldwein, K.A., Keen, M.A., Hill, P.J., Belisle, J.T., Fenton, M.J.,

2001. Different Toll-like receptor agonists induce distinct macrophage responses. J. Leukoc. Biol. 69, 1036–1044.
Julián, E., Roldán, M., Sánchez-Chardi, A., Astola, O., Agustí, G., Luquin, M., 2010. Microscopic cords, a virulence-related characteristic of Mycobacterium tuberculosis, are also present in nonpathogenic mycobacteria. J. Bacteriol. 192, 1751–60. doi:10.1128/JB.01485-09
Källenius, G., Correia-Neves, M., Buteme, H., Hamasur, B., Svenson, S.B., 2015. Lipoarabinomannan, and its related glycolipids, induce divergent and opposing immune responses to Mycobacterium tuberculosis depending on structural diversity and experimental variations. Tuberculosis (Edinb). doi:10.1016/j.tube.2015.09.005
Kalsum, S., Braian, C., Koeken, V.A.C.M., Raffetseder, J., Lindroth, M., van Crevel, R., Lerm, M., 2017. The Cording Phenotype of Mycobacterium tuberculosis Induces the Formation of Extracellular Traps in Human Macrophages. Front. Cell. Infect. Microbiol. 7, 278. doi:10.3389/fcimb.2017.00278
Kanetsuna, F., 1980. Effect of Lysozyme on Mycobacteria. Microbiol. Immunol. 24, 1151–1162. doi:10.1111/j.1348-0421.1980.tb02920.x
Kang, D.D., Lin, Y., Moreno, J.-R., Randall, T.D., Khader, S.A., 2011. Profiling early lung immune responses in the mouse model of tuberculosis. PLoS One 6, e16161. doi:10.1371/journal.pone.0016161
Kang, P.B., Azad, A.K., Torrelles, J.B., Kaufman, T.M., Beharka, A., Tibesar, E., DesJardin, L.E., Schlesinger, L.S., 2005. The human macrophage mannose receptor directs Mycobacterium tuberculosis lipoarabinomannan-mediated phagosome biogenesis. J. Exp. Med. 202, 987–99. doi:10.1084/jem.20051239
Kelley, V.A., Schorey, J.S., 2003. Mycobacterium's arrest of phagosome maturation in macrophages requires Rab5 activity and accessibility to iron. Mol. Biol. Cell 14, 3366–77. doi:10.1091/mbc.E02-12-0780
Kerns, P.W., Ackhart, D.F., Basaraba, R.J., Leid, J., Shirtliff, M.E., 2014. Mycobacterium tuberculosis pellicles express unique proteins recognized by the host humoral response. Pathog. Dis. 1–12. doi:10.1111/2049-632X.12142
Khan, N., Vidyarthi, A., Javed, S., Agrewala, J.N., 2016. Innate Immunity Holding the Flanks until Reinforced by Adaptive Immunity against Mycobacterium tuberculosis Infection. Front. Microbiol. 7, 328. doi:10.3389/fmicb.2016.00328
Kieser, K.J., Rubin, E.J., 2014. How sisters grow apart: mycobacterial growth and division. Nat. Rev. Microbiol. 12, 550–62. doi:10.1038/nrmicro3299
King, L.B., Swiatlo, E., Swiatlo, A., McDaniel, L.S., 2009. Serum resistance and biofilm formation in clinical isolates of Acinetobacter baumannii. FEMS Immunol. Med. Microbiol. 55, 414–21. doi:10.1111/j.1574-695X.2009.00538.x
Kishore, U., Ghai, R., Greenhough, T.J., Shrive, A.K., Bonifati, D.M., Gadjeva, M.G., Waters, P., Kojouharova, M.S., Chakraborty, T., Agrawal, A., 2004. Structural and functional anatomy of the globular domain of complement protein C1q. Immunol. Lett. 95, 113–128. doi:10.1016/j.imlet.2004.06.015
Kleinnijenhuis, J., Oosting, M., Joosten, L.A.B., Netea, M.G., Van Crevel, R., 2011. Innate immune recognition of Mycobacterium tuberculosis. Clin. Dev. Immunol. 2011, 405310. doi:10.1155/2011/405310
Koch, R., 1882. The etiology of tuberculosis. Berl. Klin. Wochenschr. 15, 221–30.
Kohmo, S., Kijima, T., Mori, M., Minami, T., Namba, Y., Yano, Y., Yoneda, T., Takeda, Y., Kitada, S., Yamaguchi, T., Tachibana, I., Yokota, S., 2012. CXCL12 as a biological marker for the diagnosis of tuberculous pleurisy. Tuberculosis 92, 248–252. doi:10.1016/j.tube.2012.01.001
Koliwer-Brandl, H., Syson, K., van de Weerd, R., Chandra, G., Appelmelk, B., Alber, M.,

Ioerger, T.R., Jacobs, W.R., Geurtsen, J., Bornemann, S., Kalscheuer, R., 2016. Metabolic Network for the Biosynthesis of Intra- and Extracellular α-Glucans Required for Virulence of Mycobacterium tuberculosis. PLoS Pathog. 12, e1005768. doi:10.1371/journal.ppat.1005768

Korf, J., Stoltz, A., Verschoor, J., De Baetselier, P., Grooten, J., 2005. The Mycobacterium tuberculosis cell wall component mycolic acid elicits pathogen-associated host innate immune responses. Eur. J. Immunol. 35, 890–900. doi:10.1002/eji.200425332

Kotani, T., Yurimoto, H., Kato, N., Sakai, Y., 2007. Novel acetone metabolism in a propane-utilizing bacterium, Gordonia sp. strain TY-5. J. Bacteriol. 189, 886–93. doi:10.1128/JB.01054-06

Kristian, S.A., Birkenstock, T.A., Sauder, U., Mack, D., Götz, F., Landmann, R., 2008. Biofilm formation induces C3a release and protects Staphylococcus epidermidis from IgG and complement deposition and from neutrophil-dependent killing. J. Infect. Dis. 197, 1028–35. doi:10.1086/528992

Krogh, A., Lindhard, J., 1914. On the average composition of the alveolar air and its variations during the respiratory cycle. J. Physiol. 47, 431–445. doi:10.1113/jphysiol.1914.sp001635

Krupa, A., Fol, M., Dziadek, B.R., Kepka, E., Wojciechowska, D., Brzostek, A., Torzewska, A., Dziadek, J., Baughman, R.P., Griffith, D., Kurdowska, A.K., 2015. Binding of CXCL8/IL-8 to *Mycobacterium tuberculosis* Modulates the Innate Immune Response. Mediators Inflamm. 2015, 1–11. doi:10.1155/2015/124762

Kulka, K., Hatfull, G., Ojha, A.K., 2012. Growth of Mycobacterium tuberculosis biofilms. J. Vis. Exp. e3820. doi:10.3791/3820

Lachmann, P.J., 1998. Microbial immunology: A new mechanism for immune subversion. Curr. Biol. 8, R99–R101. doi:10.1016/S0960-9822(98)70057-0

Ladel, C.H., Hess, J., Daugelat, S., Mombaerts, P., Tonegawa, S., Kaufmann, S.H.E., 1995. Contribution of α/β and γ/δ T lymphocytes to immunity againstMycobacterium bovis Bacillus Calmette Guérin: studies with T cell receptor-deficient mutant mice. Eur. J. Immunol. 25, 838–846. doi:10.1002/eji.1830250331

Laennec, R., Forbes, J., 1821. A treatise on diseases of the chest in which they are described according to their anatomical characters, and their diagnosis established on a new principle by means of acoustick instruments, Third edit. ed. Underwood London, London.

Lang, R., 2013. Recognition of the mycobacterial cord factor by Mincle: relevance for granuloma formation and resistance to tuberculosis. Front. Immunol. 4, 5. doi:10.3389/fimmu.2013.00005

Leenaars, M., Hendriksen, C.F.M., HBWM, K., MJ, N., H, H., G, K., A, L., W, P., M, van R., E, R., H, S., H, S., D, S., DES, S.-T., 2005. Critical Steps in the Production of Polyclonal and Monoclonal Antibodies: Evaluation and Recommendations. ILAR J. 46, 269–279. doi:10.1093/ilar.46.3.269

Lemassu, A., Daffé, M., 1994. Structural features of the exocellular polysaccharides of Mycobacterium tuberculosis. Biochem. J. 297 ( Pt 2, 351–7.

Lemos, M.P., McKinney, J., Rhee, K.Y., 2011. Dispensability of surfactant proteins A and D in immune control of Mycobacterium tuberculosis infection following aerosol challenge of mice. Infect. Immun. 79, 1077–85. doi:10.1128/IAI.00286-10

Lenaerts, A., Barry, C.E., Dartois, V., 2015. Heterogeneity in tuberculosis pathology, microenvironments and therapeutic responses. Immunol. Rev. 264, 288–307. doi:10.1111/imr.12252

Lenaerts, A.J., Hoff, D., Aly, S., Ehlers, S., Andries, K., Cantarero, L., Orme, I.M., Basaraba, R.J., 2007. Location of persisting mycobacteria in a Guinea pig model of tuberculosis

revealed by r207910. Antimicrob. Agents Chemother. 51, 3338–45. doi:10.1128/AAC.00276-07
Lerner, T.R., Borel, S., Gutierrez, M.G., 2015. The innate immune response in human tuberculosis. Cell. Microbiol. 17, 1277–1285. doi:10.1111/cmi.12480
Lethbridge, S., 2012. Laboratory notebook.
Liu, Y., Endo, Y., Iwaki, D., Nakata, M., Matsushita, M., Wada, I., Inoue, K., Munakata, M., Fujita, T., 2005. Human M-Ficolin Is a Secretory Protein That Activates the Lectin Complement Pathway. J. Immunol. 175.
Lopez-Marin, L.M., 2012. Nonprotein structures from mycobacteria: emerging actors for tuberculosis control. Clin. Dev. Immunol. 2012, 917860. doi:10.1155/2012/917860
Lowe, D.M., Bangani, N., Mehta, M.R., Lang, D.M., Rossi, A.G., Wilkinson, K.A., Wilkinson, R.J., Martineau, A.R., 2013. A novel assay of antimycobacterial activity and phagocytosis by human neutrophils. Tuberculosis 93, 167–178.
Luca, S., Mihaescu, T., 2013. History of BCG Vaccine. Maedica (Buchar). 8, 53–8.
Lukins, H.B., Foster, J.W., 1963. METHYL KETONE METABOLISM IN HYDROCARBON-UTILIZING MYCOBACTERIA. J. Bacteriol. 85, 1074–87.
Luo, F., Sun, X., Wang, Y., Wang, Q., Wu, Y., Pan, Q., Fang, C., Zhang, X.-L., 2013. Ficolin-2 defends against virulent Mycobacteria tuberculosis infection in vivo, and its insufficiency is associated with infection in humans. PLoS One 8, e73859. doi:10.1371/journal.pone.0073859
Madigan, M.T., Clark, D.P., Stahl, D., Martinko, J.M., 2010. Brock Biology of Microorganisms 13th Edition.
Mahamed, D., Boulle, M., Ganga, Y., Mc Arthur, C., Skroch, S., Oom, L., Catinas, O., Pillay, K., Naicker, M., Rampersad, S., Mathonsi, C., Hunter, J., Sreejit, G., Pym, A.S., Lustig, G., Sigal, A., 2017. Intracellular growth of Mycobacterium tuberculosis after macrophage cell death leads to serial killing of host cells. Elife 6, e22028. doi:10.7554/eLife.22028
Malik, Z. a, Denning, G.M., Kusner, D.J., 2000. Inhibition of Ca(2+) signaling by Mycobacterium tuberculosis is associated with reduced phagosome-lysosome fusion and increased survival within human macrophages. J. Exp. Med. 191, 287–302.
Marth, T., Kelsall, B.L., 1997. Regulation of interleukin-12 by complement receptor 3 signaling. J. Exp. Med. 185, 1987–95.
Martínez, A., Torello, S., Kolter, R., 1999. Sliding motility in mycobacteria. J. Bacteriol. 181, 7331–8.
Mashruwala, M.A., Smith, A.K., Lindsey, D.R., Moczygemba, M., Wetsel, R.A., Klein, J.R., Actor, J.K., Jagannath, C., 2011. A defect in the synthesis of Interferon-γ by the T cells of Complement-C5 deficient mice leads to enhanced susceptibility for tuberculosis. Tuberculosis (Edinb). 91 Suppl 1, S82-9. doi:10.1016/j.tube.2011.10.016
Master, S.S., Rampini, S.K., Davis, A.S., Keller, C., Ehlers, S., Springer, B., Timmins, G.S., Sander, P., Deretic, V., 2008. Mycobacterium tuberculosis Prevents Inflammasome Activation. Cell Host Microbe 3, 224–232. doi:10.1016/j.chom.2008.03.003
Matthaei, K.I., Foster, P.S., Young, I.G., 1997. The role of interleukin-5 (IL-5 ) in vivo: studies with IL-5 deficient mice. Mem. Inst. Oswaldo Cruz 92, 63–68. doi:10.1590/S0074-02761997000800010
May, A., Fischer, R.-J., Maria Thum, S., Schaffer, S., Verseck, S., Dürre, P., Bahl, H., 2013. A modified pathway for the production of acetone in Escherichia coli. Metab. Eng. 15, 218–25. doi:10.1016/j.ymben.2012.08.001
McNeil, M., Daffe, M., Brennan, P., 1991. Location of the mycolyl ester substituents in the cell walls of mycobacteria. J. Biol. Chem. 266, 13217–13223.
McNeil, M., Daffe, M., Brennan, P., 1990. Evidence for the nature of the link between the

arabinogalactan and peptidoglycan of mycobacterial cell walls. J. Biol. Chem. 265, 18200–18206.
Merle, N.S., Noe, R., Halbwachs-Mecarelli, L., Fremeaux-Bacchi, V., Roumenina, L.T., 2015. Complement System Part II: Role in Immunity. Front. Immunol. 6, 257. doi:10.3389/fimmu.2015.00257
Minnikin, D.E., Lee, O.Y.-C., Wu, H.H.., Nataraj, V., Donoghue, H.D., Ridell, M., Watanabe, M., Alderwick, L., Bhatt, A., Besra, G.S., 2015. Pathophysiological Implications of Cell Envelope Structure in Mycobacterium tuberculosis and Related Taxa, in: Ribon, W. (Ed.), Tuberculosis - Expanding Knowledge. InTech. doi:10.5772/58737
Mishra, A.K., Driessen, N.N., Appelmelk, B.J., Besra, G.S., 2011. Lipoarabinomannan and related glycoconjugates: structure, biogenesis and role in Mycobacterium tuberculosis physiology and host-pathogen interaction. FEMS Microbiol. Rev. 35, 1126–57. doi:10.1111/j.1574-6976.2011.00276.x
Mishra, B.B., Moura-Alves, P., Sonawane, A., Hacohen, N., Griffiths, G., Moita, L.F., Anes, E., 2010. Mycobacterium tuberculosis protein ESAT-6 is a potent activator of the NLRP3/ASC inflammasome. Cell. Microbiol. 12, 1046–1063. doi:10.1111/j.1462-5822.2010.01450.x
Monin, L., Khader, S.A., 2014. Chemokines in tuberculosis: The good, the bad and the ugly. Semin. Immunol. 26, 552–558. doi:10.1016/j.smim.2014.09.004
Montanaro, L., Poggi, A., Visai, L., Ravaioli, S., Campoccia, D., Speziale, P., Arciola, C.R., 2011. Extracellular DNA in biofilms. Int. J. Artif. Organs 34, 824–31. doi:10.5301/ijao.5000051
Morrison, J., Pai, M., Hopewell, P.C., 2008. Tuberculosis and latent tuberculosis infection in close contacts of people with pulmonary tuberculosis in low-income and middle-income countries: a systematic review and meta-analysis. Lancet Infect. Dis. 8, 359–368. doi:10.1016/S1473-3099(08)70071-9
Mouritsen, O.G., Zuckermann, M.J., 2004. What's so special about cholesterol? Lipids 39, 1101–1113. doi:10.1007/s11745-004-1336-x
Mukamolova, G. V., Turapov, O., Malkin, J., Woltmann, G., Barer, M.R., 2010. Resuscitation-promoting factors reveal an occult population of tubercle bacilli in sputum. Am. J. Respir. Crit. Care Med. 181, 174–180. doi:10.1164/rccm.200905-0661OC
Mulcahy, H., Charron-Mazenod, L., Lewenza, S., 2008. Extracellular DNA Chelates Cations and Induces Antibiotic Resistance in Pseudomonas aeruginosa Biofilms. PLoS Pathog. 4, e1000213. doi:10.1371/journal.ppat.1000213
Murphy, K.M., 2012. Janeway's Immunobiology, 8th ed. Garland Science, Taylor & Francis Group, LLC.
N'Diaye, E.N., Darzacq, X., Astarie-Dequeker, C., Daffé, M., Calafat, J., Maridonneau-Parini, I., 1998. Fusion of azurophil granules with phagosomes and activation of the tyrosine kinase Hck are specifically inhibited during phagocytosis of mycobacteria by human neutrophils. J. Immunol. 161, 4983–91.
Nagabhushanam, V., Solache, A., Ting, L.-M., Escaron, C.J., Zhang, J.Y., Ernst, J.D., 2003. Innate Inhibition of Adaptive Immunity: Mycobacterium tuberculosis-Induced IL-6 Inhibits Macrophage Responses to IFN- . J. Immunol. 171, 4750–4757. doi:10.4049/jimmunol.171.9.4750
Naranjo, V., Ayoubi, P., Vicente, J., Ruiz-Fons, F., Gortazar, C., Kocan, K.M., de la Fuente, J., 2006a. Characterization of selected genes upregulated in non-tuberculous European wild boar as possible correlates of resistance to Mycobacterium bovis infection. Vet. Microbiol. 116, 224–231. doi:10.1016/j.vetmic.2006.03.013

Naranjo, V., Höfle, U., Vicente, J., Martín, M.P., Ruiz-Fons, F., Gortazar, C., Kocan, K.M., De La Fuente, J., 2006b. Genes differentially expressed in oropharyngeal tonsils and mandibular lymph nodes of tuberculous and nontuberculous European wild boars naturally exposed to Mycobacterium bovis. FEMS Immunol. Med. Microbiol. 46, 298–312. doi:10.1111/j.1574-695X.2005.00035.x

Nelson, B.H., 2004. IL-2, Regulatory T Cells, and Tolerance. J. Immunol. 172, 3983–3988. doi:10.4049/jimmunol.172.7.3983

Nguyen, H.T., Wolff, K.A., Cartabuke, R.H., Ogwang, S., Nguyen, L., 2010. A lipoprotein modulates activity of the MtrAB two-component system to provide intrinsic multidrug resistance, cytokinetic control and cell wall homeostasis in Mycobacterium. Mol. Microbiol. 76, 348–64. doi:10.1111/j.1365-2958.2010.07110.x

Nielsen, P.H., Jahn, A., 1999. Extraction of EPS. Microb. Extracell. Polym. Subst. Charact. Struct. Funct. 69, 49–72. doi:10.1007/978-3-642-60147-7

Nilsson, U.R., Nilsson, B., 1984. Simplified assays of hemolytic activity of the classical and alternative complement pathways. J. Immunol. Methods 72, 49–59.

Nordenfelt, P., Waldemarson, S., Linder, A., Mörgelin, M., Karlsson, C., Malmström, J., Björck, L., 2012. Antibody orientation at bacterial surfaces is related to invasive infection. J. Exp. Med. 209, 2367–81. doi:10.1084/jem.20120325

O'Garra, A., Redford, P.S., McNab, F.W., Bloom, C.I., Wilkinson, R.J., Berry, M.P.R., 2013. The immune response in tuberculosis. Annu. Rev. Immunol. 31, 475–527. doi:10.1146/annurev-immunol-032712-095939

Ohno, N., 2012. Detrimental Effects of β (1-3),(1-6)-D-Glucans, in: Biology and Chemistry of Beta Glucan. BENTHAM SCIENCE PUBLISHERS, pp. 68–81. doi:10.2174/978160805210311101010068

Ojha, A., Anand, M., Bhatt, A., Kremer, L., Jacobs, W.R., Hatfull, G.F., 2005. GroEL1: a dedicated chaperone involved in mycolic acid biosynthesis during biofilm formation in mycobacteria. Cell 123, 861–73. doi:10.1016/j.cell.2005.09.012

Ojha, A., Hatfull, G., 2012. Biofilms of Mycobacterium tuberculosis: New Perspectives of an Old Pathogen, in: Cardona, D.P.-J. (Ed.), Understanding Tuberculosis - Deciphering the Secret Life of the Bacill. InTech, pp. 182–192. doi:10.5772/30303

Ojha, A.K., Baughn, A.D., Sambandan, D., Hsu, T., Trivelli, X., Guerardel, Y., Alahari, A., Kremer, L., Jacobs, W.R., Hatfull, G.F., 2008. Growth of Mycobacterium tuberculosis biofilms containing free mycolic acids and harbouring drug-tolerant bacteria. Mol. Microbiol. 69, 164–74. doi:10.1111/j.1365-2958.2008.06274.x

Ojha, A.K., Trivelli, X., Guerardel, Y., Kremer, L., Hatfull, G.F., 2010. Enzymatic hydrolysis of trehalose dimycolate releases free mycolic acids during mycobacterial growth in biofilms. J. Biol. Chem. 285, 17380–9. doi:10.1074/jbc.M110.112813

Orme, I.M., Robinson, R.T., Cooper, A.M., 2014. The balance between protective and pathogenic immune responses in the TB-infected lung. Nat. Immunol. 16, 57–63. doi:10.1038/ni.3048

Ortalo-Magne, A., Andersen, A.B., Daffe, M., 1996. The outermost capsular arabinomannans and other mannoconjugates of virulent and avirulent tubercle bacilli. Microbiology 142, 927–935. doi:10.1099/00221287-142-4-927

Ortalo-Magné, A., Dupont, M.-A.A., Lemassu, A., Andersen, A.B., Gounon, P., Mamadou, D., Ortalo-Magné, A., Dupont, M.-A.A., Lemassu, A., Andersen, A.B., Gounon, P., Daffé, M., Ortalo-Magne, A., Mamadou, D., 1995. Molecular composition of the outermost capsular material of the tubercle bacillus. Microbiology 141 ( Pt 7, 1609–20. doi:10.1099/13500872-141-7-1609

Pai, M., Behr, M.A., Dowdy, D.W., Dheda, K., Divangahi, M., Boehme, C.C., Ginsberg, A., Swaminathan, S., Spigelman, M., Getahun, H., Menzies, D., Raviglione, M., Barry,

C.E., Esmail, H., Barry, C.E., Young, D.B., Wilkinson, R.J., Marais, B.J., Dye, C., Swaminathan, S., Rekha, B., Havlir, D. V., Getahun, H., Sanne, I., Nunn, P., Getahun, H., Ford, N., Lonnroth, K., Jeon, C.Y., Murray, M.B., Rehm, J., Bates, M.N., Leth, F. van, Werf, M.J. van der, Borgdorff, M.W., Onozaki, I., Tiemersma, E.W., Werf, M.J. van der, Borgdorff, M.W., Williams, B.G., Nagelkerke, N.J., Vynnycky, E., Fine, P.E., Andrews, J.R., Hoa, N.B., Dowdy, D.W., Basu, S., Andrews, J.R., Lienhardt, C., Wang, L., Zhao, Y., Udwadia, Z.F., Amale, R.A., Ajbani, K.K., Rodrigues, C., Jenkins, H.E., Zelner, J.L., Kendall, E.A., Fofana, M.O., Dowdy, D.W., Dowdy, D.W., Golub, J.E., Chaisson, R.E., Saraceni, V., Firdessa, R., Reed, M.B., Bos, K.I., Comas, I., Warner, D.F., Koch, A., Mizrahi, V., Reed, M.B., Gagneux, S., Albanna, A.S., Fenner, L., Lee, R.S., Behr, M.A., Lewis, K.N., Mahairas, G.G., Sabo, P.J., Hickey, M.J., Singh, D.C., Stover, C.K., Abdallah, A.M., Simeone, R., Pai, M., Arend, S.M., Wang, J., Morrison, J., Pai, M., Hopewell, P.C., Cobat, A., Rangaka, M.X., Orme, I.M., Robinson, R.T., Cooper, A.M., Watford, W.T., Wright, J.R., Hester, C.G., Jiang, H., Frank, M.M., Ferguson, J.S., Voelker, D.R., McCormack, F.X., Schlesinger, L.S., Russell, D.G., Houben, D., Wel, N. van der, Simeone, R., Majlessi, L., Enninga, J., Brosch, R., Russell, D.G., Manca, C., Mayer-Barber, K.D., Stanley, S.A., Johndrow, J.E., Manzanillo, P.S., Cox, J.S., Pandey, A.K., Manzanillo, P.S., Shiloh, M.U., Portnoy, D.A., Cox, J.S., Kaufmann, S.H., Dorhoi, A., Schaible, U.E., Behar, S.M., Divangahi, M., Remold, H.G., Divangahi, M., King, I.L., Pernet, E., Janssen, W.J., Wolf, A.J., Samstein, M., Chackerian, A.A., Alt, J.M., Perera, T. V., Dascher, C.C., Behar, S.M., Sonnenberg, P., Lazar-Molnar, E., Barber, D.L., Mayer-Barber, K.D., Feng, C.G., Sharpe, A.H., Sher, A., Lin, P.L., Antonelli, L.R., Marakalala, M.J., Comas, I., Corbett, E.L., Marston, B., Churchyard, G.J., Cock, K.M. De, Tameris, M.D., Abel, L., El-Baghdadi, J., Bousfiha, A.A., Casanova, J.L., Schurr, E., Tobin, D.M., Lalvani, A., Behr, M.A., Sridhar, S., Thwaites, G.E., Bustamante, J., Boisson-Dupuis, S., Abel, L., Casanova, J.L., Daniels, M., Hill, A.B., Nebenzahl-Guimaraes, H., Jacobson, K.R., Farhat, M.R., Murray, M.B., Solomon, H., Pankhurst, L.J., Walker, T.M., Bradley, P., Dominguez, J., Menzies, D., Gardiner, G., Farhat, M.R., Greenaway, C., Pai, M., Farhat, M.R., Greenaway, C., Pai, M., Menzies, D., Pai, M., Sotgiu, G., Pai, M., Riley, L.W., Colford, J.M., Sorensen, A.L., Nagai, S., Houen, G., Andersen, P., Andersen, A.B., Andersen, P., Munk, M.E., Pollock, J.M., Doherty, T.M., Sester, M., Pande, T., Pai, M., Khan, F.A., Denkinger, C.M., Esmail, H., Kik, S. V., Denkinger, C.M., Chedore, P., Pai, M., Albert, H., Steingart, K.R., Boehme, C.C., Boehme, C.C., Detjen, A.K., Getahun, H., Harrington, M., O'Brien, R., Nunn, P., Peter, J.G., Swaminathan, S., Ramachandran, G., Raizada, N., Sachdeva, K.S., Sachdeva, K.S., Theron, G., Churchyard, G.J., Pai, M., Schito, M., Denkinger, C.M., Kik, S. V., Pai, M., Denkinger, C.M., Nicolau, I., Ramsay, A., Chedore, P., Pai, M., Creswell, J., Raizada, N., Wells, W.A., Sweeney, T.E., Braviak, L., Tato, C.M., Khatri, P., Berry, M.P., Xie, H., Gardiner, J.L., Karp, C.L., Zwerling, A., Mangtani, P., Roy, A., Trunz, B.B., Fine, P.E., Dye, C., Barreto, M.L., Abubakar, I., Ellis, R.D., Knight, G.M., Landry, J., Menzies, D., Nahid, P., Saukkonen, J.J., Volmink, J., Garner, P., O'Donnell, M.R., Dheda, K., Barry, C.E., Maartens, G., Dheda, K., Fox, G.J., Calligaro, G.L., Moodley, L., Symons, G., Dheda, K., Pietersen, E., Udwadia, Z.F., Alsultan, A., Peloquin, C.A., Jindani, A., Dorman, S.E., Gillespie, S.H., Merle, C.S., Lee, M., Tiberi, S., Cox, E., Laessig, K., Zumla, A., Andries, K., Matsumoto, M., Brigden, G., Getahun, H., Gunneberg, C., Granich, R., Nunn, P., Suthar, A.B., Samandari, T., Lawn, S.D., Myer, L., Edwards, D., Bekker, L.G., Wood, R., Gupta, R.K., Lawn, S.D., Getahun, H., Getahun, H., Chaisson, R.E., Raviglione, M., Denkinger, C.M., Havlir, D. V., Blanc, F.X., Karim, S.S.A., Manosuthi, W., Mfinanga, S.G., Uthman, O.A., Yan, S., Torok, M.E., Dodd, P.J., Gardiner, E., Coghlan, R., Seddon,

J.A., Dodd, P.J., Sismanidis, C., Seddon, J.A., Perez-Velez, C.M., Marais, B.J., Bauer, M., Leavens, A., Schwartzman, K., Singla, N., Singla, R., Fernandes, S., Behera, D., Dheda, K., Das, J., Satyanarayana, S., McDowell, A., Pai, M., Satyanarayana, S., Wells, W.A., Uplekar, M., Pai, M., Dowdy, D.W., Azman, A.S., Kendall, E.A., Mathema, B., Frieden, T.R., Fujiwara, P.I., Washko, R.M., Hamburg, M.A., Suarez, P.G., Comstock, G.W., Philip, R.N., Uplekar, M., Lienhardt, C., Zak, D.E., Hawn, T.R., Fletcher, H.A., Steingart, K.R., Cruciani, M., Ling, D.I., Zwerling, A., Pai, M., 2016. Tuberculosis. Nat. Rev. Dis. Prim. 2, 16076. doi:10.1038/nrdp.2016.76

Pandey, A.K.A., Sassetti, C.C.M., 2008. Mycobacterial persistence requires the utilization of host cholesterol. Proc. Natl. Acad. Sci. U. S. A. 105, 4376–80. doi:10.1073/pnas.0711159105

Pang, J.M., Layre, E., Sweet, L., Sherrid, A., Moody, D.B., Ojha, A., Sherman, D.R., 2012. The polyketide Pks1 contributes to biofilm formation in Mycobacterium tuberculosis. J. Bacteriol. 194, 715–21. doi:10.1128/JB.06304-11

Parish, T., Stoker, N.N.G., Brown, A.C., 2009. Mycobacteria Protocols, Methods in Molecular Biology. Humana Press, New Jersey. doi:10.1385/0896034712

Pasula, R., Downing, J.F., Wright, J.R., Kachel, D.L., Davis, T.E., Martin, W.J., 1997. Surfactant Protein A (SP-A) Mediates Attachment of *Mycobacterium tuberculosis* to Murine Alveolar Macrophages. Am. J. Respir. Cell Mol. Biol. 17, 209–217. doi:10.1165/ajrcmb.17.2.2469

Pedroza-Roldán, C., Guapillo, C., Barrios-Payán, J., Mata-Espinosa, D., Aceves-Sánchez, M. de J., Marquina-Castillo, B., Hernández-Pando, R., Flores-Valdez, M.A., 2016. The BCGΔBCG1419c strain, which produces more pellicle in vitro, improves control of chronic tuberculosis in vivo. Vaccine 34, 4763–4770. doi:10.1016/j.vaccine.2016.08.035

PHE, 2016. Tuberculosis in England 2016 Report (presenting data to end of 2015). Public Heal. Engl. Version 1., 173.

PHE, 2014. From evidence into action: opportunities to protect and improve the nation's health 1–28. doi:2014404

Pirson, C., Jones, G.J., Steinbach, S., Besra, G.S., Vordermeier, H.M., 2012. Differential effects of Mycobacterium bovis--derived polar and apolar lipid fractions on bovine innate immune cells. Vet. Res. 43, 54. doi:10.1186/1297-9716-43-54

Pitarque, S., Larrouy-Maumus, G., Payré, B., Jackson, M., Puzo, G., Nigou, J., 2008. The immunomodulatory lipoglycans, lipoarabinomannan and lipomannan, are exposed at the mycobacterial cell surface. Tuberculosis (Edinb). 88, 560–5. doi:10.1016/j.tube.2008.04.002

Plovsing, R.R., Berg, R.M.G., Munthe-Fog, L., Konge, L., Iversen, M., Møller, K., Garred, P., 2016. Alveolar recruitment of ficolin-3 in response to acute pulmonary inflammation in humans. Immunobiology 221, 690–697. doi:10.1016/j.imbio.2015.11.015

Poole, R.K., Trivedi, A., Singh, N., Bhat, S.A., Gupta, P., Kumar, A., 2012. Redox Biology of Tuberculosis Pathogenesis, in: Advances in Microbial Physiology. pp. 263–324.

Portevin, D., De Sousa-D'Auria, C., Houssin, C., Grimaldi, C., Chami, M., Daffé, M., Guilhot, C., 2004. A polyketide synthase catalyzes the last condensation step of mycolic acid biosynthesis in mycobacteria and related organisms. Proc. Natl. Acad. Sci. U. S. A. 101, 314–9. doi:10.1073/pnas.0305439101

Powrie, F., Menon, S., Coffman, R.L., 1993. Interleukin-4 and interleukin-10 synergize to inhibit cell-mediated immunityin vivo. Eur. J. Immunol. 23, 3043–3049. doi:10.1002/eji.1830231147

Ramakrishnan, L., 2012. Revisiting the role of the granuloma in tuberculosis. Nat. Rev. Immunol. 12, 352–66. doi:10.1038/nri3211

Ramsugit, S., Guma, S., Pillay, B., Jain, P., Larsen, M.H., Danaviah, S., Pillay, M., 2013. Pili

contribute to biofilm formation in vitro in Mycobacterium tuberculosis. Antonie van …. doi:10.1007/s10482-013-9981-6

Rastogi, S., Singh, A.K., Chandra, G., Kushwaha, P., Pant, G., Singh, K., Mitra, K., Sashidhara, K. V., Krishnan, M.Y., 2017. The diacylglycerol acyltransferase Rv3371 of Mycobacterium tuberculosis is required for growth arrest and involved in stress-induced cell wall alterations. Tuberculosis 104, 8–19. doi:10.1016/j.tube.2017.02.001

Ren, Y., Ding, Q., Zhang, X., 2014. Ficolins and infectious diseases. Virol. Sin. 29, 25–32. doi:10.1007/s12250-014-3421-2

Rifat, D., Bishai, W.R., Karakousis, P.C., 2009. Phosphate Depletion: A Novel Trigger for Mycobacterium tuberculosis Persistence. J. Infect. Dis. 200, 1126–1135. doi:10.1086/605700

Rivas-Santiago, B., Rivas Santiago, C.E., Castañeda-Delgado, J.E., León-Contreras, J.C., Hancock, R.E.W., Hernandez-Pando, R., Dauletbaev, N., Gropp, R., Frye, M., Loitsch, S., Wagner, T.O., Bargon, J., Sarkar, S., Suresh, M.R., Tabarsi, P., Chitsaz, E., Baghaei, P., Shamaei, M., Farnia, P., Marjani, M., al., et, Velayati, A.A., Masjedi, M.R., Farnia, P., Tabarsi, P., Ghanavi, J., Ziazarifi, A.H., al., et, Takiff, H., Guerrero, E., Kalita, A., Verma, I., Khuller, G.K., Hale, J.D., Hancock, R.E., Hancock, R.E., Sahl, H.G., Afacan, N.J., Yeung, A.T., Pena, O.M., Hancock, R.E., Rivas-Santiago, B., Serrano, C.J., Enciso-Moreno, J.A., Yamshchikov, A.V., Kurbatova, E.V., Kumari, M., Blumberg, H.M., Ziegler, T.R., Ray, S.M., al., et, Rivas-Santiago, B., Schwander, S.K., Sarabia, C., Diamond, G., Klein-Patel, M.E., Hernandez-Pando, R., al., et, Rivas-Santiago, C.E., Rivas-Santiago, B., Leon, D.A., Castañeda-Delgado, J., Pando, R.H., Rivas-Santiago, B., Sada, E., Tsutsumi, V., Aguilar-Leon, D., Contreras, J.L., Hernandez-Pando, R., Liu, P.T., Stenger, S., Li, H., Wenzel, L., Tan, B.H., Krutzik, S.R., al., et, Liu, P.T., Stenger, S., Tang, D.H., Modlin, R.L., Hilpert, K., Volkmer-Engert, R., Walter, T., Hancock, R.E., Spindler, E.C., Hale, J.D., Giddings, T.H., Hancock, R.E., Gill, R.T., Dorschner, R.A., Pestonjamasp, V.K., Tamakuwala, S., Ohtake, T., Rudisill, J., Nizet, V., al., et, Zanetti, M., Gennaro, R., Scocchi, M., Skerlavaj, B., Friedrich, C.L., Moyles, D., Beveridge, T.J., Hancock, R.E., Luna-Herrera, J., Martinez-Cabrera, G., Parra-Maldonado, R., Enciso-Moreno, J.A., Torres-Lopez, J., Quesada-Pascual, F., al., et, Rivas-Santiago, B., Contreras, J.C., Sada, E., Hernandez-Pando, R., Castaneda-Delgado, J., Hernandez-Pando, R., Serrano, C.J., Aguilar-Leon, D., Leon-Contreras, J., Rivas-Santiago, C., al., et, Miyakawa, Y., Ratnakar, P., Rao, A.G., Costello, M.L., Mathieu-Costello, O., Lehrer, R.I., al., et, Nizet, V., Ohtake, T., Lauth, X., Trowbridge, J., Rudisill, J., Dorschner, R.A., al., et, Zasloff, M., Sharma, S., Verma, I., Khuller, G.K., Achtman, A.H., Pilat, S., Law, C.W., Lynn, D.J., Janot, L., Mayer, M.L., al., et, 2013. Activity of LL-37, CRAMP and antimicrobial peptide-derived compounds E2, E6 and CP26 against Mycobacterium tuberculosis. Int. J. Antimicrob. Agents 41, 143–8. doi:10.1016/j.ijantimicag.2012.09.015

Rogerson, B.J., Jung, Y.-J., LaCourse, R., Ryan, L., Enright, N., North, R.J., 2006. Expression levels of Mycobacterium tuberculosis antigen-encoding genes versus production levels of antigen-specific T cells during stationary level lung infection in mice. Immunology 118, 195–201. doi:10.1111/j.1365-2567.2006.02355.x

Rose, S.J., Babrak, L.M., Bermudez, L.E., 2015. Mycobacterium avium Possesses Extracellular DNA that Contributes to Biofilm Formation, Structural Integrity, and Tolerance to Antibiotics. PLoS One 10, e0128772. doi:10.1371/journal.pone.0128772

Ruhwald, M., Aabye, M.G., Ravn, P., 2012. IP-10 release assays in the diagnosis of tuberculosis infection: Current status and future directions. Expert Rev. Mol. Diagn. doi:10.1586/erm.11.97

Russell, D.G., Barry, C.E., Flynn, J.L., 2010. Tuberculosis: what we don't know can, and

does, hurt us. Science 328, 852–6. doi:10.1126/science.1184784
Ryan, G.J., Hoff, D.R., Driver, E.R., Voskuil, M.I., Gonzalez-Juarrero, M., Basaraba, R.J., Crick, D.C., Spencer, J.S., Lenaerts, A.J., 2010. Multiple M. tuberculosis phenotypes in mouse and guinea pig lung tissue revealed by a dual-staining approach. PLoS One 5, e11108. doi:10.1371/journal.pone.0011108
Ryan, G.J., Shapiro, H.M., Lenaerts, A.J., 2014. Improving acid-fast fluorescent staining for the detection of mycobacteria using a new nucleic acid staining approach. Tuberculosis 94, 511–518. doi:10.1016/j.tube.2014.07.004
Sabio y García, C.A., Yokobori, N., Basile, J.I., Balboa, L., González, A., López, B., Ritacco, V., Barrera, S. de la, Sasiain, M. del C., 2017. C5aR contributes to the weak Th1 profile induced by an outbreak strain of Mycobacterium tuberculosis. Tuberculosis 103, 16–23. doi:10.1016/j.tube.2016.12.005
Sada-Ovalle, I., Chiba, A., Gonzales, A., Brenner, M.B., Behar, S.M., 2008. Innate Invariant NKT Cells Recognize Mycobacterium tuberculosis–Infected Macrophages, Produce Interferon-γ, and Kill Intracellular Bacteria. PLoS Pathog. 4, e1000239. doi:10.1371/journal.ppat.1000239
Saeed, W., 2012. Cavitating pulmonary tuberculosis: a global challenge. Clin. Med. (Northfield. Il). 12, 40–41. doi:10.7861/clinmedicine.12-1-40
Salina, E.G., Waddell, S.J., Hoffmann, N., Rosenkrands, I., Butcher, P.D., Kaprelyants, A.S., 2014. Potassium availability triggers Mycobacterium tuberculosis transition to, and resuscitation from, non-culturable (dormant) states. Open Biol. 4. doi:10.1098/rsob.140106
Sambandan, D., Dao, D.D.N., Weinrick, B.B.C., Vilchèze, C., Gurcha, S.S., Ojha, A., Kremer, L., Besra, G.S., Hatfull, G.F., Jacobs, W.R., 2013. Keto-Mycolic Acid-Dependent Pellicle Formation Confers Tolerance to Drug-Sensitive Mycobacterium tuberculosis. MBio 4, e00222-13. doi:10.1128/mBio.00222-13.Editor
Sani, M., Houben, E.N.G., Geurtsen, J., Pierson, J., de Punder, K., van Zon, M., Wever, B., Piersma, S.R., Jiménez, C.R., Daffé, M., Appelmelk, B.J., Bitter, W., van der Wel, N., Peters, P.J., 2010. Direct visualization by cryo-EM of the mycobacterial capsular layer: a labile structure containing ESX-1-secreted proteins. PLoS Pathog. 6, e1000794. doi:10.1371/journal.ppat.1000794
Santi, I., Dhar, N., Bousbaine, D., Wakamoto, Y., McKinney, J.D., Jakimowicz, D., 2013. Single-cell dynamics of the chromosome replication and cell division cycles in mycobacteria. Nat. Commun. 4, 2470. doi:10.1038/ncomms3470
Saraav, I., Singh, S., Sharma, S., 2014. Outcome of Mycobacterium tuberculosis and Toll-like receptor interaction: immune response or immune evasion? Immunol. Cell Biol. 92, 1–6. doi:10.1038/icb.2014.52
Sauton, B., 1912. Sur la nutrition minirale du bacille tuberculeux. Comptes Rendus Lebdomadaires des Sci. L′Academie des Sci. 92, 85–93.
Schindelin, J., Arganda-Carreras, I., Frise, E., Kaynig, V., Longair, M., Pietzsch, T., Preibisch, S., Rueden, C., Saalfeld, S., Schmid, B., Tinevez, J.-Y., White, D.J., Hartenstein, V., Eliceiri, K., Tomancak, P., Cardona, A., 2012. Fiji: an open-source platform for biological-image analysis. Nat. Methods 9, 676–82. doi:10.1038/nmeth.2019
Schlesinger, L.S., 1996. Entry of Mycobacterium tuberculosis into Mononuclear Phagocytes. Springer Berlin Heidelberg, pp. 71–96. doi:10.1007/978-3-642-80166-2_4
Schlesinger, L.S., 1993. Macrophage phagocytosis of virulent but not attenuated strains of Mycobacterium tuberculosis is mediated by mannose receptors in addition to complement receptors. J. Immunol. 150, 2920–30.
Schlesinger, L.S., Bellinger-Kawahara, C.G., Payne, N.R., Horwitz, M.A., 1990.

Phagocytosis of Mycobacterium tuberculosis is mediated by human monocyte complement receptors and complement component C3. J. Immunol. 144, 2771–80.
Schneider, B.E., Korbel, D., Hagens, K., Koch, M., Raupach, B., Enders, J., Kaufmann, S.H.E., Mittrücker, H.-W., Schaible, U.E., 2010. A role for IL-18 in protective immunity against Mycobacterium tuberculosis. Eur. J. Immunol. 40, 396–405. doi:10.1002/eji.200939583
Schoenen, H., Bodendorfer, B., Hitchens, K., Manzanero, S., Werninghaus, K., Nimmerjahn, F., Agger, E.M., Stenger, S., Andersen, P., Ruland, J., Brown, G.D., Wells, C., Lang, R., 2010. Cutting Edge: Mincle Is Essential for Recognition and Adjuvanticity of the Mycobacterial Cord Factor and its Synthetic Analog Trehalose-Dibehenate. J. Immunol. 184, 2756–2760. doi:10.4049/jimmunol.0904013
Schorey, J.S., Carroll, M.C., Brown, E.J., 1997. A macrophage invasion mechanism of pathogenic mycobacteria. Science 277, 1091–1093. doi:10.1126/science.277.5329.1091
Schwebach, J.R., Glatman-Freedman, A., Gunther-Cummins, L., Dai, Z., Robbins, J.B., Schneerson, R., Casadevall, A., 2002. Glucan is a component of the Mycobacterium tuberculosis surface that is expressed in vitro and in vivo. Infect. … 70, 2566–2575. doi:10.1128/IAI.70.5.2566
Seder, R.A., Paul, W.E., Ben-Sasson, S.Z., Legros, G.S., Plaut, M., Ben-Sasson, S.Z., Kagey-Sobotka, A., Plaut, M., Finkelman, F.D., Pierce, J.H., 1991. Production of interleukin-4 and other cytokines following stimulation of mast cell lines and in vivo mast cells/basophils. Int. Arch. Allergy Immunol. 94, 137–140. doi:10.1159/000235345
Senbagavalli, P., Geetha, S.T., Venkatesan, P., Ramanathan, V.D., 2009. Defective solubilization of immune complexes and activation of the complement system in patients with pulmonary tuberculosis. J. Clin. Immunol. 29, 674–680. doi:10.1007/s10875-009-9301-0
Sharifabadi, A.R., Hassanshahi, G., Ghalebi, S.R., Arababadi, M.K., Khorramdelazad, H., Zainodini, N., Shabani, Z., 2014. All eotaxins CCL11, CCL24 and CCL26 are increased but to various extents in pulmonary tuberculosis patients. Clin. Lab. 60, 93–97. doi:10.7754/Clin.Lab.2013.121231
Shibuya, N., Goldstein, I.J., Van Damme, E.J., Peumans, W.J., 1988. Binding properties of a mannose-specific lectin from the snowdrop (Galanthus nivalis) bulb. J. Biol. Chem. 263, 728–34.
Shimamura, M., 2008. Non-reducing end ??-mannosylated glycolipids as potent activators for invariant V??19 TCR-bearing natural killer T cells. Carbohydr. Res. doi:10.1016/j.carres.2008.04.001
Shooshtari, P., Fortuno, E.S., Blimkie, D., Yu, M., Gupta, A., Kollmann, T.R., Brinkman, R.R., Brinkman, R.R., 2010. Correlation analysis of intracellular and secreted cytokines via the generalized integrated mean fluorescence intensity. Cytometry. A 77, 873–80. doi:10.1002/cyto.a.20943
Sidobre, S., Nigou, J., Puzo, G., Rivière, M., 2000. Lipoglycans are putative ligands for the human pulmonary surfactant protein A attachment to mycobacteria. Critical role of the lipids for lectin-carbohydrate recognition. J. Biol. Chem. 275, 2415–22. doi:10.1074/JBC.275.4.2415
Sieling, P., Chatterjee, D., Porcelli, S., Prigozy, T., Mazzaccaro, R., Soriano, T., Bloom, B., Brenner, M., Kronenberg, M., Brennan, P., Et, A., 1995. CD1-restricted T cell recognition of microbial lipoglycan antigens. Science (80-. ). 269, 227–30.
Simeone, R., Bobard, A., Lippmann, J., Bitter, W., Majlessi, L., Brosch, R., Enninga, J., 2012. Phagosomal rupture by Mycobacterium tuberculosis results in toxicity and host cell death. PLoS Pathog. 8, e1002507. doi:10.1371/journal.ppat.1002507
Simmons, W.L., Dybvig, K., 2007. Biofilms protect Mycoplasma pulmonis cells from lytic

effects of complement and gramicidin. Infect. Immun. 75, 3696–9. doi:10.1128/IAI.00440-07
Singh, B., Chitra, J., Selvaraj, P., 2014. CCL2, CCL3 and CCL4 gene polymorphisms in pulmonary tuberculosis patients of South India. Int. J. Immunogenet. 41, 98–104. doi:10.1111/iji.12085
Singh, P., Goyal, A., 2013. Interleukin-6: a potent biomarker of mycobacterial infection. Springerplus 2, 686. doi:10.1186/2193-1801-2-686
Singh, P.K., Jia, H.P., Wiles, K., Hesselberth, J., Liu, L., Conway, B.A., Greenberg, E.P., Valore, E. V, Welsh, M.J., Ganz, T., Tack, B.F., McCray, P.B., Jr., 1998. Production of beta-defensins by human airway epithelia. Proc. Natl. Acad. Sci. U. S. A. 95, 14961–6.
Sochorová, Z., Petr Ačkova, D., Sitařova, B., Buriánková, K., Bezouškova, S., Benada, O., Kofroňova, O., Janeček, J., Halada, P., Weiser, J., 2014. Morphological and proteomic analysis of early stage air-liquid interface biofilm formation in Mycobacterium smegmatis. Microbiology mic.0.076174-0-. doi:10.1099/mic.0.076174-0
Sonawane, A., Santos, J.C., Mishra, B.B., Jena, P., Progida, C., Sorensen, O.E., Gallo, R., Appelberg, R., Griffiths, G., 2011. Cathelicidin is involved in the intracellular killing of mycobacteria in macrophages. Cell. Microbiol. 13, 1601–1617. doi:10.1111/j.1462-5822.2011.01644.x
Stevenson, C., Marshall, L., Morgan, D., 2006. Antimicrobial Peptides and Innate Immunity, Researchgate.Net. doi:10.1007/978-3-0348-0541-4
Stewart, P.S., Franklin, M.J., 2008. Physiological heterogeneity in biofilms. Nat. Rev. Microbiol. 6, 199–210. doi:10.1038/nrmicro1838
Stokes, R.W., Norris-Jones, R., Brooks, D.E., Beveridge, T.J., Doxsee, D., Thorson, L.M., 2004. The glycan-rich outer layer of the cell wall of Mycobacterium tuberculosis acts as an antiphagocytic capsule limiting the association of the bacterium with macrophages. Infect. Immun. 72, 5676–5686. doi:10.1128/IAI.72.10.5676-5686.2004
Stoodley, P., Nistico, L., Johnson, S., Lasko, L.-A., Baratz, M., Gahlot, V., Ehrlich, G.D., Kathju, S., 2008. Direct demonstration of viable Staphylococcus aureus biofilms in an infected total joint arthroplasty. A case report. J. Bone Joint Surg. Am. 90, 1751–8. doi:10.2106/JBJS.G.00838
Sugawara, I., Yamada, H., Hua, S., Mizuno, S., 2001. Role of Interleukin (IL)-1 Type 1 Receptor in Mycobacterial Infection. Microbiol. Immunol. 45, 743–750. doi:10.1111/j.1348-0421.2001.tb01310.x
Świerzko, A.S., Bartłomiejczyk, M.A., Brzostek, A., Łukasiewicz, J., Michalski, M., Dziadek, J., Cedzyński, M., 2016. Mycobacterial antigen 85 complex (Ag85) as a target for ficolins and mannose-binding lectin. Int. J. Med. Microbiol. 306, 212–221. doi:10.1016/j.ijmm.2016.04.004
Tailleux, L., Pham-Thi, N., Bergeron-Lafaurie, A., Herrmann, J.L., Charles, P., Schwartz, O., Scheinmann, P., Lagrange, P.H., De Blic, J., Tazi, A., Gicquel, B., Neyrolles, O., 2005. DC-SIGN induction in alveolar macrophages defines privileged target host cells for mycobacteria in patients with tuberculosis. PLoS Med. 2, 1269–1279. doi:10.1371/journal.pmed.0020381
Takade, A., Umeda, A., Matsuoka, M., Yoshida, S., Nakamura, M., Amako, K., 2003. Comparative studies of the cell structures of Mycobacterium leprae and M. tuberculosis using the electron microscopy freeze-substitution technique. Microbiol. Immunol. 47, 265–70. doi:10.1111/j.1348-0421.2003.tb03394.x
Technologies, S., 2010. Frequencies of Cell Types in Human Peripeheral Blood [WWW Document]. Poster.
Thurm, C.W., Halsey, J.F., 2005. Measurement of cytokine production using whole blood. Curr. Protoc. Immunol. Chapter 7, Unit 7.18B. doi:10.1002/0471142735.im0718bs66

Tomlin, K.L., Coll, O.P., Ceri, H., 2001. Interspecies biofilms of Pseudomonas aeruginosa and Burkholderia cepacia. Can J Microbiol 47, 949–54. doi:10.1139/w01-095
Torrado, E., Cooper, A.M., 2013. Cytokines in the Balance of Protection and Pathology During Mycobacterial Infections. Springer, New York, NY, pp. 121–140. doi:10.1007/978-1-4614-6111-1_7
Triantafilou, M., Hughes, T.R., Morgan, B.P., Triantafilou, K., 2015. Complementing the inflammasome. Immunology 147, 152–64. doi:10.1111/imm.12556
Trivedi, A., Mavi, P.S., Bhatt, D., Kumar, A., 2016. Thiol reductive stress induces cellulose-anchored biofilm formation in Mycobacterium tuberculosis. Nat. Commun. 7, 11392. doi:10.1038/ncomms11392
Trunz, B.B., Fine, P., Dye, C., 2006. Effect of BCG vaccination on childhood tuberculous meningitis and miliary tuberculosis worldwide: a meta-analysis and assessment of cost-effectiveness. Lancet 367, 1173–1180. doi:10.1016/S0140-6736(06)68507-3
Tsolaki, A.G., 2009. Innate immune recognition in tuberculosis infection. Adv. Exp. Med. Biol. 653, 185–97.
Tzeng, Y.-L., Thomas, J., Stephens, D.S., 2016. Regulation of capsule in Neisseria meningitidis. Crit. Rev. Microbiol. 42, 759–72. doi:10.3109/1040841X.2015.1022507
Underhill, D.M., Goodridge, H.S., 2012. Information processing during phagocytosis. Nat. Rev. Immunol. 12, 492–502. doi:10.1038/nri3244
van Crevel, R., van der Ven-Jongekrijg, J., Netea, M.G., de Lange, W., Kullberg, B.-J., van der Meer, J.W.., 1999. Disease-specific ex vivo stimulation of whole blood for cytokine production: applications in the study of tuberculosis. J. Immunol. Methods 222, 145–153. doi:10.1016/S0022-1759(98)00192-6
van Panhuys, N., Prout, M., Forbes, E., Min, B., Paul, W.E., Le Gros, G., 2011. Basophils Are the Major Producers of IL-4 during Primary Helminth Infection. J. Immunol. 186, 2719–2728. doi:10.4049/jimmunol.1000940
Van Rhijn, I., Nguyen, T.K.A., Michel, A., Cooper, D., Govaerts, M., Cheng, T.-Y., van Eden, W., Moody, D.B., Coetzer, J.A.W., Rutten, V., Koets, A.P., 2009. Low cross-reactivity of T-cell responses against lipids from Mycobacterium bovis and M. avium paratuberculosis during natural infection. Eur. J. Immunol. 39, 3031–41. doi:10.1002/eji.200939619
Van Wyk, N., Drancourt, M., Henrissat, B., Kremer, L., 2017. Current perspectives on the families of glycoside hydrolases of Mycobacterium tuberculosis: Their importance and prospects for assigning function to unknowns. Glycobiology. doi:10.1093/glycob/cww099
Varrot, A., Leydier, S., Pell, G., Macdonald, J.M., Stick, R. V, Henrissat, B., Gilbert, H.J., Davies, G.J., 2005. Mycobacterium tuberculosis strains possess functional cellulases. J. Biol. Chem. 280, 20181–4. doi:10.1074/jbc.C500142200
Vergne, I., Chua, J., Singh, S.B., Deretic, V., 2004a. Cell biology of mycobacterium tuberculosis phagosome. Annu. Rev. Cell Dev. Biol. 20, 367–94. doi:10.1146/annurev.cellbio.20.010403.114015
Vergne, I., Fratti, R.A., Hill, P.J., Chua, J., Belisle, J., Deretic, V., 2004b. Mycobacterium tuberculosis phagosome maturation arrest: mycobacterial phosphatidylinositol analog phosphatidylinositol mannoside stimulates early endosomal fusion. Mol. Biol. Cell 15, 751–60. doi:10.1091/mbc.E03-05-0307
Verschoor, J.A., Baird, M.S., Grooten, J., 2012. Towards understanding the functional diversity of cell wall mycolic acids of Mycobacterium tuberculosis. Prog. Lipid Res. 51, 325–39. doi:10.1016/j.plipres.2012.05.002
Vert, M., Doi, Y., Hellwich, K.-H., Hess, M., Hodge, P., Kubisa, P., Rinaudo, M., Schué, F., 2012. Terminology for biorelated polymers and applications (IUPAC Recommendations

2012). Pure Appl. Chem. 84, 377–410. doi:10.1351/PAC-REC-10-12-04
Vesosky, B., Rottinghaus, E.K., Stromberg, P., Turner, J., Beamer, G., 2010. CCL5 participates in early protection against Mycobacterium tuberculosis. J. Leukoc. Biol. 87, 1153–1165. doi:10.1189/jlb.1109742
Vilcheze, C., Morbidoni, H.R., Weisbrod, T.R., Iwamoto, H., Kuo, M., Sacchettini, J.C., Jacobs, W.R., 2000. Inactivation of the inhA-Encoded Fatty Acid Synthase II (FASII) Enoyl-Acyl Carrier Protein Reductase Induces Accumulation of the FASI End Products and Cell Lysis of Mycobacterium smegmatis. J. Bacteriol. 182, 4059–4067. doi:10.1128/JB.182.14.4059-4067.2000
Vilkas, E., Lederer, E., 1956. Isolation of a phosphatidyl-inosito-di-D-mannoside from a mycobacterial phosphatide. Bull. Soc. Chim. Biol. (Paris). 38, 111–21.
Villeneuve, C., Etienne, G., Abadie, V., Montrozier, H., Bordier, C., Laval, F., Daffe, M., Maridonneau-Parini, I., Astarie-Dequeker, C., 2003. Surface-exposed glycopeptidolipids of Mycobacterium smegmatis specifically inhibit the phagocytosis of mycobacteria by human macrophages. Identification of a novel family of glycopeptidolipids. J. Biol. Chem. 278, 51291–300. doi:10.1074/jbc.M306554200
Wagner, C., Kondella, K., Bernschneider, T., Heppert, V., Wentzensen, A., H??nsch, G.M., 2003. Post-Traumatic Osteomyelitis: Analysis of Inflammatory Cells Recruited into the Site of Infection. Shock 20, 503–510. doi:10.1097/01.shk.0000093542.78705.e3
Walters, M.C., Roe, F., Bugnicourt, A., Franklin, M.J., Stewart, P.S., 2003. Contributions of antibiotic penetration, oxygen limitation, and low metabolic activity to tolerance of Pseudomonas aeruginosa biofilms to ciprofloxacin and tobramycin. Antimicrob. Agents Chemother. 47, 317–23.
Watford, W.T., Ghio, A.J., Wright, J.R., 2000. Complement-mediated host defense in the lung. Am J Physiol Lung Cell Mol Physiol 279, L790-798.
Watford, W.T., Wright, J.R., Hester, C.G., Jiang, H., Frank, M.M., 2001. Surfactant Protein A Regulates Complement Activation. J. Immunol. 167, 6593–6600. doi:10.4049/jimmunol.167.11.6593
Watnick, P., Kolter, R., 2000. Biofilm, City of Microbes. J. Bacteriol. 182, 2675–2679. doi:10.1128/JB.182.10.2675-2679.2000
Wayne, L.L.G.L., Hayes, L.L.G., 1996. An in vitro model for sequential study of shiftdown of Mycobacterium tuberculosis through two stages of nonreplicating persistence. Infect. Immun. 64, 2062–2069. doi:
Weikert, L.F., Lopez, J.P., Abdolrasulnia, R., Chroneos, Z.C., Shepherd, V.L., 2000. Surfactant protein A enhances mycobacterial killing by rat macrophages through a nitric oxide-dependent pathway. Am. J. Physiol. - Lung Cell. Mol. Physiol. 279.
Weis, W.I., Drickamer, K., Hendrickson, W.A., 1992. Structure of a C-type mannose-binding protein complexed with an oligosaccharide. Nature 360, 127–34. doi:10.1038/360127a0
Welin, A., Eklund, D., Stendahl, O., Lerm, M., Adams, L., 2011. Human Macrophages Infected with a High Burden of ESAT-6-Expressing M. tuberculosis Undergo Caspase-1- and Cathepsin B-Independent Necrosis. PLoS One 6, e20302. doi:10.1371/journal.pone.0020302
Welin, A., Winberg, M.E., Abdalla, H., Särndahl, E., Rasmusson, B., Stendahl, O., Lerm, M., 2008. Incorporation of Mycobacterium tuberculosis lipoarabinomannan into macrophage membrane rafts is a prerequisite for the phagosomal maturation block. Infect. Immun. 76, 2882–7. doi:10.1128/IAI.01549-07
Welsh, K.J., Abbott, A.N., Hwang, S.A., Indrigo, J., Armitige, L.Y., Blackburn, M.R., Hunter, R.L., Actor, J.K., 2008. A role for tumour necrosis factor-a, complement C5 and interleukin-6 in the initiation and development of the mycobacterial cord factor trehalose 6,6???-dimycolate induced granulomatous response. Microbiology 154, 1813–1824.

doi:10.1099/mic.0.2008/016923-0
Welsh, K.J., Lewis, C.T., Boyd, S., Braun, M.C., Actor, J.K., 2012. Complement factor C7 contributes to lung immunopathology caused by Mycobacterium tuberculosis. Clin. Dev. Immunol. 2012, 429675. doi:10.1155/2012/429675
Wheeler, P.R., 2009. Analysis of lipid biosynthesis and location. Methods Mol. Biol., Methods in Molecular Biology 465, 61–81. doi:10.1007/978-1-59745-207-6
Wong, K.-W., Jacobs, W.R., Jr, 2013. Mycobacterium tuberculosis exploits human interferon γ to stimulate macrophage extracellular trap formation and necrosis. J. Infect. Dis. 208, 109–19. doi:10.1093/infdis/jit097
Woodworth, J.S., Fortune, S.M., Behar, S.M., 2008. Bacterial protein secretion is required for priming of CD8+ T cells specific for the Mycobacterium tuberculosis antigen CFP10. Infect. Immun. 76, 4199–205. doi:10.1128/IAI.00307-08
Yang, L., Haagensen, J.A.J., Jelsbak, L., Johansen, H.K., Sternberg, C., Høiby, N., Molin, S., 2008. In situ growth rates and biofilm development of Pseudomonas aeruginosa populations in chronic lung infections. J. Bacteriol. 190, 2767–76. doi:10.1128/JB.01581-07
Ye, J., Ortaldo, J.R., Conlon, K., Winkler-Pickett, R., Young, H.A., 1995. Cellular and molecular mechanisms of IFN-gamma production induced by IL-2 and IL-12 in a human NK cell line. J. Leukoc. Biol. 58, 225–33.
Yoshimoto, T., Paul, W.E., 1994. CD4pos, NK1.1pos T cells promptly produce interleukin 4 in response to in vivo challenge with anti-CD3. J. Exp. Med. 179, 1285–95.
Zambrano, M.M., Kolter, R., 2005. Mycobacterial biofilms: a greasy way to hold it together. Cell 123, 762–4. doi:10.1016/j.cell.2005.11.011
Zoubos, A.B., Galanakos, S.P., Soucacos, P.N., 2012. Orthopedics and biofilm--what do we know? A review. Med. Sci. Monit. 18, RA89-96.
Zuber, B., Chami, M., Houssin, C., Dubochet, J., Griffiths, G., Daffé, M., 2008. Direct visualization of the outer membrane of mycobacteria and corynebacteria in their native state. J. Bacteriol. 190, 5672–80. doi:10.1128/JB.01919-07

# 9 APPENDICES

## 9.1 Standard curves of cytokines/chemokines tested in planktonic and biofilm carbohydrate stimulations with whole blood

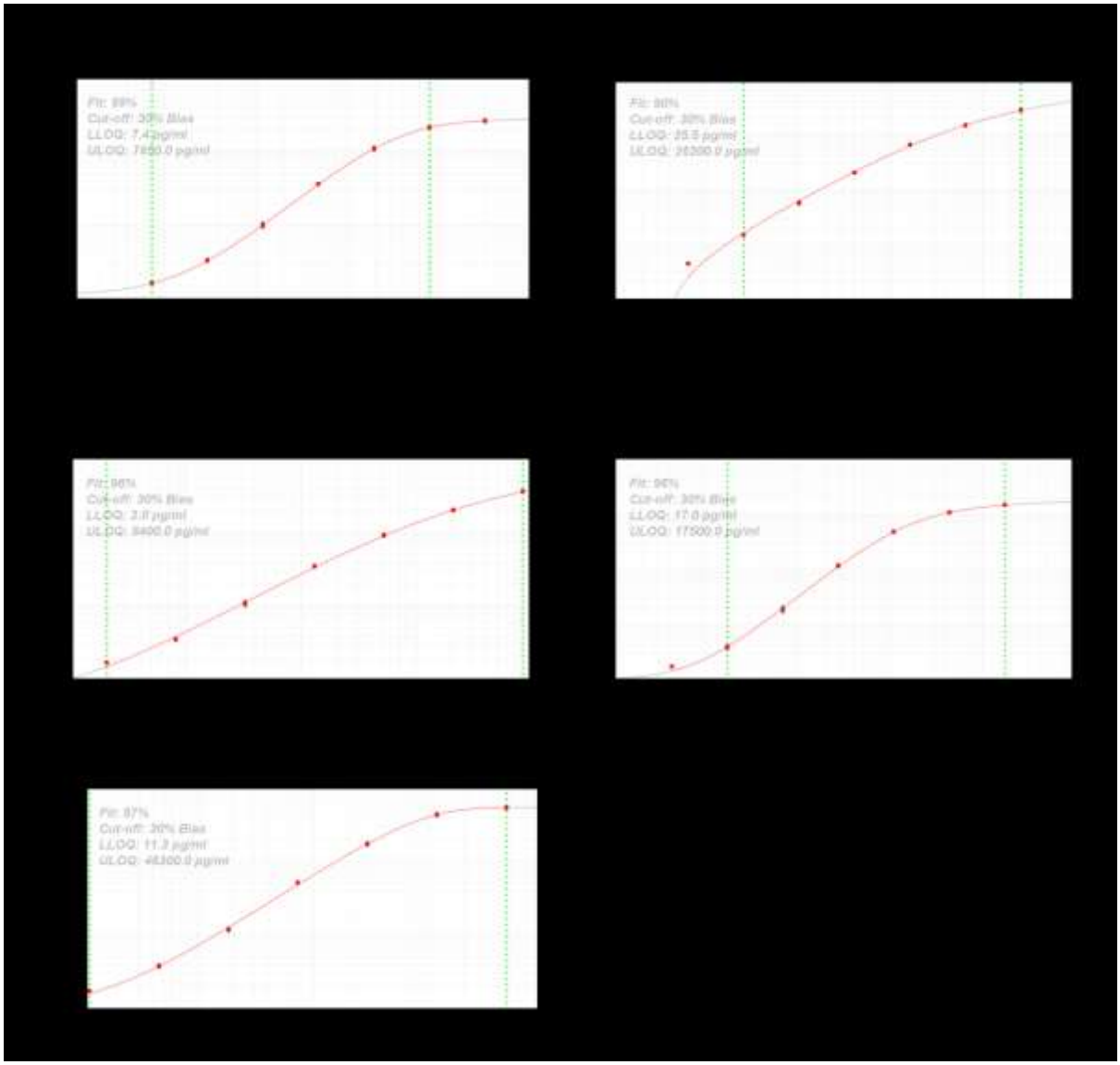

**Figure 9.1.1:** Standard curves of secreted cytokines generated using Procartaplex Th1/Th2 Panel and Procartaplex analyst software. (Affymetrics, eBiosience, USA). 7-point standard curves generated from means of duplicate standard samples, using a 5 parameter logistic fit curve. Green dotted lines show lower limit of quantitation (LLOQ) and upper limit of quantitation (ULOQ) after setting the cut-off at 30% bias (acceptable percentage variation form the ideal standard curve.) (A) IFN-γ, (B) IL-12p70, (C) IL-1b, (D) IL-2, (E) IL-4.

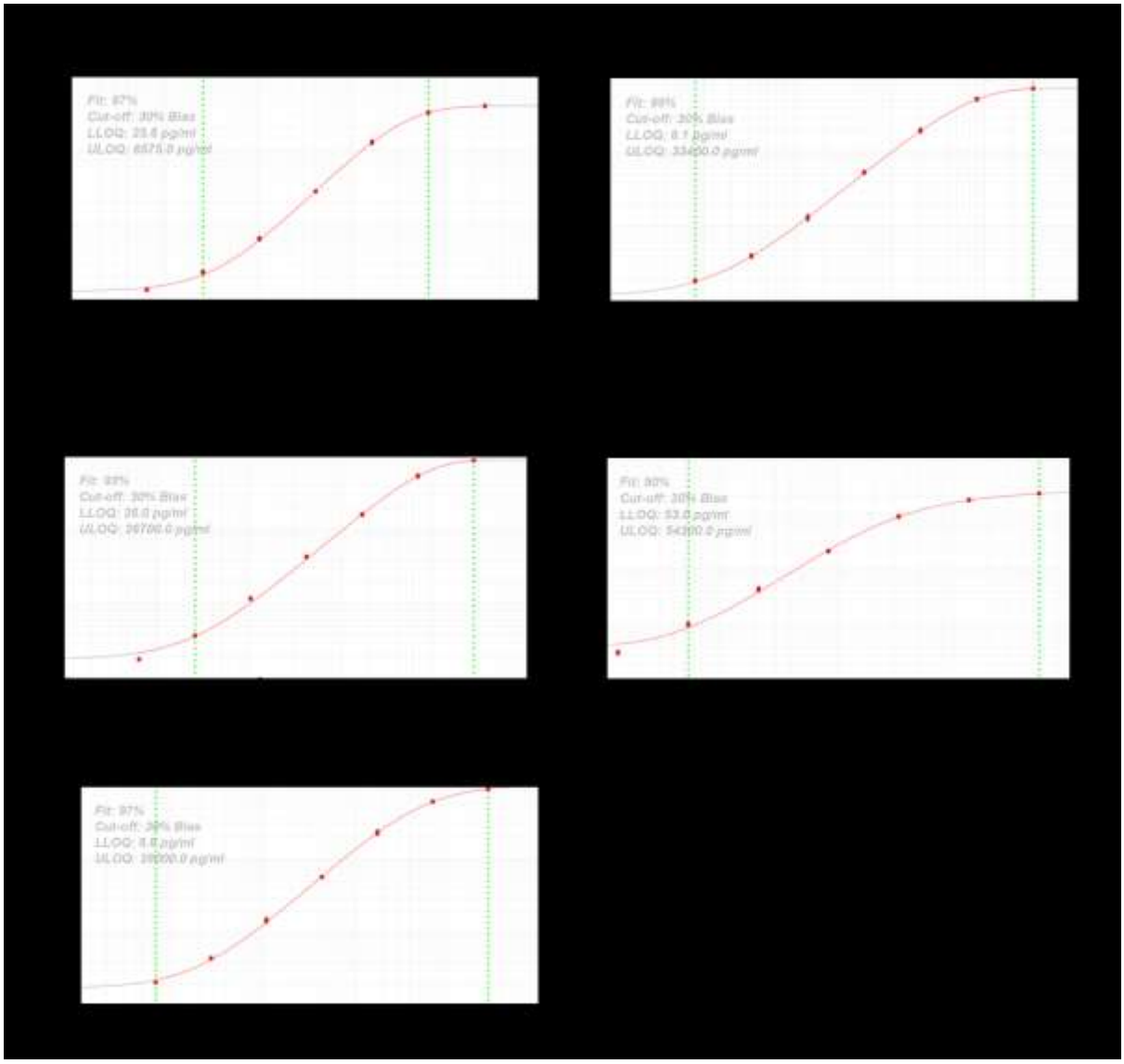

**Figure 9.1.2:** Standard curves of secreted cytokines generated using Procartaplex Th1/Th2 Panel and Procartaplex analyst software. 7-point standard curves generated from means of duplicate standard samples, using a 5 parameter logistic fit curve. Green dotted lines show lower limit of quantitation (LLOQ) and upper limit of quantitation (ULOQ) after setting the cut-off at 30% bias (acceptable percentage variation form the ideal standard curve.) (A) IL-5, (B) IL-6, (C) TNF-α, (D) GM-CSF, (E) IL-18.

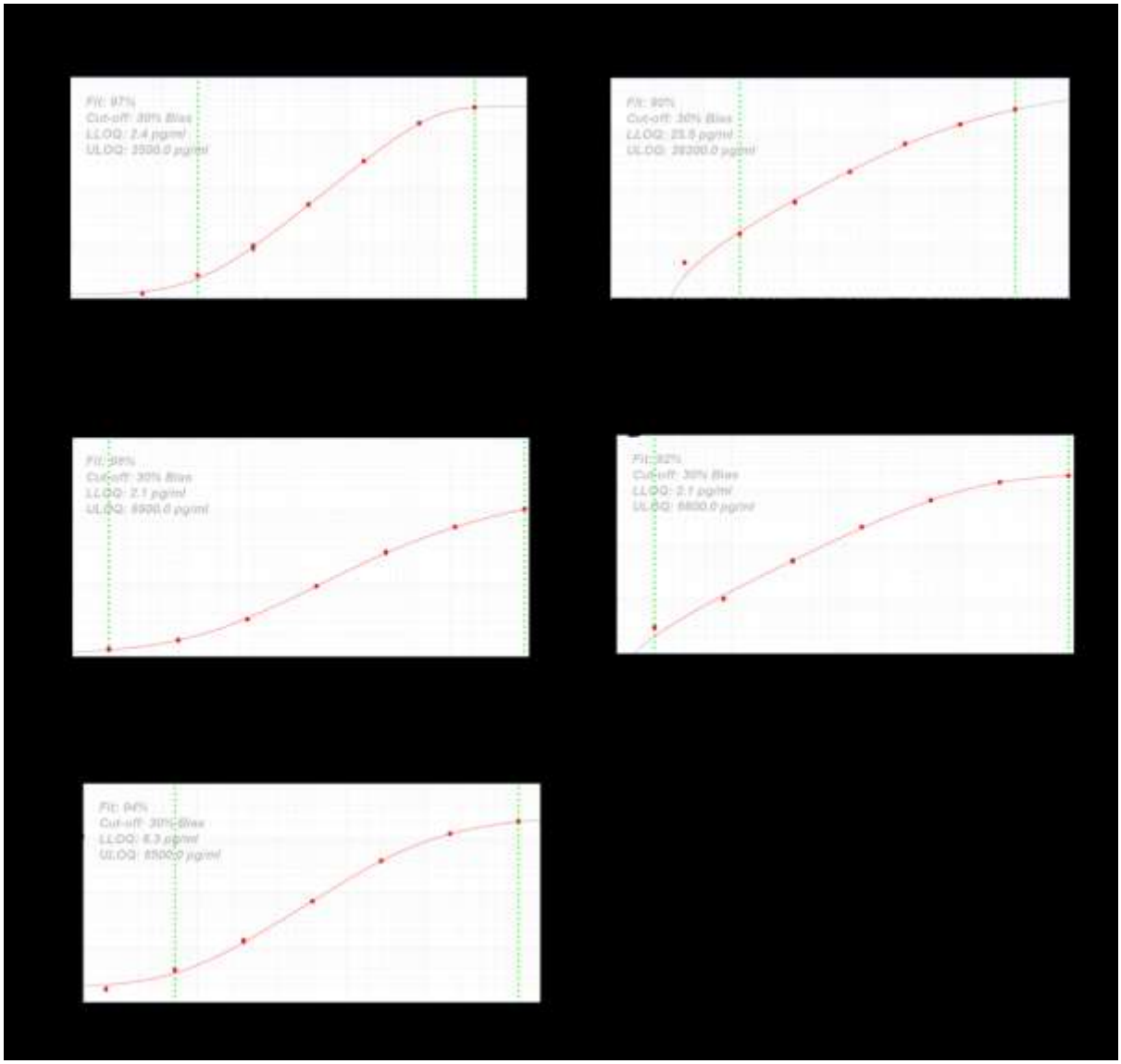

**Figure 9.1.3:** Standard curves of secreted chemokines generated using Procartaplex Th1/Th2 Panel and Procartaplex analyst software. 7-point standard curves generated from means of duplicate standard samples, using a 5 parameter logistic fit curve. Green dotted lines show lower limit of quantitation (LLOQ) and upper limit of quantitation (ULOQ) after setting the cut-off at 30% bias (acceptable percentage variation form the ideal standard curve.) (A) CCL11, (B) CXCL1, (C) CXCL8, (D) CXCL10, (E) CCL2.

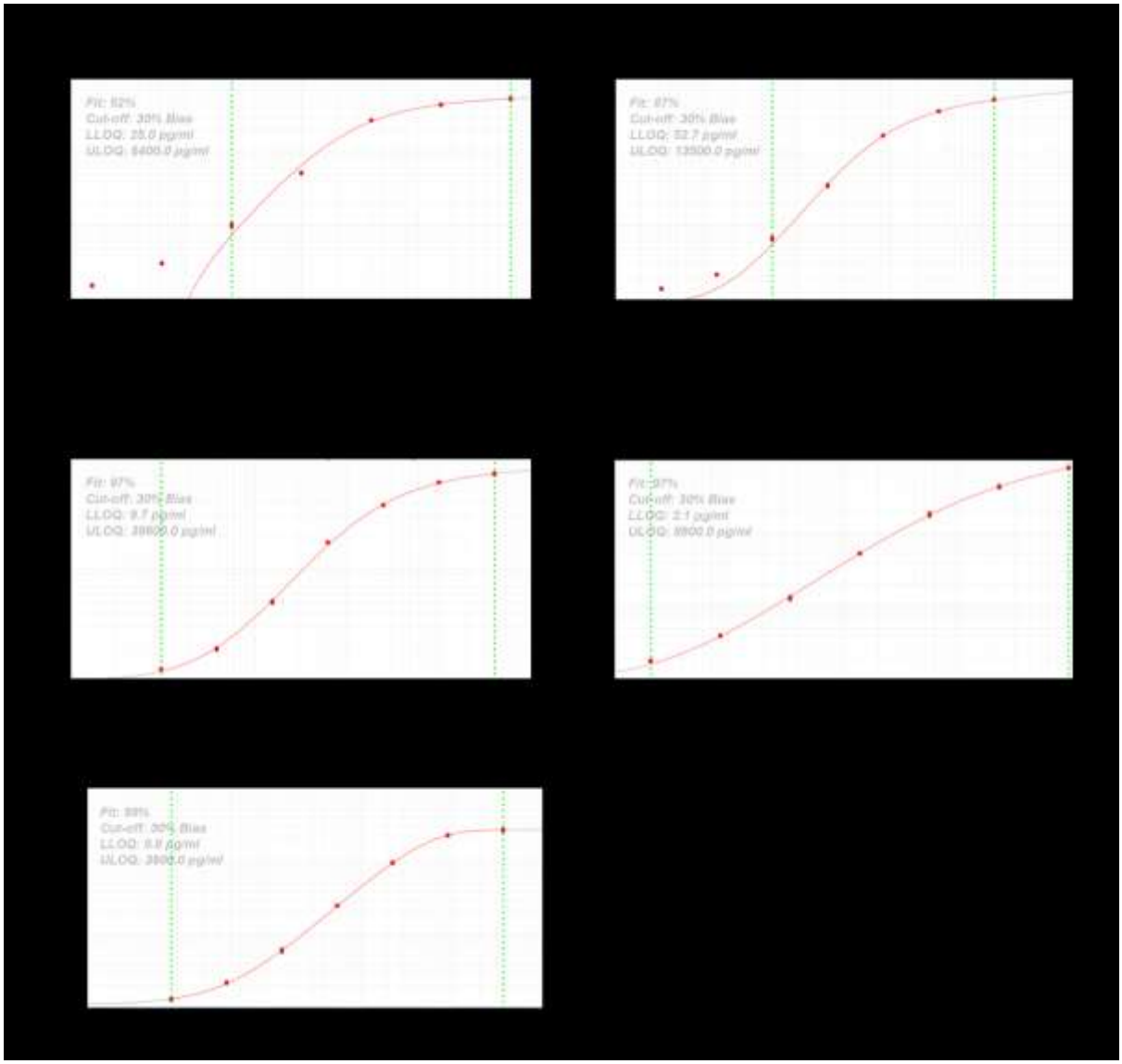

**Figure 9.1.4:** Standard curves of secreted cytokine/chemokines generated using Procartaplex Th1/Th2 Panel and Procartaplex analyst software. 7-point standard curves generated from means of duplicate standard samples, using a 5 parameter logistic fit curve. Green dotted lines show lower limit of quantitation (LLOQ) and upper limit of quantitation (ULOQ) after setting the cut-off at 30% bias (acceptable percentage variation form the ideal standard curve.) (A) CCL3, (B) CCL4, (C) CXCL12α, (D) IL-13, (E) CCL5

## 9.2 Appendix results and figures from planktonic and biofilm carbohydrate stimulations with whole blood

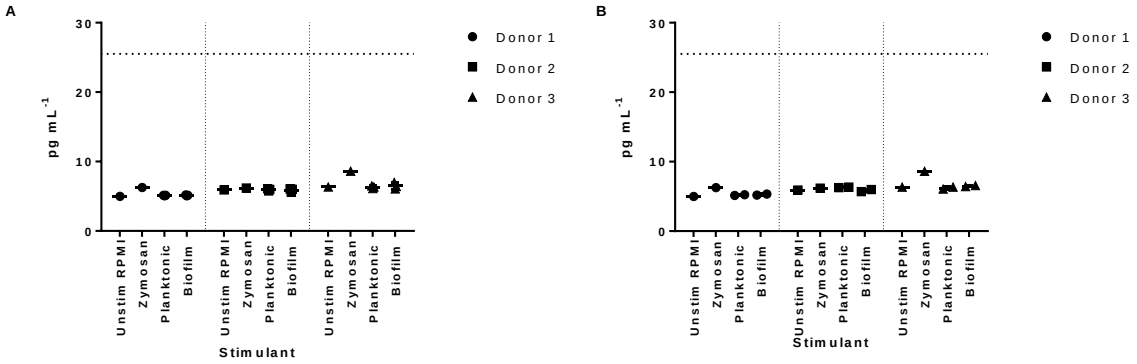


**Figure 9.2.1:** IL-12p70 response in whole blood stimulated with carbohydrate extracts from planktonic and biofilm phenotype *M. tuberculosis*. Total secreted IL-12p70 (A) in whole blood after 24h stimulation with x3 biological replicate planktonic *M. tuberculosis* **carbohydrate extracts (10 µg mL$^{-1}$)** and x3 biological replicate biofilm *M. tuberculosis* **carbohydrate extracts (10 µg mL$^{-1}$)**. Total secreted IL-12p70 (B) in whole blood after 24h stimulation with x2 biological replicate planktonic *M. tuberculosis* **carbohydrate extracts (25 µg mL$^{-1}$)** and x2 biological replicate biofilm *M. tuberculosis* **carbohydrate extracts (25 µg mL$^{-1}$)**. Negative control RPMI response (Unstim RPMI), Positive control Zymosan (10 µg mL$^{-1}$). The horizontal dotted line on each graph represents the lower limit of quantitation. Each donor blood stimulation is presented separately by vertical dotted lines. Error bars = standard deviation.

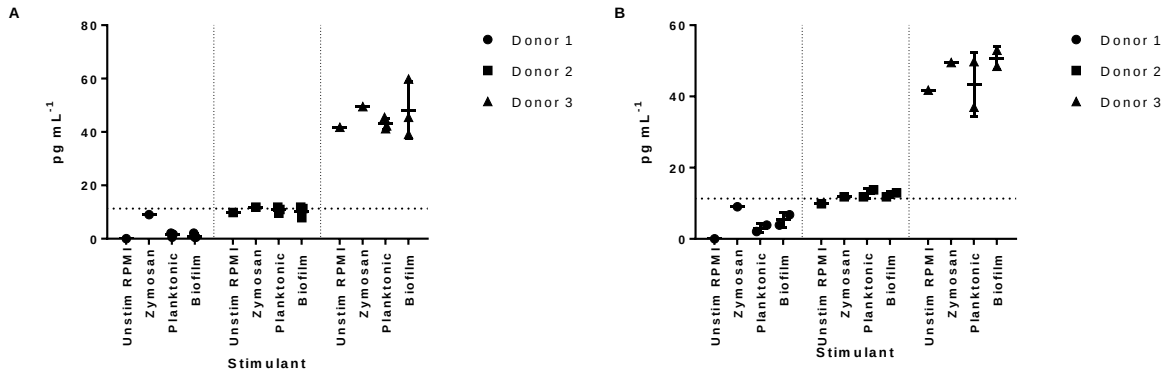


**Figure 9.2.2:** IL-4 response in whole blood stimulated with carbohydrate extracts from planktonic and biofilm phenotype *M. tuberculosis*. Total secreted IL-4 (A) in whole blood after 24h stimulation with x3 biological replicate planktonic *M. tuberculosis* **carbohydrate extracts (10 µg mL$^{-1}$)** and x3 biological replicate biofilm *M. tuberculosis* **carbohydrate extracts (10 µg mL$^{-1}$)**. Total secreted IL-4 (B) in whole blood after 24h stimulation with x2 biological replicate planktonic *M. tuberculosis* **carbohydrate extracts (25 µg mL$^{-1}$)** and x2 biological replicate biofilm *M. tuberculosis* **carbohydrate extracts (25 µg mL$^{-1}$)**. Negative control RPMI response (Unstim RPMI), Positive control Zymosan (10 µg mL$^{-1}$). The horizontal dotted line on each graph represents the lower limit of quantitation. Each donor blood stimulation is presented separately by vertical dotted lines. Error bars = standard deviation.

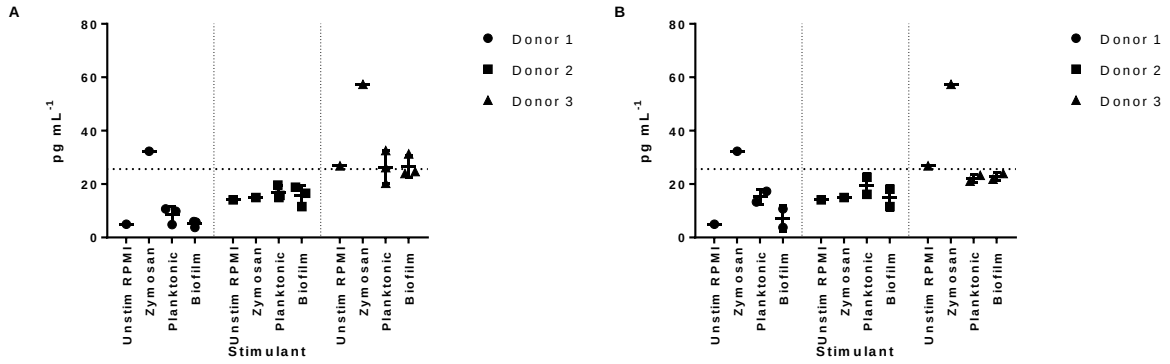


**Figure 9.2.3:** IL-5 response in whole blood stimulated with carbohydrate extracts from planktonic and biofilm phenotype *M. tuberculosis*. Total secreted IL-5 (A) in whole blood after 24h stimulation with x3 biological replicate planktonic *M. tuberculosis* **carbohydrate extracts (10 µg mL$^{-1}$)** and x3 biological replicate biofilm *M. tuberculosis* **carbohydrate extracts (10 µg mL$^{-1}$)**. Total secreted IL-5 (B) in whole blood after 24h stimulation with x2 biological replicate planktonic *M. tuberculosis* **carbohydrate extracts (25 µg mL$^{-1}$)** and x2 biological replicate biofilm *M. tuberculosis* **carbohydrate extracts (25 µg mL$^{-1}$)**. Negative control RPMI response (Unstim RPMI), Positive control Zymosan (10 µg mL$^{-1}$). The horizontal dotted line on each graph represents the lower limit of quantitation. Each donor blood stimulation is presented separately by vertical dotted lines. Error bars = standard deviation.

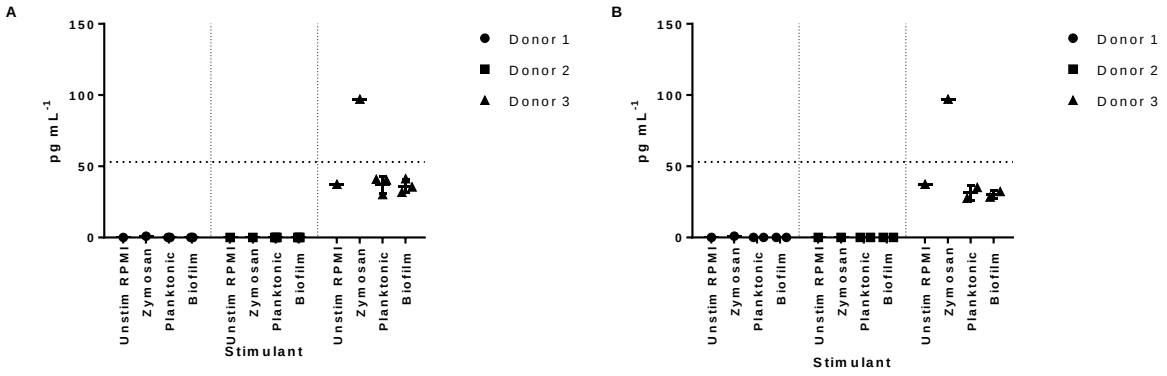


**Figure 9.2.4:** GM-CSF response in whole blood stimulated with carbohydrate extracts from planktonic and biofilm phenotype *M. tuberculosis*. Total secreted GM-CSF (A) in whole blood after 24h stimulation with x3 biological replicate planktonic *M. tuberculosis* **carbohydrate extracts (10 µg mL$^{-1}$)** and x3 biological replicate biofilm *M. tuberculosis* **carbohydrate extracts (10 µg mL$^{-1}$)**. Total secreted GM-CSF (B) in whole blood after 24h stimulation with x2 biological replicate planktonic *M. tuberculosis* **carbohydrate extracts (25 µg mL$^{-1}$)** and x2 biological replicate biofilm *M. tuberculosis* **carbohydrate extracts (25 µg mL$^{-1}$)**. Negative control RPMI response (Unstim RPMI), Positive control Zymosan (10 µg mL$^{-1}$). The horizontal dotted line on each graph represents the lower limit of quantitation. Each donor blood stimulation is presented separately by vertical dotted lines. Error bars = standard deviation.

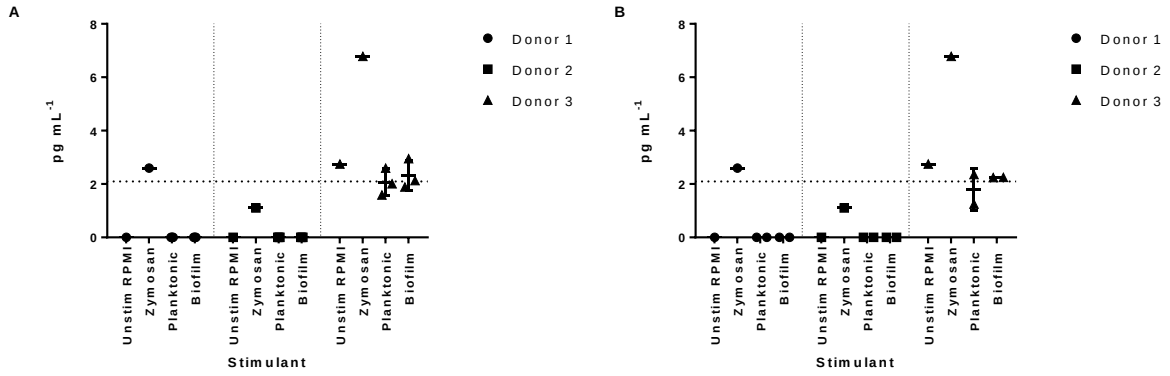


**Figure 9.2.5:** IL-13 response in whole blood stimulated with carbohydrate extracts from planktonic and biofilm phenotype *M. tuberculosis*. Total secreted IL-13 (A) in whole blood after 24h stimulation with x3 biological replicate planktonic *M. tuberculosis* **carbohydrate extracts (10 µg mL$^{-1}$)** and x3 biological replicate biofilm *M. tuberculosis* **carbohydrate extracts (10 µg mL$^{-1}$)**. Total secreted IL-13 (B) in whole blood after 24h stimulation with x2 biological replicate planktonic *M. tuberculosis* **carbohydrate extracts (25 µg mL$^{-1}$)** and x2 biological replicate biofilm *M. tuberculosis* **carbohydrate extracts (25 µg mL$^{-1}$)**. Negative control RPMI response (Unstim RPMI), Positive control Zymosan (10 µg mL$^{-1}$). The horizontal dotted line on each graph represents the lower limit of quantitation. Each donor blood stimulation is presented separately by vertical dotted lines. Error bars = standard deviation.

## 9.3 Standard curves of cytokines/chemokines/protease tested in planktonic and biofilm capsule stimulations with whole blood

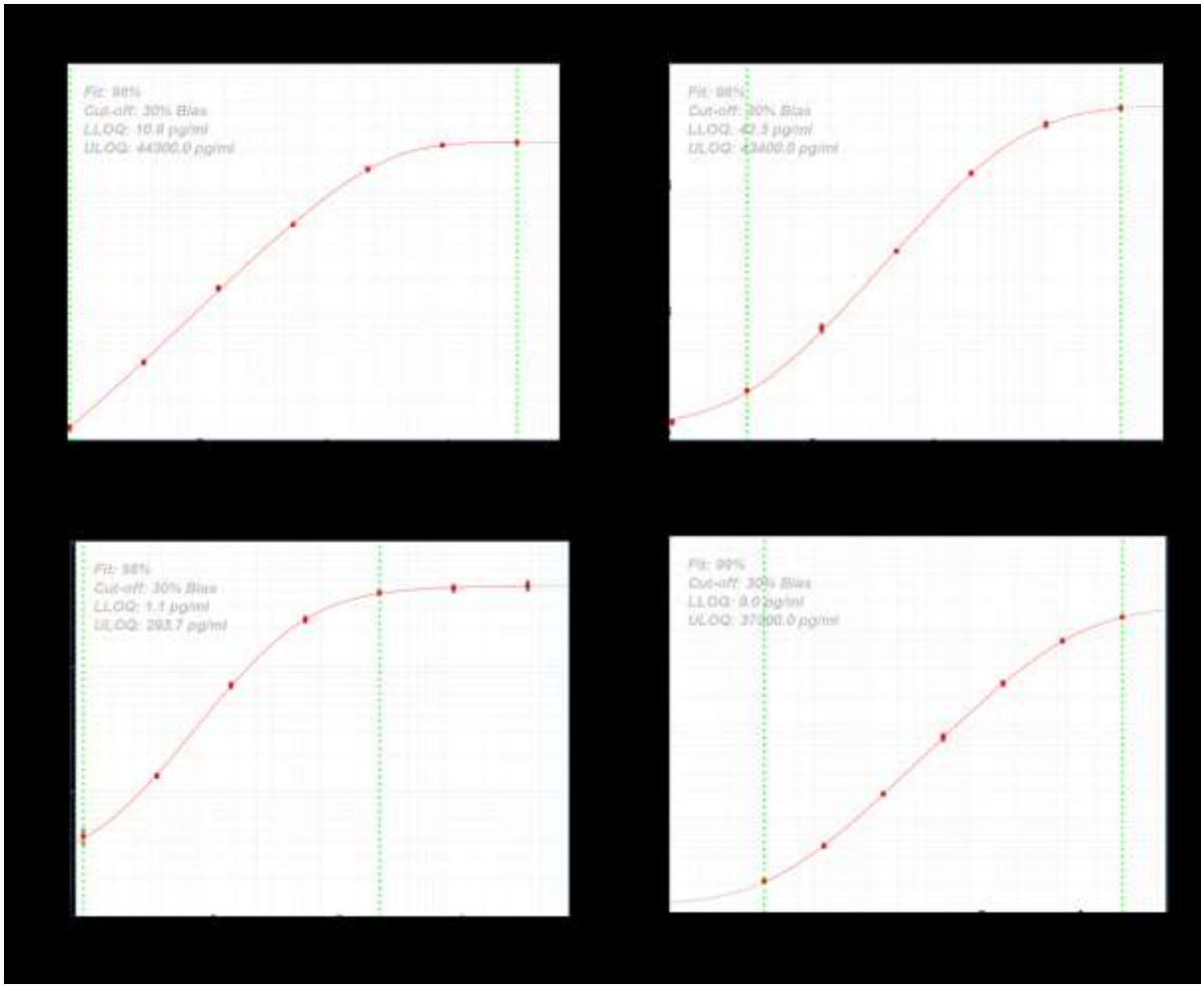

**Figure 9.3.1:** Standard curves of secreted cytokine/chemokines/protease generated using Procartaplex custom 4-plex panel and Procartaplex analyst software. 7-point standard curves generated from means of duplicate standard samples, using a 5 parameter logistic fit curve. Green dotted lines show lower limit of quantitation (LLOQ) and upper limit of quantitation (ULOQ) after setting the cut-off at 30% bias (acceptable percentage variation form the ideal standard curve.) (A) IFN-γ, (B) IL-6, (C) CCL2, (D) MMP-1.